Identification, Modeling, Dissolution, and Geochemical Evolution of Adsorption Heterogeneity of Metal Oxide Coated Sands

Alok Kumar
M.S., Southern Illinois University at Carbondale, Illinois, 1991
B.Tech., Indian School of Mines, India, 1987

A thesis submitted to the faculty of the
Oregon Graduate Institute of Science & Technology
in partial fulfillment of the requirements for the degree of
Doctor of Philosophy
in
Environmental Science and Engineering

April 1996

The dissertation "Identification, Modeling, Dissolution, and Geochemical Evolution of Adsorption Heterogeneity of Metal Oxide Coated Sands" by Alok Kumar has been examined and approved by the following Examination Committee:

William Fish, Thesis Advisor
Associate Professor

Richard L. Johnson
Associate Professor

Carl D. Palmer
Associate Professor

John C. Westall
Professor

DEDICATION

to

my parents, for inspiring me

and

my son, Ankit, and my wife, Preeti, for bringing so much joy into my life

"The great field of new discoveries .... is always the unclassified residuum. Round about the accredited and orderly facts of every science there ever floats a sort of dust-cloud of exceptional observations, of occurrences minute and irregular and seldom met with, which it always proves easier to ignore than to attend to. The ideal of every science is that of a closed and completed system of truth .... Phenomena unclassifiable within the system are paradoxical absurdities, and must be held untrue ... - one neglects or denies them with the best of scientific conscience .... Any one will renovate his science who will steadily look after the irregular phenomena. And when the science is renewed, its new formulas often have more of the voice of exception in them than of what were supposed to be the rules."

- William James
(in The Will to Believe)

ACKNOWLEDGEMENT

Four and a half years after I joined the Department of Environmental Science and Engineering, I could not have completed this thesis without the support, assistance, and assurance of my friends, colleagues, and family members. I wish to express my sincere appreciation to them.

I am grateful to my advisor, Bill Fish, for his financial support and for keeping me focussed. He gave me a lot of independence in shaping my thesis and supported my pursuit of tangentially-related and sometimes unrelated subjects. John Westall provided useful insights into various aspects of the thesis and was immensely instrumental in shaping my perception of adsorption processes. I would like to thank the members of my thesis committee, Bill Fish, Carl Palmer, Rick Johnson, and John Westall, for reviewing this work and offering insightful comments.

This research could not have been completed without the assistance of Cheryl Martin who taught me everything I know about laboratory procedures. Special thanks to Mike Elovitz and Will Romanelli in helping me fabricate experimental setups so that I could do a large number of replicate experiments; members of Dave Boone's laboratory for their insightful comments to my naive questions on microbiology and for sharing the centrifuge; Brad Beck for helping me out with computer troubles; Dirk Baron for the animated discussions; Wentai Luo, Michelle Scherer and Anabela Oliveira for their friendship.

My wife, Preeti, has put up with a lot for the duration we have been married. I cannot thank her enough for her love, patience, support, and encouragement.

TABLE OF CONTENTS

DEDICATION iii
ACKNOWLEDGEMENT v
LIST OF FIGURES x
LIST OF TABLES xvii
NOTATIONS xxvi
ABSTRACT xxx

CHAPTER 1
INTRODUCTION 1
1.1 Background 1
1.2 Statement of Research Objectives 2
1.2.1 Overall Research Objectives 2
1.2.2 Hypothesis 3
1.3 Overall Approach 4
1.4 Overview 5
1.4 References 5

CHAPTER 2
LIGANDS, METALS, AND METAL-LIGAND COMPLEXES AS DIFFERENTIAL PROBES OF SOIL ADSORPTION HETEROGENEITY ... 9
2.1 Abstract 9
2.2 Introduction 10
2.3 Definitions of Adsorption Heterogeneity and Adsorption Variability 12
2.4 Binding Strength Analysis 13
2.5 Experimental Methods 14
2.6 Results 16
2.6.1 Macroscale Adsorption Heterogeneity 16
2.6.1.1 Oxalic Acid 16
2.6.1.2 Copper 17
2.6.1.3 Cu in the Presence of Oxalate 17
2.6.2 Binding Strength Analysis of Microscale Adsorption Heterogeneity 22
2.6.2.1 Oxalic Acid 22
2.6.2.2 Copper 24
2.6.2.3 Cu in the Presence of Oxalate 24
2.7 Discussion 25
2.8 Conclusion 29

2.9 References 30

CHAPTER 3
HOMOGENEOUS-SITE ADSORPTION MODELING OF METAL OXIDE COATED SUBSOILS. 1. OXALATE and COPPER 32
3.1 Abstract 32
3.2 Introduction 33
3.3 Experimental Methods 35
3.4 Model Formulation and Parameter Estimation 35
3.5 Results 40
3.5.1 Experimental Results 40
3.5.2 Modeling Results 43
3.5.2.1 Modeling Adsorption of Oxalate onto AC 43
3.5.2.2 Modeling Oxalate on MC or MU 47
3.5.2.3 Modeling Adsorption of Cu onto AC, MC, and MU . . . 52
3.5.2.4 Sensitivity to Values of pK_a 55
3.5.2.5 Sensitivity of the Fits to the Values of N_s 55
3.6 Discussion 55
3.6.1 Modeling Adsorption of Oxalate and Cu 59
3.6.2 Heterogeneity Effects 61
3.6.3 Effect of Changes in Modeling Parameters 62
3.6.4 Linear Free Energy Relationships 63
3.6.5 Extrapolation with MINTEQA2 63
3.6.6 Valid Range of V_Y 65
3.6.7 Implications 65
3.7 References 66

CHAPTER 4
HOMOGENEOUS-SITE ADSORPTION MODELING OF METAL OXIDE COATED SUBSOILS. 2. COPPER-OXALATE COMPLEXES 70
4.1 Abstract 70
4.2 Introduction 71
4.3 Methods 71
4.4 Results 72
4.4.1 Modeling Adsorption of Cu*-Ox 79
4.4.2. Modeling Adsorption of Cu-Ox* 79
4.4.5 Modeling Simultaneous Adsorption of Cu and Oxalate 84
4.4.6 Sensitivity of Cu*-Ox Modeling to pK_a and N_s 84
4.5 Discussion 85
4.6 References 96

CHAPTER 5
SEMI-EMPIRICAL DISCRETE pK_a SPECTRUM APPROACH FOR MODELING

ADSORPTION OF OXALATE, COPPER, and COPPER-OXALATE COMPLEXES ONTO METAL OXIDE COATED SANDS 97
5.1 Abstract 97
5.2 Introduction 98
5.3 Modeling Adsorption with DPS 99
5.3.1 Modeling Adsorption on Humic Acid and Metal Oxides 99
5.3.2 Modeling Approach 100
5.4 Results 102
5.5 Discussion 112
5.6 References 118

CHAPTER 6
REMEDIATION OF METAL CONTAMINATED SUBSURFACE SOILS - DISSOLUTION AND COMPETITIVE EFFECTS 121
6.1 Abstract 121
6.2 Introduction 122
6.3 Experimental Method 124
6.4 Assumptions 125
6.5 Conditional Stability Constant Calculation 127
6.6 Results 128
6.7 Discussion 134
6.7.1 Competitive Effects 137
6.7.2 Implication 137
6.8 References 139

CHAPTER 7
GEOCHEMICAL EVOLUTION OF THE HETEROGENEITY OF SOIL ADSORPTION SITES 142
7.1 Abstract 142
7.2 Introduction 143
7.3 The Strategy for Modeling Changes in Adsorption Properties 144
7.3.1 The DLM Approach 144
7.3.2 The CDM Approach 145
7.4 Experimental Methods 149
7.5 Results 151
7.5.1 Surface Microscopy 151
7.5.2 Probing Change in Adsorption Properties with Adsorption Isotherms and Edges 151
7.5.2.1 Oxalate Isotherm 151
7.5.2.2 Cu*-Ox Isotherm 156
7.5.2.3 Oxalate pH Edges 156
7.5.2.4 Cu pH Edges 166
7.5.2.5 Cu*-Ox Edge 166

7.6 Discussion 171
7.7 References 174

CHAPTER 8
SUMMARY, IMPLICATIONS, AND FUTURE DIRECTIONS 176
8.1 Summary 176
8.1.1 Adsorption Modeling 176
8.1.2 Dissolution of Coating and its Effect on Metal Contaminant Subsoil Remediation 177
8.1.3 Change of Adsorption due to Dissolution of Coating 177
8.2 Importance of the Results 177
8.3 Future Directions 179
8.4 References 180

APPENDIX A
Data for Adsorption onto Artificially Coated Sample 181

APPENDIX B
Data for Adsorption onto Unweathered Milford Coated Sample 192

APPENDIX C
Data for Adsorption onto Weathered Milford Coated Samples 203

APPENDIX D
Data for Adsorption onto Unweathered Milford Uncoated Samples 213

APPENDIX E
Data for Adsorption onto Weathered Milford Uncoated Samples 224

APPENDIX F
Data for Ligand-Promoted Dissolution of Metal-Oxide Coating in Mini-Columns 236

VITA 240

PUBLICATIONS 241

LIST OF FIGURES

Figure 2.1. Plot of percent of oxalate adsorbed as a function of pH (pH edge) for 100 μM oxalate for Milford Coated (MC, □) and Milford Uncoated (MU, ●). 18

Figure 2.2. pH edge for 15 μM Total Cu for MC (□) and MU (●). 19

Figure 2.3. pH edge for Cu*-Ox with 1 mM oxalate and 121 μM Cu for MC (□) and MU (●). 20

Figure 2.4. pH edge for Cu*-Ox with 100 μM oxalate and 38 μM Cu for MC (□) and MU (●). 21

Figure 2.5. Binding strength analysis curves (described in the text) for a) oxalate, and b) Cu for MC. The concentration range for oxalate is 10 μM to 100 μM and the concentration range of total Cu is 5.7 μM to 15 μM. 23

Figure 2.6. Comparison of pH_{50} (pH of 50% adsorption) of oxalate, Cu, and Cu*-Ox for MC (light bars) and MU (dark bars). 26

Figure 3.1. DLM fits for adsorption of a) 10, b) 50, and c) 100 μM oxalate onto AC. The FITEQL fits are shown as ___. The dashed lines are prediction of oxalate adsorption based on effective adsorption constants. 41

Figure 3.2. DLM fits for adsorption of a) 10, b) 50, and c) 100 μM oxalate onto MC. The FITEQL fits are shown as ___. The dashed lines are prediction of oxalate adsorption based on effective adsorption constants. 42

Figure 3.3. DLM fits for adsorption of a) 5.7, and b) 15 Cu onto AC. The FITEQL fits are shown as ___. The dashed lines are prediction of oxalate adsorption based on effective adsorption constants. 44

Figure 3.4. Relationship between pH_{50} (pH of 50% adsorption) and the 6 N HCl extractable Fe and AC, MC, and MU. 45

Figure 3.5. Variation in the a) goodness of fit (V_Y) and b) effective surface complexation constants (K^{eff}) for DLM, CCM, and TLM, and oxalate concentrations of 10, 50, and 100 μM for the Artificially Coated Sample. K_{XOx2} and K_{XOx3} are the two species in DLM and CCM while K_{XOx4} is for TLM. 46

Figure 3.6. Variation in the a) goodness of fit (V_Y) and b) effective surface complexation constants (K^{eff}) for DLM, CCM, and TLM, and oxalate concentrations of 10, 50, and 100 μM for the Milford Coated Sample. K_{XOx2} and K_{XOx3} are the two species in DLM and CCM while K_{XOx4} is for TLM. 50

Figure 3.7. Variation in the a) goodness of fit (V_Y) and b) effective surface complexation constants (K^{eff}) for DLM, CCM, and TLM, and oxalate concentrations of 10, 50, and 100 μM for the Milford Uncoated Sample. K_{XOx2} and K_{XOx3} are the two species in DLM and CCM while K_{XOx4} is for TLM. 51

Figure 3.8. Variation in the a) goodness of fit (V_Y) and b) effective surface complexation constants (K^{eff}) for DLM, CCM, and TLM, and Cu concentrations of 5.7 and 15 μM for the AC, MC, and MU. 53

Figure 3.9. Relationship between the site density (N_s) and the goodness of fit (V_Y) for 10 μM (○) and 50 μM (●) oxalate, and 5.7 μM (□) and 15 μM (■) Cu. 58

Figure 3.10. Surface speciation for adsorption edges for a) 100 μM oxalate onto AC, b) 100 μM oxalate onto MC, and c) 5.7 μM Cu onto AC. Various surface species are marked on the figures. ($A = C_2O_4^{2-}$). 60

Figure 3.11. Comparison of the linear free energy relationship (LFER) and the surface complexation constant (K^{eff}) obtained for oxalate (□ and Δ) and Cu (○) for AC, MC, and MU. 64

Figure 4.1. Diffuse Layer Model (DLM) fits for adsorption of a) 8.3 μM Cu with 100 μM oxalate, and b) 38 μM Cu with 100 μM oxalate onto the Artificially Coated (AC) sample. The adsorption of Cu (only) calculated with MINTEQA2 and constants optimized with FITEQL are shown as ___. The FITEQL fits are shown as ___. The various dashed lines are prediction of adsorption based on effective surface complexation constants. 73

Figure 4.2. Diffuse Layer Model (DLM) fits for adsorption of a) 27 μM Cu with 1 mM oxalate, and b) 121 μM Cu with 1 mM oxalate onto the Artificially Coated (AC) sample. The adsorption of Cu (only) calculated with MINTEQA2 and constants optimized with FITEQL are shown as ——. We have not plotted the Cu (only) edge for 121 μM Cu because high concentration of Cu will precipitate at higher pH. The FITEQL fits are shown as ——. The various dashed lines are prediction of adsorption based on effective surface complexation constants. 74

Figure 4.3. Diffuse Layer Model (DLM) fits for adsorption of a) 100 μM oxalate with 8.3 μM Cu, and b) 100 μM oxalate with 38 μM Cu onto AC sample. The adsorption of oxalate (only) calculated with MINTEQA2 and constants optimized with FITEQL are shown as ——. The FITEQL fits are shown as ——. The various dashed lines are prediction of adsorption based on effective surface complexation constants. 76

Figure 4.4. Diffuse Layer Model (DLM) fits for adsorption of a) 100 μM oxalate with 8.3 μM Cu, and b) 100 μM oxalate with 38 μM Cu onto MU. The adsorption of oxalate (only) calculated with MINTEQA2 and constants optimized with FITEQL are shown as ——. The FITEQL fits are shown as ——. The various dashed lines are prediction of adsorption based on effective surface complexation constants. 77

Figure 4.5. The relationship for the adsorption of various concentrations of total Cu in the presence of oxalate (Cu_T^{Ox}) to the adsorption of various concentrations of Cu (Cu_T). 80

Figure 4.6. The variation in the effective surface complexation constant of Cu in the presence of oxalate (K_{XOCu1}) with respect to the total adsorbate concentrations. The adsorbate concentrations are 8.3 and 38 μM Cu with 100 μM oxalate, and 27 and 121 μM Cu with 1 mM oxalate and these are indicated on the x-axis. 81

Figure 4.7. The sensitivity of DLM fits to the choice of N_s for a) adsorption of Cu in the presence of oxalate, b) oxalate in the presence of Cu, and c) simultaneous adsorption of Cu and oxalate. The symbols □ and ○ are for adsorption of 8.3 and 38 μM Cu in the presence of 100 μM oxalate, Δ and ◇ for 27 and 121 μM Cu with 1 mM oxalate, ⊠ for 100 μM oxalate with 8.3 and 38 μM Cu, ■ for simultaneous adsorption of 8.3 μM Cu along with 100 μM oxalate,

and ● for simultaneous adsorption of 38 μM Cu and 100 μM oxalate. . 86

Figure 4.8. The near surface electrostatic parameters calculated with the DLM and plotted as a function of pH; a) the surface charge (σ) and b) electostatic correction factor (P). The symbol ○ is for simultaneous adsorption of 8.3 μM Cu along with 100 μM oxalate, Δ for simultaneous adsorption of 38 μM Cu along with 100 μM oxalate, □ for adsorption of 100 μM oxalate (only), ● and ◊ for 5.7 and 15 μM Cu (only). 92

Figure 4.9. Calculation of conditional stability constant (K_{cond}) as a function of pH for the aqueous complexation of Fe-oxalate, Al-oxalate, and Cu-oxalate. 94

Figure 5.1. Acid-base titration data generated with MINTEQA2 and fitted with two ($\Delta pK_a = 6$) and three ($\Delta pK_a = 4$) site discrete pK_a spectrum (DPS) model. 103

Figure 5.2. DPS model fit of oxalate adsorption edges for a) 10, b) 50, and c) 100 μM total oxalate onto AC with $\equiv XAH^o$ and $\equiv XA^-$ ($A = C_2O_4^{2-}$) in the one-site-class model. Insert tables show the optimal values of log K_{XOx}, as fitted with FITEQL 3.1, and the goodness of fit parameter V_Y. 104

Figure 5.3. DPS model fit of oxalate adsorption edges for a) 10, b) 50, and c) 100 μM total oxalate onto MC with $\equiv XA^-$ ($A = C_2O_4^{2-}$) in the one-site-class model. Insert tables show the optimal values of log K_{XOx}, as fitted with FITEQL 3.1, and the goodness of fit parameter V_Y. 105

Figure 5.4. DPS model fit of oxalate adsorption edges for a) 5.7 and b) 15 μM total Cu onto AC with $\equiv XOCu^+$ in the one-site-class model. Insert tables show the optimal values of log K_{XOCu}, as fitted with FITEQL 3.1, and the goodness of fit parameter V_Y. 109

Figure 5.5. DPS model fit of Cu adsorption in the ternary complex for a) 8.3 μM Cu with 100 μM oxalate, b) 38 μM Cu with 100 μM oxalate, c) 27 μM Cu with 1 mM oxalate, and d) 121 μM Cu with 1 mM oxalate onto AC with $\equiv XOCu^+$ along with the aqueous complexation of Cu and oxalate in the one-site-class model. Insert tables show the optimal values of log K_{XOCu}, as fitted with FITEQL 3.1, and the goodness of fit parameter V_Y. 110

Figure 5.6. DPS model fit of oxalate adsorption in the ternary complex for a) 100 μM with 8.3 μM Cu, and b) 100 μM oxalate with 38 μM Cu with ≡XAH° and ≡XA⁻ (A = $C_2O_4^{2-}$) in the one-site-class model. Insert tables show the optimal values of log K_{XOx}, as fitted with FITEQL 3.1, and the goodness of fit parameter V_Y. 111

Figure 5.7. Nonelectrostatic model calculations demonstrating the effect of ΔpKa values on the ability to reproduce acid-base titration curves generated with a Diffuse Layer Model with 0.05 M NaCl as background electrolyte. 116

Figure 6.1. Experimental setup for a) mini-column manifold, and b) PVC mini-columns. 126

Figure 6.2. Dissolution of Artificially Coated (AC) sample in mini-columns. The white portion of the extruded core is devoid of any coating while the darker portion is coated with goethite. 129

Figure 6.3. The change of concentration of Fe in the effluent and the change in dissolution rate with a velocity parameter V_p for Artificially Coated (AC) sample. 130

Figure 6.4. The change of concentration of Fe in the effluent and the change in dissolution rate with a velocity parameter V_p for Milford Coated (AC) sample. 131

Figure 6.5. The change of concentration of Fe in the effluent and the change in dissolution rate with a velocity parameter V_p for a) AC and b) MC. 132

Figure 6.6. The change of concentration of Fe in the effluent and the difference between effluent pH and influent pH (ΔpH) plotted with respect to change in velocity parameter V_p for a) AC and b) MC. 133

Figure 6.7. Progression of dissolution front with increasing V_p ($v_1 < v_2 < v_3$). 136

Figure 6.8. Conditional stability constant calculations for the binding of various metal ions to a) oxalate and b) EDTA. 148

Figure 7.1. Geochemical evolution of a) microscale adsorption heterogeneity and b) macroscale adsorption heterogeneity. 144

Figure 7.2. Scanning electron micrographs of a) unweathered Milford Coated (MC0) and b) weathered Milford Coated (MC3). Energy dispersive

X-ray for c) MC0 and d) MC3. 151

Figure 7.3. Scanning electron micrographs of a) unweathered Milford Uncoated (MU0) and b) weathered Milford Uncoated (MU3). Energy dispersive X-ray for c) MU0 and d) MU3. 153

Figure 7.4. Data for a) oxalate isotherm, and b) the range of site strengths calculated with the continuous distribution model at pH 7 for samples of MC. The weathering sequence is indicated by sample name followed by a number. The surficial metal oxide for the samples is listed in Table 7.2. Lines for MC0 and MC1 are overlapping and MC3 is indistinquishable from the horizontal axis. 154

Figure 7.5. Data for oxalate isotherm at pH 7 for samples of MU. The weathering sequence is indicated by sample name followed by a number. The surficial metal oxide for the samples is listed in Table 7.2. 157

Figure 7.6. Data for adsorption isotherm of Cu with 1 mM oxalate at pH 7 for samples of MC. 158

Figure 7.7. Data for a) pH edge, and b) the range of site strengths calculated with the continuous distribution model for Ox_T = 10 μM onto samples of MC. The lines in Fig. 7.7a are the CDM fits for the data. The corresponding lines in Fig. 7.7b are the calculated range of site strengths. The site strength distribution for MC2 and MC3 are indistinquishable from the horizontal axis. 159

Figure 7.8. Data for a) pH edge, and b) the range of site strengths calculated with the continuous distribution model for Ox_T = 50 μM onto samples of MC. The lines in Fig. 7.8a are the CDM fits for the data. The corresponding lines in Fig. 7.8b are the calculated range of site strengths. The site strength distribution for MC3 is indistinquishable from the horizontal axis. 164

Figure 7.9. Data for a) pH edge, and b) the range of site strengths calculated with the continuous distribution model for Ox_T = 10 μM onto samples of MU. The lines in Fig. 7.9a are the CDM fits for the data. The corresponding lines in Fig. 7.9b are the calculated range of site strengths. 165

Figure 7.10. Data for a) pH edge, and b) the range of site strengths calculated with the continuous distribution model for Cu_T = 15 μM onto

samples of MC. The lines in Fig. 7.10a are the CDM fits for the data. The corresponding lines in Fig. 7.10b are the calculated range of site strengths. The site strength distribution for MC0 and MC1 are indistinquishable from the horizontal axis. 167

Figure 7.11. Data for a) pH edge, and b) the range of site strengths calculated with the continuous distribution model for Cu_T = 15 μM onto samples of MU. The lines in Fig. 7.11a are the CDM fits for the data. The corresponding lines in Fig. 7.11b are the calculated range of site strengths. 168

Figure 7.12. Data for a) pH edge, and b) the range of site strengths calculated with the continuous distribution model for Cu_T = 27 μM with Ox_T = 1 mM onto samples of MC. The lines in Fig. 7.12a are the CDM fits for the data. The corresponding lines in Fig. 7.12b are the calculated range of site strengths. 169

Figure 7.13. Data for a) pH edge, and b) the range of site strengths calculated with the continuous distribution model for Cu_T = 27 μM with Ox_T = 1 mM onto samples of MU. The lines in Fig. 7.13a are the CDM fits for the data. The corresponding lines in Fig. 7.13b are the calculated range of site strengths. The distribution of site strengths for MU0 and MU1 are overlapping. 172

LIST OF TABLES

Table 2.1. Metal oxide coating on the Milford Coated (MC) and Milford Uncoated (MU) soils determined with 6 N HCl and ammonium-oxalate/oxalic acid (NH_4-Ox) extraction techniques (described in text). 15

Table 2.2. Oxalate pH edge adsorption characteristics for MU and MC. $\%A_{max}$, pH_{50}, pH_{min}, pH_{max} are defined in the text. 16

Table 2.3. Cu pH edge adsorption characteristics for MU and MC. 17

Table 2.4. Cu*-Ox pH edge adsorption characteristics for MU and MC. 22

Table 2.5. Log $K^{(d)}$ for oxalate for MU and MC. 22

Table 2.6. Log $K^{(d)}$ for Cu and Cu*-Ox for MU and MC. 24

Table 3.1. Parameters used for modeling adsorption of Cu and oxalate with Homogeneous-Site Surface Complexation Model (SCM), namely the Diffuse Layer Model (DLM), the Triple Layer Model (TLM), and the Constant Capacitance Model (CCM). 36

Table 3.2. Equilibrium expressions and equilibrium constants for surface protonation and the electrolyte binding reactions used for modeling Cu and oxalate adsorption with the SCMs. 38

Table 3.3. Equilibrium expressions and corresponding surface complexation reactions used for modeling adsorption of Cu and oxalate. 39

Table 3.4. Oxalate pH edge adsorption characteristics for AC, MU and MC given as the maximum percent adsorbed ($\%A_{max}$), the pH of maximum adsorption (pH_{max}), the pH of 50% adsorption (pH_{50}), and the pH of minimum adsorption (pH_{min}). 40

Table 3.5. Cu pH edge characterized by pH_{min}, pH_{50}, and pH_{max} for AC, MC, and MU. 43

Table 3.6. Effective surface complexation constants and the goodness of fit

for the adsorption of 10 μM, 50 μM, and 100 μM oxalate onto AC with DLM, CCM, and TLM. 47

Table 3.7. Effective surface complexation constants and the goodness of fit for adsorption of 10 μM, 50 μM, and 100 μM oxalate onto MC and MU with DLM and CCM. 49

Table 3.8. Effective surface complexation constants and the goodness of fit for adsorption of 10 μM, 50 μM, and 100 μM oxalate onto MC and MU with TLM. 52

Table 3.9. Effective surface complexation constants and the goodness of fit for adsorption of 5.7 μM and 15 μM Cu onto AC, MC, and MU with DLM, CCM, and TLM. 54

Table 3.10. Selected DLM fits for modeling the adsorption of oxalate and Cu onto AC with surface protonation constants for various solids (Collected from Table 1 in Huang et al. [*54*]). 56

Table 3.10 (Contd).
Selected DLM fits for modeling the adsorption of oxalate and Cu onto AC with surface protonation constants for various solids (Collected from Table 1 in Huang et al. [*54*]). 57

Table 4.1. Equilibrium expressions constants of aqueous reactions not listed in Chapter 3 but used for modeling adsorption of Cu-Oxalate with DLM, TLM, and CCM. 75

Table 4.2. Surface complexation reactions not listed in Chapter 3 but used for modeling adsorption of Cu-Oxalate with Type A and Type B ternary complexes. 75

Table 4.3. Characteristics for Cu*-Ox adsorption onto Artificially Coated (AC), Milford Coated (MC), and Milford Uncoated (MU) given as the pH of minimum adsorption (pH_{min}), pH of maximum adsorption (pH_{max}), and pH of 50% adsorption (pH_{50}). 78

Table 4.4. Effective surface complexation constant and goodness of fit for adsorption of Cu*-Ox onto AC, MC, and MU with CCM and DLM. . . 82

Table 4.5. Comparison of DLM fits for Cu-oxalate adsorption onto AC with only Type A (log $K_{XOCuOx1}$), and with Cu-only (log K_{XOCu1}) surface species. Low V_Y indicates better fit of the data. 83

Table 4.6. Effective surface complexation constant and goodness of fit for adsorption of Cu*-Ox onto AC, MC and MU with TLM. 84

Table 4.7. Surface complexation constant and goodness of fit for adsorption of Cu-Ox* onto AC, MC, and MU with CCM and DLM 85

Table 4.8. Effective surface complexation constant and goodness of fit for Adsorption of Cu-Ox* onto AC, MC, and MU with TLM. 87

Table 4.9. Effective surface complexation constant and goodness of fit for simultaneous adsorption of Cu and 100 μM onto AC, MC, and MU with CCM, DLM, and TLM. 88

Table 4.10. Selected results for modeling the adsorption of Cu*-Ox onto AC with surface protonation constants for various solids (Collected from Table 1, Huang et al. [*12*]) 89

Table 4.10 (Contd). Selected results for modeling the adsorption of Cu*-Ox onto AC with surface protonation constants for various solids (Collected from Table 1, Huang et al. [*12*]). 90

Table 5.1. Parameters used to generate synthetic acid-base titration curve with MINTEQA2. 100

Table 5.2. Parameters used to model synthetic acid-base titration curve with the discrete pK_a spectrum (DPS) approach 101

Table 5.3. Modeling adsorption of various ions with the DPS approach using the optimized surface site concentration and the pK_a spectrum. 106

Table 5.4. Effective surface complexation constant and goodness of fit for adsorption of oxalate onto AC, MC, and MU. 107

Table 5.4 (Continued). Effective surface complexation constant and goodness of fit for adsorption of oxalate onto AC, MC, and MU samples. 108

Table 5.5. Effective surface complexation constant and goodness of fit for adsorption of Cu onto AC, MC, and MU. 112

Table 5.6. Effective surface complexation constant and goodness of fit for

adsorption of Cu in the presence of oxalate onto AC, MC, and MU. . . 113

Table 5.7. Surface complexation constant and goodness of fit for adsorption of oxalate in the presence of Cu onto AC, MC, and MU. 114

Table 5.8. Comparison of DPS and SCM for their relative advantages and disadvantages in modeling adsorption of Cu, oxalate, and mixtures of Cu and oxalate onto metal oxide coated sands. 117

Table 6.1. Metal oxide coating on the Artificially Coated (AC), Milford Coated (MC), and Milford Uncoated (MU) soils determined with 6 N HCl and ammonium-oxalate/oxalic acid (NH_4-Ox) extraction techniques (described in Chapter 2). 124

Table 7.1. Equilibrium expressions for the surface complexation reactions used to reproduce the adsorption of Cu, oxalate, and Cu in the presence of oxalate in the Diffuse Layer Model (DLM). The same surface species were shown to reproduce the adsorption in Chapters 3 and 4. 147

Table 7.2. The surficial Fe and Al determined by extraction of sub-samples of weathered and unweathered samples of MC and MU with 6 N HCl and ammonium oxalate/oxalic acid (NH_4-Ox). 150

Table 7.3. Results of Continuous Distribution Model (CDM) fits for adsorption of oxalate, Cu, and Cu in the presence of oxalate (denoted here as Cu*-Ox) onto weathered and unweathered samples of MC. 155

Table 7.4. Results of CDM fits for adsorption of oxalate, Cu, and Cu*-Ox onto weathered and unweathered samples of MU. 160

Table 7.5. Optimal DLM parameters fitted to edges for Ox_T = 10 μM and 50 μM onto weathered and unweathered MC and MU. Left hand columns present best fit parameters assuming that N_s is fixed for samples of MC at 0.4 sites/nm^2 and for samples of MU at 0.3 sites/nm^2. Right hand columns present best-fit parameters when N_s is allowed to vary. 162

Table 7.5 (Continued).
Optimal DLM parameters fitted to edges for Ox_T = 10 μM and 50 μM onto weathered and unweathered MC and MU. Left hand columns present best fit parameters assuming that N_s is fixed for samples of MC at 0.4 sites/nm^2 and for samples of MU at 0.3 sites/nm^2. Right hand columns present best-fit parameters when

N_s is allowed to vary. 163

Table 7.6. Optimal DLM parameters fitted to pH edges for Cu_T = 15 μM and for Cu_T = 27 μM in the presence of Ox_T = 1 mM onto weathered and unweathered samples of MC and MU. Changing N_s did not change the fit for Cu adsorption hence results are equivalent to fits with the best V_Y. 170

Table A.1. Data for oxalate adsorption isotherm onto AC at pH 7 181

Table A.2. Data for adsorption of Ox_T = 100 μM onto AC 182

Table A.3. Data for adsorption of Ox_T = 50 μM onto AC 183

Table A.3 (Continued).
Data for adsorption of Ox_T = 50 μM onto AC 184

Table A.4. Data for adsorption of Ox_T = 10 μM onto AC 184

Table A.5. Data for adsorption of Cu_T = 5.7 μM onto AC 185

Table A.6. Data for adsorption of Cu_T = 15 μM onto AC 185

Table A.7. Data for adsorption of Cu_T = 27 μM with Ox_T = 1 mM onto AC 196

Table A.8. Data for adsorption of Cu_T = 121 μM with Ox_T = 1 mM onto AC 196

Table A.9. Data for adsorption of Cu_T = 38 μM with Ox_T = 100 μM onto AC ... 187

Table A.9 (Continued).
Data for adsorption of Cu_T = 38 μM with Ox_T = 100 μM onto AC ... 188

Table A.10. Data for adsorption of Cu_T = 8.3 μM with Ox_T = 100 μM onto AC .. 189

Table A.11. Data for adsorption of Ox_T = 100 μM with Cu_T = 38 μM onto AC ... 190

Table A.12. Data for adsorption of Ox_T = 100 μM with Cu_T = 8.3 μM onto AC .. 191

Table B.1. Data for oxalate adsorption isotherm onto MC at pH 7 192

Table B.2. Data for adsorption edge onto MC; Ox_T = 100 μM 193

Table B.3. Data for adsorption edge onto MC; Ox_T = 50 μM 194

Table B.4. Data for adsorption edge onto MC; Ox_T = 10 μM 195

Table B.5. Data for adsorption edge onto MC; Cu_T = 15 μM 196

Table B.6. Data for adsorption edge onto MC; Cu_T = 5.7 μM 197

Table B.7. Data for adsorption edge onto MC; Cu_T = 27 μM with Ox_T = 1 mM 198

Table B.8. Data for adsorption edge onto MC; Cu_T = 121 μM with Ox_T = 1 mM 199

Table B.9. Data for adsorption edge onto MC; Cu_T = 38 μM with Ox_T = 100 μM 200

Table B.10. Data for adsorption edge onto MC; Cu_T = 8.3 μM with Ox_T = 100 μM 201

Table B.11. Data for adsorption edge onto MC; Ox_T = 100 μM with Cu_T = 8.3 μM 202

Table C.1. Data for oxalate adsorption isotherm at pH 7. 203

Table C.2. Data for adsorption edge at Ox_T = 50 μM onto MC1. 204

Table C.3. Data for adsorption edge at Ox_T = 10 μM onto MC1. 204

Table C.4. Data for copper adsorption isotherm at pH 7 with Ox_T = 1 mM. 205

Table C.5. Data for adsorption edge at Cu_T = 15 μM onto MC1. 205

Table C.6. Data for adsorption edge at Cu_T = 27 μM with Ox_T = 1 mM onto MC1. 206

Table C.7. Data for oxalate adsorption isotherm at pH 7 onto MC2. 207

Table C.8. Data for adsorption edge at Ox_T = 50 μM onto MC2 208

Table C.9. Data for adsorption edge at Ox_T = 10 μM onto MC2. 208

Table C.10. Data for copper adsorption isotherm at pH 7 with Ox_T = 1 mM. 209

Table C.11. Data for adsorption edge at Cu_T = 15 μM onto MC2. 209

Table C.12. Data for adsorption edge at Cu_T = 27 μM with Ox_T = 1 mM onto MC2. 209

Table C.13. Data for oxalate adsorption isotherm at pH 7 onto MC3. 210

Table C.14. Data for adsorption edge at Ox_T = 50 μM onto MC3. 210

Table C.15. Data for adsorption edge at Ox_T = 10 μM onto MC3. 211

Table C.16. Data for copper adsorption isotherm at pH 7 with Ox_T = 1 mM. 211

Table C.17. Data for adsorption edge at Cu_T = 15 μM onto MC3. 212

Table C.18. Data for adsorption edge at Cu_T = 27 μM with Ox_T = 1 mM onto MC3 212

Table D.1. Data for oxalate adsorption isotherm onto MU at pH 7 213

Table D.2. Data for adsorption edge onto MU for Ox_T = 100 μM 214

Table D.3. Data for adsorption edge onto MU for Ox_T = 50 μM 215

Table D.4. Data for adsorption edge onto MU for Ox_T = 10 μM 216

Table D.4 (Continued).
Data for adsorption edge onto MU for Ox_T = 10 μM 217

Table D.5. Data for adsorption edge onto MU for Cu_T = 15 μM 217

Table D.6. Data for adsorption edge onto MU for Cu_T = 5.7 μM 218

Table D.7. Data for adsorption edge onto MU for Cu_T = 27 μM with Ox_T = 1 mM 219

Table D.8. Data for adsorption edge onto MU for Cu_T = 121 μM with Ox_T = 1 mM 220

Table D.9. Data for adsorption edge onto MU for Cu_T = 38 μM with Ox_T = 100 μM 220

Table D.10. Data for adsorption edge onto MU for Cu_T = 8.3 μM with

Ox_T = 100 μM 221

Table D.11. Data for adsorption edge onto MU for Ox_T = 100 μM with Cu_T = 38 μM. 222

Table D.12. Data for adsorption edge onto MU for Ox_T = 100 μM with Cu_T = 8.3 μM. 223

Table E.1. Data for adsorption isotherm onto MU1 at pH 7 224

Table E.2. Data for oxalate adsorption edge onto MU1 Ox_T = 10 μM 225

Table E.2 (Contd).
Data for oxalate adsorption edge onto MU1 Ox_T = 10 μM 226

Table E.3. Data for Cu adsorption edge onto MU1; Cu_T = 15 μM 226

Table E.4. Data for adsorption edge onto MU1 for Cu_T = 27 μM with Ox_T = 1 mM. 227

Table E.5. Data for adsorption isotherm onto MU2 at pH 7 228

Table E.6. Data for adsorption edge onto MU2 for Ox_T = 10 μM. 229

Table E.6 (Contd).
Data for adsorption edge onto MU2 for Ox_T = 10 μM. 230

Table E.7. Data for adsorption edge onto MU2 for Cu_T = 15 μM 230

Table E.8. Data for adsorption edge onto MU2 for Cu_T = 27 μM. and Ox_T = 1 mM.. 231

Table E.9. Data for adsorption isotherm onto MU3 at pH 7 232

Table E.10. Data for adsorption edge onto MU3 for Ox_T = 10 μM. 233

Table E.10 (Continued).
Data for adsorption edge onto MU3 for Ox_T = 10 μM. 234

Table E.11. Data for adsorption edge onto MU3 for Cu_T = 15 μM. 234

Table E.12. Data for adsorption edge onto MU3 for Cu_T = 27 μM. and Ox_T = 1 mM. 235

Table F.1. Data for dissolution of Fe from AC with buffered Ox_T = 1 mM at pH 4 236

Table F.2. Data for dissolution of Fe from AC with unbuffered Ox_T = 1 mM; $pH_{initial}$ = 4 237

Table F.3. Data for dissolution of Fe from MC with buffered Ox_T = 1 mM at pH 4 238

Table F.4. Data for dissolution of Fe from MC with unbuffered Ox_T = 1 mM; $pH_{initial}$ = 4 239

NOTATIONS

a	Avogadro Number
A	Specific surface area (m^2/g)
AAS	Atomic Absorption Spectrophotometry
c	Concentration in solution (mol/L)
^{c}p	Relative affinity
$^{c}p_m$	Optimized relative affinity
C_1	Inner-layer capacitance (F/m^2)
C_2	Outer-layer capacitance (F/m^2)
Cu_T	Total Cu concentration (mol/L)
Cu_T^{Ox}	Total Cu concentration in the presence of oxalate (mol/L)
Cu*-Ox	Adsorption of Cu in the presence of oxalate
Cu-Ox*	Adsorption of oxalate in the presence of Cu
CCM	Constant Capacitance Model
CDM	Continuous distribution model
DLM	Diffuse Layer Model
DPS	Discrete pK_a spectrum
EDL	Electric Double Layer
EDX	Energy dispersive X-ray
F	Faraday Constant
Fe_{aq}	Dissolved Fe
I.S.	Inner-sphere complex
K_a	Protonation Constant
K_{cond}	Conditional stability constant

K^{eff}	Effective Surface Complexation Constant
K_{Cl-}	Binding constant for Cl^-
K_{XOCu1}	Effective Surface Complexation Constant for formation of $\equiv XOCu^+$
K_{XOCu2}	Effective Surface Complexation Constant for formation of $\equiv XO^-Cu^{2+}$
K_{Na+}	Binding constant for Na^+
K_{XOx1}	Effective Surface Complexation Constant for formation of $\equiv XC_2O_4H$
K_{XOx2}	Effective Surface Complexation Constant for formation of $\equiv XC_2O_4^-$
K_{XOx3}	Effective Surface Complexation Constant for formation of $\equiv XOC_2O_4^{3-}$
K_{XOx4}	Effective Surface Complexation Constant for formation of $\equiv XOH^{2+}\text{-}HC_2O_4^-$
K_{XOx5}	Effective Surface Complexation Constant for formation of $\equiv XOH^{2+}\text{-}C_2O_4^{2-}$
$K_{XOCuOx1}$	Effective Surface Complexation Constant for formation of $\equiv XOCu(C_2O_4^{2-})^-$
$K_{XOCuOx2}$	Effective Surface Complexation Constant for formation of $\equiv X_2(C_2O_4^{2-})_2Cu$
$K_{XOCuOx3}$	Effective Surface Complexation Constant for formation of $(\equiv XOH^{2+})_2\text{-}Cu(C_2O_4)_2^{2-}$
K_{ML}	Formation constants for the metal-chelate complexes ML.
K_{MHL}	Formation constants for the metal-chelate complexes MHL
K_{MOHL}	Formation constants for the metal-chelate complexes MOHL
L	A generic ligand
M	$= N_s^T SA/a$
$\bar{n}$	Exchange stoichiometry
N_s	Site density (sites/nm^2)
N_s^T	Site density calculated with the CDM approach
NH_4-Ox	ammonium oxalate/oxalic acid extraction
Ox_T	Total oxalate concentration (mol/L)
O.S.	Outer-sphere complex
pv	Pore Volumes
ppzc	Pristine point of zero charge
pH_{50}	pH of 50% adsorption
pH_{max}	pH of maximum adsorption

pH_{min}	pH of minimum adsorption
pK_a	- log K_a
P	$\exp(\Delta zF\psi/RT)$: electrostatic correction factor
PNL	Pacific Northwest Laboratory
r_D	Dissolution Rate μmoles/pv/g
R	Gas Law Constant
S	Solids concentration (g/L)
S^*	Adsorption per unit sorbent
SCM	Surface Complexation Model
SEM	Scanning Electron Microscopy
T	Temperature
TLM	Triple Layer Model
Type A	$\equiv XOCu(C_2O_4^{2-})^-$ for both inner-sphere and outer-sphere
Type B	$\equiv X_2(C_2O_4^{2-})_2Cu$ for inner-sphere; $(\equiv XOH^{2+})_2 - Cu(C_2O_4)_2^{2-}$ for outer-sphere
V_p	Velocity parameter expressed as pore volumes per hour
V_Y	Overall variance (weighted sum of squares of residual over degrees of freedom)
α_i	Fractional distribution of the fully deprotonated ligand
α_{i-1}	Fractional distribution of ligand containing one proton
β	Heterogeneity index ($0 < \beta < 1$)
β_n	Fractional distribution of the metal M^{n+}
β_{n-1}	Fractional distribution of the hydroxylated metal ion MOH^{n-1}
Γ_{max}	maximum adsorption density (mol/L)
$\Gamma_{Cu\text{-}Ox^*}$	Adsorption of Oxalate in the presence of Cu
Γ_{Cu}	Adsorption of Cu
$\Gamma_{Cu^*\text{-}Ox}$	Adsorption of Cu in the presence of oxalate
Γ_{Ox}	Adsorption of oxalate
ψ	Potential at the surface (calculated with the Diffuse Layer Model)
ψ_o	Potential at the 'o' plane

ψ_β	Potential at the 'β' plane
α_s^{Cu}	Fractional adsorption of binding of single-ion Cu
$\alpha_s^{Cu^*\text{-}Ox}$	Fractional adsorption Cu in the presence of oxalate
σ	Surface charge (C/m^2)
ΔpK_a	$-\log K^i_{a1}K^i_{a2}$
ΔpH	Effluent pH - Influent pH
κ	${}^cp_m + \tilde{n}pH + \log c$

ABSTRACT

Identification, Modeling, Dissolution, and Geochemical Evolution of Adsorption Heterogeneity of Metal Oxide Coated Sands

Alok Kumar

Oregon Graduate Institute of Science & Technology, 1996

Supervising Professor: William Fish

Adsorption heterogeneity of subsoils may depend on the sorbate and its concentration. Ligands in natural and contaminated subsoils may dissolve substantial metal oxides thereby altering the subsoil heterogeneity. We investigated these hypotheses on sands artificially and naturally coated with various amounts of metal oxides. The adsorbates Cu, oxalate, and mixtures of Cu and oxalate (Cu-Oxalate) were used as probes of the surface.

For the concentration range studied, Binding Strength Analysis revealed that the naturally coated samples were heterogeneous at the microscale and the macroscale when oxalate was used as the probe of the surface. Cu revealed a smaller heterogeneity while Cu-Oxalate indicated an intermediate heterogeneity.

Various elaborations of homogeneous-site Surface Complexation Models (SCM), calibrated to the surface protonation properties of goethite, modeled accurately the edges of oxalate, Cu, and mixtures of Cu and oxalate. The poorer fits for large concentrations was probably because of the site heterogeneity. The accuracy of SCMs was insensitive to the choice of surface protonation constants (pK_a) and moderately sensitive to the choice of site density. The effective surface complexation constants (K^{eff}) obtained from individual edges

were somewhat different because of the concentration dependent heterogeneity. It was not always possible to use K^{eff} values for one sorbate concentration to reproduce adsorption of other concentrations of the same sorbate.

A modified version of the discrete pK_a spectrum model closely reproduced the acid-base titration curve with two adsorption sites (four pK_a's). The adsorption of all concentrations of Cu, oxalate, and Cu-Oxalate was often reproduced with only one of those sites. The competition between the dissolved Al and the surface for the oxalate in solution was accurately reproduced with both sites.

The dissolution of the oxide coating was often influenced by the pore velocity. For the naturally coated sands, the adsorption of oxalate changed measurably when nearly 70% of the 6 N HCl extractable surficial Fe and Al were removed. Adsorption of Cu in the presence and absence of oxalate changed when nearly all the surficial Fe and Al were removed. The change in adsorption included a diminished adsorption capacity and site heterogeneity.

CHAPTER 1

INTRODUCTION

1.1 Background

Hydrous metal oxides are common adsorbents in subsoils. Adsorption removes ions from solution thereby changing their mobility, their redox activity, and their potential for biotransformation (*1* and the references therein). The adsorption of ionic solutes involves specific interaction with surface functional groups (*2*). The adsorption depends on various factors including the mineralogic composition of the adsorbent, solids concentration, specific surface area, pH, and ionic strength. Ionic adsorption is typically modeled with various elaborations of the surface complexation model (SCM); the Triple Layer Model (TLM; e.g., *3 - 14*), the Diffuse Layer Model (DLM; e.g., *2, 15 - 21*), and the Constant Capacitance Model (CCM; e.g., *22 - 32*). Various SCMs differ only in the representation of the electrostatic structure at the surface. The homogeneous-site SCM formulations are often adequate for modeling adsorption of various ions onto pure phase metal oxides (*33, 34*).

Direct extrapolation of results for pure-phase metal oxides to predict in-situ ionic behavior in a naturally complex soil or subsoil assemblage is sometimes achieved by modeling soils as some combination of isolated oxides (*35, 36*). A priori determination of the appropriate combination has not been demonstrated. Some soils and aquasols coated with metal oxides (*37 - 41*) are comparatively close to a pure oxide phase and represent the best hope for diagnostic and prognostic modeling based on pure-phase metal oxide model parameters.

Oxide coated sands are proposed here to be somewhat heterogeneous in their adsorption properties and contain a range of site strengths. The presence of such microscale site heterogeneity can be estimated with binding strength analysis (BSA; *42*). The adsorption

of ions to heterogeneous subsoil particles may not always be modeled accurately with a homogeneous-site SCM. Such heterogeneous sorbents may be modeled over a wide range of conditions with a modified version of the nonelectrostatic discrete pK_a spectrum (DPS) model of Westall et al. (*43*). Soil surfaces are three dimensional and the electrostatic structure at the surface is complex. The electrostatic parameters obtained for soils with SCMs that assume a two dimensional structure will not represent reality. The near surface electrostatics may thus be neglected and the adsorption onto soils can be modeled with nonelectrostatic models containing a discrete or continuous range of adsorption energies (*43, 44*).

Ligands adsorb to soils, dissolve metal oxide/hydroxide from soils, enhance weathering of subsoil minerals, redistribute the dissolved ions, and form podzols (*45*). Ligands enhance dissolution by adsorbing to the surficial adsorption sites and forming a precursor metal-ligand complex which then detaches from the soil surface (*46 - 49*). Such dissolution may change the adsorption properties of subsoil particles.

Soils have heterogeneous adsorption sites and it is important to evaluate the effectiveness of extending the results of modeling adsorption of ions onto isolated oxides to naturally complex soils. Very few studies have done this for adsorption of metals, ligands, and metal-ligand complexes. Adsorption of ligands may dissolve surficial metal oxide thereby altering the adsorption properties. It is essential to understand the role of these processes in natural soils to accurately estimate the fate and transport of solutes and evaluate the efficiency and progress of in-situ remedial action.

1.2 Statement of Research Objectives

The primary objective of this research was to study the adsorption of metals, ligands, and mixture of metals and ligands onto oxide coated sands and to test the diagnostic and prognostic capability of various mathematical models in reproducing the mineral-solute interaction.

1.2.1 Overall Research Objectives

The *overall objectives* of the research were to study the:

1) adsorption of a model metal (Cu) and a ligand (oxalate) onto metal oxide coated sands.

2) ligand promoted dissolution of surficial metal from the metal oxide coated sands

3) long term changes in soil adsorption characteristics due to ligand promoted dissolution

The *specific objectives* of the research included:

- obtain the pH edges for adsorption of Cu, oxalate, and mixtures of Cu and oxalate.
- identify the apparent adsorption heterogeneity in the metal oxide coated sands with BSA.
- model the edges for Cu, oxalate, and mixtures of Cu and oxalate with the DLM, the CCM, the TLM, and the DPS model.
- explore the effect of flushing oxalate at various pore velocities through columns packed with metal oxide coated sands.
- obtain edges and isotherms for adsorption of Cu, oxalate, and Cu in the presence of oxalate onto the metal oxide coated sands weathered to different degree by ligand promoted dissolution.
- model the pH edges and isotherms for the weathered samples with the DLM and continuous distribution model (CDM; *44*).

1.2.2 Hypothesis

The major hypotheses proposed were:

Hypothesis 1

Soil particles are geochemically heterogeneous due to their complex mineralogic composition. Adsorption will be influenced to varying degrees by this apparent geochemical heterogeneity depending on the adsorbate and adsorbate concentrations.

Rationale

Variation in mineralogic composition of soil particles results in particle-scale variation in reactivity (microscale heterogeneity). Chemical mass action dictates that the most reactive sites will be most readily occupied by the most reactive solutes. Smaller concentrations of adsorbates will bind mostly to the stronger sites thereby revealing a smaller degree of apparent heterogeneity. Higher concentration of adsorbate will

bind to sites with a wider range of adsorption energies thereby revealing a higher degree of apparent heterogeneity. Different adsorbates coordinate with the surface functional groups by different mechanisms, e.g., some form inner-sphere complexes while some others form outer-sphere complexes. Depending on the binding mechanism, different adsorbates may reveal a slightly different apparent heterogeneity.

Hypothesis 2

Ligands dissolve adsorption sites from soil surfaces, thereby altering their microscale and macroscale adsorption heterogeneity.

Rationale

Ligands are found in natural and contaminated soils. They may preferentially adsorb to the stronger adsorption sites on soils and dissolve them. For sands coated with metal oxides, loss of stronger sites will reduce the range of adsorption energies and hence the microscale adsorption heterogeneity. For some other soils, loss of surficial oxide may reveal more adsorption sites thereby increasing the microscale site heterogeneity. Differences in fluxes of dissolution-promoting ligands through different regions of a physically heterogeneous matrix can create chemical variability in the surfaces of a material that was originally chemically homogeneous. This may increase the macroscale heterogeneity. Differences in fluxes through physically and geochemically heterogeneous formations may dissolve more metal oxide from soils containing more surficial metal than from soils containing less metal – a decrease in macroscale heterogeneity.

1.3 Overall Approach

The overall approach to testing the hypotheses and achieving the stated objectives was to conduct batch experiments for the adsorption of Cu, oxalate, and mixtures of Cu and oxalate onto metal oxide coated sands. The experimental adsorbents were sands artificially and naturally coated with various amounts of metal oxides. The pH edges were obtained for oxalate concentration (Ox_T) of 10 μM, 50 μM, and 100 μM, and Cu concentration (Cu_T) of

5.7 μM and 15 μM. The edges for mixtures of Cu and oxalate were obtained for Cu_T = 8.3 μM and 38 μM with Ox_T = 100 μM, and Cu_T = 27 μM and 121 μM with Ox_T = 1 mM. Adsorption isotherms at pH = 7 were obtained for oxalate and Cu in the presence of Ox_T = 1 mM. The pH was maintained at 7.0 with 0.01 M MOPS, a biological buffer. The ligand promoted dissolution experiments were conducted in a novel mini-column manifold with Ox_T = 1 mM at pH = 4. The pH was maintained at 4.0 with 0.01 M sodium acetate/acetic acid. All the experiments were in a background electrolyte of 0.05 M NaCl and batch adsorption experiments were for a solids concentration of 100 g/L. The data for adsorption of Cu, oxalate, and mixtures of Cu and oxalate were modeled with BSA, SCMs, DPS, and CDM techniques.

1.4 Overview

Chapter 2 explores the effect of various adsorbates and adsorbate concentrations on the apparent adsorption heterogeneity of coated sands. The third and the fourth chapters explore how effectively homogeneous-site SCMs reproduce the adsorption of Cu, oxalate, and mixtures of Cu and oxalate onto oxide coated sands. The third chapter focuses on adsorption of oxalate and Cu while the fourth focuses on adsorption of mixtures of Cu and oxalate. Chapter 5 tests how well the modified DPS approach of Westall et al. (*43*) reproduces adsorption onto mineralogically complex soils. The sixth chapter examines the role of pore velocity in dissolving metals from columns packed with oxide coated sands. Chapter 7 tests the hypothesis of geochemical evolution due to ligand promoted dissolution and identifies the criteria for the importance of this process. Chapter 8 summarizes the findings in this dissertation and identifies the important conclusions. All the experimental data are presented in Appendices A, B, C, D, E, and F.

1.4 References

(1) Mesuere, K. *Adsorption and Dissolution Reactions Between Oxalate, Chromate, and Iron Oxide Surface: Assessment of Current Modeling Concepts.* Ph.D. Dissertation, Oregon Graduate Institute of Science & Technology, December, **1991**.

(2) Dzombak, D.A. and Morel, F.M.M. *Surface Complexation Modeling: Hydrous Ferric Oxide*. John Wiley & Sons. **1990**.

(3) Davis, J.A.; James, R.O.; and Leckie, J.O.; *J. Colloid Interface Sci.*, **1978**, 63:480-499.

(4) Hayes, K.F.; Roe, A.L.; Brown, G.E.; Hodgson, K.O.; Leckie, J.O.; and Parks, G.A. *Science*, **1987**, 238:783-786.

(5) Davis, J.A. and Leckie, J.O. *Environ. Sci. Technol.* **1978**, 12, 1309.

(6) Davis, J.A. and Leckie, J.O. *J. Colloid and Interface Sci.* **1980**, 74(1), 32-43.

(7) Balistereri, L.S. and Murray, J.W. *Geochim. Cosmochim. Acta*, **1982**, 51(5), 1151-1160.

(8) Hsi, C.D. and Langmuir, D. *Geochim. Cosmochim. Acta*, **1985**, 49:1931-1941.

(9) Catts, J.G. and Langmuir, D. *J. Appl. Geochem.*, **1986**, 1:255-264.

(10) LaFlamme, B.D. and Murray, J.W. *Geochim. Cosmochim Acta*, **1987**, 51:243-250.

(11) Hunter, K.A.; Hawke, D.J.; and Choo, L.K. *Geochim. Cosmochim Acta*, **1988**, 52:627-636.

(12) Payne, T.E. and Waite, T.D. *Radiochim Acta*, **1991**, 52-53(Pt. 2):487-493.

(13) Goldberg, S. *J. Colloid and Interface Sci.* **1991**, 145(1), 1-10.

(14) Hayes, K.F. and Leckie, J.O. *J. Colloid and Interface Sci.* **1987**, 115(2), 564-572.

(15) Stumm, W.; Hohl, H.; and Dalang, F. *Croat. Chem Acta*, **1970**, 48:491-504.

(16) Huang, C.P. and Stumm, W. *J. Colloid Interface Sci.*, **1973**, 43:409-420.

(17) Harding, I.H. and Healy, T.W. *J. Colloid Interface Sci.*, **1985a**, 107:382-397.

(18) Harding, I.H. and Healy, T.W. *J. Colloid Interface Sci.*, **1985b**, 107:371-381.

(19) Dzombak, D.A. and Morel, F.M.M. *J. Colloid and Interface Sci.* **1986**, 112(2), 588-598.

(20) Mesuere, K. and Fish, W. *Environ. Sci. Technol.* **1992a**, 26(12), 2357-2364.

(21) Mesuere, K. and Fish, W. *Environ. Sci. Technol.*, **1992b**, 26(12), 2365-2370.

(22) Schindler, P.W. and Kamber, H.R. *Helv. Chim. Acta*, **1968**, 51:1781-1786.

(23) Hohl, H. and Stumm, W. *J. Colloid Interface Sci.*, **1976**, 55:281-288.

(24) Schindler, P.W.; Furst, B.; Dick, R.; and Wolf, P.U. *J. Colloid Interface Sci.*, **1976**, 55:469-475.

(25) Stumm, W.; Kummert, R. and Sigg, L. *Croat. Chem. Acta*, **1980**, 53:291-312.

(26) Sigg, L. and Stumm, W. *Colloids and Surfaces 2*, **1987**, 101-117.

(27) Sposito, G. *The Surface Chemistry of Soils*, **1984**, Oxford University Press, New York.

(28) Schindler, P.W. and Stumm, W. "The Surface Chemistry of Oxides, Hydroxides, and Oxide Minerals," in *Aquatic Surface Chemistry*, W. Stumm (ed.), Wiley-Interscience, New York, **1987**, pp. 83-110.

(29) Goldberg, S. and Sposito, G. *Soil Sci. Soc. Am. J.*, **1984a**, 48:772.

(30) Goldberg, S. and Sposito, G. *Soil Sci. Soc. Am. J.*, **1984b**, 48:779.

(31) Goldberg, S. *Soil Sci. Soc. Am. J.*, **1985**, 49:851.

(32) Goldberg, S. *J. Colloid and Interface Sci.* **1991**, 145(1), 1-10.

(33) Westall, J.C. and Hohl, H. Advan. *Colloid Interface Sci.*, **1980**, 12:265-294.

(34) Morel, F.M.M.; Yeasted, J.G.; and Westall, J.C. "Adsorption Models: A Mathematical Analysis in the Framework of General Equilibrium Calculations," in *Adsorption of Inorganics in Solid-Liquid Interfaces*, M.A. Anderson and A.J. Rubin (eds.), Ann Arbor Science, Ann Arbor, Mich., **1981**, pp. 263-294.

(35) Zachara, J.M.; Cowan, C.E.; Schmidt, R.L.; and Ainsworth, C.C. *Clays and Clay Minerals*. **1988**, 36(4), 317-326.

(36) Zachara, J.M.; Ainsworth, C.C.; Cowan, C.E.; and Resch, C.T. *Soil Sci. Soc. Am. J.* **1989**, 53, 418-428.

(37) Stahl, R.S. and James, B.R. *Soil Sci. Soc. Am. J.* **1991a**, 55, 1287-1290.

(38) Stahl, R.S. and James, B.R. *Soil Sci. Soc. Am. J.* **1991b**, 55, 1291-1294.

(39) Stahl, R.S. and James, B.R. *Soil Sci. Soc. Am. J.* **1991c**, 55, 1592-1297.

(40) Szecsody, J.E.; Zachara, J.M; and Bruckhart,P.L. *Environ. Sci. Technol.*, **1994**, 28:1706-1716.

(41) Scheiddegger, A.; Borkovec, M.; and Sticher, H. *Geoderma*. **1993**, 58, 43-65.

(42) Benjamin, M.M. and Leckie, J.O. *Environ. Sci. Technol.*, **1981**, 15(9):1050-1057.

(43) Westall, J.C.; Jones, J.D.; Turner, G.D.; and Zachara, J.M. *Environ. Sci. Technol.*, **1995**, 29:951-959.

(44) Kinniburgh, D.G.; Barker, J.A.; and Whitfield, M. *J. Colloid Interface Sci.*, **1983**, 95(2):370- 384.

(45) Lundström, U.S. *J. Soil Sci.*, **1993**, 44:121-133.

(46) Wieland, E.; Wehrli, B.; and Stumm, W. *Geochim. Cosmochim. Acta*, **1988**, 52:1969-1981.

(47) Zinder, B.; Furrer, G.; and Stumm, W. *Geochim. Cosmochim Acta*, **1986**, 50:1861-1869.

(48) Wieland, E. and Stumm, W. *Geochim. Cosmochim. Acta*, **1992**, 56:3339-3355.

(49) Furrer, G. and Stumm, W. *Geochim. Cosmochim Acta*, **1986**, 50:1847-1860.

CHAPTER 2*

LIGANDS, METALS, AND METAL-LIGAND COMPLEXES AS DIFFERENTIAL PROBES OF SOIL ADSORPTION HETEROGENEITY

2.1 Abstract

The availability and transport of solutes in the subsurface can be strongly influenced by the scale-dependent adsorption heterogeneity of the aquifer formation. Adsorption heterogeneity appears at both the micro ("heterogeneity") and the macro ("variability") scale. It has been suggested in the literature that adsorption heterogeneity should be defined only for specific adsorbate/adsorbent pairs. We have investigated the hypothesis that the observed adsorption heterogeneity is not only an inherent property of the adsorbent but depends in part on the nature and the concentration of the adsorbates. Batch experiments yielded adsorption pH edges for a ligand (oxalic acid), a metal (Cu), and a metal-ligand complex (Cu-Oxalate) adsorbing onto two related soils (Milford Coated, MC and Milford Uncoated, MU) containing different amounts of metal oxide coating. For the concentration range studied, oxalate revealed appreciable variability between MC and MU. Cu revealed a smaller degree of variability between MC and MU while Cu-Oxalate indicated an intermediate degree of variability. The effectiveness of an adsorbate to act as a probe of soil variability was found also to depend on the concentration of the adsorbate. Apparent soil variability increased with a higher concentration of oxalate but showed no concentration dependence for Cu. For Cu-Oxalate, variability depended on the concentration of both oxalate and Cu. At the microscale, oxalate exhibited appreciable heterogeneity in both soil samples whereas Cu adsorption on the same samples appeared to be quite homogeneous. Cu-Oxalate exhibited appreciable

---

*Accepted for publication in *Colloids and Surfaces A*

heterogeneity in MC for lower concentration of oxalic acid. For higher concentration of oxalate (1.0 mM) no appreciable heterogeneity was exhibited. Cu-Oxalate adsorption on MU was homogeneous for both oxalate concentrations. These results verify that both the macro and micro scale adsorption heterogeneity depends not only on the adsorbent but also on the nature and the total concentration of the adsorbate used to investigate the adsorption process.

2.2 Introduction

The availability and transport of solutes in the subsurface can be strongly influenced by the scale-dependent adsorption heterogeneity of the aquifer formation. Microscale adsorption heterogeneity on an oxide surface could result from differences in coordination of oxygen atoms that differ by the number and type of metal ions (*1*). Parfitt and Russell (2) used IR spectroscopy to identify three different types of OH groups on the 100 face of goethite: singly, doubly and triply coordinated oxygen, each with a distinct reactivity. Loganathan and Burau (*3*) identified two sites on MnO_2 for adsorption of Cd, Zn and Co. Guy, et al. (*4*) and Gadde and Laitenen (*5*) showed that the adsorption capacities for Cu and Pb were different from the capacities of Cd and Zn. They gave no explanation for the difference but it was later speculated to be due to more than one site type (*6*). Mesuere and Fish (*7*) found different adsorption capacities and degrees of competitive interactions for chromate and oxalate, effects that could be explained by multiple site types. Benjamin and Leckie (*6*) suggested that surfaces were composed of many groups of binding sites with their strength varying over more than an order of magnitude.

In discussing microscale heterogeneity, Barrow et al. (*8*) divided heterogeneity into lateral interaction, site defects, and domain defects. Lateral interaction is the effect of adsorption at one site on the energy of adsorption of adjacent sites. Site defects are defects such as vacancies, and domain defects are due to subcrystals or domains that fit imperfectly. The authors note that soil adsorption heterogeneity can be represented in three ways: 1) two or more uniform "subsurfaces", 2) a discrete distribution of sites with a few high affinity sites, a few lower affinity sites, a few more still lower affinity sites, and so on, and 3) a distribution function to describe a continuous range of site affinities. A fit of data to two uniform

Langmuir-type equations has been construed as an evidence of two "subsurfaces" with contrasting bonding energies (*9, 10*). Posner and Bowden (*11*), and Sposito (*12*) showed this conclusion was fallacious unless independent results could confirm the existence of contrasting bond energies. The discrete distribution approach results in Freundlich-type adsorption equation. A slope different from unity in the Freundlich equation suggests more than one adsorption site type, but this could also be due to polynuclear surface complexes (*13*).

Van Riemsdijk, et al. (*14, 15*) and Koopal and Van Riemsdijk (*16*) published detailed quantitative models for adsorption onto heterogeneous surfaces. Van Riemsdijk, et al. (*15*) compared the surface heterogeneity exhibited by metal (Cd) and proton adsorption using sensitivity analysis. Nederlof, et al. (*17*) discussed various techniques for solving the local isotherm problem to obtain affinity spectrum. Barrow, et al. (*8*) used a characteristic surface activity function (SAF) to quantify heterogeneity due to site defects. Binding strength analysis defines the range of binding site strengths for adsorption onto adsorptively heterogeneous surfaces without specifying a particular model of sorbate-sorbent interaction (*18*).

Nearly all studies of adsorption have treated heterogeneity, at least implicitly, as an intrinsic property of the surface. The need to specify an adsorbent/adsorbate pair for defining adsorption heterogeneity at a solid/liquid interface has been suggested (*19, 20*) but few experimental studies have explored this. We hypothesize that the observed magnitude of adsorption heterogeneity is due not only to the inherent properties of the adsorbent but depends also in part on the nature and concentration of the adsorbate.

Metals, ligands, and metal-ligand complexes adsorb onto metal oxide sites via distinctive mechanisms. Anions adsorb through a ligand exchange reaction favored at lower pH where the surface is positively charged and site hydration is favorable. In contrast, cations coordinate with surface oxygen atoms, a process favored at low surface protonation, i.e., at higher pH. Davis and Leckie (*21*) proposed that adsorption of metals as hydrolyzed species was more likely than complexation by bidentate surface sites. In contrast, ligands are not hydrolyzed and in this regard have fundamentally different surface species compared to

metals. Metals and anions can bind to different groups of sites (*22*). Anions often appear to adsorb to a uniform surface whereas some cations appear to react to a nonuniform surface (*8*). Metal-ligand complexes exhibit adsorption characteristics that are metal-like, ligand-like or a mixture of the two. Metal-like adsorption implies the pH dependence of the complexed metal is analogous to the uncomplexed metal. For ligand-like adsorption the pH dependence of the complexed metal is analogous to the uncomplexed ligand. The fractional adsorption of metals that form a metal-like complex can: 1) be independent of the ligand concentration, 2) decrease with increasing ligand concentration, or 3) increase with increasing ligand concentration (*23*). The fractional adsorption of metals that form a ligand-like complex exhibit a more complex pattern.

In our experiments, adsorption heterogeneity in both the micro and the macro scales has been investigated using a ligand, a metal and a metal-ligand complex as probes of the surface. Oxalic acid, our model ligand, is found both in natural and contaminated environments. Cu, our model metal, is toxic at high concentrations and has widespread industrial application. Cu*-Oxalate (Cu*-Ox, where the asterisk indicates that the complex is monitored by measuring Cu) is the model metal-ligand complex. The soil samples used for the experiments were selected from adjacent formations in a field site in Delaware.

2.3 Definitions of Adsorption Heterogeneity and Adsorption Variability

We have functionally defined *macroscale adsorption heterogeneity* as a difference in the binding properties of soils sampled at scales greater than the grain scale. In this paper we refer to macroscale adsorption heterogeneity as "variability". Adsorption variability is indicated by variation in values of adsorption parameters. The pH edges for ligands, metals, and metal-ligand complexes can be described by four parameters: 1) the pH of maximum adsorption (pH_{max}), 2) the pH of minimum adsorption (pH_{min}), 3) the maximum percentage adsorbed ($\%A_{max}$), and 4) the pH of 50% adsorption (pH_{50}). Though it is theoretically possible to identify these parameters for all pH edges, clear maxima are often hard to identify. Thus, pH_{50} has been used by researchers for comparing adsorption among different soils (*24*). This parameter is sensitive to experimental errors since it is located in the steepest portion of

the pH edge but it is a useful tool.

Comparison of pH_{50} effectively reveals a qualitative variability among the soil samples when a particular adsorbate type is used as a probe of the surface. When different adsorbate types (such as a cation and an anion) are used for probing an adsorbent, pH_{50} is not effective. This is because different adsorbate types exhibit different pH edge characteristics (anions adsorb more at lower pH whereas cations adsorb more at higher pH) and it is not always possible to conduct experiments for different adsorbate types under the same experimental conditions. For example, it is possible to conduct pH edge experiments for a wide range of radiolabeled oxalate concentrations. Cu adsorption pH edges cannot be obtained for a comparable range of concentrations because of solubility and detection limits. A Cu*-Ox pH edge is analogous to the pH edge of Cu but again it is not helpful to compare the pH_{50} of the two. In the case of Cu adsorption only the copper adsorbs to the surface while for Cu*-Ox adsorption there is an adsorption of both excess oxalate and Cu-Ox on the surface.

We have functionally defined *microscale adsorption heterogeneity* as the range of site strengths in a soil sample which otherwise is considered to have uniform properties at scales greater than the grain scale. In this paper we refer to microscale adsorption heterogeneity as simply "heterogeneity". The range of site strengths can be quantified by the range of the differential equilibrium constant $K^{(d)}$ as defined by Benjamin and Leckie (*18*). The range of log $K^{(d)}$ is a measure of heterogeneity and the difference in the range for different adsorbates indicate the degree to which heterogeneity depends on adsorbates.

2.4 Binding Strength Analysis

The Binding Strength Analysis of Benjamin and Leckie (*18*) is an effective tool for describing the microscale adsorption heterogeneity of oxide surfaces, although it gives no indication of the nature of the distribution of site affinities. The apparent overall adsorption equilibrium constant ($K_{e,o}$) is:

$$K_{e,o} = \frac{\Gamma[H^+]^x}{C} \qquad (2.1)$$

where, Γ is the adsorption density (moles of adsorbate/mole of adsorbent), C is the free ion

concentration in solution (moles/L), $[H^+]$ is the hydrogen ion concentration for metal adsorption (or the hydroxyl ion concentration for ligand adsorption), and x is the number of protons released during metal adsorption (or the number of protons consumed during ligand adsorption). $K_{e,o}$ is constant when $\Gamma < \Gamma_c$ (Γ_c is the critical value of adsorption density) and $K_{e,o}$ decreases when $\Gamma > \Gamma_c$. The overall constant can decrease only if the average equilibrium constant of the occupied sites becomes weaker. Benjamin and Leckie (*18*) defined a differential equilibrium constant $K^{(d)}$ which characterizes the interaction between the surface and the last increment of adsorbing atom. The calculated values of $K^{(d)}$ provide a measure of the entire range of individual site strengths. They showed that:

$$\log K^{(d)} = \log K_{e,o} - \log (1 - s) \qquad (2.2)$$

where, s is the slope at any point of the binding strength curve (Refer to Fig. 1, Benjamin and Leckie (*18*))

The heterogeneity revealed by this technique for an adsorbate/adsorbent system depends on the position of $\log \Gamma_c$ and the size of the surface concentration "window" (range of $\log \Gamma$). A larger value of $\log \Gamma_c$ suggests a smaller heterogeneity and vice versa. The narrower the $\log \Gamma$ window, the smaller the apparent heterogeneity and vice versa. Heterogeneity also depends on whether the window has been placed at the higher, middle, or lower sections of the $\log \Gamma$ axis. When the window is placed at the lower end of $\log \Gamma$ a small degree of heterogeneity is exhibited whereas for a window placed at the higher end of $\log \Gamma$ a higher degree of heterogeneity is exhibited. Using $\log K^{(d)}$ for comparing heterogeneity among adsorbents requires that the comparison be done over the same range of $\log \Gamma$, i.e., viewed through the same $\log \Gamma$ window.

2.5 Experimental methods

Two soil samples Milford "Coated" (MC) and Milford "Uncoated" (MU) were obtained through the Pacific Northwest Laboratory (PNL), Richland, Washington; both were collected from adjacent subsurface strata in Delaware. Powder XRD analysis of MC and MU shows their matrix to be primarily quartz. The coating on MC is primarily goethite (S. Smith, PNL, personal communication). MU has substantially less coating than MC but also contains

small amounts of magnetite. The samples were obtained in a desegregated state. These were then divided into two portions with a sample spliter and only one of the portions was used for subsequent experiments. The selected portion of the sample was passed through polypropylene sieves to a size fraction of 125-400 μm to reduce the heterogeneity due to particle size variation. Preliminary oxalate isotherms at pH 7 showed that narrower size-fraction soils resulted in isotherms that were more Langmuirian in nature whereas the wider size fractions gave isotherms that were more of the Freundlich type. This suggested that the narrower size-fraction soils were less adsorptively heterogeneous than the wider size fraction soils. Sieved samples were washed with ultrapure water (Nanopure, Barnstead, Boston, MA) to remove all easily removable fines. Sub-samples were extracted with 6 N HCl at 14°C to ascertain the total metal coating of each soil (Table 2.1). The soil samples were also extracted with ammonium oxalate (175 mM) + oxalic acid (100 mM) (NH_4-Ox) solution for 4 h to measure the "amorphous" portion of the metal oxide coating (Table 2.1).

Adsorption experiments were conducted at 14°C in polypropylene test tubes at atmospheric P_{CO2}. Polypropylene did not take up adsorbates from the solutions. The diffusion limitation was reduced by placing the test tubes in a multi-wheeled rotary mixer. Preliminary kinetic experiments showed equilibration time to be ≤ 48 hours for all samples. All experiments were conducted in a background electrolyte of 0.05 M NaCl. The solids:liquid ratio was always maintained at 1:10, with 150 mg of solid and 1.5 mL of solution.

The free drift pH edge experiments were conducted for oxalate, Cu and Cu*-Ox.

Table 2.1. Metal oxide coating on the Milford Coated (MC) and Milford Uncoated (MU) soils determined with 6 N HCl and ammonium-oxalate/oxalic acid (NH_4-Ox) extraction techniques (described in text).

Soil	Fe (mg/g) 6 N HCl	Al (mg/g) 6 N HCl	Fe (mg/g) NH_4-Ox	Al (mg/g) NH_4-Ox
MU	0.1	0.5	0.06	0.07
MC	0.75	1.3	0.2	0.1

Oxalate concentrations in the pH edge experiments were 10 μM, 50 μM, and 100 μM. The Cu pH edges were measured at 5.7 μM and 15 μM. Cu*-Ox pH edges were constructed for 8.3 μM and 38 μM Cu with 100 μM oxalate, and 27 μM and 121 μM Cu with 1 mM oxalate. All suspensions were prepared at a low initial pH. Various small amounts of NaOH solution (2-20 μL) were added to the test tubes which were then capped and placed on a multiwheeled rotary mixer. After 48 hours the pH in each test tube was measured with a glass electrode, the solution filtered through 0.05 μm filter, and the filtrate analyzed. The adsorbed amount was measured as the difference between the total added adsorbate and the concentration in solution.

Oxalate partitioning was measured with radiolabeled ^{14}C oxalate (NEN Research Products, 98.1 % purity. An aliquot of filtrate (750 μL) was added to 3 mL scintillation liquid (Ecolite, ICN Pharmaceuticals, Inc.) and the ^{14}C activity measured in a scintillation counter. Cu and Cu*-Ox were analyzed with atomic absorption spectrophotometry (AAS), using either flame or graphite furnace atomization.

2.6 Results

2.6.1 Macroscale Adsorption Heterogeneity

Cu, oxalate and Cu*-Ox revealed different degrees of macroscale adsorption heterogeneity ("variability") between MC and MU. Variability between MC and MU was qualitatively identified primarily by the difference in the pH_{50}.

2.6.1.1 Oxalic Acid. The pH_{50} values for MC and MU show differences indicating variability

Table 2.2. Oxalate pH edge adsorption characteristics for MU and MC. $\%A_{max}$, pH_{50}, pH_{min}, pH_{max} are defined in the text.

Soil	[Ox] = 100 μM				[Ox] = 50 μM				[Ox] = 10 μM			
	$\%A_{max}$	pH_{min}	pH_{50}	pH_{max}	$\%A_{max}$	pH_{min}	pH_{50}	pH_{max}	$\%A_{max}$	pH_{min}	pH_{50}	pH_{max}
MU	60%	10.2	6.4	6.0	65%	10.8	7.4	6.0	90%	10.4	8.4	6.0
MC	80%	11.0	7.6	5.6	90%	11.5	8.0	5.6	97%	11.0	8.5	5.6

between the soil samples (Table 2.2). The pH_{50} also suggests a greater adsorption for MC than for MU. The oxalate pH edges for MC and MU have pH_{max} ~ 5.6 and 6 respectively (Fig. 2.1,Table 2.2). The shift in the pH_{max} relative to the pK_a of oxalate (~4.2) is due to the predominance of Al oxides in the natural samples. Violante, et al. [25] observed oxalate adsorption on Al oxide to have a pH_{max} ~6. MC had a greater $\%A_{max}$ at the pH_{max} than MU presumably due to the greater metal oxide concentration and hence a greater adsorption capacity. The pH_{min} exhibits no appreciable difference for the soil samples. The values of $\%A_{max}$, pH_{50}, pH_{min}, and pH_{max} for 10 μM and 50 μM oxalate follow the same sequence as the 100 μM oxalate (Table 2.2).

2.6.1.2 Copper. The pH_{50} values for MC and MU show small differences indicating a variability between the soil samples (Table 2.3) but of smaller magnitude than observed with oxalate. The pH_{50} also suggests a greater adsorption for MC than MU. The pH edges for total Cu concentrations of 5.7 μM and 15 μM (Fig. 2.2) show no appreciable difference in the pH_{min} and pH_{max} for the soil samples.

2.6.1.3 Cu in the Presence of Oxalate. The pH_{50} values for MC and MU show differences suggesting a variability between the soil samples, both for 100 μM and 1 mM concentrations of total oxalate (Table 2.4). The pH_{50} values demonstrate that adsorption increased with a decrease in Cu concentration for a particular concentration of oxalate and with a decrease in the oxalate concentration. Cu*-Ox pH edges were found to exhibit metal-like characteristics with respect to overall pH dependence (Fig. 2.3 and 2.4). The pH_{min} and pH_{max} showed no appreciable difference between the two samples. Cu-Ox* (oxalate in Cu-oxalate) was also

Table 2.3. Cu pH edge adsorption characteristics for MU and MC.

Soil	[Cu] = 5.7 μM			[Cu] = 15 μM		
	pH_{min}	pH_{50}	pH_{max}	pH_{min}	pH_{50}	pH_{max}
MU	4.00	5.25	6.50	4.25	5.25	6.25
MC	4.00	4.80	6.50	4.00	4.80	6.00

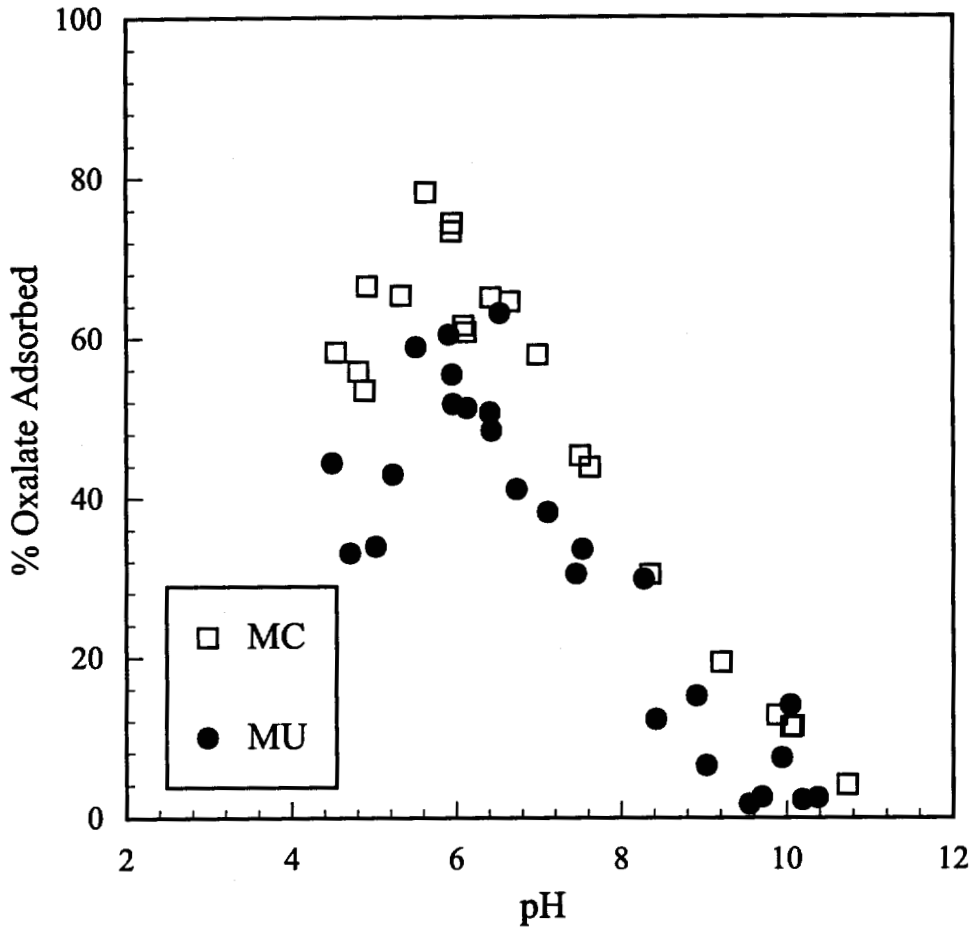

Figure 2.1. Plot of percent of oxalate adsorbed as a function of pH (pH edge) for 100 µM oxalate for Milford Coated (MC, □) and Milford Uncoated (MU, ●).

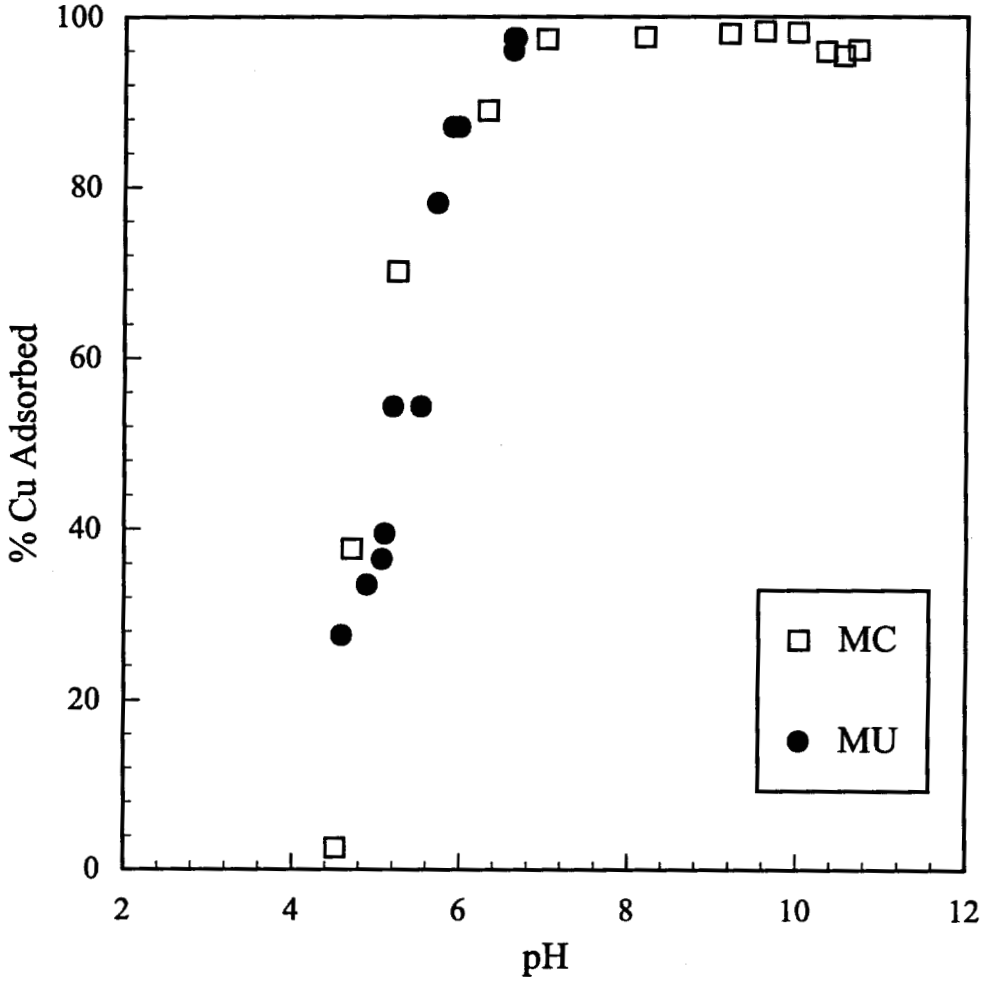

Figure 2.2. pH edge for 15 μM Total Cu for MC (□) and MU(●).

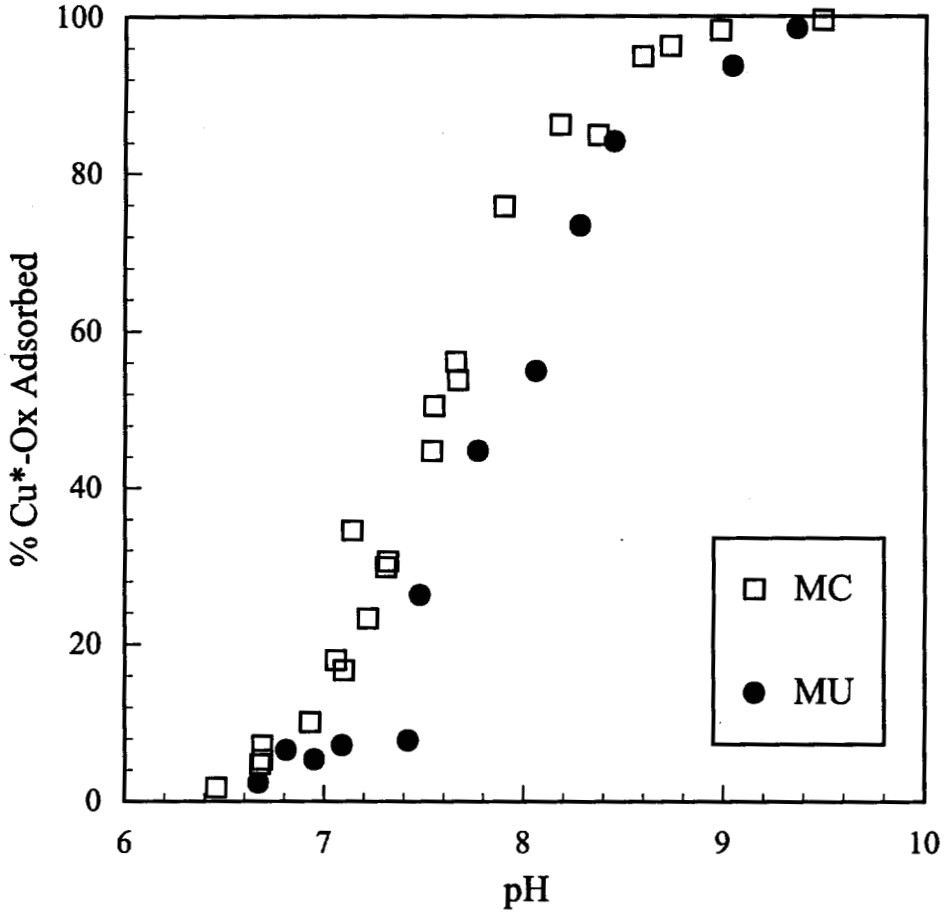

Figure 2.3. pH edge for Cu*-Ox with 1 mM oxalate and 121 μM Cu for MC (□) and MU (●).

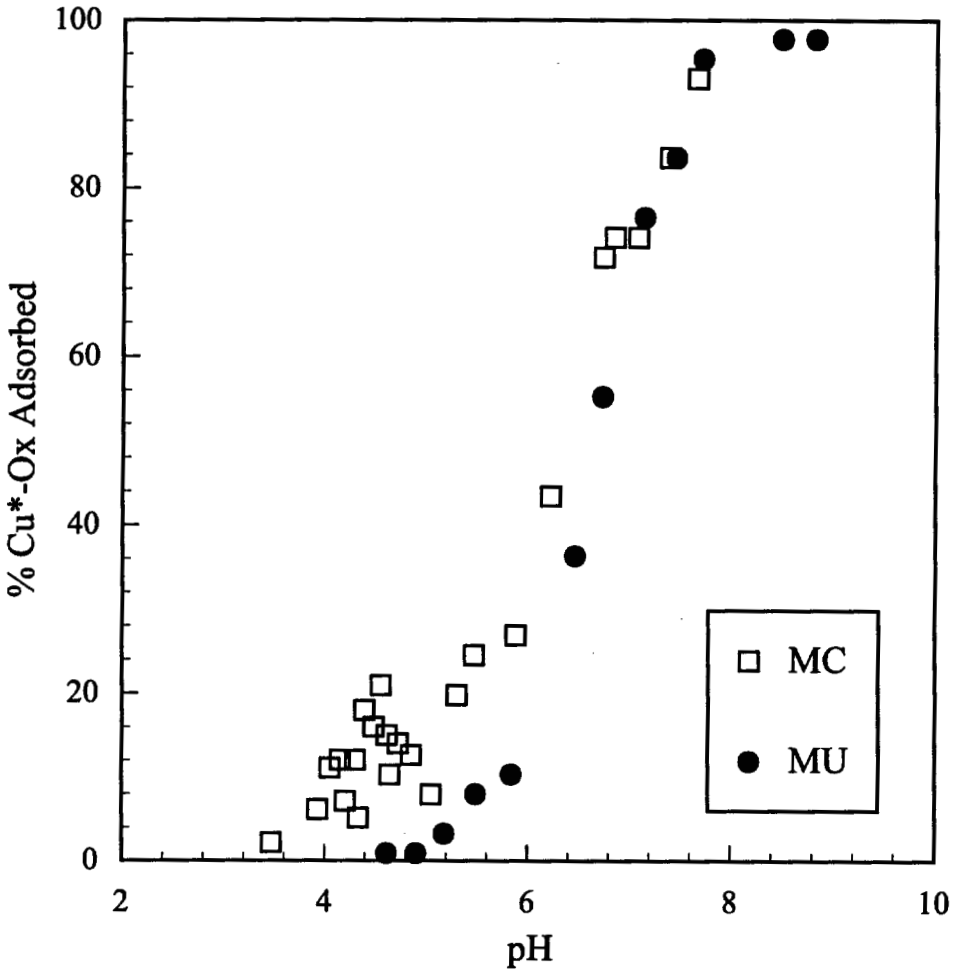

Figure 2.4. pH edge for Cu*-Ox with 100 μM and 38 μM Cu for MC (□) and MU (●).

Table 2.4. Cu*-Ox pH edge adsorption characteristics for MU and MC.

Soil	[Ox] = 1000 μM						[Ox] = 100 μM					
	[Cu] = 121 μM			[Cu] = 27 μM			[Cu] = 38 μM			[Cu] = 8.3 μM		
	pH_{min}	pH_{50}	pH_{max}	pH_{min}	pH_{50}	pH_{max}	pH_{min}	pH_{50}	pH_{max}	pH_{min}	pH_{50}	pH_{max}
MU	6.50	7.80	9.00	-	7.40	9.00	4.75	6.55	7.75	4.50	6.50	7.75
MC	6.50	7.50	9.00	-	6.80	9.00	3.50	6.40	7.50	3.50	5.60	7.25

monitored, as expected, and the relative proportion of Cu and oxalate adsorption depended on the pH and the concentration.

Solution speciation affects adsorption. Aqueous speciation calculations using MINTEQA2 show that, for the pH range of interest, the dominant aqueous oxalic acid species is $C_2O_4^{2-}$. The dominant Cu species is Cu^{2+} and the dominant Cu*-Ox species includes both CuC_2O_4 and $Cu(C_2O_4)_2^{2-}$. Surficial Fe and Al dissolve in the presence of excess oxalate. The dominant Fe and Al species in solution are: $FeC_2O_4^+$, $Fe(C_2O_4)_2^-$, $Fe(C_2O_4)_3^{3-}$, $AlC_2O_4^+$, $Al(C_2O_4)_2^-$, $Al(C_2O_4)_3^{3-}$.

2.6.2 Binding Strength Analysis of Microscale Adsorption Heterogeneity

2.6.2.1 Oxalic Acid. The BSA for oxalate (Fig. 2.5a, Table 2.5) assumes one proton is consumed for each oxalate adsorbed (i.e., x = 1). While this is not always observed over a wide pH range, it is a common assumption and is satisfactory for BSA. The pH edge data for 10 μM, 50 μM and 100 μM oxalate have been used to plot the BSA curve. MU and MC

Table 2.5. Log $K^{(d)}$ for oxalate for MU and MC.

Soil Type	log Γ_c	log $K^{(d)\ddagger}$		log $K^{(d)\dagger}$	
		Low	High	Low	High
MU	-1.6	-8.6("0.2)	-4.8("0.7)	-4.8("0.7)	-4.8("0.7)
MC	-2.7	-8.3("0.2)	-4.7("0.5)	-6.1("0.7)	-4.7("0.5)

‡ - Log $K^{(d)}$ calculated for the entire range of log Γ for which the experiment had been done. MU: (-3, -0.7), MC: (-4, -1.22)

† - Log $K^{(d)}$ calculated for log Γ over a range (-3,-2)

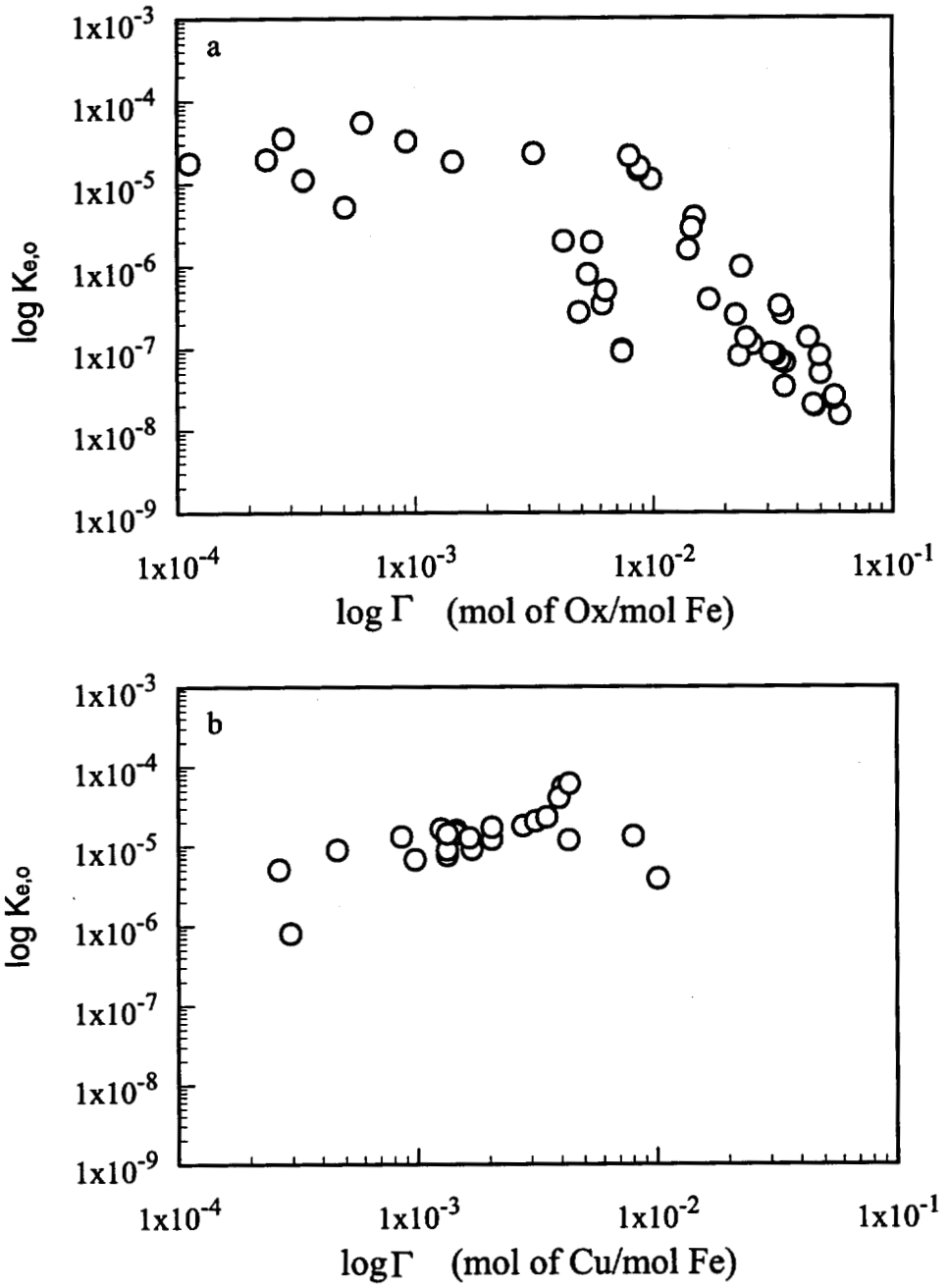

Figure 2.5. Binding Strength Analysis curves (described in the text) for a) oxalate, and b) Cu for MC. The concentration range for oxalate is 10 μM to 100 μM and the concentration range of total Cu is 5.7 μM to 15 μM.

both exhibit a wide range of log $K^{(d)}$ for oxalate varying over nearly four orders of magnitude. The critical adsorption density (log Γ_c) for MU was greater than that for MC suggesting a smaller heterogeneity for MU than MC. When MU and MC were compared for a common range of adsorption density (log Γ: [-3, -1.22]), MC exhibited notably greater heterogeneity than MU: log $K^{(d)}$ varied over 3.5 orders of magnitude for MC and over two orders of magnitude for MU.

2.6.2.2 Copper. The BSA for Cu (Fig. 2.5b, Table 2.6) assumes one proton is released for each Cu adsorbed. Again, this assumption is suitable for the BSA. Cu pH edge data for 5.7 μM and 15 μM total Cu have been used to construct the BSA curve. Log $K^{(d)}$ for MU and MC was essentially constant for the range of adsorption density studied suggesting little apparent heterogeneity in binding.

2.6.2.3 Cu in the Presence of Oxalate. The BSA for Cu*-Ox (Table 2.6) assumes one proton released for each Cu*-Ox adsorbed. This assumption was made with the rationale that Cu*-Ox adsorbs with metal-like characteristics. The pH edge data for 100 μM oxalate with 8.3 μM and 38 μM Cu and for 1 mM oxalate with 27 μM and 121 μM Cu have been used to construct BSA curves for Cu*-Ox adsorption. Cu*-Ox exhibits no appreciable heterogeneity for MU for 100 μM and 1 mM oxalate. Again, Cu*-Ox exhibits no heterogeneity for MC for the higher concentration of oxalate but for the lower concentration of oxalate it exhibits

Table 2.6. Log $K^{(d)}$ for Cu and Cu*-Ox for MU and MC.

Soil	Cu			Cu*-Ox					
				[Ox] = 1000 μM			[Ox] = 100 μM		
	log Γ_c	Low	High	log Γ_c	Low	High	log Γ_c	Low	High
MU‡	-	-5.1	-5.1	-	-7.8	-7.8	-	-6.5	-6.5
MC†	-	-5.0	-5.0	-	-7.7	-7.7	-2.8	-6.9(±0.1)	-4.8(±0.5)
								-6.5(±0.25)¶	-4.8(±0.5)¶

‡The entire range of log Γ for Cu (-3, -1). The entire range of log Γ for Cu*-Ox (-3, - 0.15)
†The entire range of log Γ for Cu (-4, -2). The entire range of log Γ for Cu*-Ox (-3, - 1.4)
¶ - Log $K^{(d)}$ calculated for MC for log Γ range (-3, -2)

heterogeneity with log $K^{(d)}$ varying over two orders of magnitude.

2.7 Discussion

Pairwise comparison of the pH_{50} of the two soils for each adsorbate under identical experimental conditions reveals that the variability among soil samples depends on the type and concentration of adsorbate (Fig. 2.6). For $Cu_T = 5.7$ μM the pH_{50} is 4.8 for MC and 5.25 for MU, reflecting a visually apparent difference in the edges for the two soils. At $Cu_T = 15$ μM, the same two pH_{50} are obtained. In contrast, the variability as revealed by pH_{50} for oxalate varies with the concentration of adsorbate. For example, MC and MU are nearly indistinguishable with 10 μM oxalate (pH_{50} = 8.5 and 8.4 respectively), but appear substantially different with 50 μM oxalate (pH_{50} = 7.4 and 8.0).

This difference in apparent variability at the macroscale can be explained by the apparent microscale heterogeneity. Cu adsorption on a given sample can be closely approximated by a homogeneous surface at the microscale. Ion partitioning to an apparently homogeneous surface is, by definition, not very sensitive to the adsorbate concentration (Fig. 2.5b). Hence, macroscale comparison of different samples on the basis of Cu adsorption are likewise insensitive to adsorbate concentrations. The concentration sensitivity of oxalate partitioning to a given sample (Fig. 2.5a) can be explained by a microscopically heterogeneous surface. Such microscale heterogeneity means that apparent macroscale variability of a subsurface formation can range from large to almost nil, depending on the amount of oxalate present.

The necessity of invoking a heterogeneous as opposed to a homogeneous surface depends on several factors besides the intrinsic heterogeneity of surface binding sites. The dependence of variability and heterogeneity on concentration is based on the surface coverage of the adsorbate and the average strength of binding. The dependence of variability and heterogeneity on the nature of the adsorbate depends on one or more of the following reasons: 1) the disparate nature of the binding of metals, ligands or metal-ligand complexes, 2) the surface coverage of the adsorbate, 3) the average strength of binding, and 4) steric effects.

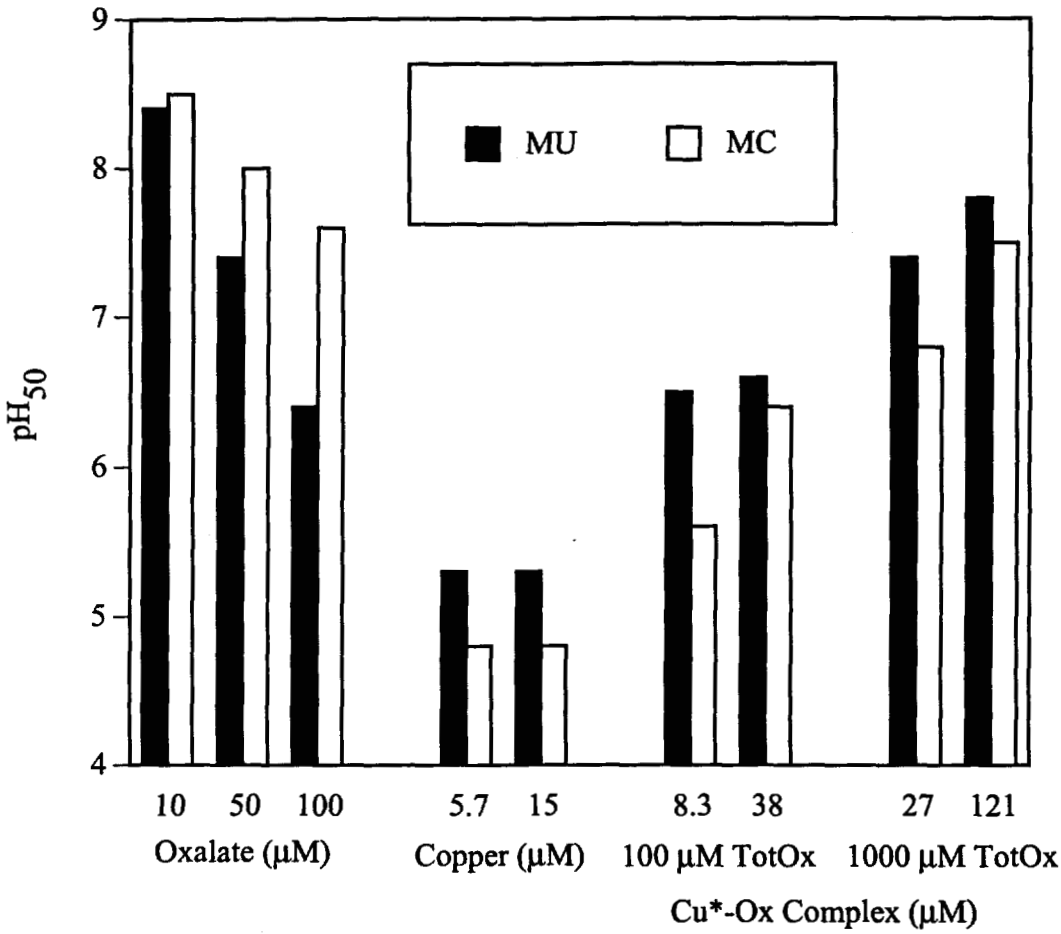

Figure 2.6. Comparison of the pH_{50} (pH of 50% adsorption) of oxalate, Cu, and Cu*-Ox for MC (light bars) and MU (dark bars)

Ions adsorb to the oxide surface as outer sphere or inner sphere complexes. An inner sphere complex signifies a direct coordination bond with a surface functional group whereas an outer sphere complex is coulombic in nature. An ion that coordinatively binds to the surface will be only partially affected by electrostatics and will be minimally susceptible to small differences in surface site density and other physical factors contributing to the site strength distribution. Ions
bound by coulombic forces will be more susceptible to the differences in site density and distribution of surface charge. Cu forms an inner sphere complex and is not a very effective probe of variability and heterogeneity. Conversely, Cu adsorption is well represented by a homogeneous surface. Oxalate forms an outer sphere complex (*26*) and is a more effective probe. Cu*-Ox complex exhibits intermediate effectiveness as a probe and probably binds to the surface with bonds that are of intermediate strength and outer sphere in nature.

The effects of surface coverage and average binding strength are interrelated. Heterogeneity is revealed only by the sites occupied by an adsorbate over the range of the edge data. At lower adsorbate concentrations nearly all sites are available over the full pH range so the adsorbate binds preferentially to the stronger sites and reveals a small heterogeneity (narrow range of binding energies). When a high concentration of adsorbate is present, most or all sites become occupied as the pH ranges from pH_{min} to pH_{max}. Strong sites will dominate near pH_{min} whereas weak sites will control the differential binding as pH_{max} is approached. These observations also can be related to the average equilibrium constant for adsorption (K^{int}), i.e., average binding strength. For lower adsorbate concentrations K^{int} is larger. At higher adsorbate concentrations both the stronger and the weaker sites are filled and a lower K^{int} is measured. If different soils have similar binding energies for their strongest sites but different ranges of binding strengths, then variability among the soils as measured by K^{int} will increase in proportion to the total adsorbate concentration.

In general, experiments with a broad span of adsorbate concentrations will reveal the greatest degree of heterogeneity regardless of the adsorbate. In our experiments, radiolabeled oxalate could be measured over more than three orders of magnitude, whereas Cu adsorption experiments were constrained to a narrower range because of analytical and solubility limits.

This practical difference explains, in part, why oxalate reveals both heterogeneity on a soil and variability among soils while Cu detects only variability and little or no heterogeneity.

Cu adsorption in mixtures of Cu and oxalate (Cu*-Ox) presents a somewhat more complicated picture than the single adsorbate experiments, but the observations fit within the general framework proposed above. Cu*-Ox reveals variability between the soil samples but reveals heterogeneity in the soil samples only at lower oxalate concentrations. Cu*-Ox adsorption was conducted in the presence of excess oxalate so the probable mechanism is that excess oxalate saturates the surface sites and Cu binds to the oxalate on the surface (≡X-Ox-Cu surface complex). When the concentration of oxalate was reduced so that the surface was no longer saturated with oxalate, the Cu could adsorb to both the oxalate on the surface and to the surface itself (≡X-Ox-Cu, ≡XO-Cu or ≡XO-Cu-Ox surface complexes). Oxalate at 1 mM saturates the metal oxide sites on both MC and MU and no heterogeneity is revealed by Cu*-Ox because the Cu encounters a purely "oxalate surface". Oxalate at 100 μM saturates the sites on MU but does not saturate the sites on MC. As a result, for lower concentrations of total oxalate Cu*-Ox reveals heterogeneity in MC (where both free and oxalate occupied sites occur) but not in MU (where only oxalate occupied sites exist).

Experiments conducted in the presence of oxalate causes dissolution of Fe and Al from the soils. This is more important for lower pH (pH < 6) conditions because dissolution decreases rapidly as pH increases. The dissolution does not affect the oxalate data presented in this paper because all the data are for pH > 6. In the case of Cu*-Ox experiments, excess oxalate induces dissolution of Fe and Al at low pH. We have estimated that the maximum Fe and Al that dissolve in the adsorption experiments was less than 10% of the total NH_4-Ox extractable Fe and Al. Under these conditions the solution concentrations of oxalate and Cu*-Ox does not change. The concentration of oxalate complexes of Fe and Al are comparable to those of Cu*-Ox complexes and probably affects the surface speciation at pH < 6. Because of the complexity of multiple adsorbing species, the full impact of Fe and Al on apparent heterogeneity is not yet known. However, such species almost certainly occur in nature and we intend to explore them in modeling studies.

Steric effects are important when several adsorbates are used to explore the

heterogeneity of an adsorbent. Larger adsorbate molecules cover more surface sites which results in an "averaging" of the surface properties over the spatial dimension of the size of the molecule. A small ion like H^+ will adsorb to each surface site whereas a larger molecule like SeO_3^{2-} will cover two to three sites (*27*). This not only diminishes the capacity of the adsorbent but also may result in smaller heterogeneity, averaged over groups of adjacent sites. Oxalate and Cu are different sizes; they could cover more than one site on the surface and the number of sites they cover may not be the same. This would cause them to exhibit a different heterogeneity and adsorption capacity between the two ions.

2.8 Conclusion

In this paper we have investigated the effect of the characteristics and concentrations of ligands, metals, and metal-ligand complexes on adsorption heterogeneity. We found that adsorbents showed different degrees of apparent adsorption heterogeneity when different adsorbates were used as probes of the surface. While oxalate is very effective in revealing variability among soils and heterogeneity in a soil, Cu exhibits a small variability among soils but no appreciable heterogeneity within each soil. Cu*-Ox exhibits an intermediate variability and heterogeneity. The results are attributed to one or more of the following: 1) differences in binding characteristics between ligands, metals and metal-ligand complexes, 2) different strength of binding, and 3) steric effects. The concentration dependence of adsorption heterogeneity can be attributed to, 1) surface coverage of an adsorbate and 2) average strength of binding. Concentration effects also influence differences among adsorbates because of practical differences in the achievable experimental concentration ranges of various adsorbates..

These results show that adsorption heterogeneity must be defined with respect to specific adsorbate/adsorbent pairs and that careful consideration must be given to the adsorbate characteristics and concentration. This complicates how one considers transport of solutes in subsurface systems that have both physical heterogeneity and chemical heterogeneity. This is further complicated by the fact that solutes are mixtures of various types of ions that are not only present as themselves but also as complexes.

2.9 References

(1) Contescu, C.; Jagiello, J. and Schwarz, J.A. *Langmuir*, **1993**, 9:1754-1765.

(2) Parfitt, R.L. and Russell, J.D. *J. Soil. Sci.*, **1977**, 28:297.

(3) Loganathan, P. and Burau, R. *Geochim. Cosmochim. Acta*, **1973**, 37:1277.

(4) Guy, R.; Chakrabarti, C. and Schramm, L. *Canad. J. Chem.*, **1975**, 53:661.

(5) Gadde, R. and Laitenen, H. *Anal. Chem.*, **1974**, 46:2022.

(6) Benjamin, M.M. and Leckie, J.O. *J. Colloid Interface Sci.*, **1981**, 79:209-221.

(7) Mesuere, K. and Fish, W. *Environ. Sci. Technol.*, **1992**, 26:2365-2370.

(8) Barrow, N.J.; Brummer, G.W. and Strauss, R. *Langmuir*, **1993**, 9:2606-2611.

(9) Holford, I.C.R.; Wedderburn, R.W.M. and Mattingly, G.E.G. *J. Soil Sci.*, **1974**, 25:242-255.

(10) Shuman, L.M. *Soil Sci. Soc. Am. Proc.*, **1975**, 39:454-458.

(11) Posner, A.M. and Bowden, J.W. *J. Soil Sci.*, **1980**, 31:1-10.

(12) Sposito, G. *Soil Sci. Soc. Am. J.*, **1982**, 46:1147-1152.

(13) Lutzenkirchen, J. and Behra, P. *Langmuir*, **1994**, 10:3916-3917.

(14) Van Riemsdijk, W.H.; Bolt, G.H.; Koopal, L.K. and Blaakmeer, J. *J. Colloid Interface Sci.*, 1986, 109:219-228.

(15) Riemsdijk, W.H.; De Wit, J.C.M.; Koopal, L.K. and Bolt, G.H. *J. Colloid Interface Sci.*, **1987**, 116:511-522.

(16) Koopal, L.K. and Van Riemsdijk, W.H. *J. Colloid Interface Sci.*, **1989**, 128:188-200.

(17) Nederlof, M.M.; Riemsdijk, W.H. and Koopal, L.K. *J. Colloid Interface Sci.*, **1990**, 135:410-426.

(18) Benjamin, M.M. and Leckie, J.O. *J. Colloid Interface Sci.*, **1981**, 83:410-419.

(19) Dabrowski, A. and Jaroniec, M. *J. Colloid Interface Sci.*, **1980**, 73:475-482.

(20) Everett, D.H. *Langmuir*, **1993**, 9:2586-2592.

(21) Davis, J.A. and Leckie, J.O. in Everett A. Jenne (Ed.), "Chemical Modeling in Aqueous Systems: Speciation, Sorption, Solubility, and Kinetics," *ACS Symposium Series, 176th Meeting of the American Chemical Society*, **1979**, 299-317, American Chemical Society, Washington, D. C.

(22) Benjamin, M.M. *Environ. Sci. Technol.*, **1983**, 17:686-692.

(23) Benjamin, M.M. and Leckie, J.O. *Environ. Sci. Technol.*, **1981**, 15:1050-1057.

(24) Ainsworth, C.C.; Girvin, D.C.; Zachara, J.M. and Smith, S.C. *Soil Sci. Soc. Am. J.*, **1989**, 53:411-417.

(25) Violante, A.; Colombo, C. and Buondonno, A. *Soil Sci. Soc. Am. J.*, **1991**, 55:65-70.

(26) Mesuere, K. and Fish, W. *Environ. Sci. Technol.*, **1992**, 26:2357-2364.

(27) Davis, J.A. and Leckie, J.O. *J. Colloid Interface Sci.*, **1980**, 74:32-43.

CHAPTER 3*

HOMOGENEOUS-SITE ADSORPTION MODELING OF METAL OXIDE COATED SUBSOILS. 1. OXALATE and COPPER

3.1 Abstract

Adsorption of oxalate and Cu onto metal oxide coated soils was modeled with three elaborations of a homogeneous-site surface complexation model (SCM): the homogeneous-site Constant Capacitance Model, the Diffuse Layer Model, and the Triple Layer Model. The adsorbents were sands naturally and artificially coated with various amounts of metal oxides. Adsorption pH edges were obtained for a single ionic strength (0.05 M NaCl) and a single solids concentration of 100 g/L using sorbate concentrations of 10, 50, and 100 μM oxalate, and 5.7 and 15 μM Cu. The adsorption models were calibrated using surface protonation properties of goethite. The adsorption pH edges for 10 and 50 μM oxalate were modeled accurately by the SCMs as were the edges for 5.7 and 15 μM Cu. We attribute the statistically poorer fits for 100 μM oxalate to heterogeneity in the adsorption energy of surface sites, evident only at high adsorbate concentrations. Site heterogeneity also caused the optimal effective surface complexation constants to be slightly different for various adsorbate concentrations. Consequently, constants optimized to a given adsorbate concentration were somewhat inaccurate when used to fit other concentrations. This was most noticeable across the wide concentration range of the oxalate edges. All models were relatively insensitive to the values of the surface protonation constants. Models were moderately sensitive to site density, with oxalate modeling more sensitive than Cu modeling.

---

*To be submitted to *Environmental Science & Technology*

3.2 Introduction

Cation and anion sorption have widespread relevance in natural systems and contaminated soils. Surface complexation modeling (SCM) is the most popular modeling approach. It treats adsorption conveniently as a chemical coordination reaction. The basic SCM has been elaborated to include representations of columbic or electrostatic forces near the surface. The most commonly used SCMs are the Constant Capacitance Model (CCM) (e.g., *1 - 11*), the Diffuse Layer Model (DLM) (e.g., *12 - 19*), and the Triple Layer Model (TLM) (e.g., 20 - 31). The inclusion of electric double layer models has also allowed modeling of interparticle interaction and electrokinetic behavior (e.g., coagulation and electrophoretic mobility, *32 - 35*).

SCMs are often used as a diagnostic tool for testing how well we understand fundamental processes at the mineral-water interface. Specific model constructs may help us relate observed phenomena to processes at the molecular scale. SCMs also are often proposed as a prognostic tool in which laboratory or limited field parameterization is used to predict chemical behavior for the range of conditions found in the environment. For all the success in representing laboratory data, SCMs have been disappointing in their fulfillment of diagnostic and prognostic goals.

SCMs have limited diagnostic ability because, ironically, they are "too successful". If properly calibrated, SCMs using any of the electric double layer models yield results that fit most chemical data (*36, 37*). We gain little insight as to which formulation most closely describes molecular scale processes. Within any particular model, we cannot find a unique parameterization that would give information about the thermodynamics of the surface reactions. For instance, the layer capacitances in TLM or CCM are not unique and bear little relationship to the actual capacitance of the surface layer.

SCMs also often fall short as a prognostic tool. They replicate laboratory data easily but cannot always predict behavior in the environment. Most experiments are done on isolated oxides and there is no method for directly extrapolating such results to predict in-situ ionic behavior on a naturally complex soil or subsoil assemblage. Soils are often modeled as some combination of isolated oxides (*38, 39*) but a priori determination of this combination

has not been demonstrated. However in some soils and aquasols, particles are coated with metal oxides (*40* and references therein), so that the surface is comparatively close to a pure oxide phase. These soils should represent the best hope for prognostic modeling based on pure-phase model parameters. Based on this rationale, sands synthetically coated with Mn- and Fe-oxides are used for studies of adsorption (*41 - 43*) and dissolution (*44*).

Adsorption onto metal oxides is modeled with either a multiple site-type formulation or a single site-type multiple surface reaction formulation (*19*). The former is generally construed to represent adsorption to a heterogeneous surface while the latter represents adsorption to a homogeneous surface. We term these two modeling approaches as the heterogeneous-site surface complexation model and the homogeneous-site surface complexation model. In fact, both multiple site and multiple reaction formulations incorporate an apparent heterogeneity because both approaches allow for a number of adjustable parameters.

The site heterogeneity of coated sands depends on the concentration of the adsorbate (demonstrated in Chapter 2). Smaller concentration of adsorbate binds to only a few sites on the surface and reveals a small heterogeneity. Larger concentration of adsorbate binds to more sites on the surface and reveals a greater heterogeneity. It is important to test if the SCMs are capable of reproducing adsorption onto materials that exhibit such concentration dependent heterogeneity.

In this chapter we focus on the homogeneous-site SCM for reproducing the adsorption of Cu and oxalate. In Chapter 5 we will focus on the use of the heterogeneous-site formulation. In this chapter we describe 1) the accuracy of SCMs in diagnosing and predicting adsorption onto somewhat heterogeneous sands naturally and artificially coated with various amounts of metal oxides, 2) the applicability of models calibrated to the acid-base properties of pure-phase metal oxides for modeling adsorption onto oxide-coated sands, and 3) the sensitivity of models of oxide-coated sands to the choice of surface protonation constants (pK_a) and site density (N_s).

We accurately reproduced moderately wide ranges of adsorbate concentrations with SCMs and that the models were insensitive to the choice of protonation constants. The

surface complexation constants obtained for individual sorbate concentrations were generally similar for different concentrations for the same sorbate but in some cases they varied significantly with concentration. As a result we were not always able to use constants for one sorbate concentration to reproduce the adsorption of another concentration of the sorbate.

3.3 Experimental methods

The three metal oxide coated sand samples, Artificially Coated (AC), Milford Coated (MC) and Milford Uncoated (MU), were obtained from the Pacific Northwest Laboratory (PNL), Richland, Washington. AC is a washed silica sand on which a coating of Fe oxyhydroxide (primarily goethite) was precipitated (*44*). Detailed description of MC and MU is presented in Section 2.5.

AC was passed through polypropylene sieves to isolate a nominal size fraction of 125-300 μm. As with MC and MU sieved samples of AC were washed with ultrapure water (Nanopure, Barnstead, Boston, MA) to eliminate most fines. HCl (6 N, 14°C) extractable Fe was determined for AC to be 1.8 mg/g of soil. The methodology for adsorption experiments is presented in Section 2.5. Free-drift pH edge experiments were conducted for a background electrolyte of 0.05 M NaCl and a solids concentration of 100 g/L. The adsorbate concentrations were maintained at oxalate concentration (Ox_T) of 10 μM, 50 μM, and 100 μM and Cu concentration (Cu_T) of 5.7 μM and 15 μM. The oxalate-induced dissolution of metal oxide coatings was monitored by measuring the Fe and Al in solution, with atomic absorption spectrophotometry (AAS), at the end of the adsorption experiment.

3.4 Model Formulation and Parameter Estimation

The goal of our modeling was to see if single-site type SCMs using protonation constants obtained for goethite or other defined phases work well for adsorption of a metal (Cu) and a ligand (oxalate) onto metal oxide coated sands over a range of pH. We optimized the effective surface complexation constant (K^{eff}) with the nonlinear fitting program FITEQL 3.1 using the default error estimates (*45*). The pH edges for different ion concentrations were modeled individually. Then, K^{eff} values obtained from modeling one sorbate concentration

Table 3.1. Parameters used for modeling adsorption of Cu and oxalate with Homogeneous-Site Surface Complexation Model (SCM), namely the Diffuse Layer Model (DLM), the Triple Layer Model (TLM), and the Constant Capacitance Model (CCM).

Parameters		DLM	TLM		CCM
			O.S[§]	I.S[¶]	
Site density (N_s), sites/nm^2 Oxalate:	AC	0.30	3.01	0.36	0.60
	MC	0.40	10.03	0.40	0.20
	MU	0.30	6.02	0.30	0.30
Specific surface area (g/m^2)	AC	10	10		10
	MC	3	3		3
	MU	2	2		2
Solid : Solution (g/L)		100	100		100
Inner-layer capacitance (C_1) F/m^2			0.8		1.06
Outer-layer capacitance (C_2) F/m^2			0.2		

[§]Outer Sphere Complex, Oxalate only
[¶]Inner Sphere Complex, Cu only

were used to reproduce adsorption edges for other sorbate concentrations. This extrapolation was performed with MINTEQA2, which gave results identical to the fits obtained with FITEQL 3.1. We used the same equilibrium constants for aqueous reactions while modeling with FITEQL and MINTEQA2.

In FITEQL 3.1 the goodness of fit is given by the overall variance (V_Y) which is calculated as the weighted sum of squares of residuals divided by the degrees of freedom. Value of V_Y between 0.1 and 20 indicate a good fit (*19*). $V_Y > 20$ suggests that the model is inappropriate and a $V_Y < 0.1$ suggests too many adjustable parameters.

The parameters needed for surface complexation modeling are the solids concentration, the specific surface area, the N_s, and, for the CCM and TLM, the capacitances for the assumed planes. The specific values for these parameters are listed in Table 3.1. The surface area was estimated from those obtained at PNL (*46*) which is satisfactory for

demonstrating the effectiveness of SCMs. Mesuere and Fish (*17*) suggest three criteria for obtaining good estimates of N_s: 1) optimal for modeling acid-base titration data for the sorbent, 2) falls within the range of independently determined N_s values, and 3) exceeds the maximum adsorption density (Γ_{max}) of the sorbates.

Soils are mineralogically complex and their surface chemical properties are difficult to characterize (*47*). Acid-base equilibration in a titration of a natural soil requires hours to days, during which dissolution of metal oxides can skew solution and surface speciation in ways that are almost impossible to predict. Additionally, acid-base titration of sand-size soil samples cannot be performed accurately with classical potentiometric techniques because of the small specific surface area (*48*). There is no database from which to infer an acceptable range of N_s for soils and N_s values smaller than those obtained for metal oxides have been used for modeling adsorption onto soils (*39*).

Due to these practical limitations we chose the third option of Mesuere and Fish (*17*) in which the oxalate isotherm at pH 7 (not shown here) is used to determine Γ_{max}, since no dissolution occurs at this pH. N_s is calculated using: $N_s = a\Gamma_{max} / SA$, where, a is the Avogadro number, S is the solids concentration (g/L), and A is the specific surface area (m^2/g). As a further check on the validity of this N_s, FITEQL 3.1 was applied to the overall data set for all edges for a sorbate, assuming a wide range of N_s. The N_s that gave the minimum V_Y should be greater than or equal to N_s obtained from the equation above.

The modeling criterion was the ability to consistently model adsorption over a wide range of concentration with the minimum number of uniquely defined surface species. We assumed for all models that the surface species have 1 : 1 (site : sorbate) stoichiometries (*17, 19*). A three-state, amphiprotic surface site $\equiv XO^-$, $\equiv XOH^o$, and $\equiv XOH^{2+}$ was assumed for all modeling. Because of the experimental problems noted above in the discussion of N_s, pK_a's for natural soils are difficult to obtain experimentally. Consequently, we used pK_a's fitted to goethite titration data for most of our modeling. The pK_a values used for modeling are presented in Table 3.2. Some modeling was done with pK_a's measured for other metal oxides to test the sensitivity of SCMs to the choice of pK_a.

Oxalate was assumed to adsorb via ligand exchange with surface hydroxyl groups.

Table 3.2. Equilibrium expressions and equilibrium constants for surface protonation and the electrolyte binding reactions used for modeling Cu and oxalate adsorption with the SCMs.

Equilibrium expression	Model	log K
$[\equiv XOH_2^+] = [\equiv XOH^o]\{H^+\}\exp(-F\psi_o/RT)(K_{a1})^{-1}$	DLM	-7.9[¶]
	TLM	-8.3[¥]
	CCM	-7.9[†]
$[\equiv XO^-] = [\equiv XOH^o]\{H^+\}^{-1}\exp(F\psi_o/RT)K_{a2}$	DLM	-10.02[¶]
	TLM	-10.30[¥]
	CCM	-10.02[†]
$[\equiv XOH_2^+ - Cl^-] = [\equiv XOH^o]\{H^+\}\{Cl^-\}\exp(F(\psi_\beta - \psi_o)/RT)K_{Cl-}$	TLM	9.2[‡]
$[\equiv XO^- - Na^+] = [\equiv XOH^o]\{H^+\}^{-1}\{Na^+\}\exp(F(\psi_o-\psi_\beta)/RT)K_{Na+}$	TLM	-9.2[‡]

[¶]Van Geen et al. (*50*)
[¥]Mesuere and Fish (*17*)
[†]assumed to be the same as the DLM hydrolysis constants from Van Geen et al. (*50*)
[‡]assumed to be the same as the electrolyte reaction constants in Mesuere and Fish (*17*)
{ } activity

The oxalate surface species used in the DLM and CCM were $\equiv XC_2O_4H^o$, $\equiv XC_2O_4^-$, and a physically unrealistic species, $\equiv XOC_2O_4^{3-}$. Although $\equiv XC_2O_4H^o$, and $XC_2O_4^-$ alone reproduce the low pH points of the edge, $\equiv XOC_2O_4^{3-}$ is needed to predict adsorption at pH > 7 (see Fig 1c in *17*). The outer-sphere oxalate species in the TLM were $\equiv XOH_2^+ - C_2O_4^{2-}$ and $\equiv XOH_2^+ - HC_2O_4^-$. All the oxalate species used here are the same as those used by Mesuere and Fish (*17*) to model oxalate adsorption onto goethite. Cu was assumed to adsorb via an inner-sphere complex between Cu and the surface oxide group ($\equiv XOCu^+$) (*19, 51, 52*). Cu was also modeled in the TLM as a possible outer-sphere complex ($\equiv XO^- - Cu^+$). A summary of the surface complexation reactions used in the modeling is presented in Table 3.3. Ion activities were corrected with the Davies equation and in accordance with the FITEQL 3.1 user manual (*45*).

Table 3.3. Equilibrium expressions and corresponding surface complexation reactions used for modeling adsorption of Cu and oxalate.

Equilibrium expressions	log K[a]
$\{H_2C_2O_4\} = \{C_2O_4^{2-}\}\{H^+\}^2K_{ox1}$	5.52[¶]
$\{HC_2O_4^-\} = \{C_2O_4^{2-}\}\{H^+\}K_{ox2}$	4.27[¶]
$\{FeC_2O_4^+\} = \{Fe^{3+}\}\{C_2O_4^{2-}\}K_{FeOx1}$	7.58[§]
$\{Fe(C_2O_4^{2-})_2^-\} = \{Fe^{3+}\}\{C_2O_4^{2-}\}^2K_{FeOx2}$	13.81[§]
$\{Fe(C_2O_4^{2-})_3^{3-}\} = \{Fe^{3+}\}\{C_2O_4^{2-}\}^3K_{FeOx3}$	18.60[§]
$\{AlC_2O_4^+\} = \{Al^{3+}\}\{C_2O_4^{2-}\}K_{AlOx1}$	6.10[§]
$\{Al(C_2O_4^{2-})_2^-\} = \{Al^{3+}\}\{C_2O_4^{2-}\}^2K_{AlOx2}$	11.09[§]
$\{Al(C_2O_4^{2-})_3^{3-}\} = \{Al^{3+}\}\{C_2O_4^{2-}\}^3K_{AlOx3}$	15.12[§]
[a] T = 25°C and I = 0 M	

Surface Complexation Reactions	Model
Oxalate	
$[\equiv XC_2O_4H^o] = [\equiv XOH^o]\{C_2O_4^{2-}\}\{H^+\}^2K_{XOx1}$	DLM, CCM[‡]
$[\equiv XC_2O_4^-] = [\equiv XOH^o]\{C_2O_4^{2-}\}\{H^+\}\exp(F\psi_o/RT)K_{XOx2}$	DLM, CCM[‡]
$[\equiv XOC_2O_4^{3-}] = [\equiv XOH^o]\{C_2O_4^{2-}\}\{H^+\}^{-1}\exp(3F\psi_o/RT)K_{XOx3}$	DLM, CCM[‡]
$[\equiv XOH_2^+ - C_2O_4^{2-}] = [\equiv XOH^o]\{C_2O_4^{2-}\}\{H^+\}\exp(F(2\psi_\beta-\psi_o)/RT)K_{XOx4}$	TLM[†]
$[\equiv XOH_2^+ - HC_2O_4^-] = [\equiv XOH^o]\{C_2O_4^{2-}\}\{H^+\}^2\exp(F(\psi_\beta-\psi_o)/RT)K_{XOx5}$	TLM[†]
Copper	
$[\equiv XOCu^+] = [\equiv XOH^o][Cu^{2+}]\{H^+\}^{-1}\exp(-F\psi_o/RT)K_{XOCu1}$	DLM,CCM,TLM[‡]
$[\equiv XO^- - Cu^{2+}] = [\equiv XOH^o]\{H^+\}^{-1}\{Cu^{2+}\}\exp(F(\psi_o-2\psi_\beta)/RT)K_{XOCu2}$	TLM[†]

[¶]Mesuere and Fish (*17*), [§]Smith and Martell (*49*)
[‡]Inner sphere complex, [†]Outer sphere complex, { } activity

3.5 Results

3.5.1 Experimental Results

The pH edges for Ox_T = 10, 50, and 100 μM, on all materials, were typical of anions (e.g., AC data shown in Fig. 3.1, Table 3.4). Adsorption diminished with rising pH but in some cases 15 - 20 % oxalate remained adsorbed at pH 10. Oxalate adsorption onto AC resembled adsorption onto goethite (*17*). Essentially 100% of the oxalate was adsorbed for pH < 6.5. The percent adsorption of 10 μM oxalate onto AC drops steeply for pH > 7. Higher concentrations of oxalate (50 and 100 μM) show "broader" edges: proportionally less binding at pH 7 and proportionally more at pH 10.

MC and MU differ from AC in that their coatings contain significant amounts of Al which dissolves at low pH. Unlike the results for AC, oxalate adsorption onto the naturally coated MC and MU has a relatively narrow maximum and declines for pH < 5.5 (Figure 3.2). This decline occurs at pH values above the pK_{a2} of oxalic acid (≈ 4.2) which typically corresponds to pH of maximum adsorption (pH_{max}). A decline in oxalate adsorption below pH 6 is also reported for Al_2O_3 (*53*). Significant surficial Al dissolved during adsorption and the resulting Al-oxalate species in solution may explain the results. MC and MU differ from AC by showing distinct saturation effects. As with AC, the relative proportion of oxalate adsorption on MC and MU at pH < 7 declines with increasing Ox_T.

The pH edges for Cu_T = 5.7 and 15 μM, were characteristic of cations: adsorption

Table 3.4. Oxalate pH edge adsorption characteristics for AC, MU and MC given as the maximum percent adsorbed ($\%A_{max}$), the pH of maximum adsorption (pH_{max}), the pH of 50% adsorption (pH_{50}), and the pH of minimum adsorption (pH_{min}).

Soil	[Ox] = 100 μM				[Ox] = 50 μM				[Ox] = 10 μM			
	$\%A_{max}$	pH_{min}	pH_{50}	pH_{max}	$\%A_{max}$	pH_{min}	pH_{50}	pH_{max}	$\%A_{max}$	pH_{min}	pH_{50}	pH_{max}
AC	100%	10.5	8.6	4.0	100%	11.5	9.1	4.0	100%	11.0	8.9	4.0
MU	60%	10.2	6.4	6.0	65%	10.8	7.4	6.0	90%	10.4	8.4	6.0
MC	80%	11.0	7.6	5.6	90%	11.5	8.0	5.6	97%	11.0	8.5	5.6

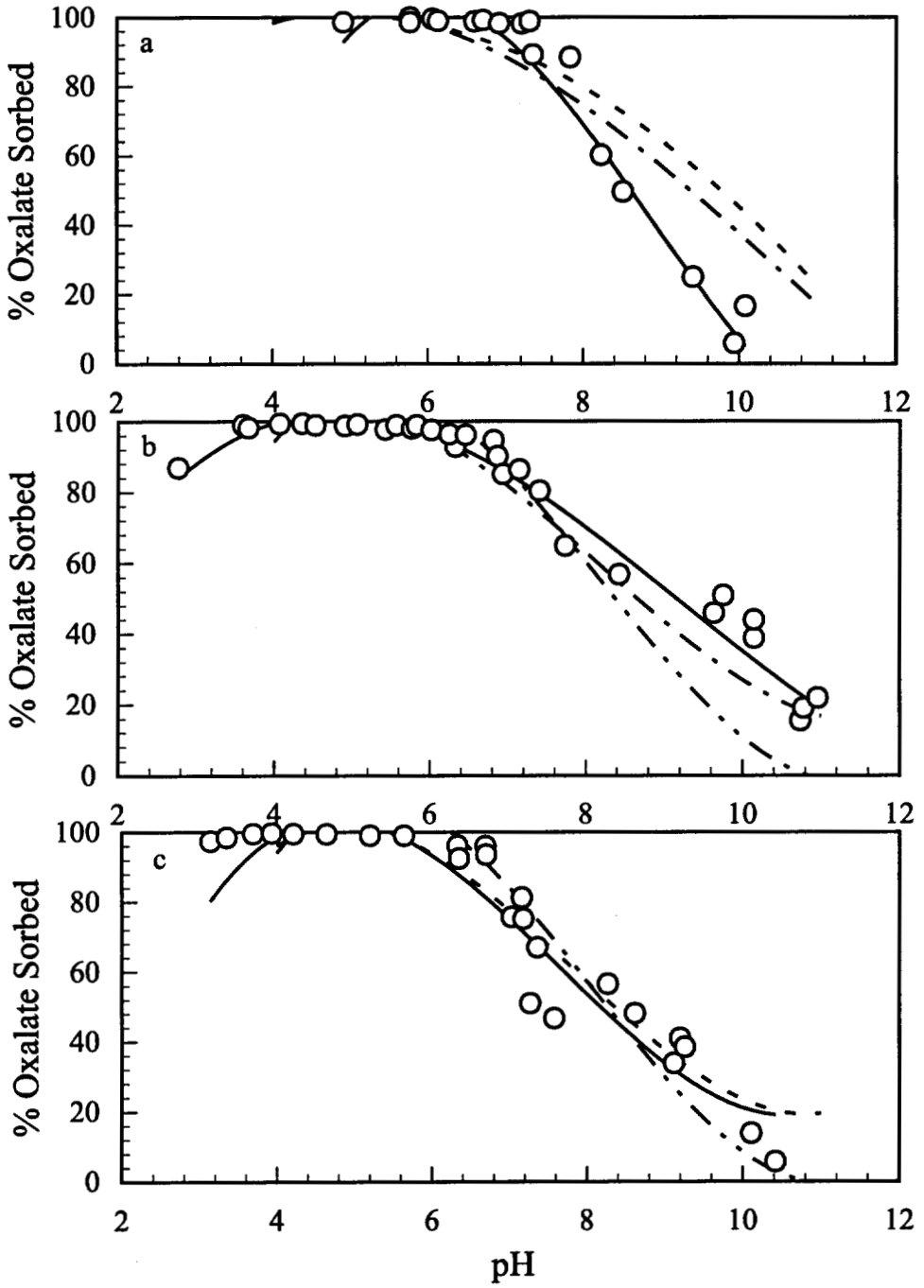

Figure 3.1. DLM fits for adsorption of a) 10, b) 50, and c) 100 μM oxalate onto AC. The FITEQL fits for the data is shown as ——— . The dashed lines are prediction of oxalate adsorption based on effective adsorption constants for 10 μM oxalate (— · · · —), 50 μM oxalate (- - - -), and 100 μM oxalate (— · —).

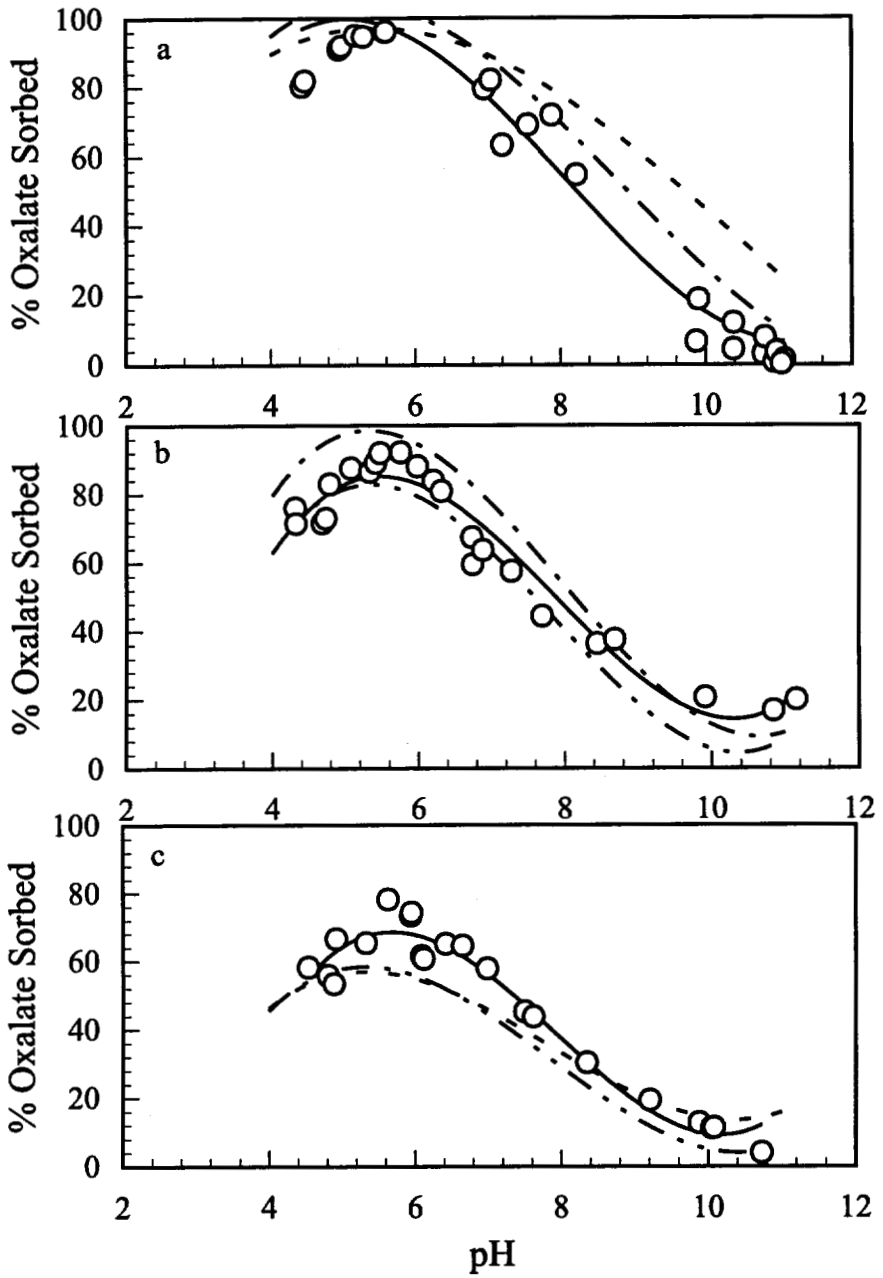

Figure 3.2. DLM fits for adsorption of a) 10, b) 50, and c) 100 μM oxalate onto MC. The FITEQL fits for the data is shown as ——— . The dashed lines are prediction of oxalate adsorption based on effective adsorption constants for 10 μM oxalate (— · · —), 50 μM oxalate (- - - -), and 100 μM oxalate (— · —).

Table 3.5. Cu pH edge characterized by pH_{min}, pH_{50}, and pH_{max} for AC, MC, and MU.

Soil	[Cu] = 5.7 μM			[Cu] = 15 μM		
	pH_{min}	pH_{50}	pH_{max}	pH_{min}	pH_{50}	pH_{max}
AC	3.50	4.55	5.50	3.00	4.75	6.00
MU	4.00	5.25	6.50	4.25	5.25	6.25
MC	4.00	4.80	6.50	4.00	4.80	6.00

was negligible at pH ≤ 4 but increased sharply and reached essentially 100% above pH 5.5 (illustrated in Fig. 3.3 and Table 3.5). Cu edges onto AC, MC, and MU are similar to those for goethite and hydrous ferric oxide. For AC, increasing Cu_T from 5.7 to 15 μM had little effect on the relative proportion of Cu bound as a function of pH, indicating that site saturation was not approached in the Cu experiments.

The pH at 50% adsorption (pH_{50}) obtained from an adsorption edge is a convenient qualitative measure of the affinity of a surface for an ion. For anions, pH_{50} increases with the overall binding affinity, while for cations, pH_{50} drops as binding affinity rises. Values of pH_{50} for oxalate and Cu show that adsorption affinity follows the sequence AC > MC > MU (Tables 3.4 and 3.5). As expected and as shown in Figure 3.4, values of pH_{50}, i.e., overall affinity, correlated with the 6 N HCl extractable portion of the surficial Fe.

3.5.2 Modeling Results

3.5.2.1 Modeling Adsorption of Oxalate onto AC

Edges for Ox_T = 10 μM and 50 μM (Fig 3.1a, b), were adequately modeled by DLM and CCM, (V_Y < 20; Fig. 3.5 and Table 3.6). These models somewhat accurately reproduced Ox_T = 100 μM but gave a larger V_Y (Fig. 3.5), slightly overpredicting the adsorption at pH > 9 (Fig. 3.1c). The pH edge was modeled adequately with $\equiv XC_2O_4^-$ and $\equiv XOC_2O_4^{3-}$. Despite its use in previous studies (*17*) $\equiv XC_2O_4H^o$ was unnecessary for pH 4 to 12.

TLM results (in Fig. 3.5 Table 3.6) were similar to those of DLM and CCM. Although the pH edges for 10 and 50 μM oxalate were accurately modeled, the pH edge for 100 μM oxalate gave statistically poorer fit (V_Y > 20). The fit slightly overpredicted

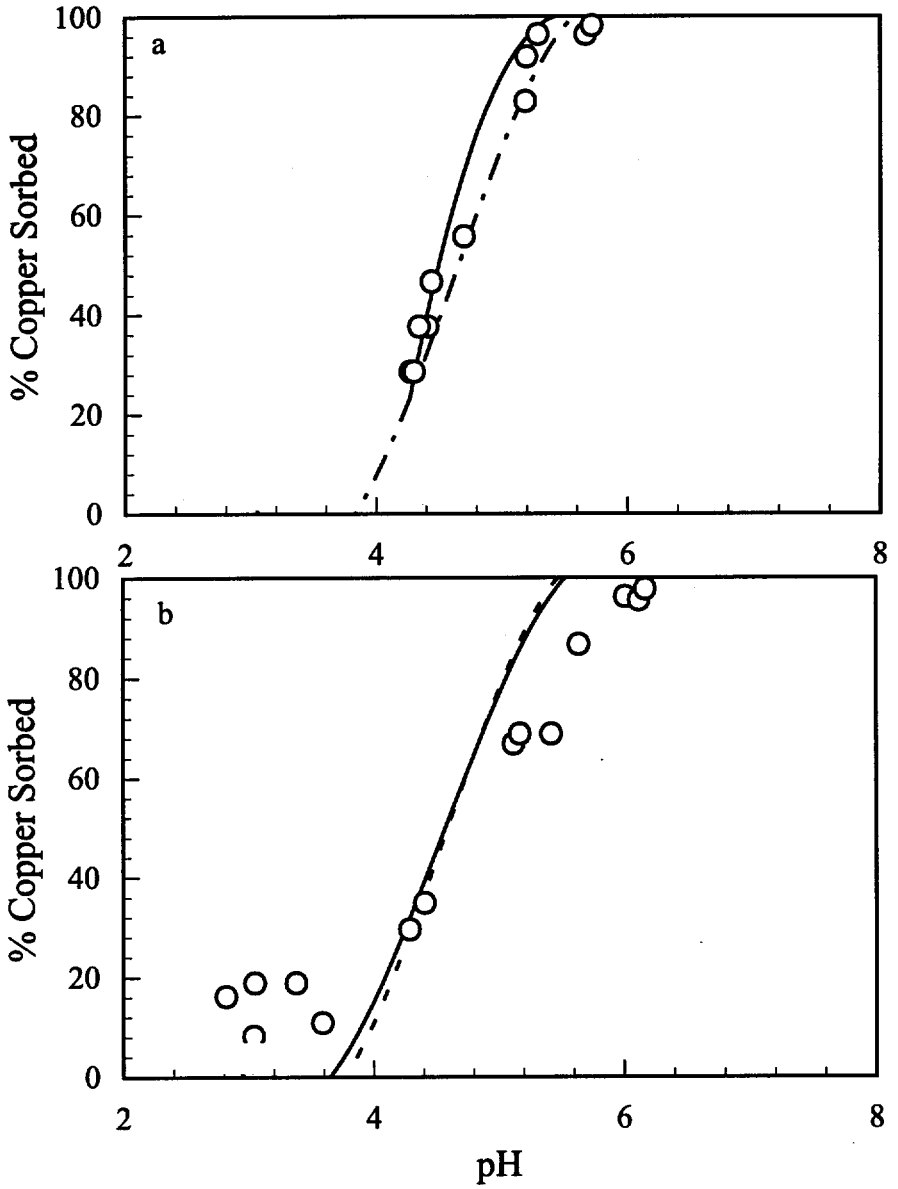

Figure 3.3. DLM fits for adsorption of a) 5.7, b) 15 μM Cu onto AC. The FITEQL fits for the data is shown as ——— . The dashed lines are prediction of oxalate adsorption based on effective adsorption constants for 5.7 μM Cu (- - - ·), and 15 μM Cu (— - —).

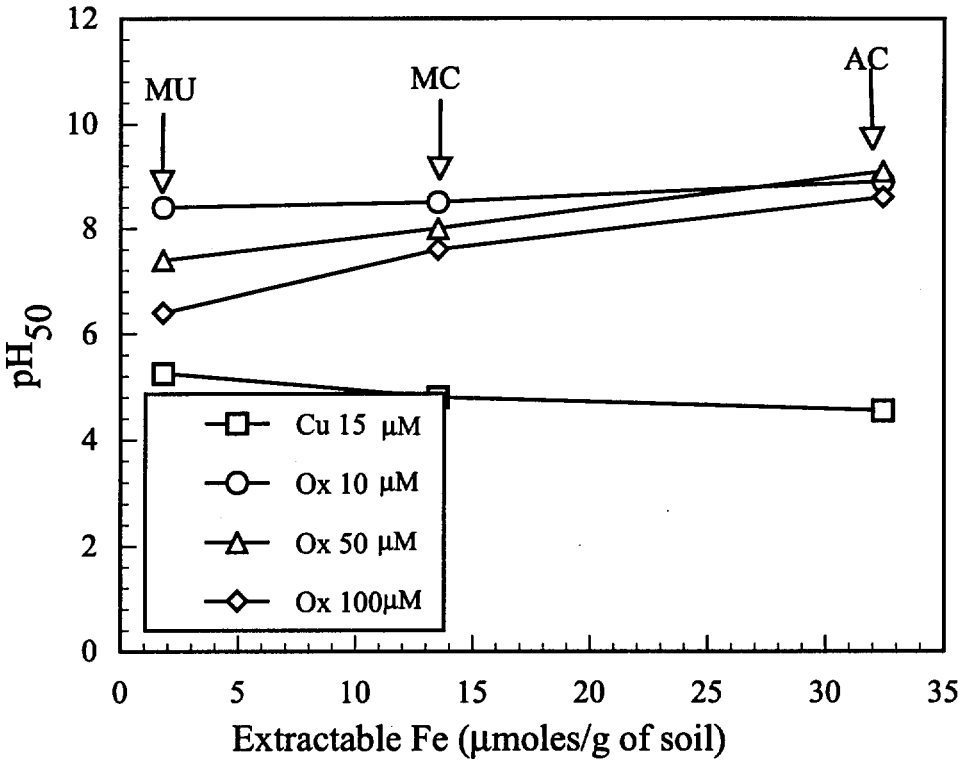

Figure 3.4. Relationship between pH_{50} (pH of 50% adsorption) and the 6 N HCl extractable Fe for AC, MC, and MU.

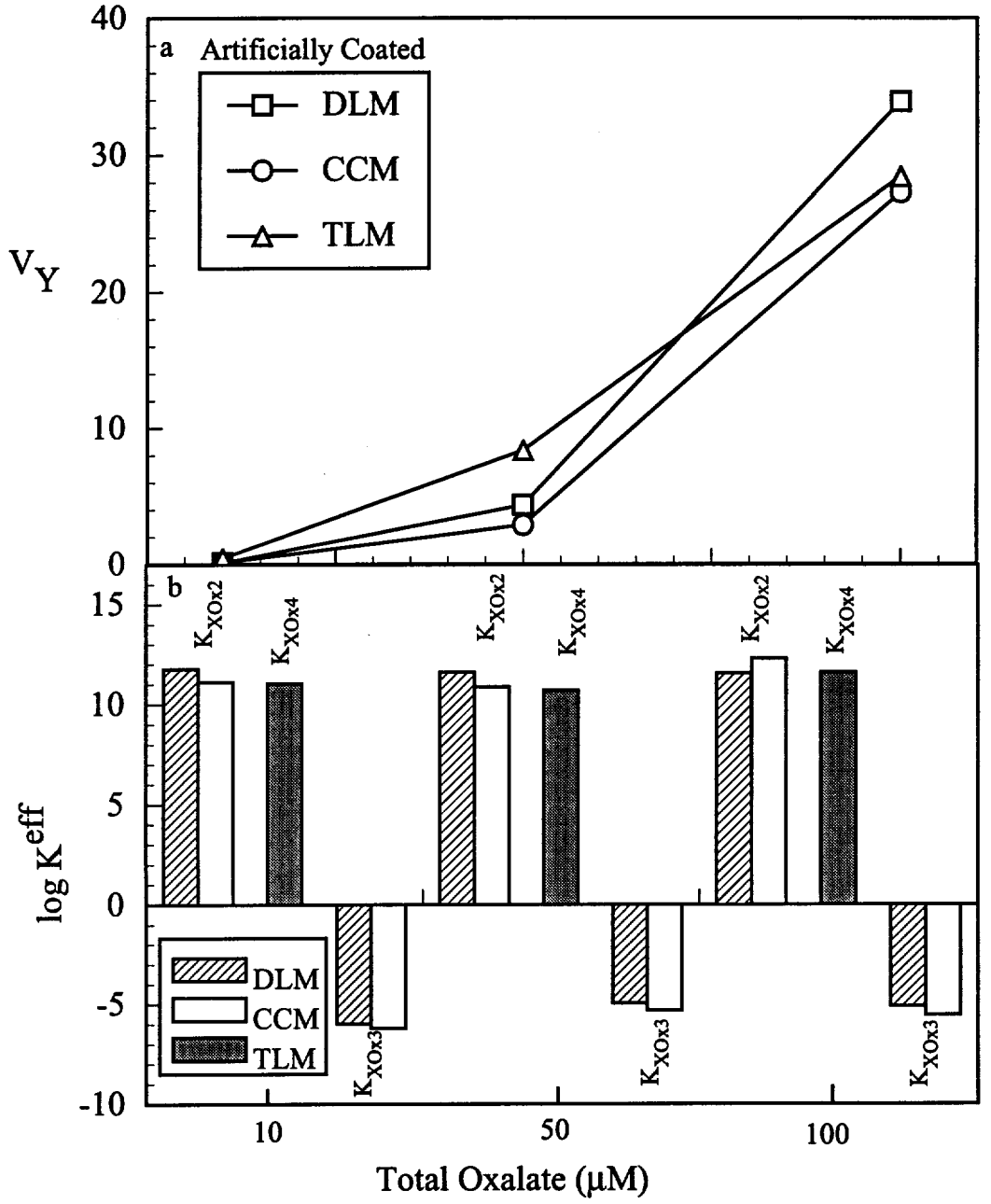

Figure 3.5. Variation in the a) goodness of fit (V_Y) and b) effective surface complexation constants (K^{eff}) for DLM, CCM, and TLM, and oxalate concentrations of 10, 50, and 100 μM for the Artificially Coated Sample. K_{XOx2}, and K_{XOx3} are the two species in DLM and CCM while K_{XOx4} is for TLM.

adsorption for pH 6 - 8 but accurately predicted adsorption for pH > 8. The surface species $\equiv XOH_2^+ - C_2O_4^{2-}$ alone was adequate for pH 4 - 12; $\equiv XOH_2^+ - HC_2O_4^-$ added no improvement to the values of V_Y in the model fits.

We used MINTEQA2 with equilibrium reaction constants listed in Table 3.2 to reproduce the adsorption pH edges for various Ox_T using K^{eff} optimized by FITEQL 3.1 to a single value of Ox_T. As illustrated in Figure 3.1a, the K^{eff} for Ox_T = 50 μM and 100 μM slightly underpredicted the adsorption of Ox_T = 10 μM at pH < 7 but overpredicted adsorption for pH > 8. For Ox_T = 50 μM, K^{eff} for Ox_T = 10 μM underpredicted adsorption for pH > 8 but K^{eff} for Ox_T = 100 μM oxalate closely predicted adsorption (see Fig. 3.1b). The data for 100 μM Ox_T were represented almost equally well by constants for any concentration. Thus, extrapolating from low to high concentration of oxalate worked well but extrapolation from high to low concentrations was less satisfactory, at least for pH > 8.

3.5.2.2 Modeling Oxalate on MC or MU

The adsorption of oxalate onto MC and MU was modeled in two steps. The first was

Table 3.6. Effective surface complexation constants and the goodness of fit for the adsorption of 10 μM, 50 μM, and 100 μM oxalate onto AC with DLM, CCM, and TLM.

Model	[Ox] μM	V_Y	log K_{XOx2}	log K_{XOx3}	log K_{XOx4}
DLM	100	33.9	11.03±0.02	-5.11±0.02	
	50	4.35	11.1±0.07	-4.96±0.02	
	10	0.13	11.76±0.21	-5.99±0.26	
CCM	100	27.29	10.68±0.02	-5.55±0.01	
	50	2.89	10.86±0.07	-5.33±0.02	
	10	0.12	11.59±0.18	-6.21±0.25	
TLM	100	28.43			11.60±0.01
	50	8.36			12.29±0.02
	10	0.44			11.53±0.11

to model the pH edge for data at pH > 6 where dissolution of surface coatings was unimportant. The second was to model the entire pH edge by using the data for Al dissolution and including reactions for formation of Al-oxalate complexes in solution. The first step optimized N_s, which was then used to model the entire pH edge. We modeled adsorption without including readsorption of Al-oxalate because it is not a dominant process. Fe dissolution was not included because of the low solubility of Fe (its observed concentration was more than an order of magnitude smaller than Al).

Oxalate adsorption onto MC (Fig. 3.2) and MU was modeled with DLM and CCM using the surface species $\equiv XC_2O_4^-$ and $\equiv XOC_2O_4^{3-}$ for pH > 6. The results of the fitting procedure is listed in Table 3.7. The adsorption of Ox_T = 10 and 50 μM were accurately modeled. For Ox_T = 100 μM, the fit was accurate but V_Y was larger. For the entire pH range (pH 4 - 11) modeling adsorption of Ox_T = 100 μM with DLM gave $V_Y < 20$. In all other case fits was statistically poorer with $V_Y > 20$ (shown in Fig. 3.6 and 3.7, and Table 3.7). The adsorption of Ox_T = 10 μM was somewhat overpredicted at pH < 6 probably because of the large errors in data for low concentrations of dissolved Al (Fig. 3.2c). The optimal values of log K^{eff} did not vary appreciably with Ox_T. The goodness of fit was statistically better at low Ox_T than at high Ox_T but most of the difference in V_Y can be attributed to larger absolute errors in the higher concentration data.

Modeling with TLM showed trends very similar to those observed for DLM and CCM. Although the adsorption of oxalate was modeled accurately, the fit for Ox_T = 100 μM was statistically poorer and gave $V_Y > 20$ (as shown in Fig. 3.6 and 3.7, and Table 3.8). The entire edge (pH 4 - 11) was modeled by including dissolution of Al and its aqueous complexation with oxalate. The results were nearly the same as those obtained with DLM and CCM (Table 3.8).

Attempts to reproduce adsorption of various Ox_T with K^{eff}, a single value optimized to one Ox_T, exhibited trends similar to that observed for AC. As shown in Fig. 3.2, K^{eff} for Ox_T = 50 μM and 100 μM overpredicted the adsorption of Ox_T = 10 μM. K^{eff} for Ox_T = 10 μM underpredicted adsorption of 50 μM for pH > 8 whereas K^{eff} for Ox_T = 100 μM overpredicted adsorption for pH < 8. The adsorption of Ox_T = 100 μM was closely modeled

Table 3.7. Effective surface complexation constants and the goodness of fit for adsorption of 10 μM, 50 μM, and 100 μM oxalate onto MC and MU with DLM and CCM.

Model	[Ox] μM	Condition	V_Y	log K_{Ox2}	log K_{Ox3}
DLM, MC	100	pH > 6	50.04	11.53±0.03	-4.26±0.04
		All Points	11.26	11.87±0.02	-4.72±0.04
	50	pH > 6	3.21	11.04±0.04	-4.26±0.04
		All Points	4.72	11.21±0.03	-4.27±0.05
	10	pH > 6	0.59	11.45±0.25	-5.06±0.15
		All Points	0.53	11.21±0.26	-5.00±0.14
CCM, MC	100	pH > 6	41.01	12.91±0.02	-4.98±0.04
		All Points	47.03	13.64±0.02	-5.73±0.06
	50	pH > 6	11.21	12.66±0.03	-5.10±0.05
		All Points	20.35	13.19±0.02	-5.17±0.06
	10	pH > 6	0.46	12.63±0.13	-5.98±0.25
		All Points	0.31	12.61±0.11	-5.98±0.26
DLM, MU	100	pH > 6	23.98	12.43±0.03	-5.29±0.07
		All Points	27.68	12.59±0.02	-5.61±0.07
	50	pH > 6	12.67	11.83±0.03	-4.39±0.06
		All Points	9.45	11.89±0.03	-4.32±0.06
	10	pH > 6	1.11	12.41±0.08	-5.20±0.20
		All Points	3.26	10.78±0.08	-4.28±0.07
CCM, MU	100	pH > 6	24.26	12.46±0.02	-5.82±0.06
		All Points	30.97	12.67±0.02	-6.08±0.06
	50	pH > 6	14.69	12.18±0.03	-5.05±0.05
		All Points	10.03	12.37±0.02	-5.02±0.06
	10	pH > 6	0.96	12.63±0.07	-5.88±0.40
		All Points	2.28	12.50±0.07	-5.72±0.30

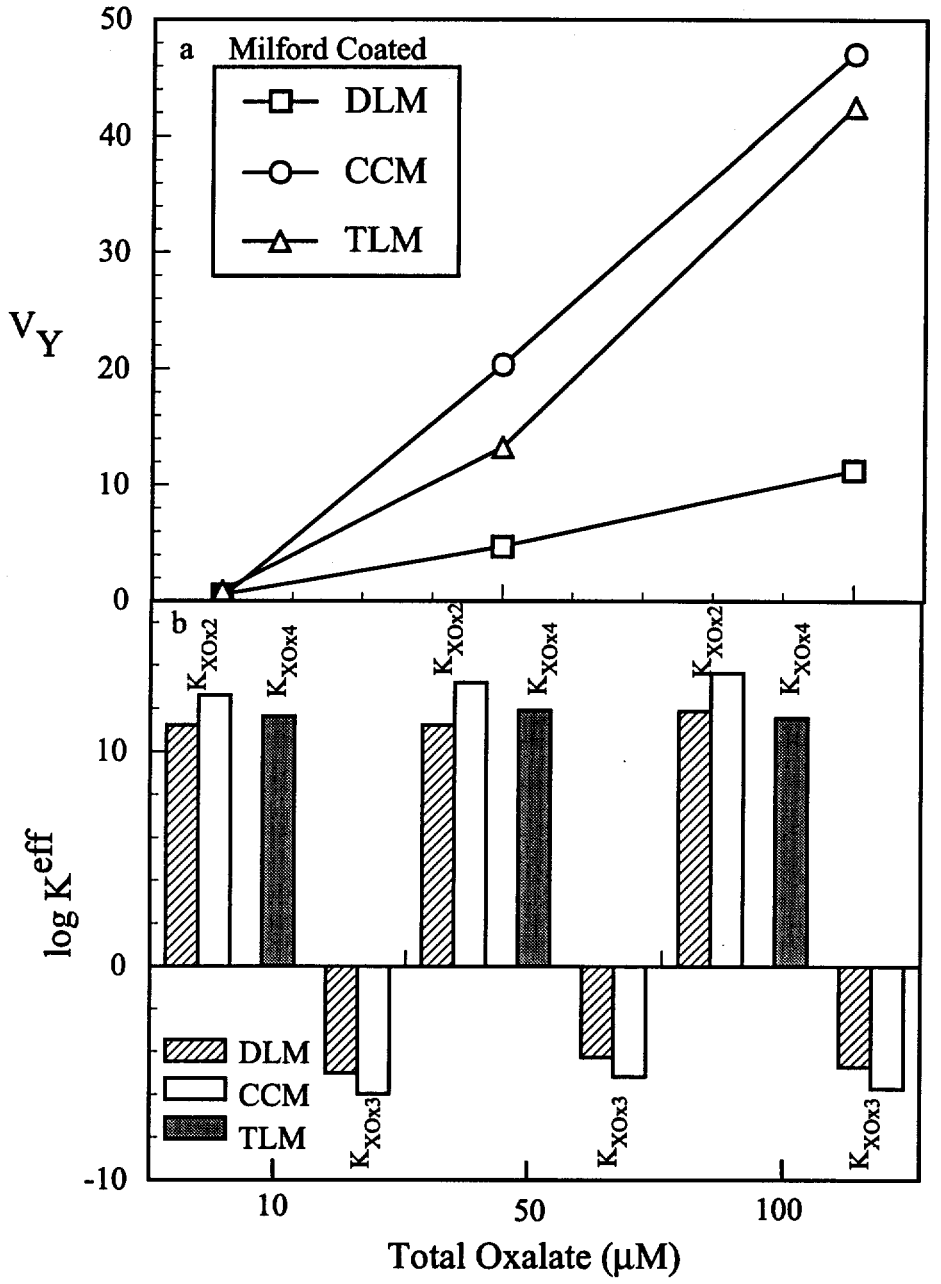

Figure 3.6. Variation in the a) goodness of fit (V_Y) and b) effective surface complexation constants (K^{eff}) for DLM, CCM, and TLM, and oxalate concentrations of 10, 50, and 100 μM for the Milford Coated Sample. K_{XOx2}, and K_{XOx3} are the two species in DLM and CCM while K_{XOx4} is for TLM.

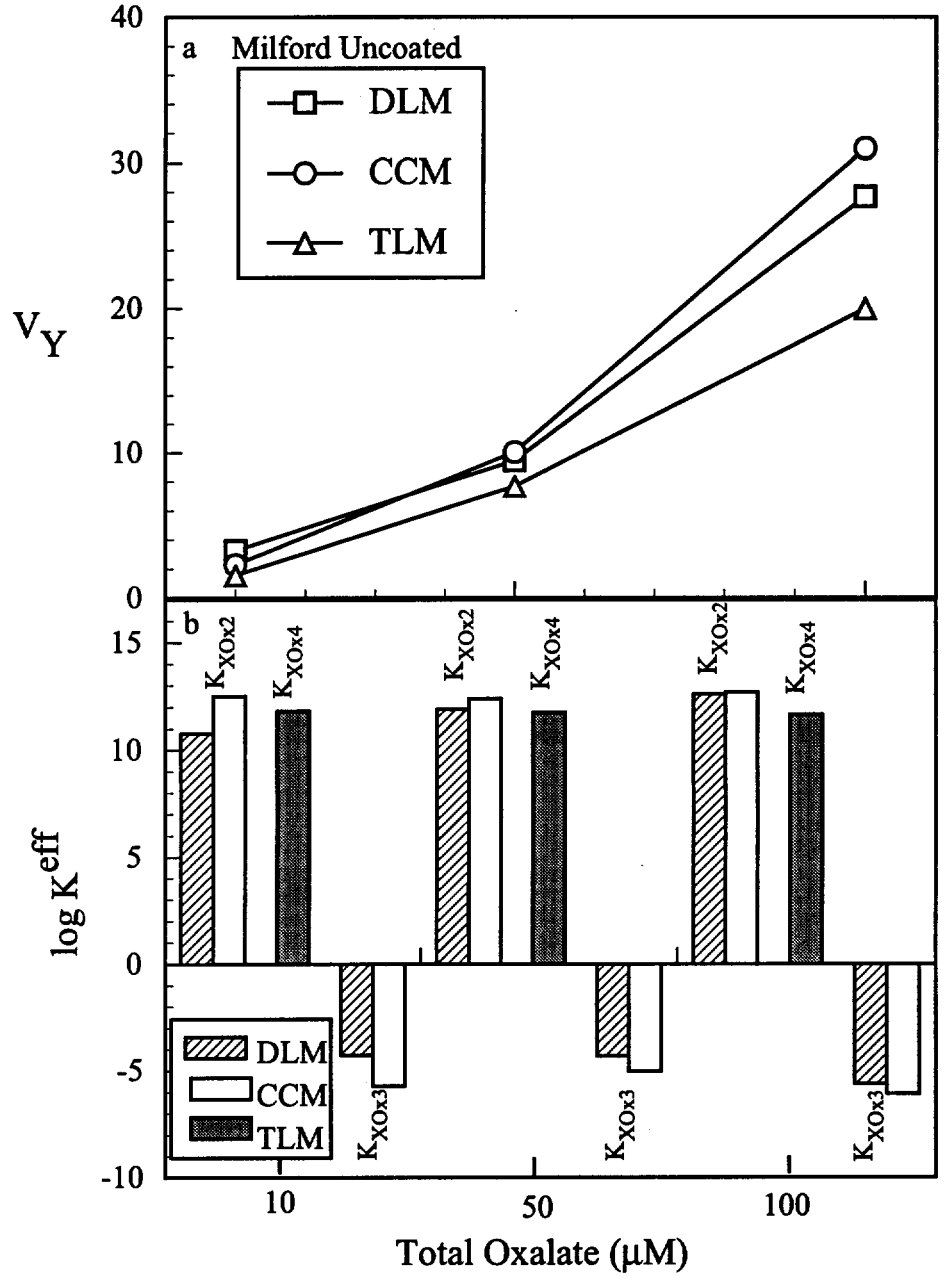

Figure 3.7. Variation in the a) goodness of fit (V_Y) and b) effective surface complexation constants (K^{eff}) for DLM, CCM, and TLM, and oxalate concentrations of 10, 50, and 100 μM for the Milford Uncoated Sample. K_{XOx2}, and K_{XOx3} are the two species in DLM and CCM while K_{XOx4} is for TLM.

Table 3.8. Effective surface complexation constants and the goodness of fit for adsorption of 10 μM, 50 μM, and 100 μM oxalate onto MC and MU with TLM.

Model	[Ox] μM	Conditions	V_Y	log K_{Ox4}
TLM, MC	100	pH > 6	43.05	11.50±0.01
		Entire Edge	42.49	11.56±0.01
	50	pH > 6	5.64	11.61±0.02
		Entire Edge	13.27	11.90±0.02
	10	pH > 6	0.96	11.55±0.07
		Entire Edge	0.89	11.63±0.06
TLM, MU	100	pH > 6	16.75	11.54±0.01
		Entire Edge	19.99	11.66±0.01
	50	pH > 6	8.15	11.67±0.02
		Entire Edge	7.67	11.74±0.02
	10	pH > 6	0.83	11.90±0.07
		Entire Edge	1.55	11.82±0.05

with K^{eff} for a Ox_T = 50 μM and 10 μM except for pH 5 - 7.

3.5.2.3 Modeling Adsorption of Cu onto AC, MC, and MU

The surface species ≡XOCu$^+$ modeled adsorption of Cu onto AC, MC, and MU with DLM and CCM (*19*). The fits were accurate ($0.1 \leq V_Y \leq 4$) for both concentrations of Cu. As illustrated in Figures 3.3a, 3.3b, and by the range of V_Y values in Figure 3.8 and Table 3.9, fits were better for Cu_T = 5.7 μM than for Cu_T = 15 μM. The K^{eff} values for larger Cu_T was always smaller than the K^{eff} value of smaller Cu_T.

Both inner-sphere (≡XOCu$^+$) and outer-sphere (≡XO$^-$ - Cu^{2+}) complexes accurately modeled the adsorption of Cu onto AC, MC, and MU with TLM ($0.1 < V_Y < 4$). The results for the outer-sphere Cu complex are not shown because spectroscopic and other data show that Cu forms inner-sphere complexes (*51, 52*). The K^{eff} for one Cu_T somewhat accurately predicted the adsorption for another Cu_T (Fig. 3.3a, b). K^{eff} for 15 μM Cu slightly

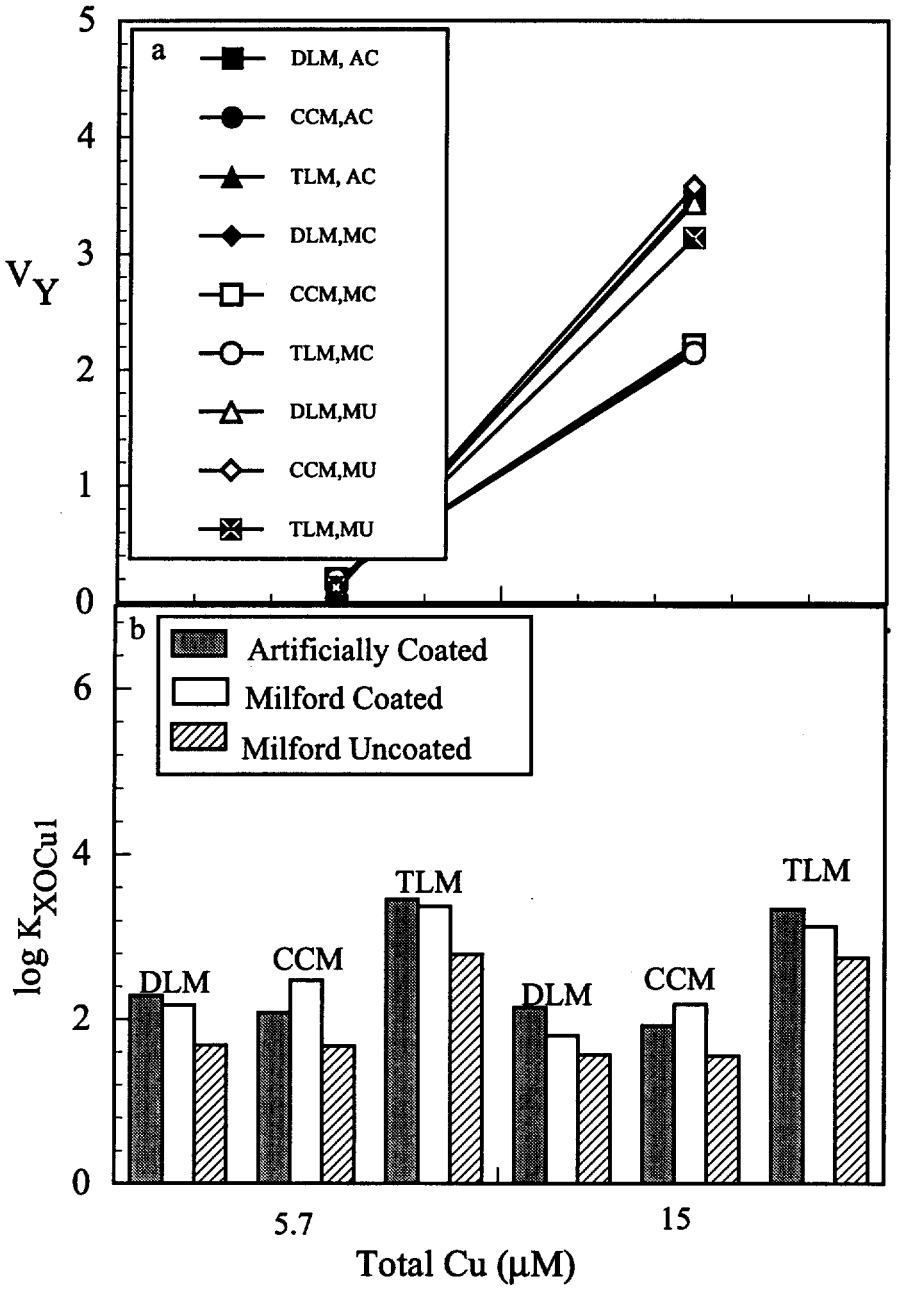

Figure 3.8. Variation in the a) goodness of fit (V_Y) and b) effective surface complexation constant (log K_{XOCu1}) for DLM, CCM, and TLM, and Cu concentrations of 5.7 and 15 μM for the AC, MC, and MU.

Table 3.9. Effective surface complexation constants and the goodness of fit for adsorption of 5.7 μM and 15 μM Cu onto AC, MC, and MU with DLM, CCM, and TLM.

Model	[Cu] μM	V_Y	log K_{XOCu1}
DLM, AC	15.0	3.47	2.14±0.10
	5.70	0.10	2.29±0.15
CCM, AC	15.0	3.48	1.92±0.10
	5.70	0.10	2.08±0.15
TLM, AC	15.0	3.48	3.34±0.10
	5.7.0	0.10	3.45±0.15
DLM, MC	15.0	2.17	1.80±0.13
	5.70	0.20	2.17±0.10
CCM, MC	15.0	2.22	2.18±0.13
	5.70	0.20	2.47±0.10
TLM, MC	15.0	2.15	3.13±0.13
	5.70	0.20	3.37±0.10
DLM, MU	15.0	3.44	1.56±0.07
	5.70	0.13	1.68±0.20
CCM, MU	15.0	3.58	1.55±0.07
	5.70	0.13	1.67±0.20
TLM, MU	15.0	3.14	2.75±0.07
	5.70	0.13	2.79±0.20

underpredicted the adsorption of Cu_T = 5.7 μM but the difference was small.

3.5.2.4 Sensitivity to Values of pK_a

Adsorption onto AC was accurately modeled with the DLM using a range of different pK_a's corresponding to various metal oxides (listed in Table 3.10). The choice of acid-base parameters had little effect on the goodness of fit (V_Y) and only slightly affected the values of the optimized K^{eff}. Values of K^{eff} for oxalate (K_{XOx2}) did not change significantly for different pK_a's whereas K^{eff} values for the other oxalate species (K_{XOx3}) and for Cu (K_{XOCu1}) were more sensitive to pK_a values. Although not shown here, the trends did not change for other SCMs (CCM and TLM) or for other sorbents (MC and MU).

3.5.2.5 Sensitivity of the Fits to the Values of N_s

The adsorption of oxalate and Cu was modeled with a wide range of N_s values. The fits depended on the type and total concentration of sorbate (illustrated Fig. 3.9). Cu adsorption pH edges were modeled with the same V_Y for a three orders of magnitude variation of N_s. In contrast, the oxalate pH edges exhibited a distinct minimum in V_Y as a function of N_s and the minimum was shallower for Ox_T = 10 μM than for Ox_T = 50 μM. The same trends were also present for the adsorption of oxalate and Cu onto MC and MU with CCM and TLM.

3.6 Discussion

The adsorption of a relatively wide range of oxalate and Cu onto metal-oxide coated sands was modeled with homogeneous-site SCMs. Only at higher sorbate concentrations and for pH > 7 did the model fits deteriorate somewhat. The fits for both sorbates were insensitive to the choice of pK_a's. Adsorption of oxalate was sensitive to the changes in N_s but the adsorption of comparable concentration of Cu was insensitive to changes in N_s. K^{eff} was a function of the total sorbate concentration. The K^{eff} obtained from one sorbate concentration did not always accurately reproduce adsorption for other sorbate concentrations.

Table 3.10. Selected DLM fits for modeling the adsorption of oxalate and Cu onto AC with surface protonation constants for various solids (Collected from Table 1 in Huang et al. [*54*]).

Solid	Sorbate	pK_{a1}	pK_{a2}	V_Y	log K_{XOx2}	log K_{XOx3}	log K_{XOCu1}
γ-Al_2O_3	Ox_T = 10 μM	7.2	9.5	0.14	11.97±0.26	-5.13±0.26	
		5.7	11.5	0.17	12.06±0.13	-7.19±0.34	
α-Al_2O_3		8.5	9.7	0.26	11.53±0.38	-5.93±0.31	
$Fe(OH)_3$		5.1	10.7	0.16	12.06±0.14	-6.61±0.29	
α-FeOOH		7.0	8.4	0.17	12.13±0.50	-3.53±0.24	
		4.2	10.8	0.16	12.06±0.14	-6.71±0.30	
γ-FeOOH		3.9	10.5	0.15	12.06±0.14	-6.40±0.28	
TiO_2		5.4	6.4	0.10	13.95±0.21	-0.97±0.22	
		2.6	9.4	0.16	12.12±0.18	-4.97±0.26	
γ-Al_2O_3	Cu_T = 15 μM	7.2	9.5	3.39			1.44±0.11
		5.7	11.5	3.10			0.12±0.11
α-Al_2O_3		8.5	9.7	3.49			2.74±0.11
$Fe(OH)_3$		5.1	10.7	2.94			-0.32±0.11

Table 3.10 (Continued). Selected DLM fits for modeling the adsorption of oxalate and Cu onto AC with surface protonation constants for various solids (Collected from Table 1 in Huang et al. [*54*]).

Solid	Sorbate	pK_{a1}	pK_{a2}	V_Y	log K_{Ox2}	log K_{Ox3}	log K_{XOCu1}
α-FeOOH	Cu_T = 15 μM	7.0	8.4	3.36			1.25±0.11
		4.2	10.8	2.50			-0.87±0.10
γ-FeOOH		3.9	10.5	2.30			-1.00±0.09
TiO_2		5.4	6.4	3.14			-0.09±0.11
		2.6	9.4	1.65			-1.23±0.08

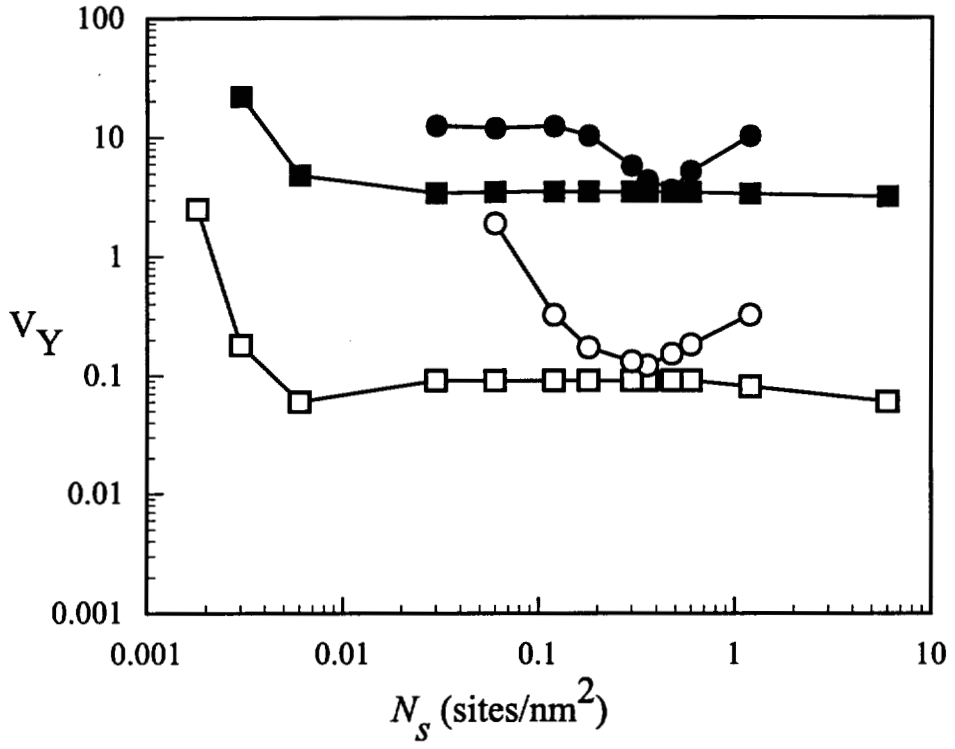

Figure 3.9. Relationship between the site density (N_s) and the goodness of fit (V_Y) for 10 μM (O) and 50 μM (●) oxalate, and 5.7 μM (□) and 15 μM (■) Cu.

3.6.1 Modeling Adsorption of Oxalate and Cu

The adsorption of oxalate was modeled with DLM and CCM over pH 4 - 11 with $\equiv XC_2O_4^-$ and $\equiv XOC_2O_4^{3-}$. The surface species $\equiv XC_2O_4H^o$ was omitted from DLM and CCM models of oxalate adsorption because it is important only at pH < 4.2 (see Fig. 1c in Mesuere and Fish [*17*]). The species $\equiv XC_2O_4^-$ is important for pH < 7 while the physically unrealistic species $\equiv XOC_2O_4^{3-}$ is important at pH > 7 (Fig. 3.10a, b). Nowack and Sigg (*55*) were able to model the broad adsorption edge of EDTA with a binuclear complex at low pH and a mononuclear complex at high pH. We attempted to circumvent the use of the improbable species $\equiv XOC_2O_4^{3-}$ by employing the strategy of Nowack and Sigg (*55*) but were unsuccessful.

The adsorption of oxalate was modeled with TLM with the outer-sphere surface species $\equiv XOH_2^+ - C_2O_4^{2-}$ for pH 4 - 11. The species $\equiv XOH_2^+ - HC_2O_4^-$ is important only at pH < 4 and was omitted. We modeled the edges without invoking any unrealistic species perhaps because the TLM represents the electrostatic effects more realistically than DLM and CCM.

Cu forms an inner-sphere complex (*51, 52*) but we modeled the Cu pH edges successfully with both inner-sphere and outer-sphere species. This latitude in modeling also has been observed by other researchers. Goldberg (*11*) reports that the adsorption of borate can be modeled with both inner-sphere and outer-sphere complexed species. Adsorption of Ca, Mg, Cd, Cu, and Pb are well modeled with inner-sphere complexes (*2, 3, 13*) and with-outer sphere complexes (*22, 56*).

The upward shift in pH_{max} for oxalate on MC and MU is similar to the shift observed by Violante et al. (*53*) for adsorption of oxalate onto Al_2O_3. They do not comment on the possible reasons, but the shift could be due to oxalate-induced dissolution of Al and the competition between dissolved Al and the surface sites for oxalate in solution. Ligand-induced dissolution is favored at lower pH and the dissolved Al outcompetes the surface for the oxalate in solution at pH < 6.

Oxalate in the edge experiments always dissolved less than 5 μM Fe from AC and the pH edges were modeled without including Fe-oxalate complexes in solution. Adsorption of

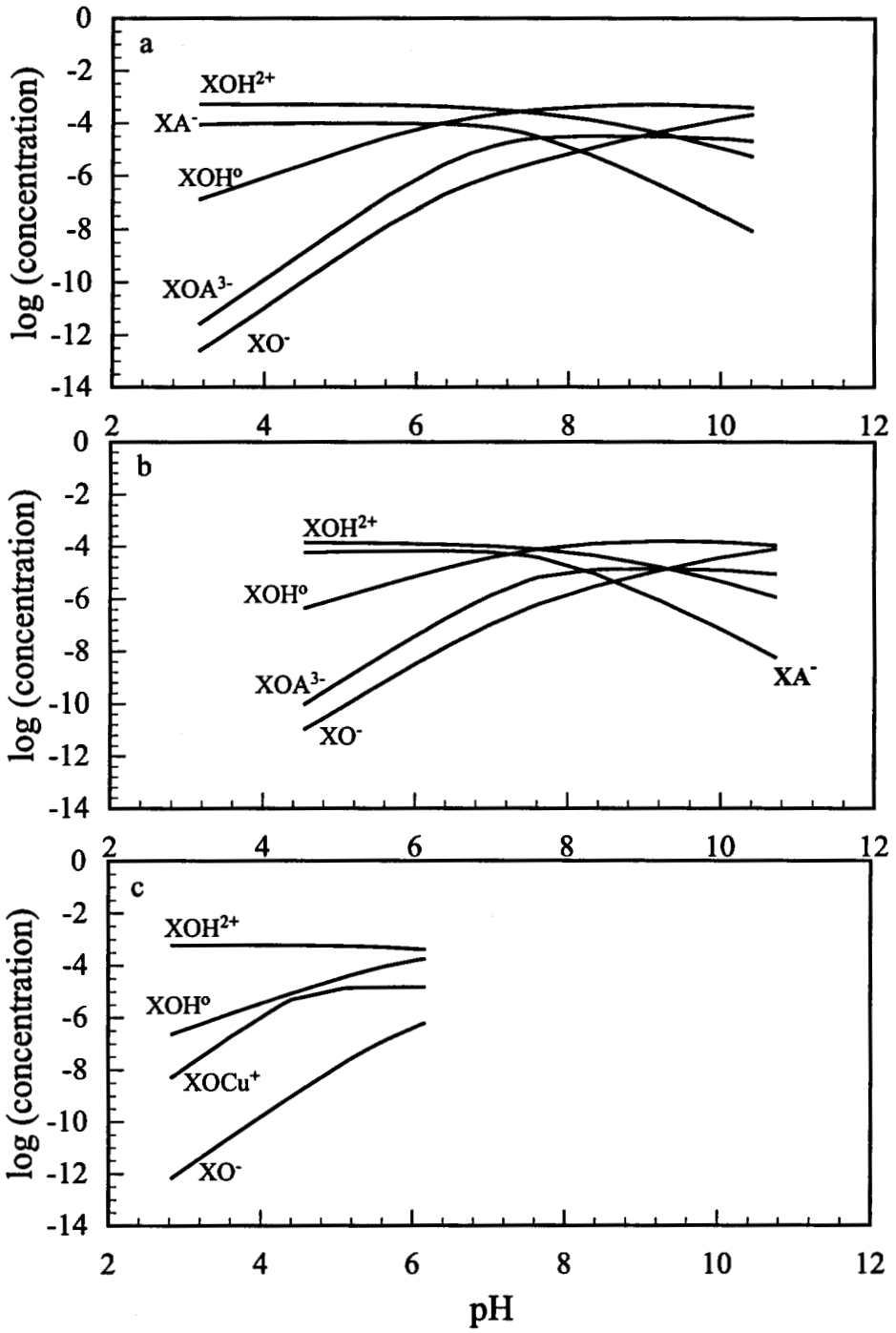

Figure 3.10. Surface speciation for adsorption edges of a) 100 μM oxalate onto AC, b) 100 μM oxalate onto MC, and c) 5.7 μM Cu onto AC. Various surface species are marked on the figures. ($A = C_2O_4^{2-}$).

the same concentration of oxalate onto MC and MU dissolved an order of magnitude more Al than Fe hence the decrease in oxalate adsorption below pH 6 was modeled by including the competition between the surface and the dissolved Al for oxalate. Modeling results not presented here show that this effect is not specific to Al and will be evident if significant concentrations of other metals, including Fe, dissolved during adsorption.

Dissolution of surficial metal oxides can change the surface properties of the coated sands. Experiments were done to monitor the effect of dissolution on adsorption properties. Substantially more metal oxides than the total oxalate extractable portion had to be removed to see perceptible changes in adsorption of oxalate.

3.6.2 Heterogeneity Effects

Adsorption onto AC, MC, and MU was adequately modeled with homogeneous-site SCMs for a relatively wide range of sorbate concentrations. A greater value of V_Y for large concentration of sorbate (Fig. 3.5 - 3.8) may be due to the heterogeneity of adsorption energies. There are numerous pieces of experimental evidence for the presence of site heterogeneity.

Modeling individual concentrations of a sorbate gave slightly different K^{eff} values. K_{XOCu1} always decreased with an increase in sorbate concentration (see Fig. 3.8 and Table 3.9). A decrease in K^{eff} with increase in sorbate concentration can be explained by the presence of sites with distinctly different binding energies. We were unable to always get distinct trends for the change in K^{eff} values for different oxalate concentrations (Fig. 3.5 - 3.7 and Table 3.6 - 3.8). The absence of distinct trends for oxalate adsorption is primarily because the K^{eff} values are influenced by the difference in the concentration of dissolved metal for different oxalate concentrations. The difference in the K^{eff} values for individual adsorbates translated into inaccuracy in extrapolation of constants to predict adsorption at various concentrations.

We simultaneous fit all data for a sorbate to obtain an overall K^{eff}. The overall log K^{eff} for Cu (obtained with DLM for AC) was 2.19 which was within the range of K^{eff} values obtained from individual Cu edges with the DLM (shown in Table 3.9). Similarly the overall K^{eff} values for oxalate (obtained with DLM for AC) were 11.03 and -5.06 (for $\equiv XC_2O_4^-$ and

$\equiv XOC_2O_4^{3-}$ respectively). The overall K^{eff} values obtained with such optimization depends on the number of data points for individual edges and on the ability to fit individual edges. The overall K^{eff} values for Cu_T = 5.7 and 15 μM was very close to the K^{eff} value for Cu_T = 15 μM. The overall K^{eff} value for Ox_T = 10, 50, and 100 μM was similar to the K^{eff} for Ox_T = 100 μM. Thus, the overall K^{eff} value is skewed towards the larger sorbate concentration. We did not use the overall K^{eff} because it will overpredict site heterogeneity for small sorbate concentration. It is also not always possible to obtain data for a wide range of concentrations. Constants obtained from a smaller data set often has to be extrapolated to obtain adsorption at other sorbate concentrations.

Surface heterogeneity is manifested in the "spreading out" of the pH edge. Sharp pH edges with distinct inflection points are obtained when the surface sites are well characterized by a single binding energy that is titrated during the experiment. Sites that are sufficiently heterogeneous to require multiple binding energies are titrated one after the other and result in a "spread out" edge with a broad inflection.

Anion pH edge are often spread out because of the solution protonation reactions of the weak-acid anions. However, oxalate is nearly fully deprotonated (to $C_2O_4^{2-}$) over the pH range 5 - 11. The "spread out" pH edge in this case cannot be attributed to the protonation of oxalate but rather to the heterogeneity of adsorption energies and the titration of different sites during adsorption.

Although the adsorption onto slightly heterogeneous surfaces can be modeled with a single site and multiple reactions, larger heterogeneity cannot be modeled with this assumption because of smaller number of adjustable parameters. Using multiple site formulations should be more effective in modeling the adsorption on strongly heterogeneous surfaces, i.e., the heterogeneity revealed by higher concentrations of sorbate, because of larger number of adjustable parameters. This approach will be pursued in Chapter 5.

3.6.3 Effect of Changes in Modeling Parameters

As explained earlier, it is difficult to obtain pK_a values from acid-base titration of soils. Our finding (Table 3.10) suggests that adsorption modeled with a wide range of pK_a's fit the data accurately and often results in somewhat similar values of K^{eff}. Accurate measure of the

pK_a's are not essential and that almost any literature value can be used effectively. Although this insensitivity is good for modeling, it makes the models ineffective for diagnosing microscale adsorption processes.

The fit for oxalate was more sensitive to N_s than the fit for Cu (Fig. 3.9). Other researchers (*52, 57, 58*) report metal adsorption to be insensitive to N_s. A possible reason for this difference between Cu and oxalate may be that oxalate forms an outer-sphere complex that is less stable than an inner-sphere complex (*59*) and hence its fit my be more sensitive to N_s.

3.6.4 Linear Free Energy Relationships

The K^{eff} values obtained for oxalate and Cu with the DLM approach can be compared with values obtained by other researchers by comparing the computed K^{eff} values it with the linear free energy relationship (LFER) for cations and anions obtained by Dzombak and Morel (*19*). The K_{XOx2} values for AC, MC, and MU (marked as Δ and □ in Figure 3.11) agree well with the LFER for anions and K_{XOCu1} values (marked as ○ in Figure 3.11) also agrees with LFER for cations. AC, MC, and MU can be treated as a homogeneous HFO for a moderately wide range of sorbate concentration.

3.6.5 Extrapolation with MINTEQA2

The K^{eff} obtained from one sorbate concentration does not always accurately reproduce the adsorption for other sorbate concentrations over the entire pH (Fig. 3.1, 3.2, and 3.3). Such extrapolation accurately reproduced Cu adsorption and oxalate adsorption for pH < 7. Oxalate adsorption for pH > 7 is sometimes underpredicted and at other times overpredicted. This appears to be due to heterogeneity in adsorption energies. Smaller sorbate concentrations bind to mainly the stronger sites on the surface and the K^{eff} value is larger. Larger sorbate concentrations bind to both the stronger sites and the weaker sites on the surface and the K^{eff} value is smaller. When we try to use constants for smaller concentration to reproduce adsorption of larger concentration, we are imposing a larger K^{eff} value on a concentration that will give a smaller K^{eff} and we overestimate the adsorption. Conversely, when we try to use constants for larger concentration to reproduce adsorption of smaller concentration, we are trying to impose a smaller K^{eff} value on a concentration that

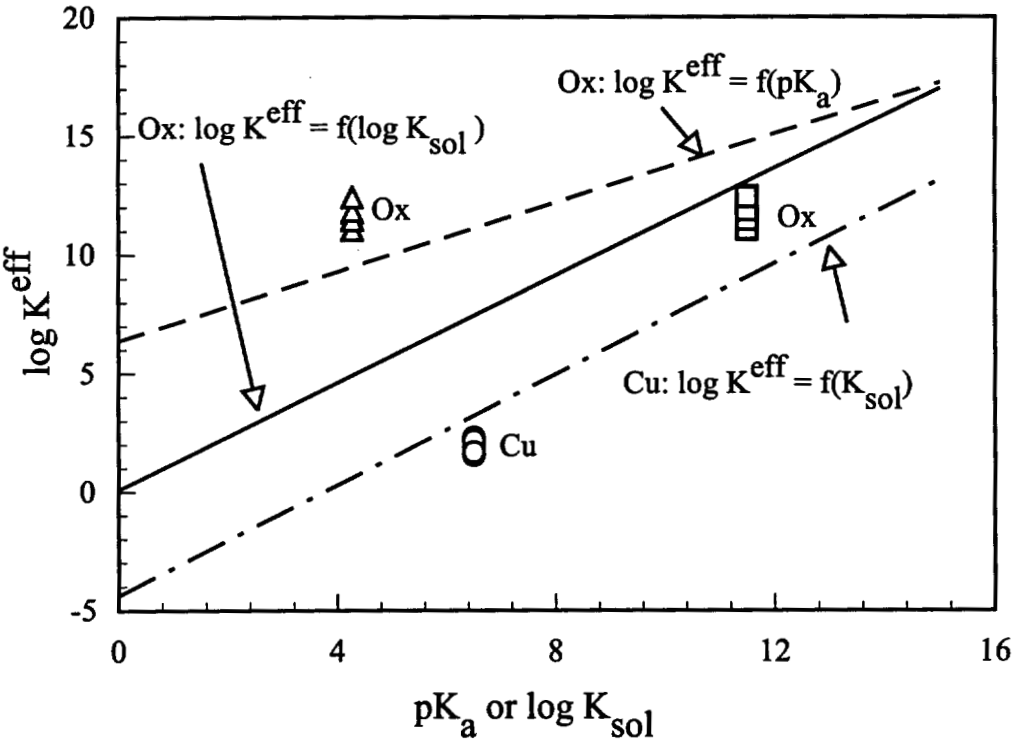

Figure 3.11. Comparison of the linear free energy relationship (LFER) and the surface complexation constants (K^{eff}) obtained for oxalate (□ and Δ) and Cu (O) for AC, MC, and MU.

will give a larger K^{eff} and we underestimate the adsorption. When sorbate concentrations are not very different similar heterogeneity is revealed and K^{eff} for one concentration reproduces the adsorption of the other concentration. When sorbate concentrations are vastly different, K^{eff} from one concentration overpredicts the heterogeneity revealed by smaller concentrations and underpredicts the heterogeneity revealed by higher concentrations.

3.6.6 Valid Range of V_Y

The range of V_Y values (V_Y = 0.1 - 20) suggested by Dzombak and Morel (*19*) give a convenient measure of acceptable fits. A value of V_Y outside this range does not always indicate an inability to fit the entire pH edge. V_Y incorporates both the accuracy of the fit and the scatter in the data. Values outside this range may be obtained for adsorption onto soil even though the fits are accurate because of the scatter in the data. Adsorption of Ox_T = 100 μM was modeled with $V_Y > 20$ with DLM (see Fig. 3.1c), CCM, and TLM but the fits were accurate when compared to the scatter in the data. Although this range of V_Y (0.1 - 20) is a good guideline, the accuracy of the fit should be decided with visual inspection of the fit and the data even if V_Y lies outside this prescribed range.

3.6.7 Implications

Adsorption onto metal-oxide coated soils can be modeled with the assumption of a pure phase metal-oxide surface. A homogeneous-site formulation reproduces the adsorption of a moderately wide range of sorbate concentration. Fits are insensitive to changes in pK_a's and literature values for pure phase oxides can be used for modeling adsorption onto these soils. This insensitivity makes SCMs ineffective for diagnosing microscale adsorption processes. Inaccurate estimates of N_s will influence the adsorption of oxalate but will not influence the adsorption of Cu. An important goal of modeling is to predict the adsorption for a wide range of sorbate concentration based on constants obtained from a sparse data set. For extrapolation beyond the range of concentrations for which the K^{eff} values are obtained there will be errors in estimates of the adsorbed amount because of the heterogeneity in adsorption site types.

3.7 References

(1) Schindler, P.W. and Kamber, H.R. *Helv. Chim. Acta*, **1968**, 51:1781-1786.

(2) Hohl, H. and Stumm, W. *J. Colloid Interface Sci.*, **1976**, 55:281-288.

(3) Schindler, P.W.; Furst, B.; Dick, R.; and Wolf, P.U. *J. Colloid Interface Sci.*, **1976**, 55:469-475.

(4) Stumm, W.; Kummert, R. and Sigg, L. *Croat. Chem. Acta*, **1980**, 53:291-312.

(5) Sigg, L. and Stumm, W. *Colloids and Surfaces 2*, **1987**, 101-117.

(6) Sposito, G. *The Surface Chemistry of Soils*, **1984**, Oxford University Press, New York.

(7) Schindler, P.W. and Stumm, W. "The Surface Chemistry of Oxides, Hydroxides, and Oxide Minerals," in *Aquatic Surface Chemistry*, W. Stumm (ed.), Wiley-Interscience, New York, **1987**, pp. 83-110.

(8) Goldberg, S. and Sposito, G. *Soil Sci. Soc. Am. J.*, **1984a**, 48:772.

(9) Goldberg, S. and Sposito, G. *Soil Sci. Soc. Am. J.*, **1984b**, 48:779.

(10) Goldberg, S. *Soil Sci. Soc. Am. J.*, **1985**, 49:851.

(11) Goldberg, S. *Soil Sci. Soc. Am. J.*, **1985**, 50:1154.

(12) Stumm, W.; Hohl, H.; and Dalang, F. *Croat. Chem Acta*, **1970**, 48:491-504.

(13) Huang, C.P. and Stumm, W. *J. Colloid Interface Sci.*, **1973**, 43:409-420.

(14) Harding, I.H. and Healy, T.W. *J. Colloid Interface Sci.*, **1985a**, 107:382-397.

(15) Harding, I.H. and Healy, T.W. *J. Colloid Interface Sci.*, **1985b**, 107:371-381.

(16) Dzombak, D.A. and Morel, F.M.M. *J. Colloid and Interface Sci.* **1986**, 112(2), 588-598.

(17) Mesuere, K. and Fish, W. *Environ. Sci. Technol.* **1992a**, 26(12), 2357-2364.

(18) Mesuere, K. and Fish, W. *Environ. Sci. Technol.*, **1992b**, 26(12), 2365-2370.

(19) Dzombak, D.A. and Morel, F.M.M. *Surface Complexation Modeling: Hydrous Ferric Oxide*. John Wiley & Sons. **1990**.

(20) Davis, J.A.; James, R.O.; and Leckie, J.O.; *J. Colloid Interface Sci.*, **1978**, 63:480-499.

(21) Hayes, K.F.; Roe, A.L.; Brown, G.E.; Hodgson, K.O.; Leckie, J.O.; and Parks, G.A. *Science*, **1987**, 238:783-786.

(22) Davis, J.A. and Leckie, J.O. *Environ. Sci. Technol.* **1978**, 12, 1309.

(23) Davis, J.A. and Leckie, J.O. *J. Colloid and Interface Sci.* **1980**, 74(1), 32-43.

(24) Balistereri, L.S. and Murray, J.W. *Geochim. Cosmochim. Acta*, **1982**, 51(5), 1151-1160.

(25) Hsi, C.D. and Langmuir, D. *Geochim. Cosmochim. Acta*, **1985**, 49:1931-1941.

(26) Catts, J.G. and Langmuir, D. *J. Appl. Geochem.*, **1986**, 1:255-264.

(27) LaFlamme, B.D. and Murray, J.W. *Geochim. Cosmochim Acta*, **1987**, 51:243-250.

(28) Hunter, K.A.; Hawke, D.J.; and Choo, L.K. *Geochim. Cosmochim Acta*, **1988**, 52:627-636.

(29) Payne, T.E. and Waite, T.D. *Radiochim Acta*, **1991**, 52-53(Pt.2):487-493.

(30) Goldberg, S. *J. Colloid and Interface Sci.* **1991**, 145(1), 1-10.

(31) Hayes, K.F. and Leckie, J.O. *J. Colloid and Interface Sci.* **1987**, 115(2), 564-572.

(32) Lyklema, J. *J. Colloid Interface Sci.*, **1977**, 58:242-250.

(33) Hiemenz, P.C. *Principles of Colloid and Surface Chemistry*, Mercel Dekker, New York, **1977**.

(34) Smith, A.L. "Electrical Phenomena Associated with the Solid-Liquid Interface," in *Dispersion of Powders and Liquids*, 3rd ed. G.D. Parfitt (ed.) Applied Science Publishers, London, **1981**, pp. 75-80.

(35) Hunter, R.J. *Zeta Potential in Colloid Science*, Academic Press, New York, **1981**.

(36) Westall, J.C. and Hohl, H. Advan. *Colloid Interface Sci.*, **1980**, 12:265-294.

(37) Morel, F.M.M.; Yeasted, J.G.; and Westall, J.C. "Adsorption Models: A Mathematical Analysis in the Framework of General Equilibrium Calculations," in *Adsorption of Inorganics in Solid-Liquid Interfaces*, M.A. Anderson and A.J. Rubin (eds.), Ann Arbor Science, Ann Arbor, Mich., **1981**, pp. 263-294.

(38) Zachara, J.M.; Cowan, C.E.; Schmidt, R.L.; and Ainsworth, C.C. *Clays and Clay Minerals.* **1988**, 36(4), 317-326.

(39) Zachara, J.M.; Ainsworth, C.C.; Cowan, C.E.; and Resch, C.T. *Soil Sci. Soc. Am. J.* **1989**, 53, 418-428.

(40) Scheiddegger, A.; Borkovec, M.; and Sticher, H. *Geoderma.* **1993**, 58, 43-65.

(41) Stahl, R.S. and James, B.R. *Soil Sci. Soc. Am. J.* **1991a**, 55, 1287-1290.

(42) Stahl, R.S. and James, B.R. *Soil Sci. Soc. Am. J.* **1991b**, 55, 1291-1294.

(43) Stahl, R.S. and James, B.R. *Soil Sci. Soc. Am. J.* **1991c**, 55, 1592-1297.

(44) Szecsody, J.E.; Zachara, J.M; and Bruckhart,P.L. *Environ. Sci. Technol.*, **1994**, 28:1706-1716.

(45) Herbelin, A.L. and Westall, J.C. *FITEQL: A Computer Program for Determination of Chemical Equilibrium Constants*, Version 3.1, Report 94-01, Department of Chemistry, Oregon State University, Corvallis, OR, **1994**.

(46) S. Smith, Personal Communication, **1995**, Pacific Northwest Laboratory, Richland, WA.

(47) Bolt, G.H. and van Riemsdijk, W.H. "Surface Chemical Processes in Soil," in *Aquatic Surface Chemistry*, W. Stumm (ed.), Wiley-Interscience, New York, **1987**, pp. 127-164.

(48) Bürgisser, C.S.; Scheidegger, A.M.; Borkovec, M.; and Sticher, H. *Langmuir.* **1994**, 10(3), 855-860.

(49) Smith, R.M. and Martell, A.E. *Critical Stability Constants: Other Organic Ligands*, **1977**, Vol. 3, Plenum Press, New York.

(50) Van Geen, A.; Robertson, A.P.; and Leckie, J.O. *Geochim. Cosmochim. Acta.* **1994**, 58(9), 2073-2086.

(51) Motschi, H. *Colloids Surfaces*, **1984**, 9:333-347.

(52) Hayes, K.F. *Equilibrium, Spectroscopic and Kinetic Studies of Ion Adsorption at the Oxide/Aqueous Interface*, **1987**, Ph.D. Dissertation, Stanford University, Stanford, CA.

(53) Violante, A.; Colombo, C.; and Buondonno, A. *Soil Sci. Soc. Am. J.* **1991**, 55, 65-70.

(54) Huang, C.P,.; Hsieh, S.; Park, S.W.; Corapcioglu, M.O.; Bowers, A.R.; Elliott, H.A. "Chemical interactions between heavy metal ions and hydrous solids," in *Metal Speciation, Separation, and Recovery*, Ed. Parretson, J.W. and Passino, R., Proceedings of the International Symposium on Metal Speciation, Separation, and Recovery, Chicago, Illinois, July 27 - August 1, **1986**, 437-474, Lewis Publishers, Inc.

(55) Bernd, N. and Sigg, L. *J. Colloid Interface Sci.*, **1996**, 177:106-121.

(56) Balisterieri, L.S. and Murray, J.W. *Amer. J. Sci.*, **1981**, 281:788-806.

(57) Kent, D.B.; Tripathy, V.S.; Ball, N.B.; and Leckie, J.O. 1986, Stanford Tech. Rept. #294, **1986**, Stanford CA; also NUREG Rept. CR-4897, SAND 86-7175 (1988).

(58) Hayes, K.F.; Redden, G.; Ela, W.; and Leckie, J.O. *J. Colloid Interface Sci.*, **1991**, 142(2):448-469.

(59) Stumm, W. *Chemistry of Solid-Water Interface-Processes at the Mineral-Water and Particle-Water Interface in Natural Systems*, **1992**, John Wiley & Sons, Inc.

CHAPTER 4*

HOMOGENEOUS-SITE ADSORPTION MODELING OF METAL OXIDE COATED SUBSOILS. 2. COPPER-OXALATE COMPLEXES

4.1 Abstract

Adsorption from mixtures of a model metal (Cu) and a model ligand (oxalate) onto metal oxide-coated sands was measured as a function of pH at a single ionic strength (0.05 M NaCl), a single solids concentration (100 g/L), and at adsorbate concentrations of 8.3 and 38 μM Cu in the presence of 100 μM oxalate, and 27 and 121 μM Cu in the presence of 1 mM oxalate. Data were fitted with surface complexation models assuming a homogeneous surface and a 1:1 (site : adsorbate) stoichiometry. We modeled the adsorption of Cu and oxalate in the mixture by including Cu-only and oxalate-only surface species along with aqueous complexation of Cu and oxalate. Excess oxalate in solution dissolved metal oxides from the surface. The dissolved metal did not influence Cu adsorption but did diminish adsorption of oxalate in the ternary system. We were unable to extrapolate effective surface complexation constants obtained from the edge for one concentration of Cu-Oxalate to accurately reproduce the adsorption for other concentrations. The ability to reproduce the adsorption of mixtures of Cu and oxalate was insensitive to the choice of surface protonation constants and the electrical double layer model but was moderately sensitive to the choice of the site density.

---

* To be submitted to *Environmental Science & Technology*

4.2 Introduction

In the presence of ligands, metals can adsorb to a mineral surface with both ligand-like and metal-like characteristics (*1*). Some metal-ligand complexes bind strongly to the oxide surface whereas others remain mostly in solution so that the ligand competes with the surface for coordination of the metal ion (*2*). Vuceta (*3*) shows that citrate and EDTA suppress the adsorption of Pb and Cu onto α - quartz. Huang et al. (*4*) find that adsorption of Cd, Zn, Pb, and Cu onto SiO_2, γ - Al_2O_3 and two Delaware soils is enhanced by humic acid, NTA, glycine, and tartrate. Richter and Theis (*5*) show that citrate and cyanide suppress the adsorption of Ni onto oxide surfaces. Cu adsorption is also greater in the presence of NTA, glycine and aspartic acid (*6*). Elliott and Huang (*6*) studied Cu adsorption onto γ-Al_2O_3 in the presence of chelates and propose a model to qualitatively explain the adsorption characteristics. Cu in the presence of EDTA forms a ligand-like complex with the surface (*7*). Cu adsorption onto silica gel increases in the presence of 2,2',6',2"-terpyridine, 2-pyridine methanol, and 2-aminomethyl pyridine but decreases in the presence of picolinic acid, salicylic acid, and 5-sulfosalicylic acid (*8*). However, the applicability of these findings to natural porous media, such as oxide coated soils, has been little studied.

We investigated the effect of oxalate on the adsorption of Cu onto natural and synthetic metal-oxide coated sands. Cu is a typical, moderately strongly adsorbing transition metal; oxalate is a more weakly binding ligand that is common both in natural soils and contaminated sites. Our goal was also to reproduce adsorption of mixtures of Cu and oxalate (Cu-Oxalate) with homogeneous-site surface complexation models (SCMs) calibrated to the single-adsorbate adsorption of oxalate and Cu. The specific goals were the same as those of Chapter 3. Extending our studies of the homogeneous-site models to metal-ligand mixtures provides a more stringent test because mixtures of metals and ligands increase the complexity of the adsorption system and provide a tighter constraint on the model.

4.3 Methods

The experimental methods and conditions were the same as those discussed in the experimental section of Chapters 2 and 3. The pH edges for Cu-oxalate were obtained for

a constant ionic strength of 0.05 M NaCl and a constant solids concentration of 100 g/L. We used Cu concentration (Cu_T) of 8.3 and 38 μM with oxalate concentration (Ox_T) of 100 μM oxalate, and Cu_T = 27 and 121 μM with Ox_T = 1 mM. For convenience we use Cu*-Ox to denote adsorbed Cu measured in the presence of oxalate, and Cu-Ox* to denote adsorbed oxalate in the presence of Cu. Cu*-Ox was calculated as the difference of total Cu and Cu in solution as analyzed with atomic absorption spectrophotometry (AAS), using either flame or graphite furnace atomization. Cu-Ox* was measured by spiking solutions with small amounts of radiolabeled ^{14}C oxalate (NEN Research Products, 98.1 % purity) and relating Cu-Ox* to the amount of ^{14}C activity adsorbed from solution.

The modeling approach was the same as in Chapter 3. A minimum number of surface species was used to reproduce the Cu-Oxalate edges. Adsorbed metal species in the presence of ligands are often modeled as either a surface-metal-ligand (Type A or Type I; *1, 6, 7, 9, 10*) or a surface-ligand-metal (Type B or Type II; *2*) ternary surface complexes. We first tested if we could reproduce the adsorption of Cu and oxalate in the mixture with Cu-only and oxalate-only species along with aqueous complexes of Cu and oxalate. We also tested if using Type A and Type B species improved the fit. We used surface species with 1:1 (site : sorbate) stoichiometry for most of our modeling. Adding a surface species with a 2:1 stoichiometry only marginally improved the fit for Cu-oxalate system. This species is important only at pH < 4.5 and was not used here. The site densities (N_s) used for modeling Cu-oxalate adsorption were the same as those used previously for modeling the respective single-adsorbate edges (Chapter 3). For modeling the simultaneous adsorption of oxalate and Cu we used the N_s for oxalate because oxalate adsorption is sensitive to N_s whereas Cu adsorption is relatively insensitive to N_s. The aqueous reactions and the surface complexation reactions used for modeling and not listed in Chapter 3 are listed in Tables 4.1 and 4.2, respectively.

4.4 Results

Cu*-Ox edges shown in Figures 4.1 and 4.2 exhibit characteristics typical of metals with adsorption increasing with pH. However, the Cu*-Ox edges were less sharp than the

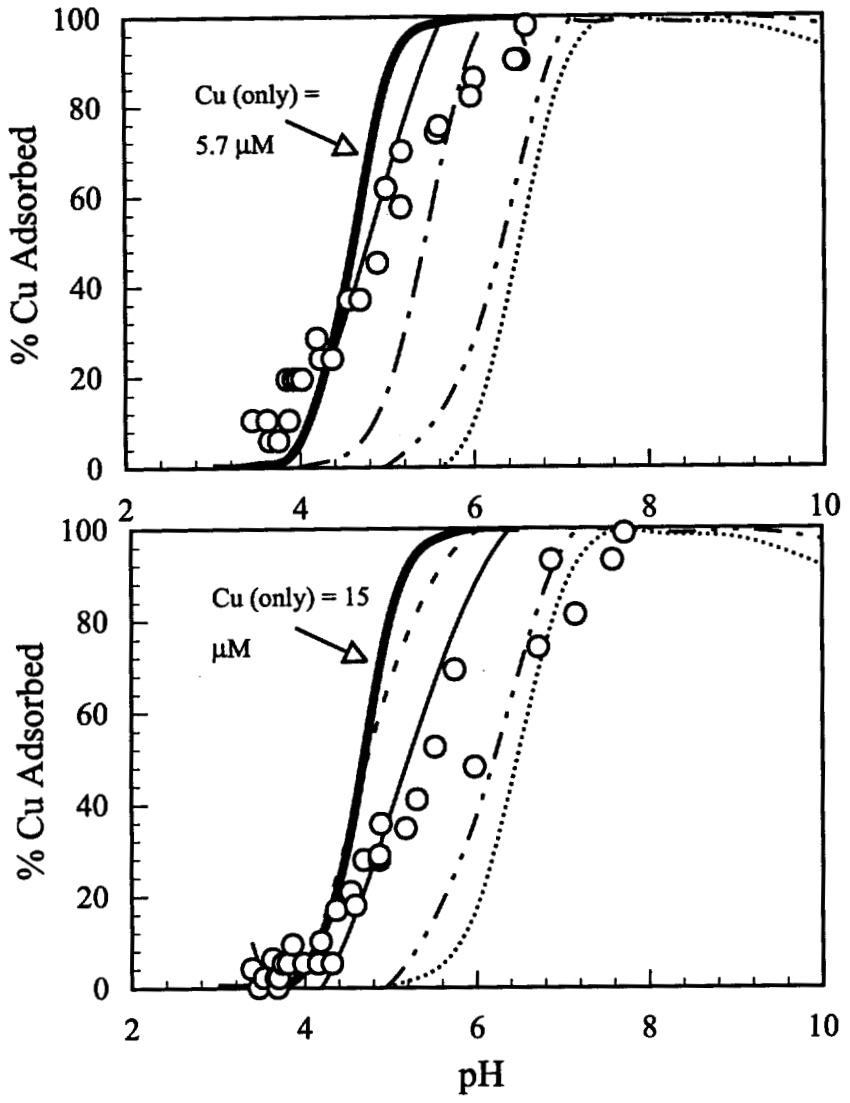

Figure 4.1. Diffuse Layer Model (DLM) fits for adsorption of a) 8.3 μM Cu with 100 μM oxalate, and b) 38 μM Cu with 100 μM oxalate onto the Artificially Coated (AC) sample. The adsorption of Cu (only) calculated with MINTEQA2 and constants optimized with FITEQL are shown as ▬▬ . The FITEQL fits are shown as ——. The various dashed lines are predictions of adsorption based on effective adsorption constants for 8.3 μM Cu with 100 μM oxalate (– - – -), 38 μM Cu with 100 μM oxalate (- - - -), 27 μM Cu with 1 mM oxalate (— - - -), and 121 μM Cu with 1 mM oxalate (·····).

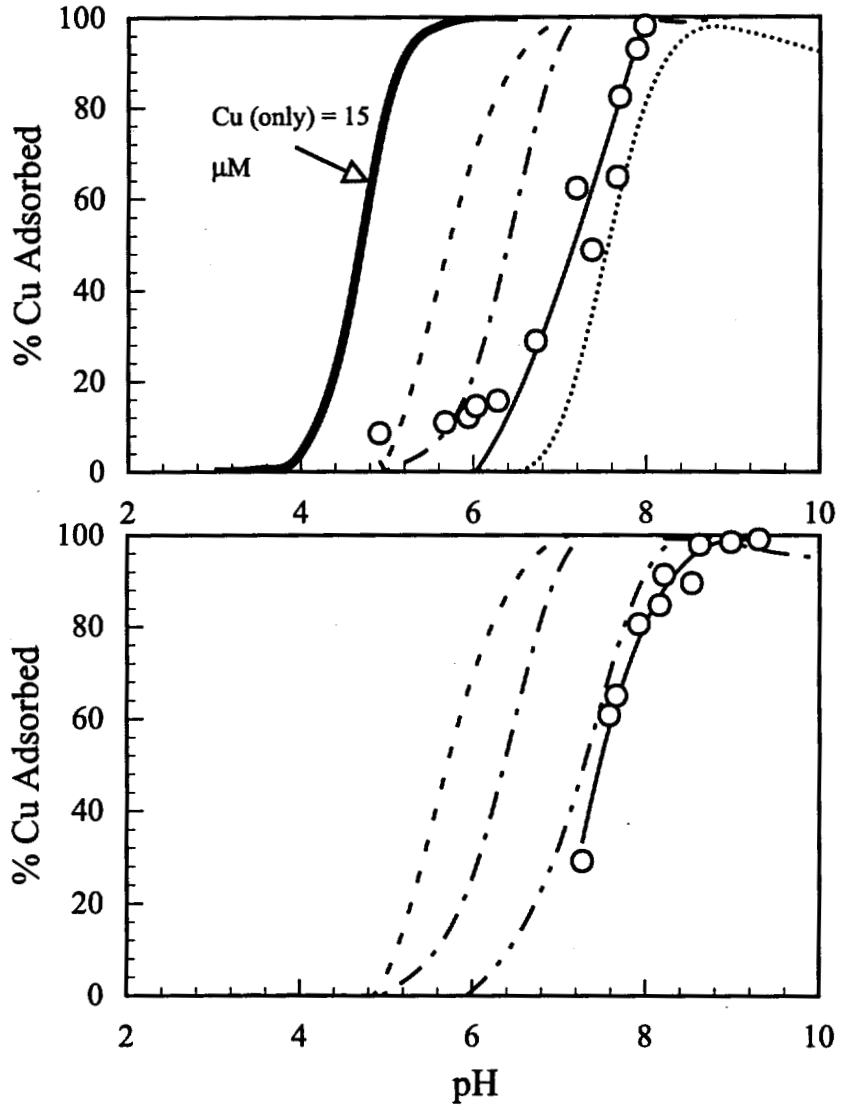

Figure 4.2. Diffuse Layer Model (DLM) fits for adsorption of a) 27 μM Cu with 1 mM oxalate, and b) 121 μM Cu with 1 mM oxalate onto the Artificially Coated (AC) sample. The adsorption of Cu (only) calculated with MINTEQA2 and constants optimized with FITEQL are shown as ▬▬ . We have not plotted the Cu (only) edge for 121 mM Cu because high concentration of Cu will precipitate at higher pH. The FITEQL fits are shown as ——. The various dashed lines are predictions of adsorption based on effective adsorption constants for 8.3 μM Cu with 100 μM oxalate (- - - -), 38 μM Cu with 100 μM oxalate (– - – -), 27 μM Cu with 1 mM oxalate (— - - -), and 121 μM Cu with 1 mM oxalate (·····).

Table 4.1. Equilibrium expressions constants of aqueous reactions not listed in Chapter 3 but used for modeling adsorption of Cu-Oxalate with DLM, TLM, and CCM.

Equilibrium Expressions	log K[a]
$[CuC_2O_4] = [Cu^{2+}][C_2O_4^{2-}]K_{CuOx,1}$	6.23[§]
$[Cu(C_2O_4)_2^{2-}] = [Cu^{2+}][C_2O_4^{2-}]^2K_{CuOx,2}$	10.27[§]

[a] T = 25°C and I = 0 M

[§]Smith and Martell (*11*)

Cu edges in Chapter 3. The position of Cu*-Ox edge as indicated by pH of minimum adsorption (pH_{min}), pH of maximum adsorption (pH_{max}), and pH of 50% adsorption (pH_{50}) (presented in Table 4.3) depended on Ox_T and Cu_T. For the same Ox_T, an increase in Cu_T diminished the fractional Cu*-Ox adsorption, i.e., the edge shifted to the right. For similar Cu_T, an increase in Ox_T also diminished the fractional Cu*-Ox adsorption, i.e., the edge shifted to the right. In contrast, single-adsorbate Cu edges showed little sensitivity to Cu_T. Cu-Ox* edges shown in Figures 4.3 and 4.4 were obtained only for Ox_T = 100 μM in the presence of Cu_T = 8.3 and 38 μM. Reliable Cu-Ox* adsorption data could not be obtained for Ox_T = 1 mM because of the small proportion of adsorbed Ox_T and the associated large errors. Cu-Ox* edges were similar to oxalate edges. The pH_{max} for AC was at pH ≈ 4

Table 4.2. Surface complexation reactions not listed in Chapter 3 but used for modeling adsorption of Cu-Oxalate with Type A and Type B ternary complexes.

Equilibrium Expressions	Model
<u>Cu in the presence of oxalate</u>	
$[\equiv XOCu(C_2O_4^{2-})^-] = [\equiv XOH^o]\{Cu^{2+}\}\{C_2O_4^{2-}\}\{H^+\}^{-1}$ $\exp(F\psi_o/RT)K_{XOCuOx1}$	DLM,CCM,TLM[‡]
$[\equiv X_2(C_2O_4^{2-})_2Cu] = [\equiv XOH^o]^2\{Cu^{2+}\}\{C_2O_4^{2-}\}^2\{H^+\}^2K_{XOCuOx2}$	DLM,CCM,TLM[‡]
$[(\equiv XOH^{2+})_2 - Cu(C_2O_4)_2^{2-}] = [\equiv XOH^o]^2\{Cu^{2+}\}\{C_2O_4^{2-}\}^2$ $\{H^+\}^2\exp(F(\psi_o-2\psi_\beta)/RT)K_{XOCuOx3}$	TLM[†]

[‡]Inner sphere complex, [†]Outer sphere complex

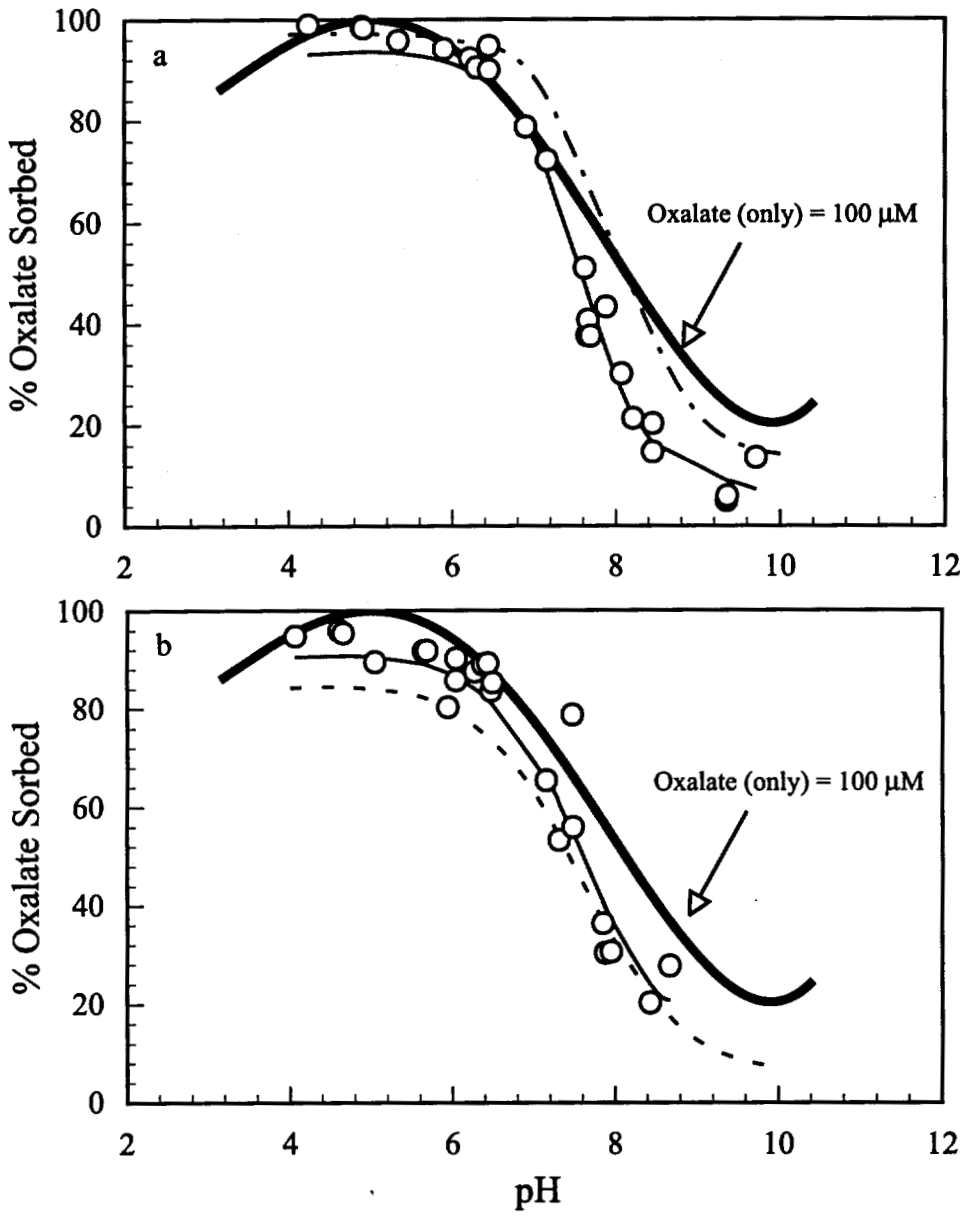

Figure 4.3 DLM fits for adsorption of a) 100 µM oxalate with 8.3 µM Cu, and b) 100 µM oxalate with 38 µM Cu onto AC. The adsorption of oxalate (only) calculated with MINTEQA2 and constants optimized with FITEQL are shown as ▬▬ . The FITEQL fits for the data is shown as ——— . The dashed line is the prediction of oxalate adsorption based on effective adsorption constants for 100 µM oxalate with 8.3 µM Cu (- - -) and 100 µM oxalate with 38 µM Cu (— - —).

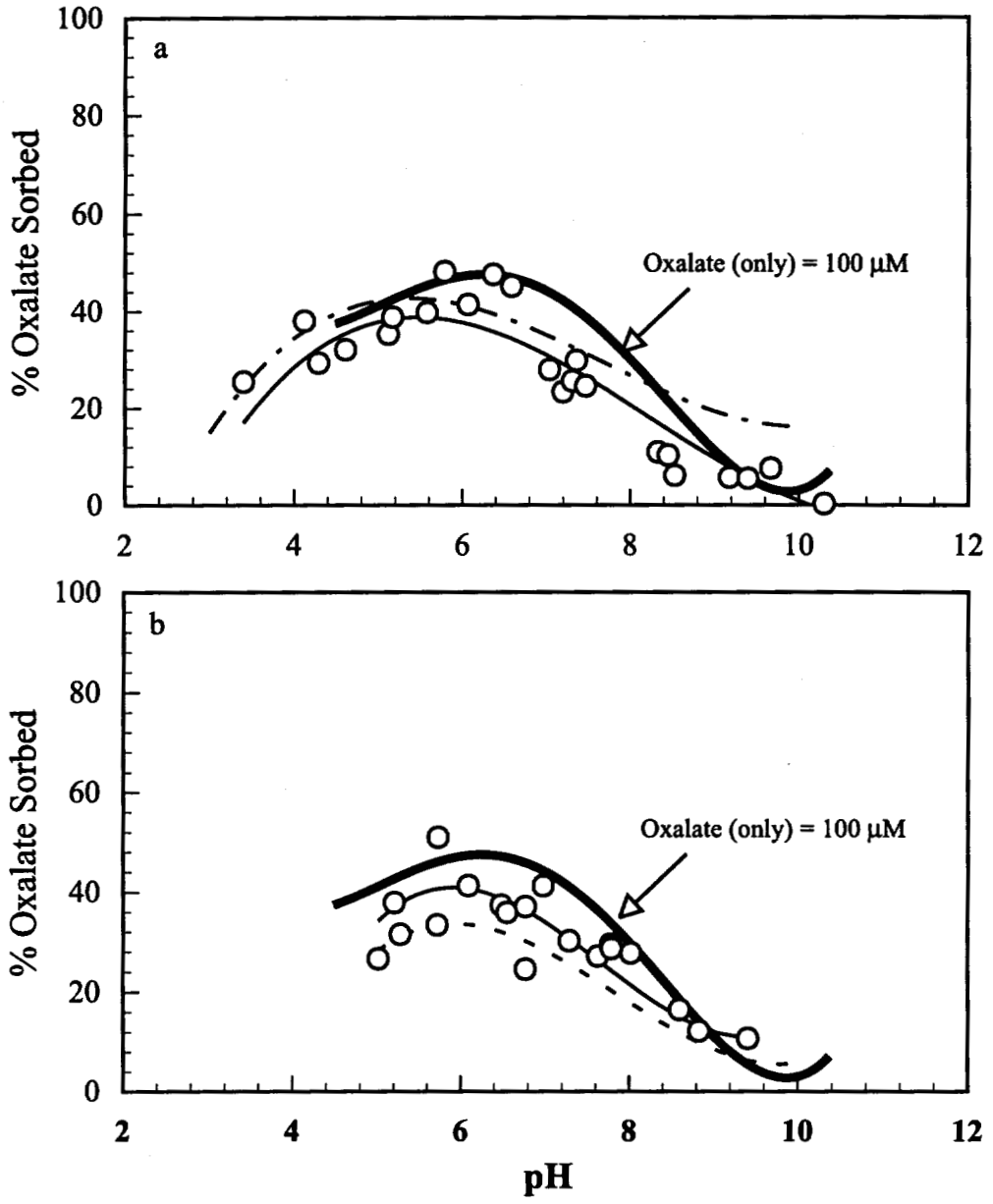

Figure 4.4. DLM fits for adsorption of a) 100 µM oxalate with 8.3 µM Cu, and b) 100 µM oxalate with 38 µM Cu onto MU. The adsorption of oxalate (only) calculated with MINTEQA2 and constants optimized with FITEQL are shown as ▬▬ . The FITEQL fits for the data is shown as ——— . The dashed line is the prediction of oxalate adsorption based on effective adsorption constants for 100 µM oxalate with 8.3 µM Cu (- - -) and 100 µM oxalate with 38 µM Cu (— · —).

Table 4.3. Characteristics for Cu*-Ox adsorption onto Artificially Coated (AC), Milford Coated (MC), and Milford Uncoated (MU) given as the pH of minimum adsorption (pH_{min}), pH of maximum adsorption (pH_{max}), and pH of 50% adsorption (pH_{50}).

Soil	[Ox] = 1000 μM						[Ox] = 100 μM					
	[Cu] = 121 μM			[Cu] = 27 μM			[Cu] = 38 μM			[Cu] = 8.3 μM		
	pH_{min}	pH_{50}	pH_{max}	pH_{min}	pH_{50}	pH_{max}	pH_{min}	pH_{50}	pH_{max}	pH_{min}	pH_{50}	pH_{max}
MU	6.50	7.80	9.00	-	7.40	9.00	4.75	6.55	7.75	4.50	6.50	7.75
MC	6.50	7.50	9.00	-	6.80	9.00	3.50	6.40	7.50	3.50	5.60	7.25
AC	6.75	7.45	8.50	-	7.25	8.00	3.50	5.60	7.50	3.00	4.90	6.50

whereas for MC and MU it shifted upward to $pH_{max} \simeq 6$. The pH_{min} for AC, MC, and MU was at pH > 10.

MINTEQA2 calculations with constants in Table 4.1 and Table 3.3 showed that $C_2O_4^{2-}$, $Cu(C_2O_4)_2^{2-}$ and CuC_2O_4 were the dominant aqueous species over the pH range of interest. Aqueous $C_2O_4^{2-}$ was always in excess of bound forms. The concentrations of $Cu(C_2O_4)_2^{2-}$ and $CuC_2O_4^{\circ}$ differed by half a log unit over the pH range of interest and their relative importance varied with Ox_T. In the presence of Ox_T = 1 mM, $Cu(C_4O_4)_2^{2-}$ was the dominant aqueous Cu species whereas $CuC_2O_4^{\circ}$ was the dominant aqueous Cu species in the presence of Ox_T =100 μM.

The surface and aqueous species that must be included in the adsorption model were deduced by comparing the adsorption of an ion in the presence and absence of another ion. The ratio of adsorbed oxalate in the presence of Cu to the adsorption in the absence of Cu ($\Gamma_{Cu\text{-}Ox^*}$ and Γ_{Ox}, respectively) and the ratio of adsorbed Cu in the presence of oxalate to that in the absence of oxalate ($\Gamma_{Cu^*\text{-}Ox}$ and Γ_{Cu}, respectively) are measures of the influence of one ion on the adsorption of another. A ratio of one indicates no influence and the adsorption may be modeled as if it were a single adsorbate system. A ratio different from one suggests the contrary.

$\Gamma_{Cu\text{-}Ox^*}/\Gamma_{Ox}$ equal to one for pH 3.5 to 8.5 indicating that oxalate in the presence of lower Cu concentrations may be modeled with only the oxalate species. $\Gamma_{Cu^*\text{-}Ox}/\Gamma_{Cu}$ was

calculated from the edges for Cu*-Ox and Cu although total Cu was different in the presence and absence of oxalate. We plotted $\Gamma_{Cu^*\text{-}Ox}/\Gamma_{Cu}$ against the ratio of total Cu in the presence of oxalate (Cu_T^{Ox}) and total Cu in the absence of oxalate (Cu_T), i.e., plotted Cu_T^{Ox}/Cu_T vs $\Gamma_{Cu^*\text{-}Ox}/\Gamma_{Cu}$ (Figure 4.5). Linear regression on this data ($r^2 = 0.98$) showed that for $Cu_T^{Ox}/Cu_T = 1$ (same total Cu in the presence and absence of oxalate), $\Gamma_{Cu^*\text{-}Ox}/\Gamma_{Cu} \approx 0.71$ for pH 4 to 6. Thus, the influence of oxalate on the adsorption of Cu must be accounted for in the model.

4.4.1 Modeling Adsorption of Cu*-Ox

Models using a Cu surface species $\equiv XOCu^+$ along with aqueous complexes of Cu and oxalate closely reproduced Cu adsorption onto AC in the presence of $Ox_T = 100$ μM and 1 mM, as shown in Fig. 4.1 and 4.2 and Table 4.4. The adsorption of Cu*-Ox onto MC was also modeled with the DLM and CCM with the same surface species, and with similar results (Table 4.4). For MU, the fits deteriorated for $Cu_T = 121$ μM with $Ox_T = 1$ mM. A Type A ternary complex ($\equiv XOCuC_2O_4^-$; *8, 10*) did not improve the fit and at higher adsorbate concentrations ($Cu_T = 121$ μM with $Ox_T = 1$ mM) gave a statistically poorer fit (Table 4.5). Including the Type B species also did not improve the fit. For the TLM, Cu*-Ox adsorption onto AC, MC, and MU was modeled with an inner-sphere Cu species $\equiv XOCu^+$ (see Table 4.6). Using an inner-sphere Type A and an outer-sphere Type B species ($(\equiv XOH_2^+)_2$-$Cu(C_2O_4)_2^{2-}$), only marginally improved the fit and was omitted. For most cases smaller adsorbate concentrations gave a larger optimal effective surface complexation constant (K^{eff}) (Fig. 4.6).

We obtained the best extrapolation when we used the K^{eff} values from one Ox_T to reproduce the Cu*-Ox edges for the same Ox_T but at different Cu_T (Fig. 4.1 and 4.2). We could not accurately extrapolate K^{eff} obtained for Cu adsorption in the presence of one Ox_T to reproduce Cu adsorption in the presence of another Ox_T. Thus, the K^{eff} for a given Cu_T and Ox_T underpredicted the adsorption of smaller Cu_T and Ox_T but overpredicted the adsorption of larger Cu_T and Ox_T.

4.4.2. Modeling Adsorption of Cu-Ox*

With the DLM and CCM we were able to model oxalate adsorption onto AC in the presence of Cu using only the oxalate surface species $\equiv XC_2O_4^-$ and $\equiv XOC_2O_4^{3-}$ (Table 4.7 and

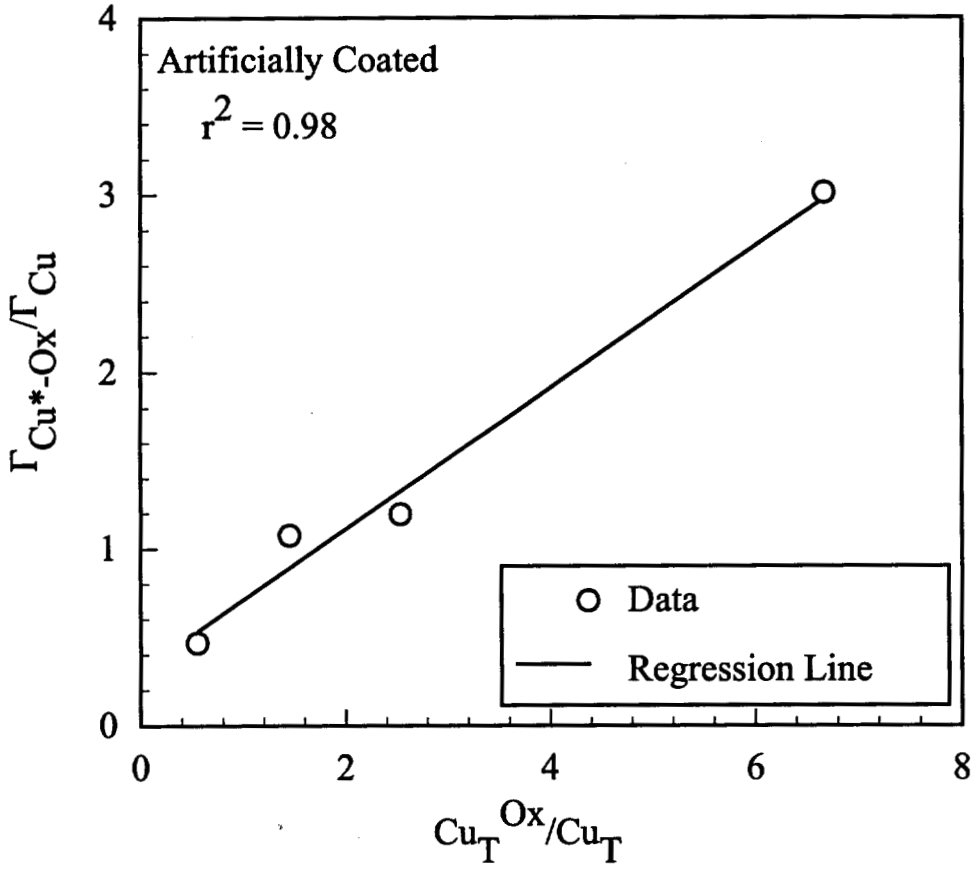

Figure 4.5. The relationship for the adsorption of various concentrations of total Cu in the presence of oxalate ($Cu_T{}^{Ox}$) to the adsorption of various concentrations of Cu (Cu_T).

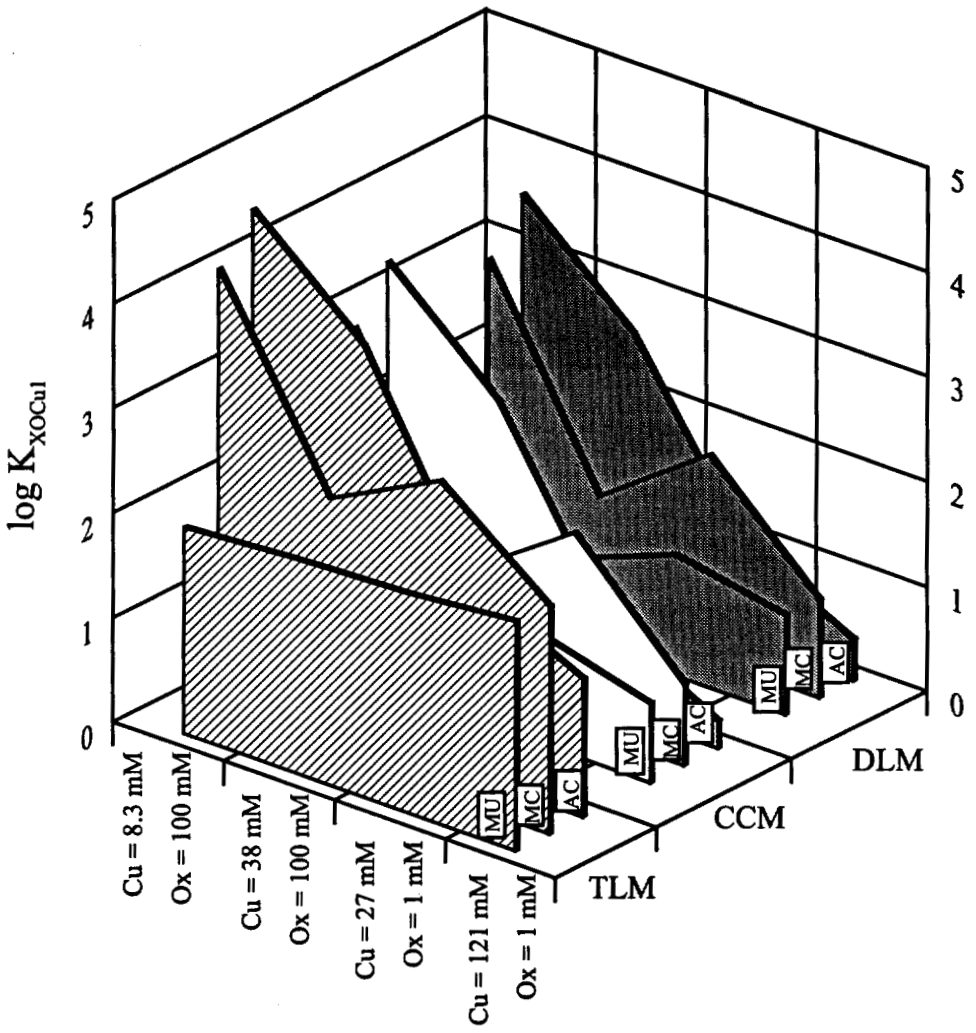

Figure 4.6. The variation in the effective surface complexation constant of Cu in the presence of oxalate (K_{XOCu1}) wth respect to the total adsorbate concentrations. The adsorbate concentrations are 8.3 and 38 μM Cu with 100 μM oxalate, and 27 and 121 μM Cu with 1 mM oxalate and these are indicated on the x-axis.

Table 4.4. Effective surface complexation constant and goodness of fit for adsorption of Cu*-Ox onto AC, MC, and MU with CCM and DLM.

Model	[Ox] μM	[Cu] μM	V_Y	log K_{XOCu1}
AC, DLM	100	8.3	0.85	3.52±0.11
		38.0	11.35	2.56±0.04
	1000	27.0	7.58	0.94±0.06
		121.0	2.9	0.39±0.06
AC, CCM	100	8.3	0.86	3.52±0.11
		38.0	11.53	2.56±0.02
	1000	27.0	7.82	0.83±0.06
		121.0	2.55	0.26±0.02
MC, DLM	100	8.3	1.16	3.06±0.15
		38.0	18.03	1.17±0.05
	1000	27.0	7.51	1.94±0.06
		121.0	11.82	0.93±0.01
MC, CCM	100	8.3	1.17	3.05±0.15
		38.0	18.44	1.11±0.06
	1000	27.0	7.9	1.85±0.07
		121.0	7.79	0.77±0.01
MU, DLM	100	8.3	1.03	0.94±0.18
		38.0	1.19	0.74±0.06
	1000	27.0	3.57	1.15±0.04
		121.0	117.2	0.95±0.02
MU, CCM	100	8.3	1.06	0.87±0.17
		38.0	1.45	0.65±0.06
	1000	27.0	3.64	1.04±0.04
		121.0	85.43	0.75±0.02

Table 4.5. Comparison of DLM fits for Cu-oxalate adsorption onto AC with only Type A (log $K_{XOCuOx1}$), and with Cu-only (log K_{XOCu1}) surface species. Low V_Y indicates better fit of the data.

Ox_T μM	Cu_T μM	log $K_{XOCuOx1}$	log K_{XOCu1}	V_Y
100	8.3	5.20±0.12		0.99
			3.52±0.11	0.85
	38	4.51±0.04		12.62
			2.56±0.04	11.35
1000	27	2.95±0.04		3.73
			0.94±0.14	7.58
	121	2.84±0.09		36.74
			0.39±0.06	2.9

the model fit in Fig. 4.3). This is not surprising given that Ox_T = 100 μM was in twelvefold excess of Cu_T = 8.3 μM. However, for Cu_T = 38 μM, the oxalate-only model still gave acceptable (though less good) fits even though oxalate was in less than threefold excess. The edges for MC and MU were modeled with the same species by including Al dissolved from the surface, its complexation in solution, and the competition between dissolved Al and the surface for oxalate (see Table 4.7, Fig. 4.4). For TLM the outer-sphere species $\equiv XOH_2^+$-$C_2O_4^{2-}$ alone reproduced Cu-Ox* on AC (V_Y always < 26 in Table 4.8) and Cu-Ox* on MC and MU was modeled with the same surface species after accounting for the Al dissolved from the surface.

The K^{eff} values fitted to one Cu-oxalate edge reasonably reproduced the Cu-Ox* data for other Cu_T and Ox_T, although the extrapolated predictions are systematically slightly over or under the data, as shown in Figs. 4.3 and 4.4. Extrapolating from 8.3 μM to 38 μM Cu_T underpredicts oxalate adsorption by about 10%, whereas the reverse extrapolation overpredicts adsorption.

Table 4.6. Effective surface complexation constant and goodness of fit for adsorption of Cu*-Ox onto AC, MC and MU with TLM.

Model	[Ox] μM	[Cu] μM	V_Y	log K_{XOCu1}
TLM, AC	100	8.3	0.85	4.68±0.12
		38.0	11.15	3.74±0.03
	1000	27.0	8.81	1.82±0.06
		121.0	3.44	1.31±0.02
TLM, MC	100	8.3	1.15	4.27±0.15
		38.0	17.55	2.45±0.06
	1000	27.0	7.99	2.99±0.07
		121.0	24.77	2.17±0.01
TLM, MU	100	8.3	1.07	1.97±0.18
		38.0	0.74	2.04±0.06
	1000	27.0	3.79	2.09±0.04
		121.0	229.34	2.19±0.03

4.4.5 Modeling Simultaneous Adsorption of Cu and Oxalate

Binary Cu ($\equiv XOCu^+$) and oxalate ($\equiv XC_2O_4^-$ and $\equiv XOC_2O_4^{3-}$) species modeled simultaneous adsorption of Cu and oxalate onto AC, MC, and MU with DLM and CCM (V_Y < 50 in all but one case; Table 4.9). For the TLM, the same Cu species and an outer-sphere oxalate species ($\equiv XOH_2^+$-$C_2O_4^{2-}$) together reproduced the adsorption of Cu and oxalate onto AC and MC. Adsorption onto MU was accurately modeled for Cu_T = 8.3 μM but was less well modeled for Cu_T = 38 μM (Table 4.9).

4.4.6 Sensitivity of Cu*-Ox Modeling to pK_a and N_s

A wide range of surface protonation constant (pK_a) values worked well for Cu in the presence of oxalate (indicated in Table 4.10). The insensitivity to the pK_a values did not change with an order of magnitude change in Ox_T. The optimized K^{eff} values were sensitive to the choice of pK_a values. Although not shown here, the adsorption of Cu-Ox*, and

Table 4.7. Surface complexation constant and goodness of fit for adsorption of Cu-Ox* onto AC, MC, and MU with CCM and DLM

Model	[Ox] μM	[Cu] μM	V_Y	log K_{XOx2}	log K_{XOx3}
DLM, AC	100	8.3	8.04	11.08±0.02	-6.01±0.04
		38	12.12	11.52±0.02	-5.59±0.06
CCM, AC	100	8.3	7.06	10.85±0.02	-6.42±0.04
		38	9.95	11.22±0.02	-5.85±0.05
DLM, MC	100	8.3	20.81	11.61±0.01	-4.76±0.08
CCM, MC	100	8.3	N.C[¶]		
DLM, MU	100	8.3	13.73	11.97±0.02	-5.38±0.09
		38	19.40	12.27±0.02	-4.23±0.11
CCM, MU	100	8.3	27.02	12.27±0.02	-5.94±0.10
		38	12.42	12.56±0.02	-4.99±0.11

[¶]No Convergence: Can neglect the a species by assigning log K_{XOx3} = -12 to achieve convergence

simultaneous adsorption of Cu and oxalate were also insensitive to the pK_a values.

As with Cu (only) adsorption, the adsorption of Cu in the ternary complex was modeled accurately for most cases with more than two orders of magnitude variation in N_s (Fig. 4.7a). The range of N_s values was narrower for 121 μM Cu. For oxalate concentration in the ternary complex (100 μM) comparable to the highest Cu concentration (121 μM) the range of N_s values that accurately reproduced the oxalate edges was much smaller (Fig. 4.7b). The simultaneous adsorption of both Cu (8.3 and 38 μM) and oxalate (100 μM) in the mixture was also sensitive to N_s (Fig. 4.7c) because oxalate was always in excess (Ox_T > Cu_T).

4.5 Discussion

The adsorption of mixtures of Cu and oxalate onto sands coated with various amounts of Fe and Al oxides was modeled with SCMs with pK_a values for goethite and N_s for single

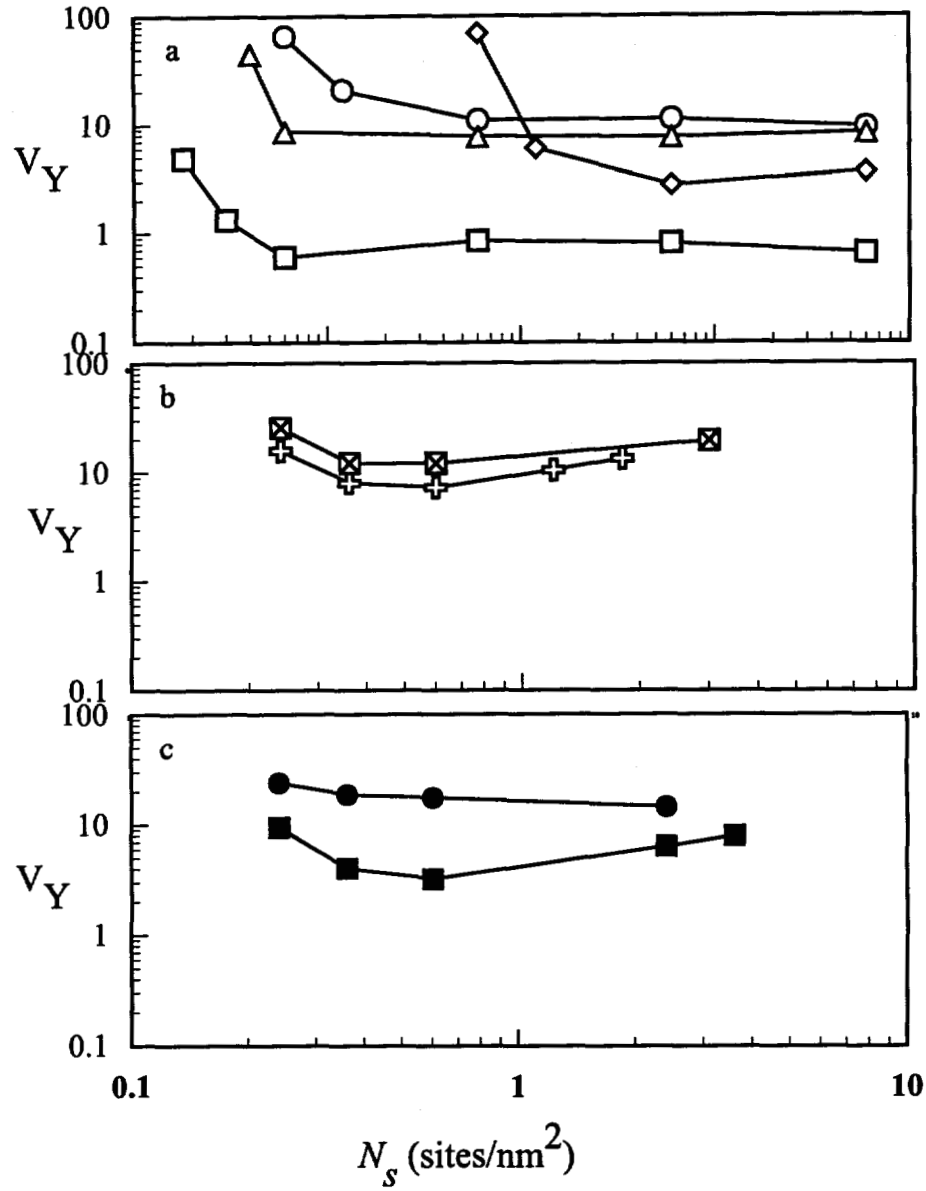

Figure 4.7. The sensitivity of DLM fits to the choice of N_s for a) adsorption of Cu in the presence of oxalate, b) adsorption of oxalate in the presence of Cu, and c) simultaneous adsorption of Cu and oxalate. The symbols □ and O are for adsorption of 8.3 and 38 μM Cu in the presence of 100 μM oxalate, △ and ◇ for 27 and 121 μM Cu with 1 mM oxalate, ✣ and ⊠ for 100 μM oxalate with 8.3 and 38 μM Cu, ■ for simultaneous adsorption of 8.3 μM Cu along with 100 μM oxalate and ● for simultaneous adsorption of 38 μM Cu and 100 μM oxalate.

Table 4.8. Effective surface complexation constant and goodness of fit for Adsorption of Cu-Ox* onto AC, MC, and MU with TLM.

Sample	[Ox] μM	[Cu] μM	V_Y	log K_{XOx3}
AC	100	8.26	25.9	10.99±0.01
		38	19.32	11.06±0.01
MC	100	8.26	20.16	11.81±0.01
MU	100	8.26	17.66	11.53±0.01
		38	14.61	11.76±0.01

ion adsorption of Cu and oxalate. Including either a Type A or a Type B ternary complex did not improve the fit and in some cases gave poorer fits. The modeling was accurate over a wide range of conditions for AC and MC. For MU, fit was poorer for the adsorption of Cu_T = 121 μM with Ox_T = 1 mM.

In the presence of oxalate, Cu adsorption is depressed at the higher pH values (Fig.4.1 and 4.2). The fractional adsorption of Cu in the absence of any complexing ligand is calculated as:

$$\alpha_s^{Cu} = \frac{[\equiv XOCu^+]}{[Cu^{2+}] + [\equiv XOCu^+]} \qquad (4.1)$$

The fractional adsorption of Cu in the presence of oxalate (assuming no ternary surface complexes) is calculated as:

$$\alpha_s^{Cu^{2+}\text{-}Ox} = \frac{[\equiv XOCu^+]}{[CuC_2O_4^0] + [Cu^{2+}] + [\equiv XOCu^+] + [Cu(C_2O_4)_2^{2-}]} \qquad (4.2)$$

Oxalate is in the fully deprotonated form at pH > 4.5. The adsorption of oxalate also decreases at pH > 4. Although the surface is more favored for Cu adsorption at higher pH, oxalate in solution competes with the surface sites to form stable Cu-oxalate complexes in solution. This competition between the surface and the oxalate in solution diminishes

Table 4.9. Effective surface complexation constant and goodness of fit for simultaneous adsorption of Cu and 100 μM onto AC, MC, and MU with CCM, DLM, and TLM.

Sample	Cu_T μM	Model	V_Y	log K_{XOx2}	log K_{XOx3}	log K_{XOCu1}	log K_{OxC4}
AC	8.3	DLM	3.74	10.96±0.02	-6.13±0.03	2.18±0.12	
		CCM	3.51	10.72±0.02	-6.41±0.03	1.62±0.12	
		TLM	12.47			3.49±0.13	11.01±0.01
	38	DLM	25.2	10.87±0.02	-5.83±0.05	1.16±0.05	
		CCM	19.8	10.51±0.03	-6.00±0.03	0.59±0.05	
		TLM	32.64			2.48±0.05	11.01±0.01
MC	8.3	DLM	9.74	11.61±0.02	-5.01±0.08	1.90±0.17	
		CCM	N.C.[¶]				
		TLM	29.57			2.70 ±0.16	11.80±0.01
MU	8.3	DLM	5.31	11.98 ±0.02	-5.64 ±0.11	0.45 ±0.21	
		CCM	12.72	12.28 ±0.02	-6.07 ±0.11	0.51 ±0.21	
		TLM	9.12			6.85±0.19	11.55±0.01
	38	DLM	11.34	11.99 ±0.03	-5.84 ±0.13	0.37 ±0.06	
		CCM	9.4	12.44 ±0.02	-5.65 ±0.12	0.33 ±0.12	
		TLM	90.46			0.12±0.02	11.67±0.01

Table 4.10. Selected results for modeling the adsorption of Cu*-Ox onto AC with surface protonation constants for various solids (Collected from Table 1, Huang et al. [*12*])

Solid	Ox_T	Cu_T	Model	pK_{a1}	pK_{a2}	V_Y	log K_{XOCu1}
γ-Al_2O_3	100 μM	38 μM	DLM	7.2	9.5	10.69	1.89±0.03
				5.7	11.5	8.31	0.70±0.03
α-Al_2O_3				8.5	9.7	11.58	3.15±0.03
$Fe(OH)_3$				5.1	10.7	6.91	0.33±0.03
α-FeOOH				7	8.4	10.42	1.71±0.03
				4.2	10.8	4.32	-0.06±0.03
γ-FeOOH				3.9	10.5	3.68	-0.14±0.03
TiO_2				5.4	6.4	8.58	0.48±0.02
				2.6	9.4	3.27	-0.30±0.02
γ-Al_2O_3	1 mM	27 μM	DLM	7.2	9.5	6.76	0.52±0.06
				5.7	11.5	4.13	0.10±0.05
α-Al_2O_3				8.5	9.7	8.17	1.36±0.06
$Fe(OH)_3$				5.1	10.7	3.43	0.06±0.04

Table 4.10 (Continued). Selected results for modeling the adsorption of Cu*-Ox onto AC with surface protonation constants for various solids (Collected from Table 1, Huang et al. [*12*]).

Solid	Ox_T	Cu_T	Model	pK_{a1}	pK_{a2}	V_Y	log K_{XOCu1}
α-FeOOH	1 mM	27 μM	DLM	7	8.4	6.92	0.37±0.06
				4.2	10.8	2.96	0.04±0.04
γ-FeOOH				3.9	10.5	2.89	0.04±0.04
TiO_2				5.4	6.4	5.08	-0.38±0.05
				2.6	9.4	2.82	0.02±0.04

fractional Cu adsorbed at higher pH values.

The adsorption of Cu in the presence of oxalate is modeled by including the adsorption of Cu (only) along with and the aqueous complexation of Cu and oxalate. Oxalate concentrations of 100 μM and 1 mM do not saturate all adsorption sites in AC and MC. Cu binds to any available sites and hence can be modeled by a Cu only surface species. For MU, Ox_T = 1 mM nearly saturates the surface sites and we are unable to obtain good fits for adsorption of Cu_T = 121 μM (large V_Y values in Table 4.4 and 4.6). Similarly, we were able to use a oxalate (only) surface species along with aqueous complexation of Cu and oxalate to reproduce the adsorption of Ox_T = 100 μM in the presence of Cu. Oxalate is always in excess ($Ox_T > 3Cu_T$) and its adsorption can be modeled by neglecting any Cu that may adsorb on the surface as a Cu-oxalate ternary complex. The simultaneous adsorption of Cu and oxalate was modeled with Cu (only) and oxalate (only) surface species.

The surface charge (σ) for adsorption of Cu in the presence of Ox_T = 100 μM mimics the charge developed by the single adsorbate Ox_T = 100 μM (see Fig. 4.8a) because oxalate is always in excess. For the same pH range, the electrostatic correction factor (P) for adsorption of Cu-oxalate mixture did not vary more than Cu (only) or oxalate (only) adsorption (Fig. 4.8b). Near surface electrostatic forces do not seem to influence the adsorption of Cu and oxalate in the ternary system any more than in the Cu and oxalate single adsorbate systems.

For adsorption of Cu in the presence oxalate, when we used $\equiv XOCu^+$ we were able to somewhat accurately extrapolate K^{eff} values obtained for Cu adsorption in the presence of one ligand concentration to reproduce adsorption of other concentrations of Cu in the presence of same concentration of the ligand (Fig. 4.1 and 4.2). We were however unable to extrapolate K^{eff} values for Cu adsorption between different concentrations of the ligand. The extrapolation did not improve even when we used Type A ternary complexes. Such inaccuracy in extrapolation is due to deficiencies in extrapolating site heterogeneity and competition over different concentration ranges.

The site heterogeneity revealed by an adsorbate depends on the total adsorbate concentration, as indicated in Chapter 2. When Cu in the presence of oxalate is used to probe

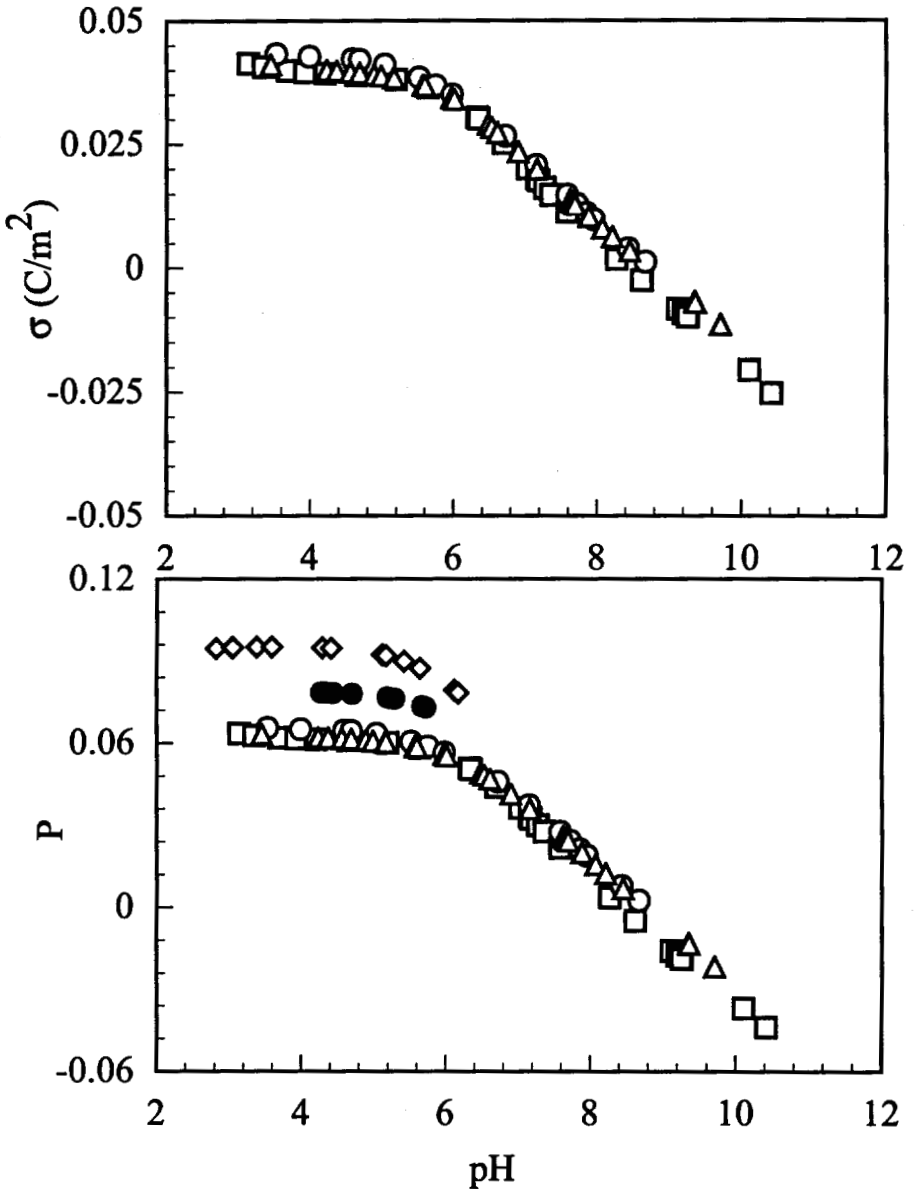

Figure 4.8. The near surface electrostatic parameters calculated with the DLM and plotted as a function of pH; a) the surface charge (σ) and b) electrostatic correction factor (P). The symbols O is for simultaneous adsorption of 8.3 μM Cu along with 100 μM oxalate, Δ for simultaneous adsorption of 38 μM Cu along with 100 μM oxalate, □ for adsorption of 100 μM oxalate (only), ● and ◇ for 5.7 and 15 μM Cu (only).

the surface, larger Cu_T reveals greater site heterogeneity since it binds to more site types on the soil surface. The K^{eff} values in this case is smaller because it includes binding to both weaker and stronger sites (Tables 4.4 - 4.7). Smaller adsorbate concentrations preferentially bind to stronger adsorption sites and the K^{eff} values are larger. The optimal K_{XOCu1} values decreased with increase in Cu_T and Ox_T (e.g., Table 4.4). For DLM, log K_{XOCu1} = 3.52 for Cu_T = 8.3 μM with Ox_T = 100 μM whereas log K_{XOCu1} = 0.39 for Cu_T = 121 μM with Ox_T = 1 mM. For the same concentration of oxalate, inaccuracy in extrapolating constants for Cu binding may be due primarily to site heterogeneity and secondarily due to competition. For different ligand concentrations inaccuracy in extrapolation may be primarily due to competition and secondarily due to site heterogeneity.

Excess oxalate dissolves Al and Fe from the oxide surface during equilibration and changes the equilibrium speciation. The dissolution is not important for the adsorption of Cu in the presence of Ox_T = 1 mM because Cu adsorption is negligible below pH 6 and dissolution is unimportant at pH > 6. However, in the presence of Ox_T = 100 μM a significant portion of the Cu*-Ox edge lies in the pH range of 4 - 6 and can be influenced by shifts in equilibrium due to dissolution of metal oxides. The concentration of dissolved Fe was small (< 5 μM) for Ox_T = 100 μM, and was neglected. For MC and MU, the concentration of dissolved Al was more than an order of magnitude greater than the concentration of dissolved Fe. The adsorption of Cu*-Ox onto MC and MU could be successfully modeled without including dissolved Al (e.g., see Table 4.4) but reproducing the adsorption of Cu-Ox* required including the competition between the surface and the dissolved Al for the oxalate (e.g., see Table 4.7).

Conditional stability constants (K_{cond}) (*13*) suggest Fe-oxalate is more stable than Al-oxalate or Cu-oxalate at pH < 4 (illustrated in Fig. 4.9). Al-oxalate is more stable than Cu-oxalate at pH < 6. Although Fe-oxalate in solution is more favored than Cu-oxalate it is unimportant in our experiments because of its small concentration. A large concentration of dissolved Al will compete with Cu for the oxalate in solution and will not change the adsorption of Cu in the presence of oxalate. In addition, the Cu*-Ox edges for AC, MC, and MU (characterized in Table 4.3) are similar, although the concentrations of dissolved metal

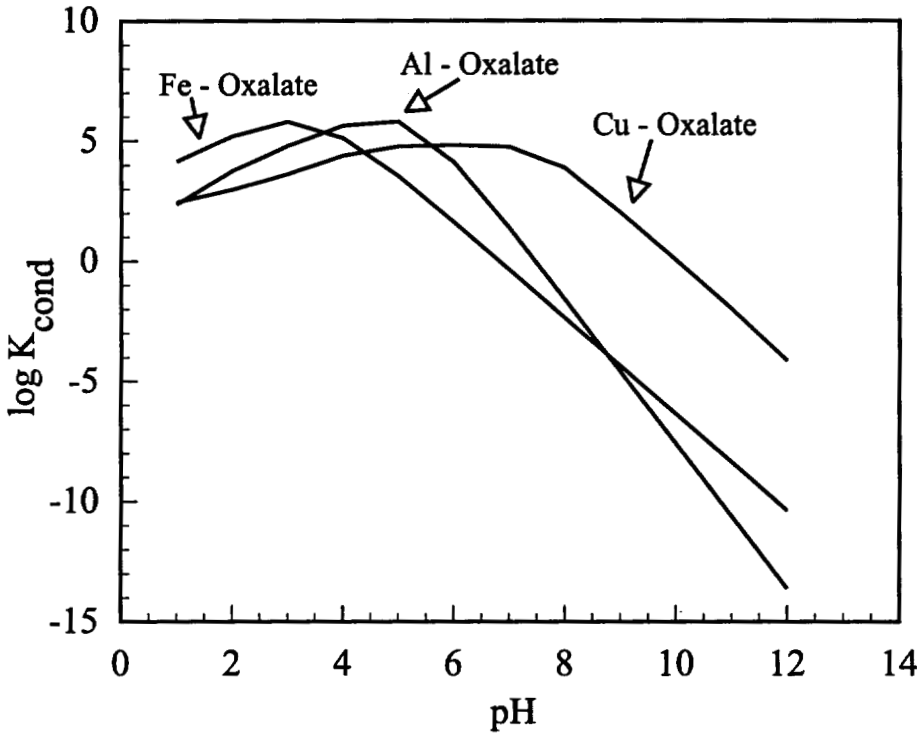

Figure 4.9. Calculation of conditional stability constant (K_{cond}) as a function of pH for the aqueous complexation of Fe-oxalate, Al-oxalate, and Cu-oxalate

oxide is significantly different indicating the insensitivity of the edge to dissolved oxides.

The modeling of Cu*-Ox adsorption was insensitive to N_s and pK_a. The adsorption of Cu-Ox* and simultaneous adsorption of Cu and oxalate was sensitive to N_s but insensitive to pK_a. Insensitivity of the fits to modeling parameters (N_s and pK_a) suggests that errors in estimates of these parameters will not influence the fits to the data. This is encouraging because it is very difficult to obtain accurate estimates of these parameters for natural soil samples. Conversely, such insensitivity makes the SCMs ineffective for diagnosing microscale adsorption processes.

A homogeneous-site SCM calibrated to the acid-base properties of goethite, and to the adsorption of single adsorbate Cu and oxalate reproduced the adsorption of a moderately wide range of concentrations of Cu and oxalate in the ternary system. The ability to model the edge was insensitive to the values of pK_a and sensitive to the values of N_s. The simultaneous adsorption of Cu and oxalate onto some coated sands was not always reproduced accurately with SCMs. It was not always possible to use K^{eff} values obtained from one Cu-Oxalate edge to reproduce adsorption for the other concentrations.

4.6 References

(1) Benjamin, M.M. and Leckie, J.O. *Environ. Sci. Technol.*, **1981**, 15(9):1050-1057.

(2) Davis, J.A. and Leckie, J.O. *Environ. Sci.Technol.*, **1978**, 12(12):1309-1315.

(3) Vuceta, J. *Adsorption of Pb(II) and Cu(II) on α - Quartz from Aqueous Solution: Influence of pH, Ionic Strength, and complexing Ligands*, Ph.D. Thesis, **1976**, California Institute of Technology, Pasadena, CA.

(4) Huang, C.P.; Elliott, H.A.; and Ashmead, R.M. *J. Water Poll. Cont. Fed.*, **1977**, 49:745.

(5) Richter, R.O. and Theis, T.L. "Adsorption Reactions of Nickel Species at Oxides Surface," *175th National Meeting of the American Chemical Society*, Anaheim, Calif., **1978**, March 12-17.

(6) Elliott, H.A. and Huang, C.P. *J. Colloid Interface Sci.*, **1979**, 70(1):29-45.

(7) Bowers, A.R. and Huang, C.P. *J. Colloid Interface Sci.*, **1986**, 110(2):575-590.

(8) Park, Y.J.; Jung, K.H.; and Park, K.K. *J. Colloid Interface Sci.*, **1995**, 172:1-12.

(9) Bourg, A.C. and Schindler, P.W. *Chimia*, **1978**, 32:116.

(10) Schindler, P.W. in *Mineral-Water Interface Geochemistry*, M.F. Hochella, Jr., and A.F. White (eds), Reviews in Mineralogy, **1990**, Vol. 23, Mineralogical Society of America, Washington D.C.

(11) Smith, R.M. and Martell, A.E. *Critical Stability Constants: Other Organic Ligands*, **1977**, Vol. 3, Plenum Press, New York.

(12) Huang, C.P,.; Hsieh, S.; Park, S.W.; Corapcioglu, M.O.; Bowers, A.R.; Elliott, H.A. "Chemical Interactions Between Heavy Metal Ions and Hydrous solids," in *Metal Speciation, Separation, and Recovery*, Ed. Parretson, J.W. and Passino, R., Proceedings of the International Symposium on Metal Speciation, Separation, and Recovery, Chicago, Illinois, July 27 - August 1, **1986**, 437-474.

(13) Bowers, A.R. and Huang, C.P. *Wat. Res.*, **1987**, 21(7):757-764.

CHAPTER 5*

SEMI-EMPIRICAL DISCRETE pK_a SPECTRUM APPROACH FOR MODELING ADSORPTION OF OXALATE, COPPER, and COPPER-OXALATE COMPLEXES ONTO METAL OXIDE COATED SANDS

5.1 Abstract

Sands coated with metal oxides are often heterogeneous and contain multiple site classes. We modified the discrete pK_a spectrum (DPS) approach of Westall et al. (*1*) to model the adsorption of Cu, oxalate, and mixtures of Cu and oxalate onto somewhat heterogeneous sands artificially and naturally coated with various amounts of Fe and Al oxides. Although the acid-base titration curve was closely reproduced with two adsorption sites (a four pK_a model), the adsorption of a moderately wide range of concentrations of Cu, oxalate, and mixtures of Cu and oxalate was often reproduced with only one of those sites. Only the competition between the dissolved Al and the surface for the oxalate was more accurately reproduced with both sites.

---

* To be submitted to *Environmental Science & Technology*

5.2 Introduction

Various elaborations of the homogeneous-site surface complexation model (SCM) are commonly used to reproduce adsorption of metals, ligands, and metal-ligand complexes, including the Diffuse Layer Model (DLM), the Constant Capacitance Model (CCM), and the Triple Layer Model (TLM). Despite their general success they often poorly reproduce adsorption across large sorbate concentrations, probably because of the site heterogeneity, or a distribution of adsorption energies. Models that account for heterogeneous binding energies (See Table 1 in Westall et al. [*1*]) have mostly been developed to describe metal or proton coordination with humic materials and only some of these have been extended for adsorption onto minerals or soils (*2, 3*). One method is to invert an isotherm via the Fredholm integral of the first kind to derive a continuous distribution of "local" site strengths. However, this problem is ill posed and requires specialized semi-analytical techniques (*4 - 9*) and numerical methods (*2, 3, 10, 11*). To circumvent these difficulties, site strengths are sometimes assumed to have a predetermined continuous (*12*) or discrete (*1*) distribution. The assumption of a discrete distribution is often more useful and reliable than a continuous distribution (*13, 14*).

Some models of binding heterogeneity explicitly account for coulombic forces at the surface (*5, 6, 15 - 17*) but Westall et al. (*1*) argue persuasively that such electrostatic correction factors are invalid for complex adsorbents. Some of the basic assumptions of the electrostatic model, which was originally formulated for the Hg electrode, are overextended when applied even to pure metal oxides. These assumptions break down totally for adsorption onto complex structures such as humic substances and soils. Explicit representation of near-surface electrostatics does not inherently make a model more correct in its ability to represent reality: a nonelectrostatic discrete pK_a spectrum (DPS) successfully reproduces the adsorption of Co onto a natural humic material as a function of pH, for two ionic strengths, and over a wide range of Co concentrations (*1*).

Although the adsorption heterogeneity of humic substances is somewhat similar to that of the mineral components of soils, humic functional groups (e.g., carboxylic, phenolic) are distinctly different from metal oxides and clay minerals. In particular, adsorption sites on

metal oxides and clay edges are amphoteric: they gain and lose protons to attain positive and negative charge. Most humic functional groups only lose protons at common environmental pH values and thus attain only a negative charge. Cations and anions bind strongly to many common minerals, but only cations bind to humic materials. Also, the titration curves for different ionic strengths are parallel for humic materials (*1*) but intersect at the pristine point of zero charge (ppzc) for pure oxides (*18*).

The goal of this research was to extend the DPS approach of Westall et al. (*1*) from humate-metal binding to modeling the adsorption of metals and anions onto metal oxides. The extended model was tested for adsorption of Cu, oxalate, and Cu-Oxalate onto metal oxide coated sands: Artificially Coated (AC), Milford Coated (MC), and Milford Uncoated (MU).

5.3 Modeling Adsorption with DPS

5.3.1 Modeling Adsorption on Humic Acid and Metal Oxides

As indicated earlier, humates and metal oxides must be modeled with slightly different techniques. Na^+ exchange is important for humates (*19*) and implicitly accounts for some electrostatic effects in noncoulombic models of humic materials (*1*). Na^+ does not adsorb significantly on metal oxides. It is also not possible for a single Na^+ exchange reaction to account for the effects of ionic strength on metal oxide adsorption because the potentiometric titration curves for metal oxides intersect at the ppzc and diverge at higher or lower pH. Additional exchange reactions may reproduce the ionic strength dependence, they introduce more adjustable parameters. Parameter fitting routines such as FITEQL 3.1 can be unstable when more than four parameters are simultaneously optimized.

Humates are easily titrated to obtain acid-base titration curves. Similar titration is not always possible for coated sands because of mineral dissolution. While models of humic acids are calibrated to acid-base curves for individual humic acids, models of coated sands are more reliably calibrated to acid-base properties of isolated oxides. Titration data for humates are successfully modeled with only the ionization of the neutral monoprotic-acid sites (*1*).

Table 5.1. Parameters used to generate synthetic acid-base titration curve with MINTEQA2.

Surface Hydrolysis Reactions	**log K**
$[\equiv XOH_2^+] = [\equiv XOH^o]\{H^+\}\exp(-F\psi_o/RT)K_{a1}^{-1}$	-7.9†
$[\equiv XO^-] = [\equiv XOH^o]\{H^+\}^{-1}\exp(F\psi_o/RT)K_{a2}$	-10.7†
MINTEQA2 Model Parameters	**Values**
Solid Concentration (g/L)	3.5
Surface Area (m^2/g)	66
Site Concentration (mol/L)	5.75×10^{-4}
MINTEQA2 Setup Format	
Components: H^+, Na^+, Cl^-	
Adsorption Model: Diffuse Layer Model	
Input: Total H^+	
Calculate: pH	

†Mesuere and Fish (*20*)

Amphoteric metal oxides require modeling by diprotic acid sites, so adsorption onto metal oxides is optimized for twice as many pK_a values. An increase in adjustable parameters makes the fitting more arbitrary.

Westall et al. (*1*) model humate acid-base titration data with four sites having distinct pK_a's fixed at set intervals ($\Delta pK_a = 2$) prior to parameter fitting. Those researchers found that only two sites (corresponding to $pK_a = 6, 8$) contribute to the adsorption of Co. Natural oxide coated sands are composed of various mineral assemblages. So appropriate pK_a's cannot be predicted in advance.

5.3.2 Modeling Approach

The approach of Westall et al. (*1*) was modified to reproduce adsorption of an anion (oxalate), and a cation (Cu), as well as Cu-Oxalate mixtures onto metal oxide coated sands. The adsorption data modeled in this chapter was obtained in Chapters 2, 3, and 4. As in Westall et al. (*1*), the first step was to optimize the number of site classes, the total

Table 5.2. Parameters used to model synthetic acid-base titration curve with the discrete pK_a spectrum (DPS) approach

Surface Hydrolysis Reactions
$[\equiv X_iOH_2^+] = [\equiv X_iOH^o]\{H^+\}K^i_{a1}{}^{-1}$ (i = 1, n)
$[\equiv X_iO^-] = [\equiv X_iOH^o]\{H^+\}^{-1}K^i_{a2}$ (i = 1, n)
FITEQL Problem Setup Strategy
Components: H^+, X_iOH, Na^+, Cl^- (i = 1, n)
Species: H^+, OH^-, $X_iOH_2^+$, X_iO^-, Na^+, Cl^- (i = 1, n)
ΔpK_a: Constant
Adjustable Parameter: Individual pK_a Values
Optimize: T_{XiOH}
Serial Data
Total H^+, pH, Na^+, Cl^-
Solution From FITEQL Optimization
pK^i_{a1}: 5, 8
pK^i_{a2}: 11, 14
$T_{XOH(i)}$ (mol/L): 1.81×10^{-4}, 4.98×10^{-4}

concentration of sites, and the pK_a values from acid-base titration curves. Because acid-base titration of coated sands is experimentally difficult, we used literature values of goethite pK_a's (*20*) to generate a synthetic acid-base titration curve with MINTEQA2 using a DLM and assuming a background electrolyte of 0.05 M NaCl (see Table 5.1 for details of the procedure). Following Westall et al. (*1*) we used FITEQL 3.1 (*21*) to model the titration curve without correcting for electrostatic surface forces. The input parameters are summarized in Table 5.2. To complete the optimization, the pK_a values were changed while ΔpK_a (- log $K^i_{a1}K^i_{a2}$) was kept constant.

The surface sites, $\equiv X_iOH^o$ (i = number of site classes), gain or lose protons to form $\equiv X_iOH_2^+$ and $\equiv X_iO^-$, hence two pK_a values were needed for each site class. One, two, and

three discrete site classes were considered and ΔpK_a for each was kept constant (= 6). The pK_a pair for each class was varied heuristically until the best fit was obtained as gauged by a low value of V_Y. The ΔpK_a used here is larger than that used for SCMs. As explained in the discussion section, larger ΔpK_a compensate for the absence of electrostatic factor. It also minimizes the number of site classes needed, hence the number of adjustable parameters. Equilibrium expression and equilibrium constants for aqueous reactions were the same as those used in Chapters 3 and 4. Surface species were defined as $\equiv XC_2O_4H^o$ or $\equiv XC_2O_4^-$ for oxalate and $\equiv XOCu^+$ for Cu. For Cu in the ternary complex (denoted as Cu*-Ox), we used $\equiv XOCu^+$ along with the aqueous complexation of Cu and oxalate. Model parameters are summarized in Table 5.3. When sites were assumed to be unimportant they were assigned a very small effective surface complexation constant value ($\log K^{eff} = -12$).

5.4 Results

Two site classes ($pK^i_{a1} = 5, 8$ and $pK^i_{a2} = 11, 14$) reproduced the acid-base titration curves within ± 20% relative error (Fig. 5.1). The error is mostly due to small inflections, and the overall agreement is quite good. The model fit with three site classes ($pK^i_{a1} = 4, 6, 8$ and $pK^i_{a2} = 10, 12, 14$) tracked the titration curve more closely but we used two site classes for modeling adsorption of Cu and oxalate because the goal of the DPS approach is to model with a "small" set of surface sites. The range of pK_a values is greater than that for humic acid (*1*) probably because the average pK_a for Fe and Al oxides is generally higher than that for humic acid.

Either oxalate surface species ($\equiv XC_2O_4H^o$ or $\equiv XC_2O_4^-$) modeled adsorption of 10, 50, and 100 μM oxalate onto AC with similar accuracy as shown by the relatively close matches of the model curves and the data points in Fig. 5.2 and the similar V_Y values in Table 5.4. When we used only one site class we could closely reproduce the adsorption of 10 μM total oxalate (Ox_T) but the fits for the broader edges of Ox_T = 50 and 100 μM were somewhat less good. The fits were slightly improved when adsorption was modeled as simultaneous binding of oxalate to both sites to form $\equiv XC_2O_4^-$ as we did subsequently for MU and MC (Table 5.4, Fig. 5.3). When we assumed the surface species to be $\equiv XC_2O_4H^o$, we were unable to obtain

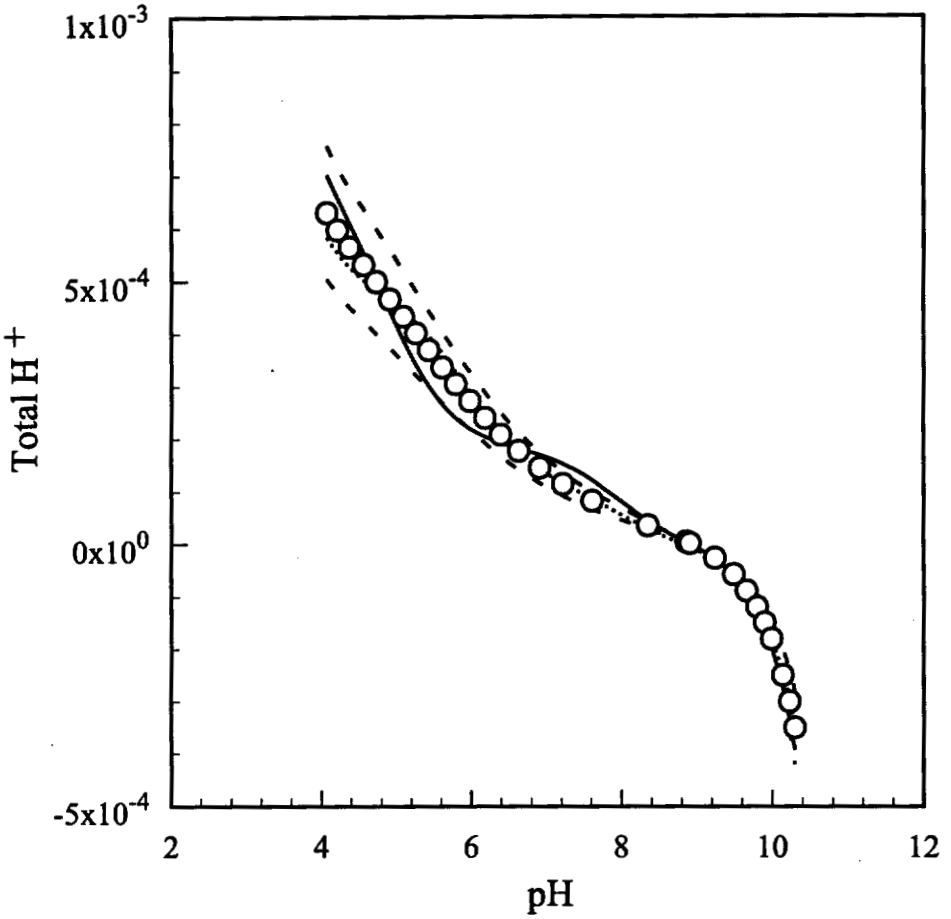

Figure 5.1. Acid-base titration data generated with MINTEQA2 and fitted with two ($\Delta pK_a = 6$; ———) and three ($\Delta pK_a = 4$, ...) site discrete pKa spectrum (DPS) model. The - - - - lines indicate ±20% standard error.

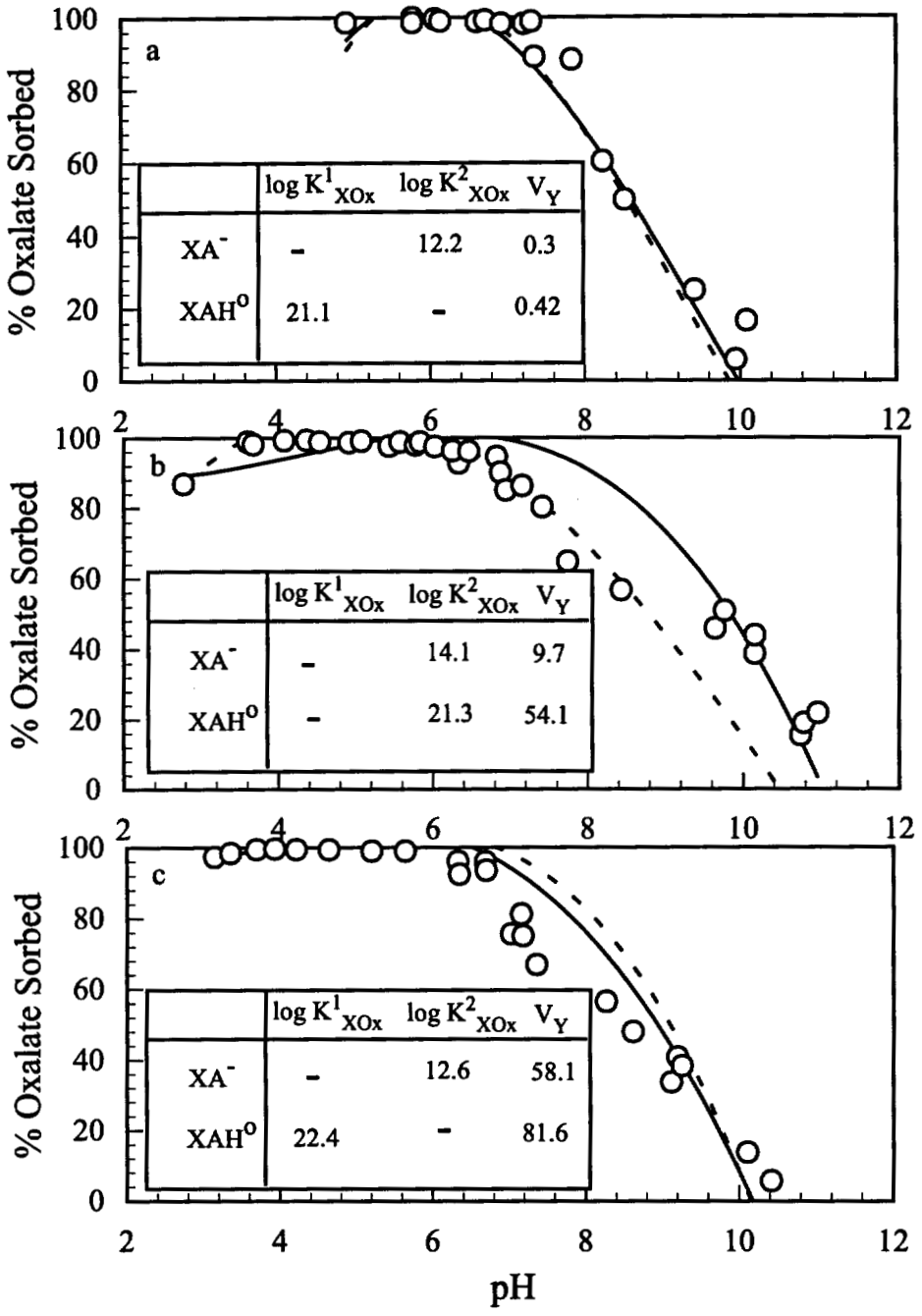

Figure 5.2. DPS model fit of oxalate adsorption edges for a) 10 μM, b) 50 μM, and c) 100 μM total oxalate onto AC with XAH^o (———) and XA^- (- - - -) ($A = C_2O_4^{2-}$) in the one-site-class model. Insert tables show the optimal values of log K_{XOx}, as fitted with FITEQL 3.1, and the goodness of fit parameter V_Y.

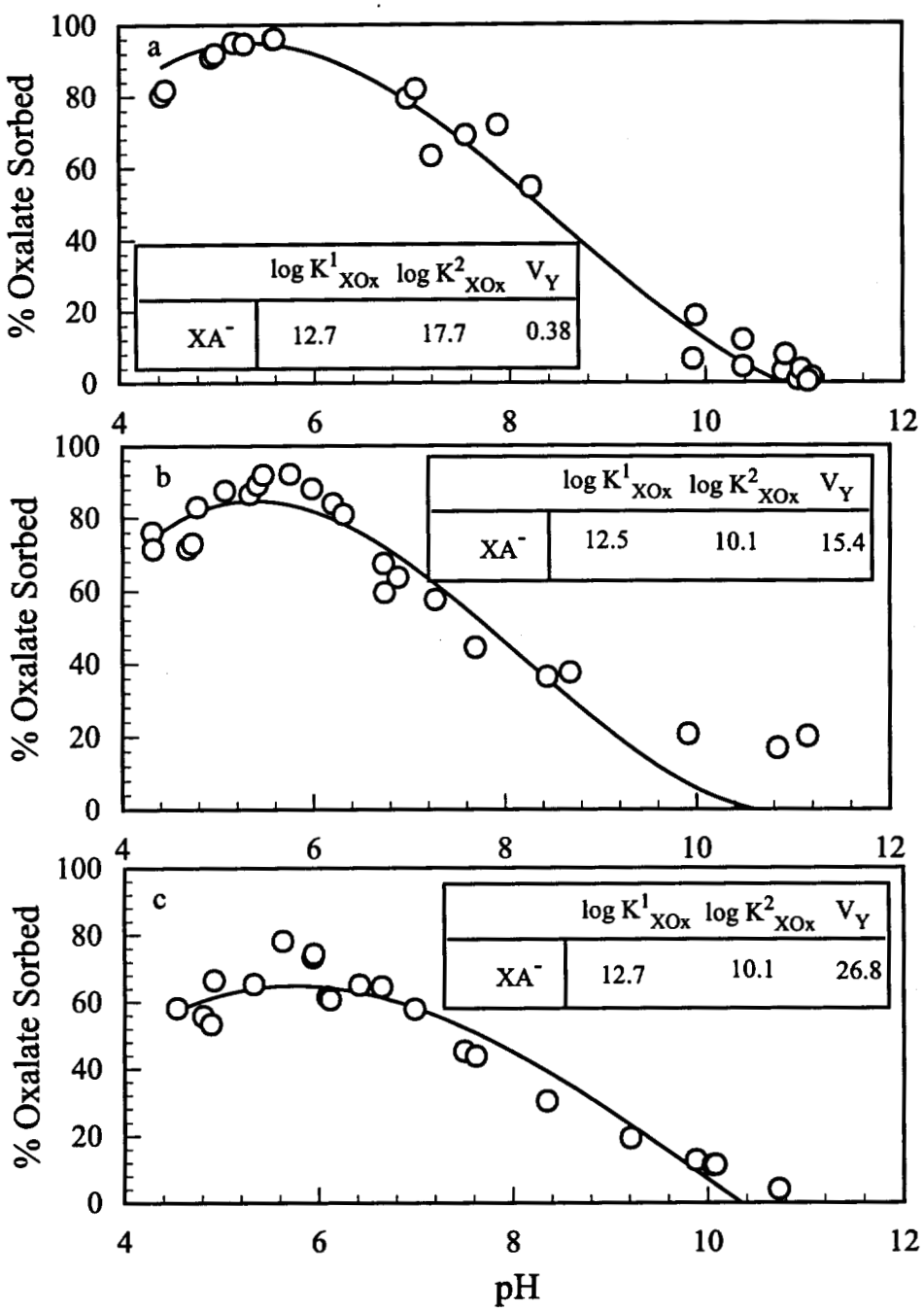

Figure 5.3. DPS model fit of oxalate adsorption edges for a) 10 μM, b) 50 μM, and c) 100 μM total oxalate onto MC with XA^- (————) ($A = C_2O_4^{2-}$) in the two-site-class model. Insert tables show the optimal values of log K_{XOx}, as fitted with FITEQL 3.1, and the goodness of fit parameter V_Y.

Table 5.3. Modeling adsorption of various ions with the DPS approach using the optimized surface site concentration and the pK_a spectrum.

Adsorption Reactions
Oxalate
$[\equiv X_iC_2O_4H^o] = [\equiv X_iOH^o]\{C_2O_4^{2-}\}\{H^+\}^2K^i_{XOx1}$ (i = 1, n)
$[\equiv X_iC_2O_4^-] = [\equiv X_iOH^o]\{C_2O_4^{2-}\}\{H^+\}K^i_{XOx2}$ (i = 1, n)
Copper
$[\equiv X_iOCu^+] = [\equiv X_iOH^o]\{Cu^{2+}\}\{H^+\}^{-1}K^i_{XOCu}$ (i = 1, n)
Input for Ion Adsorption Modeling with FITEQL
pK^i_{a1}: 5, 8
pK^i_{a2}: 11, 14
$T_{XOH(i)}$ (mol/L): $1.81x10^{-4}$, $4.98x10^{-4}$
Various aqueous components and species
Various components and species related to each adsorption site
Serial Data
$[\ ]_T$[¶], $[\ ]_s$[§], pH, Na^+, Cl^-
Parameter to be Optimized
[¥]log K^{eff}

[¶]Total Concentration of Ion
[§]Adsorbed Concentration of Ion
[¥]log of Surface Complexation Constant

convergence with adsorption to both sites - one of the sites was unimportant.

The oxalate edges for MC and MU differ from AC. The adsorption on the natural sands is maximum at pH ~ 6, as shown in Figure 5.3, due to the competition between the surface and dissolved Al for the oxalate in solution at lower pH (Al is dissolved from the natural materials (Chapter 3). The adsorption of Ox_T = 10 μM onto both MC and MU was accurately modeled with one site and any one species (Table 5.4). The fits for Ox_T = 50 μM and 100 μM also were better when we used both sites along with the species $\equiv XC_2O_4^-$.

Table 5.4. Effective surface complexation constant and goodness of fit for adsorption of oxalate onto AC, MC, and MU.

[Ox]	V_Y	log K^1_{XOx1}	log K^2_{XOx1}	V_Y	log K^1_{XOx2}	log K^2_{XOx2}
AC:	0.42	21.12±0.15	x	0.79	13.03±0.11	x
10 μM	0.44	x	21.49±0.15	0.30	x	12.16±0.13
	NC[¶]			NC[¶]		
AC:	54.12	21.34±0.05	x	9.67	14.06±0.02	x
50 μM	54.94	x	20.81±0.05	11.8	x	13.68±0.03
	NC[¶]			9.95	14.05±0.02	10.15±0.45
AC:	81.59	22.36±0.02	x	68.4	13.31±0.01	x
100 μM	84.26	x	21.91±0.02	58.15	x	12.56±0.01
	NC[¶]			36.1	13.11±0.01	10.53±0.01
MC:	0.86	20.75±0.16	x	0.54	13.06±0.09	x
10 μM	0.98	x	28.09±0.18	0.67	x	19.79±0.14
	N.C.			0.38[‡]	12.72±0.12	17.66±0.41
MC:	45.21	19.71±0.04	x	34.71	13.29±0.02	x
50 μM	55.25	x	18.86±0.05	36.95	x	11.39±0.04
	NC[¶]			15.37[‡]	12.51±0.03	10.10±0.03
MC:	136.3	19.52±0.02	x	57.4	13.25±0.01	x
100 μM	176	x	18.88±0.03	123	x	10.80±0.02
	NC[¶]			26.79[‡]	12.73±0.02	10.07±0.02
MU:	3.22	20.74±0.08	x	0.36	12.66±0.05	x
10 μM	3.67	x	27.94±0.09	0.39	x	19.85±0.07
	NC[¶]			0.37	12.65±0.05	15.39±1.42
MU:	85.05	19.36±0.03	x	26.21	12.68±0.01	x
50 μM	95.38	x	18.01±0.03	77.8	x	10.71±0.03
	NC[¶]			15.9	12.42±0.02	9.54±0.03

[‡] Used for Fig. 2; [¶]No Convergence: One of the sites seems unimportant; x = -12

Table 5.4 (Continued). Effective surface complexation constant and goodness of fit for adsorption of oxalate onto AC, MC, and MU samples.

[Ox]	V_Y	log K^1_{XOx1}	log K^2_{XOx1}	V_Y	log K^1_{XOx2}	log K^2_{XOx2}
MU:	181.1	18.48±0.01	x	50.57	12.46±0.01	x
100 μM	243.7	x	16.89±0.02	133.8	x	10.05±0.01
	NC[¶]			20.12	12.19±0.01	9.56±0.02

[¶]No Convergence: need to neglect one site; x = -12

The adsorption of Cu concentration (Cu_T) of 5.7 μM and 15 μM onto AC, MC, and MU were accurately reproduced with any one site, as shown in Fig. 5.4 and Table 5.5. More than one site overdefined the adsorption. For adsorption of Cu_T = 5.7 μM onto AC and MU we obtained $V_Y < 0.1$ because the default error estimates were too small. We did not change the error estimates because we wanted to model various sorbate concentrations with minimum change in model parameters.

As with SCMs, the adsorption of Cu on the presence of oxalate was modeled with species $\equiv XOCu^+$ along with aqueous complexes of Cu and oxalate. The adsorption of Cu in the ternary complex was modeled for all soils with any one of the sites. As shown in Table 5.6 ($0.1 < V_Y < 20$) and Fig. 5.5 we obtained good fits to the edge data. Modeling with two sites did not converge suggesting one of the sites was unimportant. For AC, the adsorption of oxalate in the mixture was modeled with the same accuracy with any one site when the assumed species was $\equiv XC_2O_4H^\circ$ (Table 5.7). With $\equiv XC_2O_4^-$ we obtained better fits when adsorption was modeled with only the second site (pK_a = 8, 14). The fits obtained with two species were the same (Fig. 5.6) but the fitting was unstable and did not converge when we used both sites to reproduce adsorption onto AC. For MC and MU, the adsorption of oxalate in the presence of Cu was better reproduced when we used both surface sites and the species $\equiv XC_2O_4^-$. The species $\equiv XC_2O_4H^\circ$ always gave statistically poorer fits when one site was used and never converged when both sites were used.

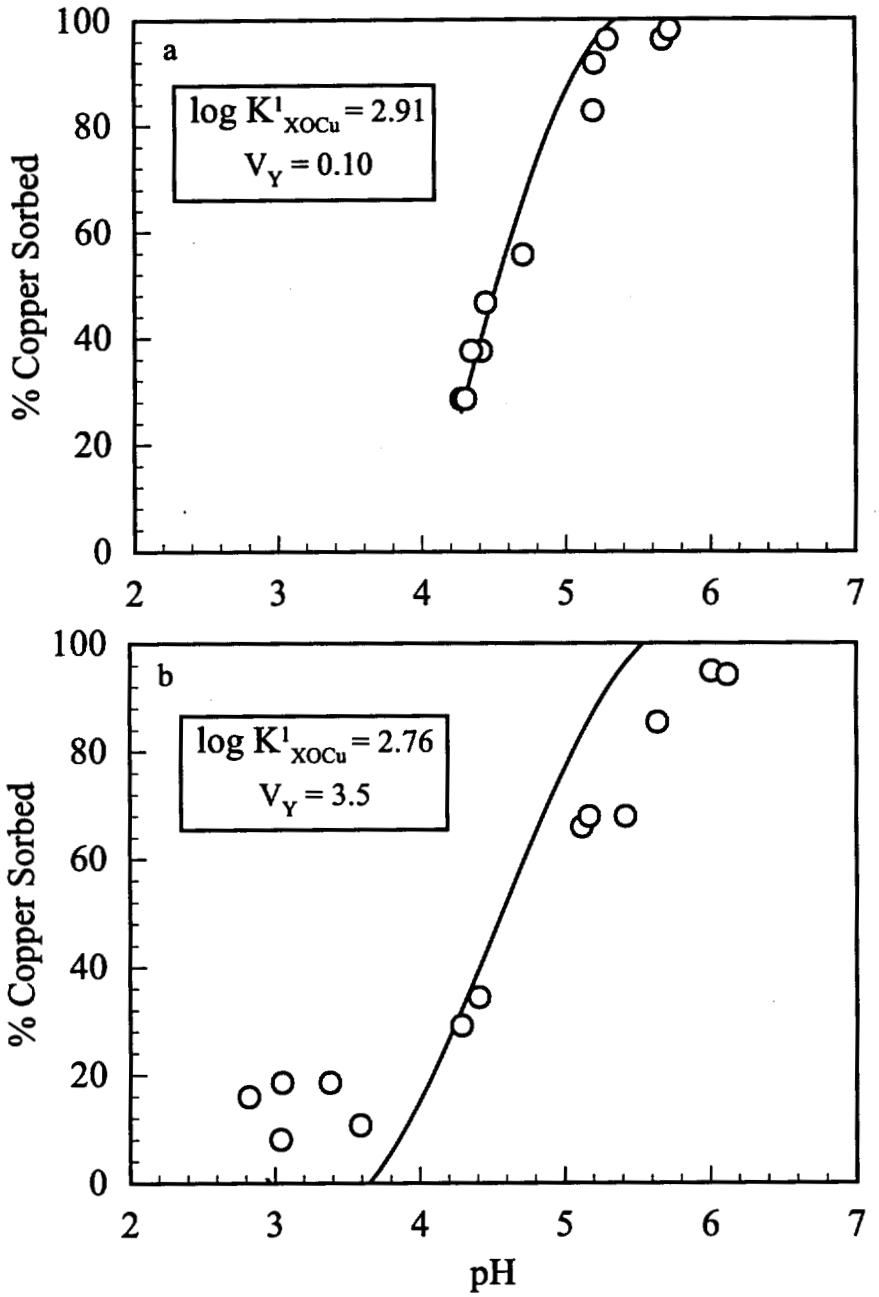

Figure 5.4. DPS model fit of Cu adsorption edges for a) 5.7 μM, and b) 15 μM total Cu onto AC with $XOCu^+$ in the one-site-class model. Insert tables show the optimal values of log K_{XOCu}, as fitted with FITEQL 3.1, and the goodness of fit parameter V_Y.

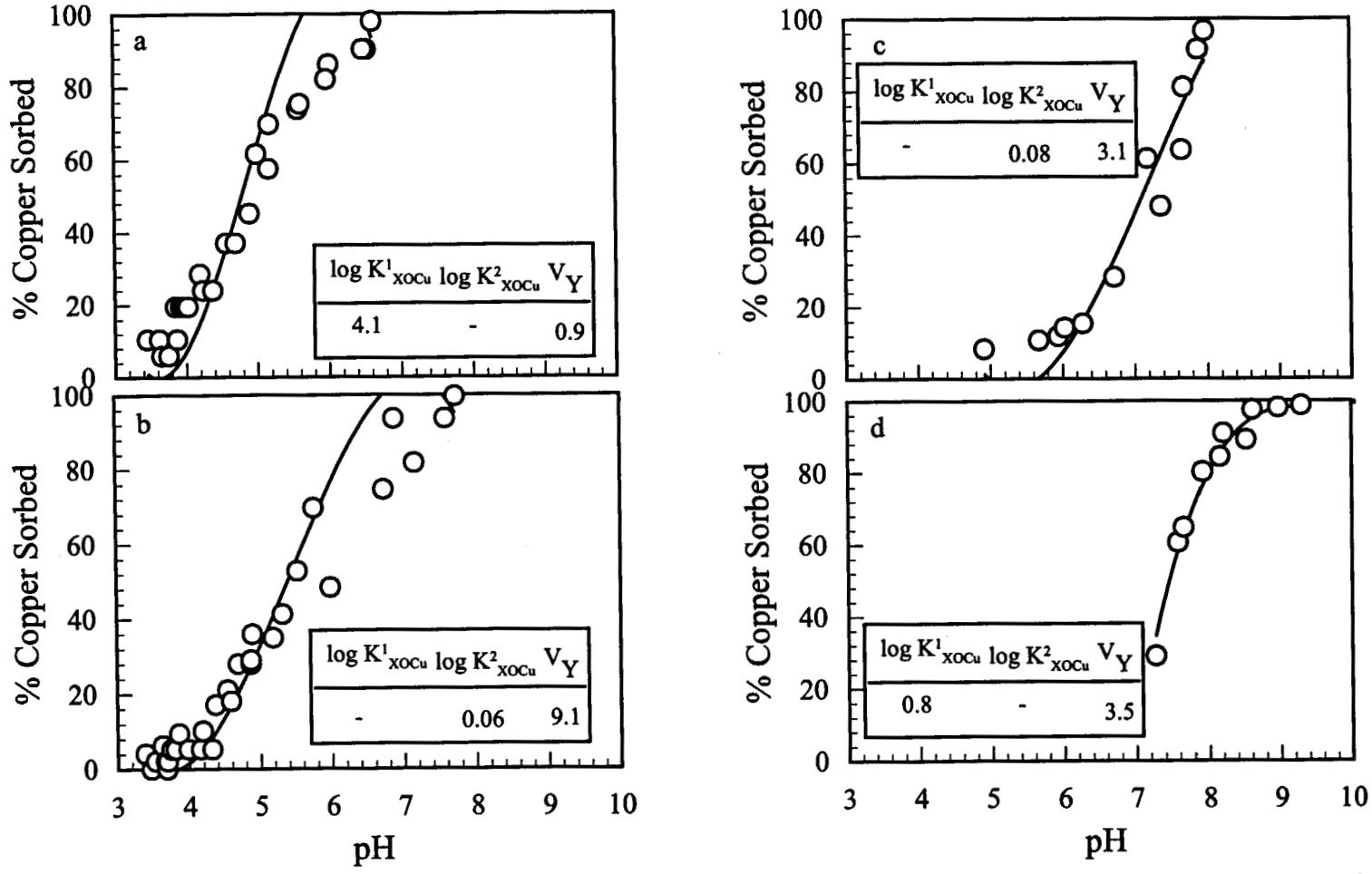

Figure 5.5. DPS model fit of Cu adsorption in the ternary complex for a) 8.3 μM Cu with 100 μM oxalate, b) 38 μM with 100 μM oxalate, and c) 27 μM Cu with 1 mM oxalate, and d) 121 mM Cu with 1 mM oxalate onto AC with $XOCu^{+}$ along with aqueous complexation of Cu and oxalate in the one-site-class model. Insert tables show the optimal values of log K_{XOCu}, as fitted with FITEQL 3.1, and the goodness of fit parameter V_Y.

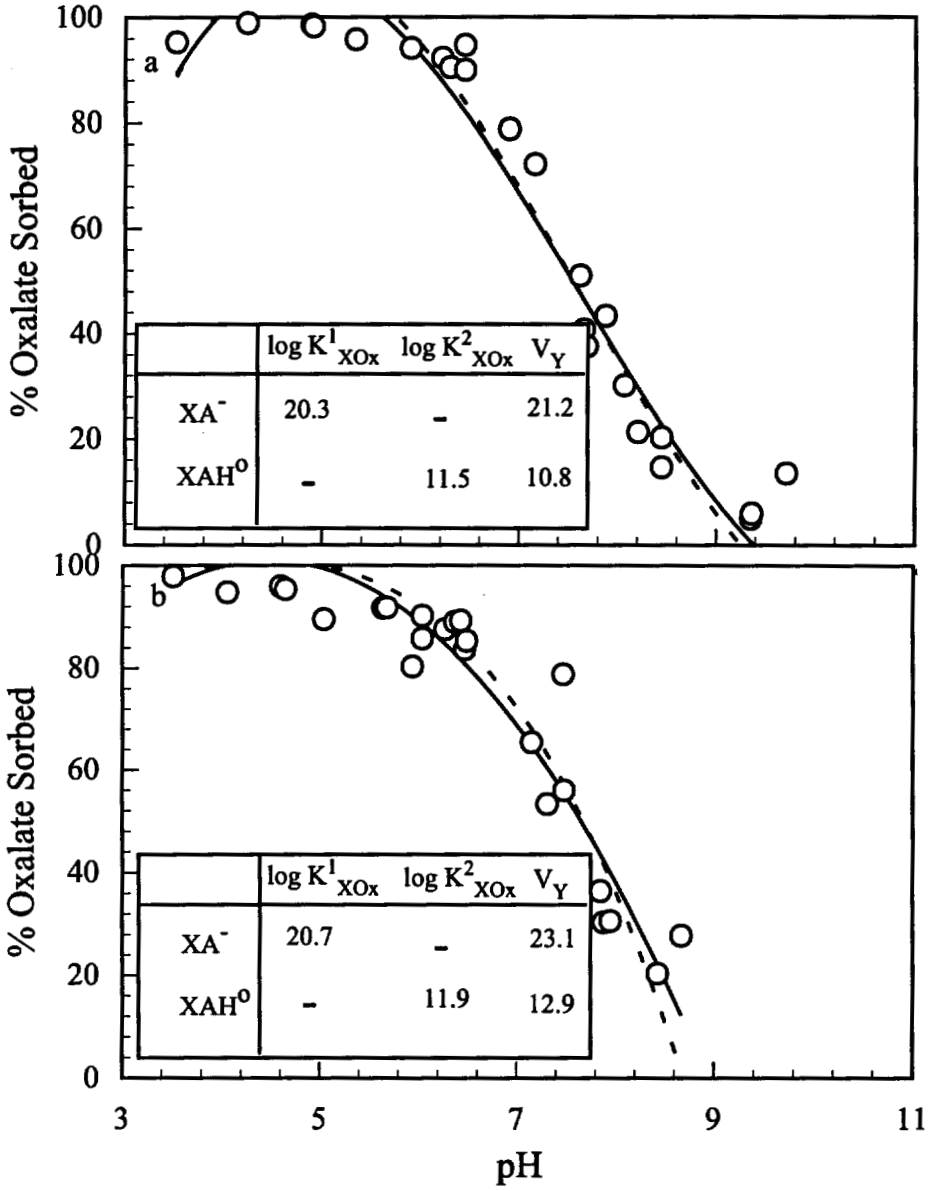

Figure 5.6. DPS model fit of oxalate adsorption in the ternary complex for a) 100 μM oxalate with 8.3 μM Cu, and b) 100 μM oxalate with 38 μM Cu onto AC with XAH^o (—————) and XA^- (- - - -) (A = $C_2O_4^{2-}$) in the one-site-class model. Insert tables show the optimal values of log K_{XOx}, as fitted with FITEQL 3.1, and the goodness of fit parameter V_Y.

Table 5.5. Effective surface complexation constant and goodness of fit for adsorption of Cu onto AC, MC, and MU.

[Cu]	V_Y	$\log K^1_{XOCu}$	$\log K^2_{XOCu}$
AC: 5.7 μM	0.10	2.91±0.16	x
	0.05	x	-0.42±0.16
AC: 15 μM	3.49	2.76±0.11	x
	2.92	x	-0.67±0.11
MC: 5.7 μM	0.21	2.29±0.11	x
	0.15	x	-0.91±0.10
MC: 15 μM	2.25	2.00±0.13	x
	1.97	x	-1.20±0.11
MU: 5.7 μM	0.14	1.49±0.20	x
	0.08	x	-1.55±0.17
MU: 15 μM	3.68	1.38±0.08	x
	1.54	x	-1.65±0.06

‡ Used for Fig. 4; x = -12

5.5 Discussion

A simple nonelectrostatic, discrete pK_a spectrum model reproduced the adsorption of a moderately wide concentration of Cu, oxalate, and mixtures of Cu and oxalate. The DPS approach modeled a moderately wide range of Cu and Cu-Oxalate onto AC, MC, and MU with one site. Adsorption of small Ox_T was accurately modeled with one site and any one species whereas a larger concentrations of oxalate were sometimes better reproduced with two sites and with $\equiv XC_2O_4^-$. Also with the DPS we did not have to invoke the physically unrealistic species $\equiv XOC_2O_4^{3-}$ as we had to with the DLM and CCM to model the higher pH points of the edge.

The DPS will be most conveniently applied if it is possible to determine in advance the

Table 5.6. Effective surface complexation constant and goodness of fit for adsorption of Cu in the presence of oxalate onto AC, MC, and MU.

[Ox] μM	[Cu] μM	V_Y	log K^1_{XOCu}	log K^2_{XOCu}
AC: 100	8.3	0.86	4.13±0.12	x
		0.53	x	0.90±0.11
	38.0	11.34	3.18±0.03	x
		5.93	x	0.06±0.03
AC: 1000	27.0	8.39	1.27±0.06	x
		3.07	x	0.08±0.04
	121.0	3.45	0.79±0.02	x
		13.27	x	-0.29±0.02
MC: 100	8.3	1.18	3.18±0.15	x
		0.75	x	0.16±0.13
	38.0	18.95	1.20±0.05	x
		11.56	x	-0.90±0.04
MC: 1000	27.0	8.76	1.89±0.07	x
		3.09	x	0.21±0.05
	121.0	6.23	0.65±0.01	x
		22.83	x	-0.57±0.01
MU: 100	8.3	1.11	0.63±0.17	x
		0.45	x	-1.10±0.15
	38.0	2.09	0.35±0.05	x
		0.95	x	-1.42±0.04
MU: 1000	27.0	4.02	0.67±0.04	x
		3.64	x	-0.47±0.03
	121.0	14.47	0.07±0.02	x
		32.53	x	-0.93±0.01

‡ Used for Fig. 5; x = -12

Table 5.7. Surface complexation constant and goodness of fit for adsorption of oxalate in the presence of Cu onto AC, MC, and MU.

Ox	Cu	V_Y	log K^1_{XOx1}	log K^2_{XOx1}	V_Y	log K^1_{XOx2}	log K^2_{XOx2}
AC:	8.3	21.22	20.26±0.01	x	150.8	12.67±0.01	x
100		39.7	x	19.36±0.02	10.8	x	11.47±0.01
		N.C.			Error		
	38	23.04	20.66±0.01	x	143.6	13.28±0.01	x
		40.31	x	19.69±0.02	12.9	x	11.88±0.01
		N.C.			Error		
MC:	8.3	208.9	19.8±0.02	x	97.9	13.04±0.01	x
100		258.7	x	18.82±0.02	242.3	x	10.39±0.01
		N.C.			11.5	12.45±0.02	9.97±0.01
MU:	8.3	253.8	17.64±0.01	x	92.5	12.29±0.01	x
100		376.6	x	13.94±0.01	107.9	x	9.84±0.01
		N.C.			11.5	11.94±0.02	9.63±0.01
	38	225.1	18.76±0.02	x	17.7	12.6±0.01	x
		411.3	x	15.40±0.02	191.6	x	10.36±0.01
		N.C.			10.6	12.49±0.01	9.45±0.04

‡ Used for Fig. 6; ¶No Convergence: One of the sites seems unimportant; x = -12

sites that are involved in adsorption by aligning the pK_a values in the spectrum with estimates of pK_a values for the soils. The pK_a values for a defined mixed oxide suspension can be calculated from those of the component pure phases (*23, 24*). Although, in principle, this approach should work for soils, their mineralogical complexity often renders such calculation inaccurate. Evaluation of the chemical composition of coated sands often does not indicate which phase will be dominant in the adsorption process. The adsorption of Cu, oxalate, and Cu-Oxalate is not sensitive to changes in pK_a and different values of pK_a model the data with the same accuracy (Chapters 3 and 4). The pK_a values of isolated oxides are highly variable and different values are obtained by different researchers so were unable to determine a priori

the sites that will most significantly contribute to adsorption.

A SCM typically uses one site (two pK_a's), an electrostatic model, and a small ΔpK_a. Bolt and Van Riemsdijk (*25*) opine that titration data for metal oxides should be modeled with a small ΔpK_a (*26*) (typically around 2). We found the best fit of the acid-base titration curves for goethite with the DPS model using two sites (four pKa's), no near-surface electrostatics, and a $\Delta pK_a = 6$. The multiple pK_a's and a larger ΔpK_a help the DPS model account for the near-surface electrostatics. We demonstrated this by showing that a single-site, non-electrostatic model ($\Delta pK_a = 2$) gives a vastly different titration curve than a single-site DLM with the same hypothetical pK_a values (as shown in Fig. 5.7a). In Figure 5.7b, increasing the ΔpK_a (to 8) for the single-site non-electrostatic model makes the predicted titration curve similar to that of the curve obtained with DLM ($\Delta pK_a = 2$). Thus the DPS model the absence of electrostatics can be compensated by a large ΔpK_a. As the number of sites in the nonelectrostatic model is increased, a smaller ΔpK_a can be used. Increasing the number of sites and having a smaller ΔpK_a makes the DPS fits smoother. In this sense, there is a trade off between a "realistic" ΔpK_a and the number of adjustable parameters needed to obtain it. An acid-base titration curve can be modeled with a single-site DLM or a multi-site DPS with a larger ΔpK_a with similar accuracy.

Acid-base titration data typically span many orders of magnitude of proton concentration (*22*) and so must be modeled with a larger number of site classes than does anion and cation binding data, which typically are obtained for a smaller concentration range. A smaller number of sites will model the adsorption data accurately. To model the data for Co binding to humic acid Westall et al. (*1*) assume some sites to be unimportant based on the results of the optimization procedure.

Similar problem sometimes exists in choosing species required to model anion adsorption. Although both $\equiv XC_2O_4H^\circ$ and $\equiv XC_2O_4^-$ reproduced the adsorption of lower oxalate concentrations, we obtained better fits when we used $\equiv XC_2O_4^-$ to reproduce the adsorption of larger concentrations. This corroborates our results with SCMs in Chapter 3. For the SCM approach, oxalate edges were modeled with the fully deprotonated oxalate ($C_2O_4^{2-}$) coordinating with the positively charged ($\equiv XOH_2^+$ or $\equiv X^+$) or negatively charged

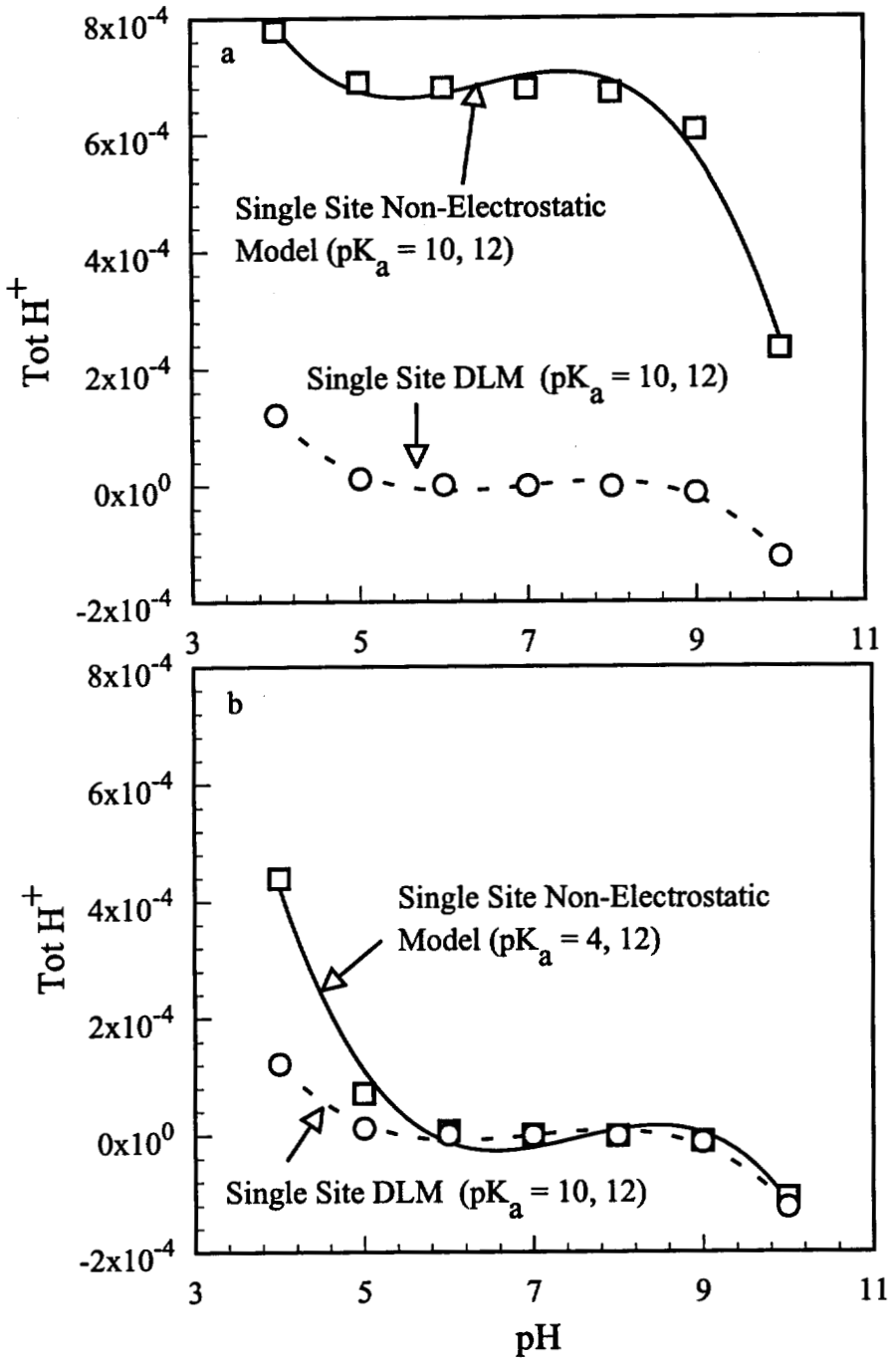

Figure 5.7. Nonelectrostatic model calculations demonstrating the effect of ΔpK_a values on the ability to reproduce acid-base titration curves generated with a Diffuse Layer Model with 0.05 M NaCl as background electrolyte.

($\equiv XO^-$) surface. We were able to neglect the coordination of $HC_2O_4^-$ to the positively charged surface to form a neutrally charged species $\equiv XC_2O_4H^\circ$. Based on chemical insight and such literature evidence it is possible to neglect a surface species when more than one surface species can form.

The key to extending the DPS model to reproduce binding onto oxides is the ability to consistently determine which sites and which species will be important and unimportant for adsorption of various sorbates. The present formulation of the DPS model does not provide insight into how this can be achieved for soils that are inherently complex in their mineralogic composition. Westall (*27*) is developing a version of FITEQL that will automatically assign small log K^{eff} (= -12) to sites that do not contribute to adsorption. Development of such a model will improve the ability to fit a wide range of data with the DPS approach.

We observed various advantages and disadvantages for modeling ion adsorption with SCM and DPS approaches (listed in Table 5.8). (For details of SCM results see Chapter 3 and 4). Both SCM and DPS modeled low to moderate concentration of Cu, oxalate, and Cu-Oxalate mixtures with somewhat similar accuracy. Although the results with both approaches were similar, DPS provides a more flexible platform for modeling adsorption onto somewhat

Table 5.8. Comparison of DPS and SCM for their relative advantages and disadvantages in modeling adsorption of Cu, oxalate, and mixtures of Cu and oxalate onto metal oxide coated sands.

No	Properties	SCM	DPS
1	The ability to obtain a good fit depends on concentration of anion	Y	Y
2	The ability to obtain a good fit depends on concentration of cation	N	N
3	Easily select a consistent set of surface species over another	N	Y
4	Easily select a consistent set of surface sites for various sorbates	Y	N
5	Easily models site heterogeneity	N	Y
6	Easily models competition	Y	Y

Y = Yes
N = No

heterogeneous adsorbents.

The two models often provide similar insights into adsorption mechanism. Both indicate Cu in the presence and absence of oxalate coordinates directly with the surface. Two species $\equiv XC_2O_4^-$ and $\equiv XOC_2O_4^{3-}$ (a physically unrealistic species) reproduced oxalate adsorption with DLM and CCM whereas one species $\equiv XOH_2^+\text{-}C_2O_4^{2-}$ reproduced adsorption with TLM. The DPS model was advantageous in that it consistently reproduced adsorption of oxalate with one species $\equiv XC_2O_4^-$ and we did not invoke a physically unrealistic species to model the oxalate edge at the higher pH.

The extension of the DPS model to cation and anion binding is promising. It shows a direction to a flexible platform for surface complexation based modeling and avoids the uncertainties and problems of electrostatic models used in conventional SCMs. In its present formulation it is not yet clear how specific reactions, species, and sites can be a priori selected to analyze the adsorption data. Although the present formulation somewhat limits its use in natural conditions improvements in automatic assigning of sites (*27*) will greatly improve its usefulness.

5.6 References

(1) Westall, J.C.; Jones, J.D.; Turner, G.D.; and Zachara, J.M. *Environ. Sci. Technol.*, **1995**, 29:951-959.

(2) Contescu, C.; Jagiello, Jacek; and Schwarz, J.A. *Langmuir*, **1993**, 9:1754-1765.

(3) Černik, M.; Borkovec, M.; and Westall, J.C. *Environ. Sci. Technol.*, **1995**, 29(2)413-425.

(4) Nederlof, M.M.; van Riemsdijk, W.H.; and Koopal L.K. *Environ. Sci. Technol.*, **1992**, 26:763-771.

(5) De Witt, J.C.M.; van Riemsdijk, W.H.; and Koopal L.K. *Environ. Sci. Technol.*, **1993a**, 27:2005-2014.

(6) De Witt, J.C.M.; van Riemsdijk, W.H.; and Koopal L.K. *Environ. Sci. Technol.*, **1993b**, 27:2015-2022.

(7) Nederlof, M.M.; De Witt, J.C.M.; Van Riemsdijk, W.H.; and Koopal L.K. *Environ. Sci. Technol.*, **1993**, 26:763-771.

(8) Nederlof, M.M.; Van Riemsdijk, W.H.; and Koopal L.K. *Environ. Sci. Technol.*, **1994**, 28:1037-1047.

(9) Benedetti, M.F.; Milne, C.J.; Kinniburgh, D.G.; Van Riemsdijk, W.H.; and Koopal, L.K. *Environ. Sci. Technol.*, **1995**, 29:446.

(10) Jagiello, J.; Bandosz, T.; Putyera, K.; and Schwarz, J.A. *J. Colloid Interface Sci.*, **1995**, 172:341-346.

(11) Borkovec, M.; Rusch, U.; Černík, M.; Koper, G.J.M.; and Westall, J.C. *Colloids and Surfaces*, **1996**, in press.

(12) Perdue, E.M. and Lytle, C.R. *Environ. Sci. Technol.*, **1983**, 17:654-660.

(13) Dzombak, D.A.; Fish, W.; and Morel, F.M.M. *Environ. Sci. Technol.*, **1986**, 20(7):669-675.

(14) Fish, W.; Dzombak, D.A.; and Morel, F.M.M. *Environ. Sci. Technol.*, **1986**, 20(7):676-683.

(15) Rudzinski, W.; Charmas, R.; Partyka, S.; Thomas, F.; and Bottero, J.Y. *Langmuir*, **1992**, 8:1154-1164.

(16) Koopal, L.K. and Van Riemsdijk, W.H. *J. Colloid Interface Sci.*, **1993**, 128(1):188-200.

(17) Tipping, E.; Reddy, E.E.; and Hurley. *Environ. Sci. Technol.*, **1990**, 24:1700-1705.

(18) Mesuere, K. *Adsorption and Dissolution Reactions Between Oxalate, Chromate, and Iron Oxide Surface: Assessment of Current Modeling Concepts*. Ph.D. Dissertation, Oregon Graduate Institute of Science & Technology, December, **1991**.

(19) Bonn, B.A. and Fish, W. *J. Soil Sci.*, **1993**, 44:335-345.

(20) Mesuere, K. and Fish, W. *Environ. Sci. Technol.* **1992**, 26(12), 2357-2364.

(21) Herbelin, A.L. and Westall, J.C. *FITEQL: A Computer Program for Determination of Chemical Equilibrium Constants*, Version 3.1, Report 94-01, Department of Chemistry, Oregon State University, Corvallis, OR, **1994**.

(22) Dzombak, D.A. and Morel, F.M.M. *Surface Complexation Modeling: Hydrous Ferric Oxide*. John Wiley & Sons. **1990**.

(23) Parks, G.A. *Chem. Rev.*, **1965**, 65:177.

(24) Schwarz, J.A; Driscoll, C.T; and Bhanot, A.K. *J Colloid and Interface Sci.*, **1984**,

97(1):55-61.

(25) Bolt, G.H. and Van Riemsdijk, W.H. *Soil Chemistry B. Physiological Models*, G.H. Bolt (ed.), **1982**, 2nd ed., p. 459, Elsvier, Amsterdam, 1982.

(26) Koopal, L.K.; Van Riemsdijk, W.H.; and Roffey, M.G. *J. Colloid and Interface Sci.*, **1987**, 118(1):117-136.

(27) Westall, J.C. Personal Communication, **1996**, Oregon State University, Oregon.

CHAPTER 6

REMEDIATION OF METAL CONTAMINATED SUBSURFACE SOILS - DISSOLUTION AND COMPETITIVE EFFECTS

6.1 Abstract

Metal-contaminated soil can be washed by flushing metal-binding ligand through the subsoil formations. However the ligand also may promote substantial dissolution of natural metal (hydr)oxides. The dissolved natural metals, such as Fe and Al, may complex with much of the added ligand, thus reducing the ligands effectiveness in extracting the targeted contaminant metals. The competition depends on the relative affinity of the ligand for the natural and contaminated metal but also depends on the relative rates of contaminant desorption/dissolution and natural metal dissolution. In compacted medium, dissolution can be transport limited and the kinetics may depend on the flow velocity. We used laboratory experiments to quantify the effect of pore velocity on dissolution of metal from sands artificially and naturally coated with various amounts of metal oxides. Oxalate, our model chelate, rapidly dissolved Al, and dissolved Fe at a slower rate. The dissolution of surficial oxide was strongly dependent on the pore velocity when the influent solution was not buffered. In the presence of buffered oxalate, the pore velocity affected the dissolution from only the naturally coated sample. Conditional stability constant calculations show that high concentration of dissolved Fe will reduce the efficiency of metal contaminant removal. In some cases, the more soluble, dissolved Al may also reduce the efficiency of contaminant removal.

6.2 Introduction

The most frequently encountered metal contaminants in the subsurface are Pb, Hg, As, Cr, Cd, and Cu (*1*). Such metal contaminants can be remediated by, 1) solidification/immobilization, 2) ex-situ and in-situ soil washing (*1 - 4*), and 3) electrokinetic remediation (*5 - 7*). While the first technique immobilizes the contaminant in-situ, the other techniques are effectively used for removing the contaminant from the soil.

Metal contaminated subsurface soil is effectively cleaned ex-situ by flushing chelate through heaps of soil or in-situ by flushing chelate through subsurface formations. The dissolution of contaminant is enhanced with extractants such as surfactants, chelates, or acid/alkaline solution (*8*). Citric acid, acetate, oxalate, NTA, EDTA, and DTPA form soluble and mobile complexes with Ni, Cu, Fe, Co, etc. (*9 - 13*). The metal-chelate complexes are then either drained from ex-situ heaps or else pumped from the subsurface and treated ex-situ.

The efficiency of in-situ soil washing and ex-situ heap leaching depends on the type and concentration of the complexant, the pH, the ionic strength, and the flow rate. The total amount of metal contaminant removed is not improved by increasing the flow rate but the time for complete removal of contaminants is significantly reduced (*2*). Davis and Singh (*2*) suggest washing first with water at pH = 2 at rapid flow rate and then with EDTA at smaller flow rate to remove recalcitrant residual contaminants. Some problems that plague consistent performance are:

1. strong complexants are moderately to strongly adsorbing so it is difficult to transport chelate to contaminated zones of an adsorption medium unless "swamping" concentrations are used.
2. flushing a swamping concentration of chelate to saturate the adsorption sites induces substantial dissolution of surficial metal from the soil.
3. the dissolved natural metals compete with the metal contaminant for the chelate in solution thereby reducing the efficiency of contaminant removal.

Although various studies have evaluated the effectiveness of soil washing in removing metal from contaminated soil, few have discussed the effect of dissolved natural metals on the complexation of metal contaminant with a chelate. Davis and Singh (*2*) do not discuss the

effect of dissolution on remediation. Elliott et al. (*14*) do not observe change in removal of Pb in the presence of dissolved Fe because of slow kinetics of Fe dissolution.

Selective extraction of metal contaminant without dissolving surficial metal oxide is often desirable. Strongly alkaline extracting solution may be used to prevent dissolution (*15*). Metal adsorption in subsurface soil is not always reversible and a substantial amount of the metal contaminant is immobilized in the micropores or as solid solution. Dissolving the surficial metal oxide in these cases will mobilize trapped contaminants and may be beneficial. It is important to understand what will control dissolution in compacted subsurface strata.

Strong chelates and H^+ coordinate with metal (hydr)oxides on soils on a short time scale and dissolve the same sites at longer time scales. The surface controlled dissolution occurs through adsorption, formation of a precursor complex, and release of the metal from the surface (*16 - 18*). A combination of the surface complexation approach and the principle of surface controlled dissolution (*16, 19*) effectively interprets the dissolution of kaolinite (*20, 21*), hematite (*22, 23*), δ-Al_2O_3 and BeO (*16*), ferrihydrite (*24*), anorthite (*25*), Fe(III) (*19*), olivine (*26*), and hematite and magnetite (*27*).

The rate of proton induced dissolution is nonlinearly dependent on the concentration of adsorbed protons whereas the rate of ligand promoted dissolution is linearly proportional to the concentration of adsorbed ligand (*16, 19*). Proton promoted dissolution is significant but in the presence of ligands is often eclipsed by ligand promoted dissolution. Various studies have investigated the surface controlled process but only a few have investigated the effect of transporting dissolution inducing reagents through a geochemically reactive compacted medium.

The movement of dissolution fronts and concomitant occurrence of side reactions in the subsurface will influence the in-situ removal of contaminants from subsurface soil. Although the movement of dissolution fronts has been studied to explain formation of podzols (*28*) no study to our knowledge has explored its effect on remediation of contaminants. The primary goal of this research was to experimentally evaluate the effect of pore velocity on the dissolution of metal oxide coating from soils, particularly with respect to the degree of pH buffering. We then theoretically explored the effect of the dissolved metal oxide on, 1) the

binding of chelate to the coating and 2) the removal of metal contaminants from the subsurface with in-situ remediation techniques. We used sand artificially and naturally coated with various amounts of metal oxides for our experiments. We used oxalate as the model chelate because it is a moderately strong complexant and occurs naturally in soils.

We found that the dissolution of surficial oxide depended strongly on the pore velocity for an unbuffered influent solution but in the presence of buffered oxalate, the pore velocity affected the dissolution from only the naturally coated sample. The complexation of metal contaminant with chelates is sometimes influenced by dissolved Al but is always influenced by high concentration of dissolved Fe.

6.3 Experimental Method

We conducted experiments on sands naturally and artificially coated with varying amounts of Fe and Al oxides. Milford Coated (MC) and Artificially Coated (AC) samples were obtained from the Pacific Northwest Laboratory (PNL), Richland, WA. MC was collected from adjacent subsurface strata in Delaware. AC was prepared at the PNL (*29*). The Details of sample preparation and experimental conditions are presented in Chapter 2. Sub-samples of MC and MU were extracted with 6 N HCl to measure the "total" surficial coating and ammonium oxalate/oxalic acid solution to measure the "amorphous" portion of the coating. The surficial metal oxide content obtained with the extraction techniques are presented in Table 6.1.

Table 6.1. Metal oxide coating on the Artificially Coated (AC), Milford Coated (MC), and Milford Uncoated (MU) soils determined with 6 N HCl and ammonium-oxalate/oxalic acid (NH_4-Ox) extraction techniques (described in Chapter 2).

Soil	Fe (mg/g) 6 N HCl	Al (mg/g) 6 N HCl	Fe (mg/g) NH_4-Ox	Al (mg/g) NH_4-Ox
AC	1.8	-	-	-
MC	0.75	1.3	0.2	0.1

To eliminate the abrasion of particles in stirred reactors we dissolved the surficial metal oxides in a mini-column manifold (illustrated in Fig. 6.1a). The top reservoir contained 1 mM oxalate with background electrolyte of 0.05 M NaCl. The influent solution was buffered at pH 4 with 0.01 M sodium acetate/acetic acid. The lower reservoir maintained a constant head with a non-metallic float valve. A PVC tube (0.25" diameter) was attached to the second reservoir. The PVC mini-columns (6" long and 0.25" in diameter) were attached to the PVC tube with a section of Tygon tubing.

The PVC mini-columns illustrated in Figure 6.1b were closed with PVC end caps at top and bottom. We used PVC because it is unreactive and opaque. We inserted plugs of acid washed glass wool into the top and bottom of the column to evenly distribute influent over the cross-section. The middle of the column was packed with 12 to 15 g of metal oxide coated sand. A 0.2 μm polycarbonate filter (Poretics) was placed between the bottom glass wool and the bottom end cap to keep fines from escaping.

All components of the mini-column manifold were washed with nonionic detergent, rinsed, acid-washed, and rinsed again before assembly. Oxalate was flushed through the setup for ~ 72 hours after which mini-columns, wet packed with oxide coated sands, were attached to the experimental setup. We measured the effluent every day for total elution volume, pH, and concentration of Fe and Al. We tested for colloidal Fe and Al by dividing the effluent into two portions, one was filtered through a 0.05 μm filter and the other was acidified with 6 N HCl. The treatments showed negligible difference in total Fe and Al. We analyzed Fe and Al in solution with atomic absorption spectrophotometry (AAS), using either flame or graphite furnace atomization.

6.4 Assumptions

For MC, the 6 N HCl extractable Fe and Al was significantly greater than the oxalate extractable portion (Table 6.1). The oxalate extractable portion of the coating dissolves relatively rapidly because it is the "amorphous" portion of the coating. The remaining coating dissolves slowly because of its crystallinity. We monitored the dissolution of the surficial coating until the oxalate extractable portion of the coating was removed because this

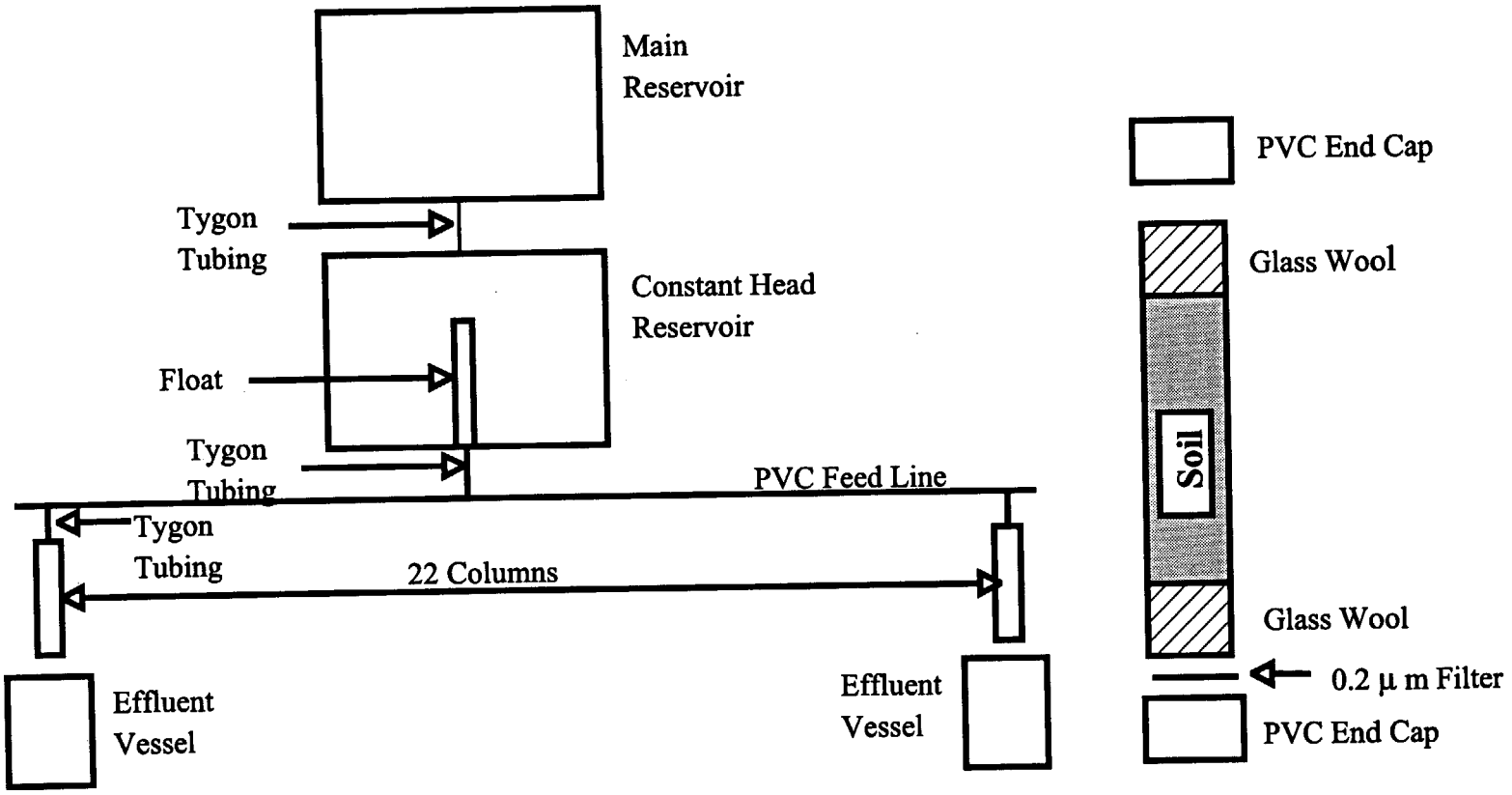

Figure 6.1. Experimental Setup for a) mini-column manifold, and b) PVC mini-columns.

relatively rapidly dissolving portion may be most significant in influencing the remediation of metal contaminants. In our experiments the oxalate extractable Al dissolved readily (by the passage of 5 pore volumes of 1 mM oxalate at pH 4) whereas the oxalate extractable Fe dissolved slowly. We were only able to obtain distinct trends for dissolution of Fe.

We neglected dissolution of silica because it is important primarily at higher pH (*21, 30, 31*). In the presence of small concentration of Al, the dissolution of silica is suppressed because Al adsorbs on the silica and prevents OH^- ions from approaching the silica surface (*31 - 33*).

We plotted the data with respect to a velocity parameter (V_p) expressed as pore volumes passed per unit time (pv/hr):

$$V_p = \frac{(\textit{total volume of effluent})}{(\textit{sampling interval})\ (\textit{volume of the column})\ \textit{porosity}} \qquad (6.1)$$

The porosity of the column was assumed to be 0.3. The essential observations and conclusions are not affected by the exact porosity that is assumed.

6.5 Conditional Stability Constant Calculation

We used the conditional stability constants (*34, 35*) to theoretically analyze the effect of dissolved Fe and Al on the removal of various metal contaminants. Dominance of one metal-chelate complex over another over a wide pH range cannot be ascertained from the values of the stability constants over a wide pH range due to formation of metal hydroxides, acid speciation of the ligand, and formation of secondary metal complexes (*35*). The conditional stability constant accounts for various aqueous complexes in the presence of chelates:

$$K_{cond} = \alpha_i \beta_n K_{ML} + \alpha_{i-1} \beta_n K_{MHL} + \alpha_i \beta_{n-1} K_{MOHL} \qquad (6.2)$$

where: α_i is the fractional distribution of the fully deprotonated ligand

α_{i-1} is the fractional distribution of ligand containing one proton

β_n is the fractional distribution of the metal M^{n+}

β_{n-1} is the fractional distribution of the hydroxylated metal ion MOH^{n-1}

K_{ML}, K_{MHL}, and K_{MOHL} are the formation constants for the metal-chelate complexes

ML, MHL, and MOHL

Bowers and Huang (*34*) explain that the ability of relatively insoluble metals, like Fe(III), to compete with a soluble metal will depend on the concentration of the soluble metal. The partitioning of chelate between a comparatively insoluble metal and a more soluble metal will approach the ratio of the conditional stability constants as the concentration of the soluble metal decreases to the solubility limit of the less soluble metal.

6.6 Results

The coating from AC was stripped from the top to the bottom of the column as a coherent dissolution front (illustrated in Fig. 6.2). The concentration of dissolved Fe (Fe_{aq}) did not vary with V_p when the influent oxalate was buffered at pH 4 (shown in Fig. 6.3). Fe_{aq} equalled 0.45 mM for V_p ranging from 0 to 0.9 pv/hr. The dissolution rate (r_D) thus increased in linear proportion to V_p, i.e., $\partial r_D/\partial V_p = 0.4$ μmoles/pv/g (Fig. 6.3).

Unlike AC, Fe_{aq} data for MC diminished when V_p was increased and the influent solution was buffered at pH = 4. As shown in Figure 6.4, increasing the V_p from 0 to 0.2 pv/hr reduced Fe_{aq} from 0.1 mM to 0.045 mM. Fe_{aq} decreased slightly with further increase in V_p. We performed t-test on the data for $V_p > 0.1$ (neglecting data for $V_p < 0.1$). The two groups of data points at $0.1 < V_p < 0.25$ and at $0.35 < V_p < 0.55$ gave a significant t value of 5 whereas the critical t value at 5% significance level for a single tailed t-test is ~ 1.76. This suggests that there indeed was a decrease in Fe_{aq} when V_p increased from 0.15 pv/hr to 0.5 pv/hr. Like AC, the calculated r_D values for MC increased proportionally with increase in V_p, i.e., $\partial r_D/\partial V_p = 0.035$ μmoles/pv/g. Both Fe_{aq} and r_D were an order of magnitude smaller for MC than for AC, probably because the natural oxides were more crystalline or more tightly affixed to the mineral matrix. Thus, the rate of dissolution from AC is limited only at the macroscale by the rate of advection while that from MC is limited at the microscale due to film diffusion. This is explained in details in the discussion section.

Unbuffered influent solutions showed a different dependence on V_p than the buffered

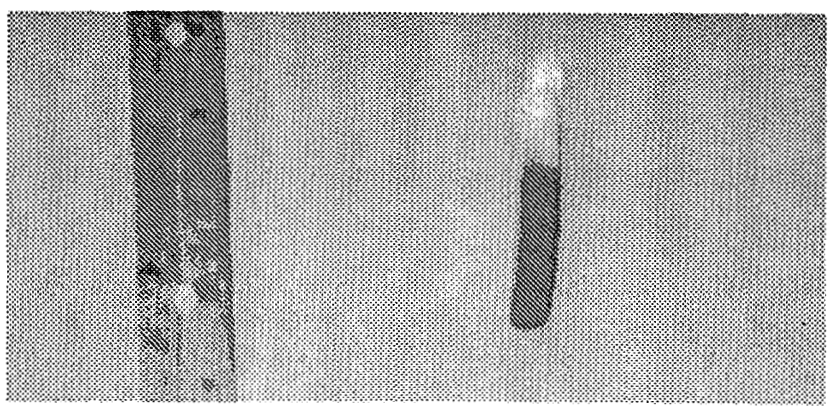

Figure 6.2. Dissolution of Artificially Coated (AC) sample in the mini-columns. The white portion of the extruded core is devoid of any coating while the darker portion is coated with goethite.

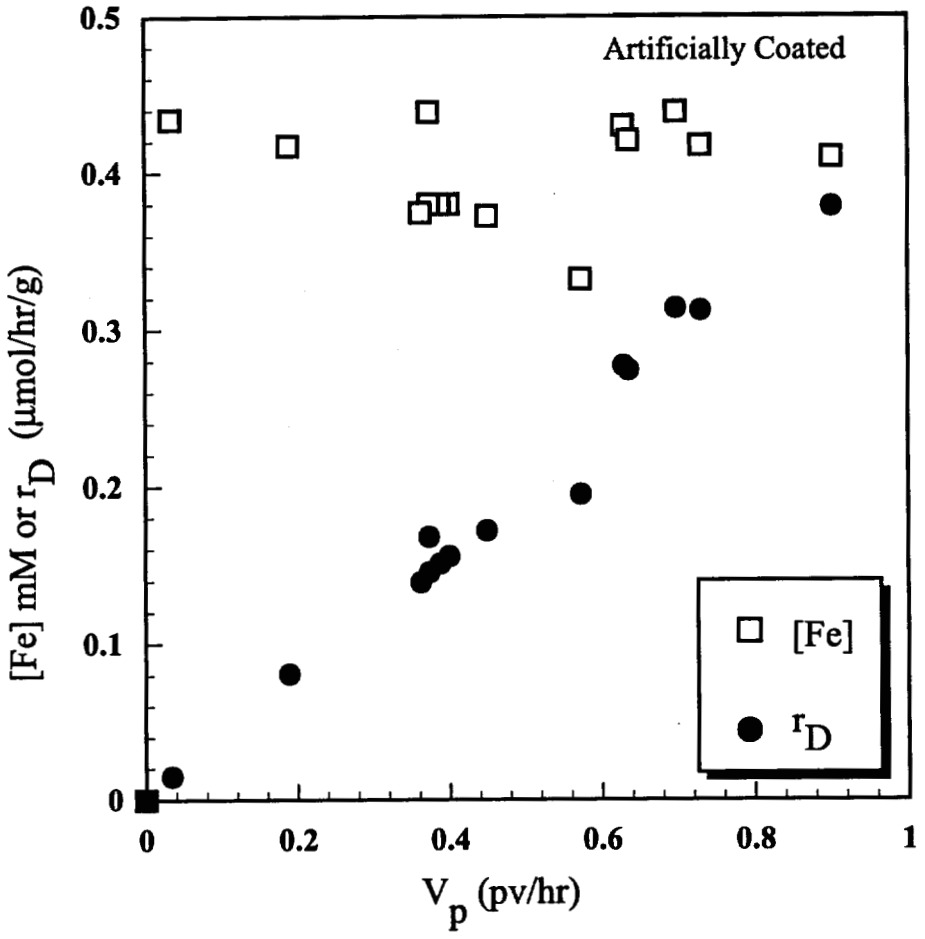

Figure 6.3. The change of concentration of Fe in the effluent and the change in dissolution rate (r_D) with V_p for Artificially Coated (AC) sample.

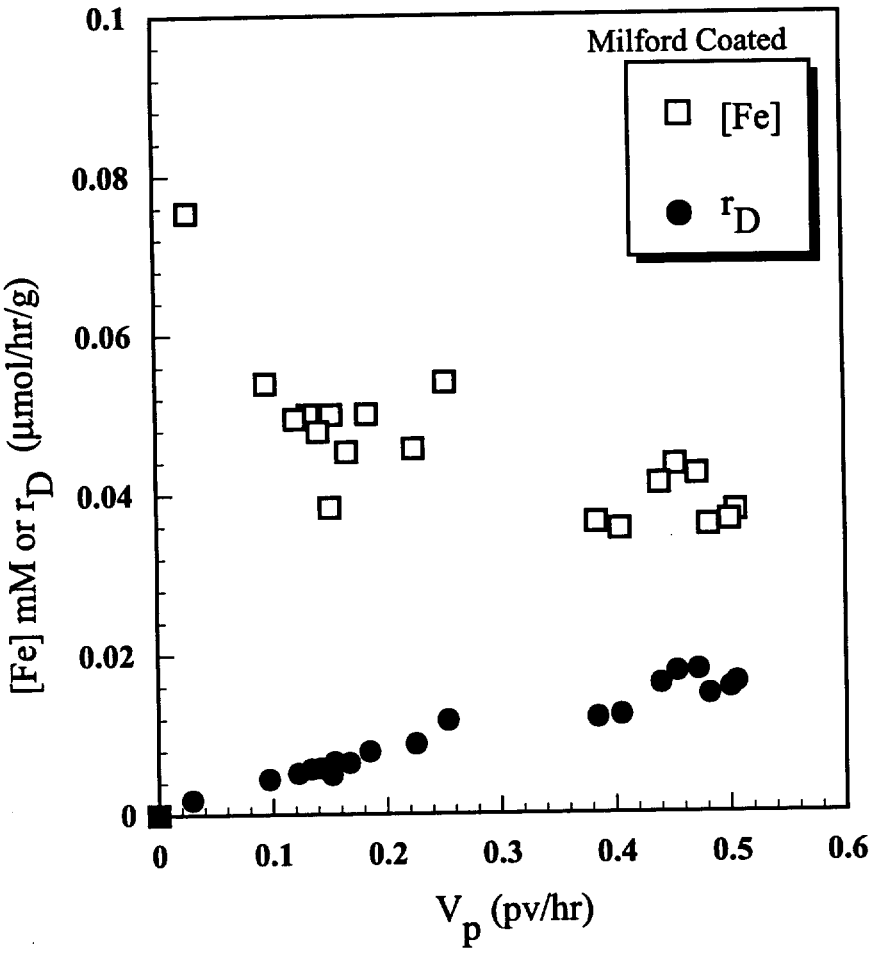

Figure 6.4. The change of concentration of Fe in the effluent and the change in dissolution rate with V_p for Milford Coated (MC) sample.

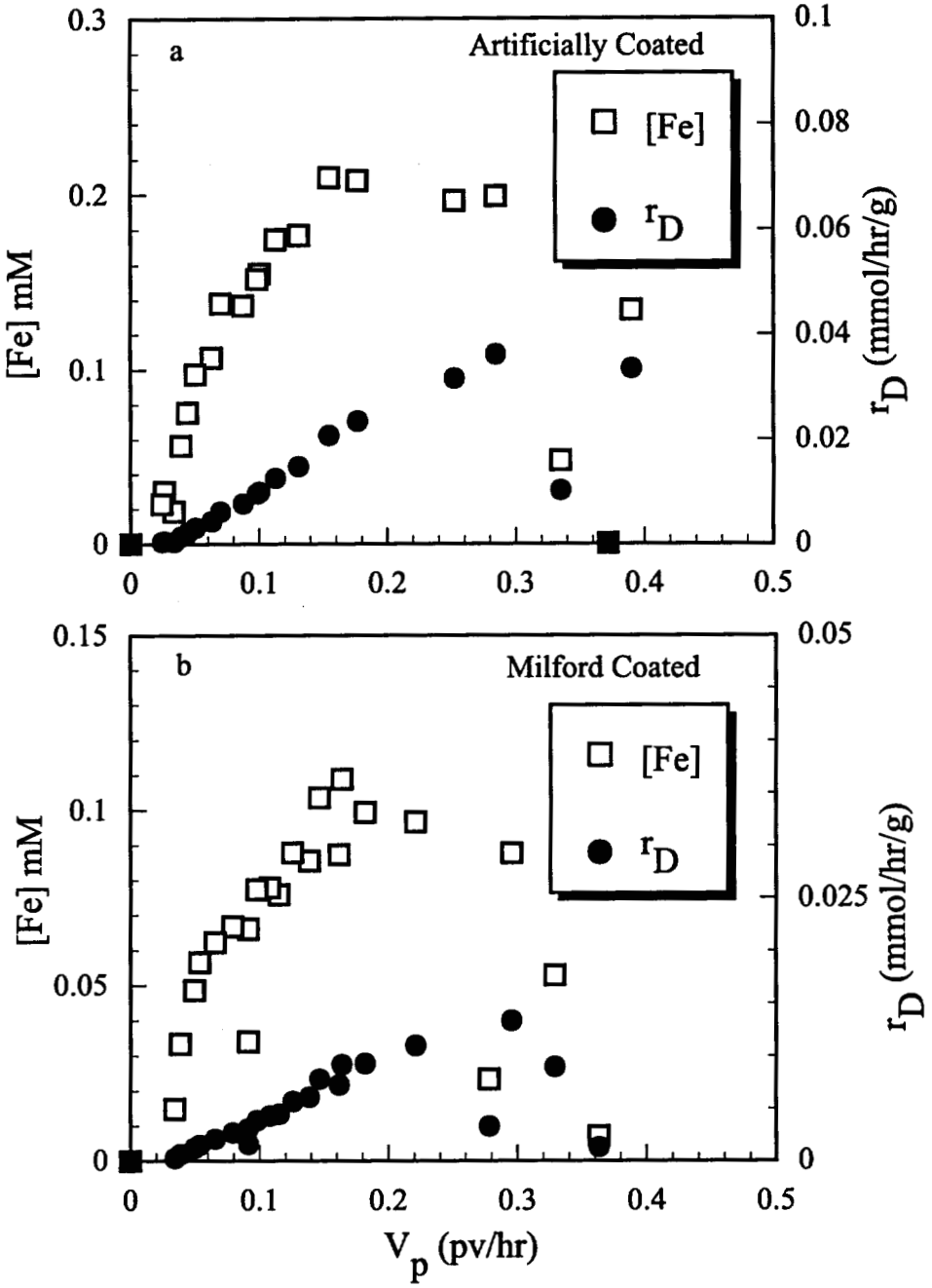

Figure 6.5. The change of concentration of Fe in the effluent and the change in dissolution rate with a velocity parameter V_p for a) AC, and b) MC.

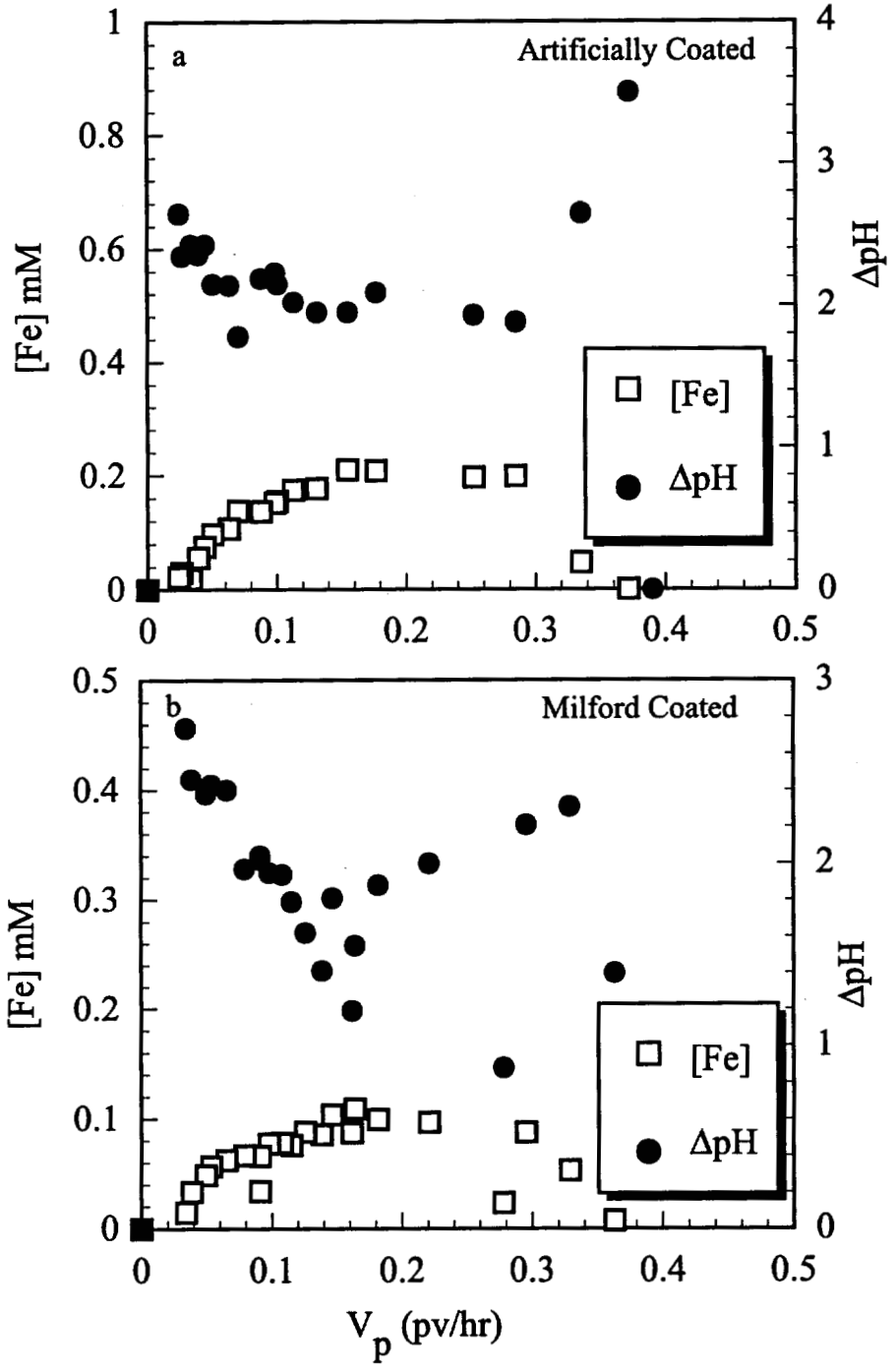

Figure 6.6. The change of concentration of Fe in the effluent and the difference between effluent pH and influent pH (ΔpH) plotted with respect to change in velocity parameter (V_p) for a) AC, and b) MC.

influent solution. In all cases (illustrated in Fig. 6.5 and 6.6), the Fe_{aq} initially increased with V_p, reached a maximum, and decreased with further increase in V_p. The scatter in the data at higher V_p is due to experimental difficulty in maintaining a high flow rate and in sampling the large volume eluted at high flow rates.

For AC, Fe_{aq} rose to 0.2 mM as V_p was increased from 0 to 0.15 pv/hr (see Fig. 6.5a). At higher V_p, Fe_{aq} was constant at about 0.2 mM but declined for $V_p > 0.25$ pv/hr. The change in Fe_{aq} was accompanied by a change in the difference between the effluent and influent pH (ΔpH; shown in Fig. 6.5b). Smaller Fe_{aq} at small V_p corresponded with larger ΔpH whereas larger Fe_{aq} at higher V_p corresponded with smaller ΔpH. The ΔpH eventually plateaued at ~ 2, corresponding to the plateau in Fe_{aq} at 0.2 mM. As with the buffered influent solution, r_D in the unbuffered system rose in proportion to V_p, i.e., $\partial r_D/\partial V_p = 0.14$ μmoles/pv/hr (for $V_p > 0.03$ pv/hr; Fig. 6.5a). The value of r_D for the unbuffered influent was smaller than that for buffered influent. Unlike the buffered influent solution there was no net dissolution of metal oxides between 0 and 0.03 pv/hr probably because dissolved Fe-oxalate complexes readsorbed to the coated sand.

In case of MC (as illustrated in Fig. 6.6a), Fe_{aq} increased to 0.1 mM with increase in V_p to 0.15 pv/hr. Unlike AC, Fe_{aq} did not plateau but declined at higher V_p. The ΔpH diminished with increasing Fe_{aq} and reached a plateau at ΔpH ~ 1.5 corresponding to the maximum Fe_{aq} (Fig. 6.6b). The dissolution rate increased in proportion to V_p, i.e., $\partial r_D/\partial V_p$ = 0.06 μmoles/pv/hr (for $V_p > 0.03$ pv/hr). The value of r_D was nearly the same for the buffered and unbuffered influent solution.

6.7 Discussion

Dissolution of Fe coating from AC is fast relative to the flow rate and dissolution equilibrium is achieved at the pore scale. In Figure 6.3, Fe_{aq} = 0.45 mM saturated 1 mM oxalate and was invariant with V_p. The concentration of dissolved metal in the pore water is not limited by pore scale transport processes. However, the overall metal removed from the column is limited by the rate of advection and may be modeled as a moving boundary problem.

For MC, Fe_{aq} decreased with diminishing V_p. The equilibrium for MC was affected by micropores and was slowly achieved in ~ 48 hours in batch experimental conditions, as mentioned in Chapter 2. At the pore scale, local equilibrium may be achieved at very small V_p. At higher V_p, pore scale equilibrium is disturbed and the system is pushed away from equilibrium. The amount of dissolved metal is diluted by increasing amounts of influent solution flushed through the column at higher V_p. Dissolution in this case is diffusion limited at the microscale and the rate may be calculated with a film diffusion model.

For unbuffered influent solution, Fe_{aq} increased with increase in V_p, reached a maximum, and then decreased (e.g., Fig. 6.5). The corresponding change in ΔpH, which decreased and then plateaued, gives us insight into the V_p dependence (e.g., Fig. 6.5b). Dissolution occurred over a small region at the influent portion of the column. Surface controlled dissolution produces alkalinity (*24*):

Fe-O-Fe-l-OH + L = Fe-O-Fe-l-L + OH^-	Adsorption of ligand
Fe-O-Fe-l-L = Fe-O-l-FeL	Formation of precursor complex
Fe-O-l-FeL + H_2O → Fe-l-OH + FeL + OH^-	Detachment of the metal ion

Such reactions would raise the pH of the influent solution and thereby slowing down ligand induced dissolution. The progression of dissolution front with variation in V_p is illustrated in Figure 6.7. For small V_p the dissolution occurs over a small portion of the column and the corresponding Fe_{aq} is small. This corresponds to a larger ΔpH. As V_p increases, the influent acidity is pushed further through the column, the dissolution occurs over a larger portion of the column, the ΔpH is smaller, and therefore Fe_{aq} is large. For $V_p > 0.15$ pv/hr, the influent acidity broke through the column, the ΔpH was constant, and as a result Fe_{aq} plateaued. Still larger V_p diminished Fe_{aq} because of dilution effect.

The values of r_D were an order of magnitude greater for AC than for MC because the coating of AC was less crystalline. For AC, r_D was greater for buffered influent than for unbuffered influent. Interestingly, the value of r_D was nearly the same when coating was dissolved from MC with either buffered or unbuffered influent solution. The value of $\partial r_D/\partial V_p$ was greater for dissolution of AC with buffered influent (= 0.4 μmoles/pv/g) than with unbuffered influent (= 0.14 μmoles/pv/g). The value of $\partial r_D/\partial V_p$ was nearly the same when

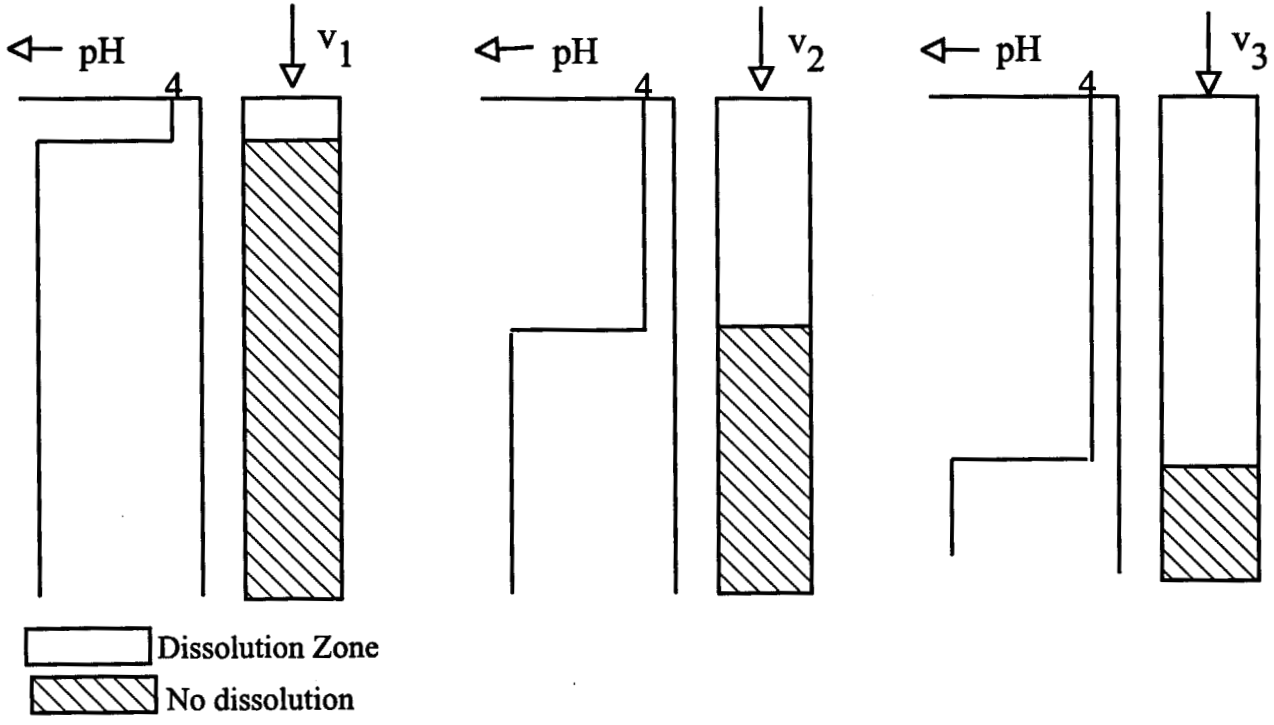

Figure 6.7. Progression of dissolution front with increasing flow velocity in the column ($v_1 < v_2 < v_3$).

MC was dissolved with buffered (= 0.035 μmoles/pv/g) and unbuffered (= 0.06 μmoles/pv/g) oxalate.

6.7.1 Competitive Effects

The dissolved surficial metal will compete with metal contaminant to form stable metal-chelate complexes in solution. Substantial concentration of dissolved surficial metal diminishes the adsorption of oxalate at pH < 6 (demonstrated in Chapter 3). Dissolved Al does not influence the adsorption of Cu in the presence of oxalate but dissolved Fe may influence the adsorption of Cu (explained in Chapter 4). The stability of a metal contaminant in a chelate solution depends on the concentration of other dissolved metals. The efficiency of soil washing with a chelate depends on how effectively a metal contaminant competes with the dissolved metal to form stable metal-chelate complexes. For oxalate, Fe and Al form stable complexes at pH < 6 and various metal contaminants (illustrated in Fig. 6.8a) will not be efficiently removed in the presence of dissolved Fe and Al. For some other chelates like EDTA (a chelate generally proposed for flushing metals), Fe forms a more stable complex at pH < 6 than other metal contaminants (illustrated in Fig. 6.8b) and in its presence metal contaminant removal will not be efficient (Fig. 6.8b). However, Al forms less stable metal-chelate complexes than other metals and in its presence metal contaminant can be efficiently removed.

6.7.2 Implication

Our results indicate that chelates dissolve significant coating and when the influent solution is buffered the dissolution rate may be limited by diffusion in some samples. In others dissolution may be at equilibrium but the total amount of metal dissolved may depend on advection. Increasing V_p (the flushing rate) may not reduce the time required to remediate the contaminated subsoil. Larger V_p will enhance the dissolution of the coating, will reduce the total amount of the contaminant metal that can be complexed by the chelate, and the dissolved metal-chelate complex may require ex-situ treatment prior to disposal. Small V_p will consume less wash solution and require less pumping per unit time but will increase the time in which the site can be remediated.

Adding buffer to the influent solution will simplify the geochemsitry of the remediation

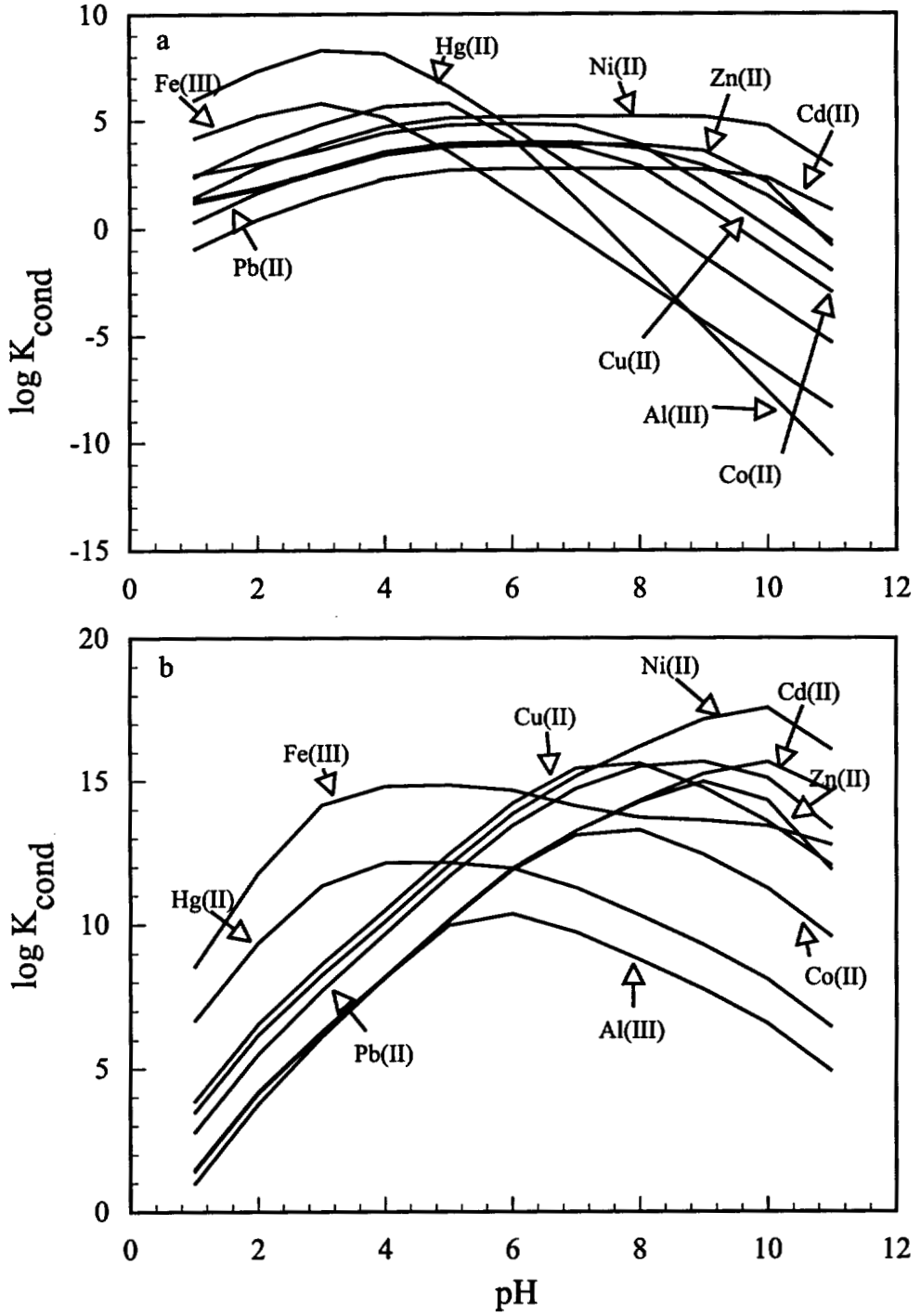

Figure 6.8. Conditional stability constant calculations for the binding of various metal ions to a) oxalate, and b) EDTA.

process. Geochemical equilibrium models will reproduce the geochemistry and film diffusion will reproduce the kinetics of dissolution. In the absence of a buffer there will be less control on the process because of the progress of the dissolution front. The change in pH will be severely dependent on V_p.

Although using buffer is recommended, it will add to the cost of remediation. A fixed buffer concentration may be insufficient in controlling pH in some regions of a geochemically heterogeneous medium. Regions of higher surficial metal typically have greater adsorption capacity and will contain more metal contaminant. Remediation of such a zone will produce greater alkalinity and will provide lesser control on the pH. In subsurface soil, some buffers, like acetate, may be used as a substrate by the indigenous microbial population. Adding buffer in this case may not achieve its intended purpose of maintaining a constant pH.

Remediation of geochemically heterogeneous subsurface soil may result in side reactions that may not be always predictable with buffered and unbuffered influents. This will greatly complicate analysis of data and will add to the uncertainty in monitoring the progress of in-situ removal of metal contaminants.

6.8 References

(1) Yarlagadda, P.S.; Matsumoto, M.R.; Van Benschoten, J.E.; and Kathuria, A.J. *J Environ. Eng.*, **1995**, 121(4):276-286.

(2) Davis, A.P. and Singh, I. *J. Environ. Eng.*, **1995**, 121(2):174-185.

(3) Jones, T.L. and Ghassemi, A. "Modern In-Field Process System - Case Study: Soil Washing," in *Remediation of Hazardous Waste Contaminated Soils*, Wise, D.L. and Trantola, D.J. (eds.), Mercel Dekker, Inc., **1994**, pp. 719-744.

(4) Van Riemsdijk, W.H. and Van der Zee, S.E.A.T.M. *Geochim. Cosmochim. Acta*, **1989**, 44:143-158.

(5) Probstein, R.F. and Hisks, R.E. *Science*, **1993**, 26:498-503.

(6) Acar, Y.B. and Alshawabkeh, A.N. *Environ. Sci. Technol.*, **1994**, 28:2638-2650.

(7) Hicks, R.E. and Tandorf, S. *Environ. Sci. Technol.*, **1994**, 28:2203-2210.

(8) Raghavan, R.; Coles, E.; and Dietz, D. *Cleaning Excavated Soil Using Extraction Agents:*

A State-of-the-Art Review, *EPA/600/2-89/034*, Environmental Protection Agency, Cincinnati, Ohio, **1989**.

(9) Dennis, R.M.; Dworkin, D., and Zupko, A.J. "Soil Washing Processes for Site Remediation," In *Remediation of Hazardous Waste Contaminated Soils*, Wise, D.L. and Trantola, D.J. (eds.), Mercel Dekker, Inc., **1994**, pp. 719-744.

(10) Lindsay, W.L. *Chemical Equilibria in Soils*, John Wiley & Sons, New York, **1979**.

(11) Swanson, J.L. *Effects of Organic Complexants on the Mobility of Low-Level Waste Radionuclides in Soils: Status Report*, *PNL-3927*, Pacific Northwest Laboratory, Richland, Washington, **1981**.

(12) Swanson, J.L. *Mobility of Organic Complexes of Nickel and Cobalt in Soils*, *PNL-4796*, Pacific Northwest Laboratory, Richland, Washington, **1983**.

(13) Means, J.L.; Crerar, D.A. and Duguid, J.O. *Science*, **1978**, 200:1477-1481.

(14) Elliott, H.A.; Linn, J.H. and Shields, G.A. *Hazardous Waste & Hazardous Materials*, **1989**, 6(3)223-229.

(15) PEI Associates Inc., *Electromembrane Processes for Recovery of Lead from Contaminated Soils*, National Science Foundation, Grant No. ISI-8560730, **1986**.

(16) Furrer, G. and Stumm, W. *Geochim. Cosmochim. Acta*, **1986**, 50:1847-1860.

(17) Stumm, W.; Furrer, G.; Wieland, E.; and Zinder, B.; "The Effects of Complex-Forming Ligands on the Dissolution of Oxides and Aluminosilicates," in *The Chemistry of Weathering*, J.L. Drever (ed.), **1985**, 55-74, Reidel Publishing Co.

(18) Stumm, W.; Furrer, G. and Kunz, B. *Croat. Chem. Acta.*, **1983**, 56:593-611.

(19) Zinder, B.; Furrer, G.; and Stumm, W. *Geochim. Cosmochim. Acta*, **1986**, 50:1861-1869.

(20) Wieland, E. and Stumm, W. *Geochim. Cosmochim. Acta*, **1992**, 56:3339-3355.

(21) Chim, P-K. F. and Mills, G.L. *Chem. Geol.*, **1991**, 90:307-317.

(22) Torres, R.; Blesa, M.A. and Matijević, E. *J. Colloid Interface Sci.*, **1989**, 131(2):567-579.

(23) Chang, H.-C. and Matijević, E. *J. Colloid Interface Sci.*, **1983**, 92:479.

(24) Lin, C-F. and Benjamin, M.M. *Environ. Sci. Technol.*, **1990**, 24:126-134.

(25) Amrhein, C. and Suarez, D.L. *Geochim. Cosmochim Acta*, **1988**, 52:2785-2793.

(26) Wogelius, R.A. and Walther, J.V. *Geochim. Cosmochim. Acta*, **1991**, 55:943-954.

(27) Torres, R.; Blesa, M.A. and Matijević, E. *J. Colloid Interface Sci.*, **1990**, 134(2):475-485.

(28) Lundström, U.S. *J. Soil Sci.*, **1993**, 44:121-133.

(29) Szecsody, J.E.; Zachara, J.M; and Bruckhart,P.L. *Environ. Sci. Technol.*, **1994**, 28:1706-1716.

(30) Bennett, P.C.; Melcer, M.E.; Siegel, D.I. and Hassett, J.P. *Geochim. Cosmochim. Acta*, **1988**, 52:1521-1530.

(31) Iler, R.K. *The Chemistry of Silica*, **1979**, John Wiley, New York, pp. 866.

(32) Lewin, J.C. *Geochim. Cosmochim. Acta*, **1961**, 21:182.

(33) Beckwith, R.S. and Reeve, R. *Geochim. Cosmocim. Acta*, **1969**, 33:745-750.

(34) Bowers, A.R. and Huang, C.P. *Wat.Res.*, **1987**, 21(7):757-764.

(35) Ringbom, A. and Wanninen, E. "Complexation Reactions," in *Treatise on Analytical Chemistry* Part 1, Vol. 2 2nd edition, Kolthoff, I. and Ewing, P. (eds.), **1979**, Wiley, New York.

CHAPTER 7*

GEOCHEMICAL EVOLUTION OF THE HETEROGENEITY OF SOIL ADSORPTION SITES

7.1 Abstract

Weathering reactions in natural and contaminated subsurface soils often dissolve hydrous metal oxides from these soils. Dissolution of hydrous metal oxides can alter the adsorption properties of subsoil particles. We tested this hypothesis by dissolving different amounts of oxide coatings from Milford Coated (MC) and Milford Uncoated (MU) sands. We then obtained isotherms and pH edges for these "weathered" samples as well as for "unweathered" MC and MU. For MC, the adsorption of oxalate did not measurably change until after about 70% of the 6 N HCl extractable surficial Fe and Al were removed. Cu edges in the presence and absence of oxalate did not change until nearly all the surficial Fe and Al were lost. For MU, the adsorption of oxalate and Cu in the presence and absence of oxalate changed only when nearly all of the oxide coating was removed. The change in the adsorption characteristics was represented by a diminished site density, a decline in the average binding strength, and a loss of sites with larger adsorption energies.

---

* To be submitted to *Environmental Science & Technology*

7.2 Introduction

Hydrous metal oxides are important products of weathering and soil formation processes (*1*). They do not readily dissolve at typical soil pH (2) but can be dissolved and transported by organic chelators produced biologically in the soil (e.g., *3 - 6*) or introduced to the soil by humans (e.g., *7 - 11*). In anaerobic, organic rich environments, reduction by microorganisms dissolves Fe and Mn oxides from soils (*12, 13*).

Ligand-promoted dissolution occurs through adsorption of a ligand, formation of the precursor metal-ligand complex, and release of the metal from the surface (e.g., *14 - 17*). Chelator induced dissolution is usually much faster than proton promoted dissolution at typical soil pH values (*10, 17, 18*). The detachment of the surface metal is further enhanced by reductive dissolution (e.g., *9, 19*) and photoreductive dissolution (*20, 21*) where electron transfer follows adsorption.

We hypothesize that weathering reactions may change the adsorption of soils by, 1) inducing large scale variability in the adsorption properties of chemically homogeneous but physically heterogeneous soils, 2) altering the microscale adsorption heterogeneity within all or part of a soil formation, and 3) reducing the adsorption heterogeneity among different soils. The hypothesis is based on the rationale that soils are often heterogeneous in their adsorption characteristics and contain a wide range of adsorption energies. Ligands may preferentially coordinate onto the strongest adsorption sites on soil surface and may preferentially dissolve the stronger binding sites. As illustrated in Figure 7.1a, this may dissolve the stronger sites more readily than the weaker sites thereby altering the distribution of adsorption energies and reducing the overall site density (N_s). At the larger spatial scales, differential flow of ligands/acids through regions of higher permeability will preferentially dissolve surficial metal creating localized zones of metal depletion (illustrated in Fig. 7.1b). Evidence for the effect of pore velocity on dissolution rate is presented in Chapter 6. The solubilized metal can also be redeposited in strata with different geochemical environment creating localized zones of metal enrichment, as in spodosol soils (22). Over long time scales, the presence of physical heterogeneity can increase the macro-scale geochemical variability of the subsurface.

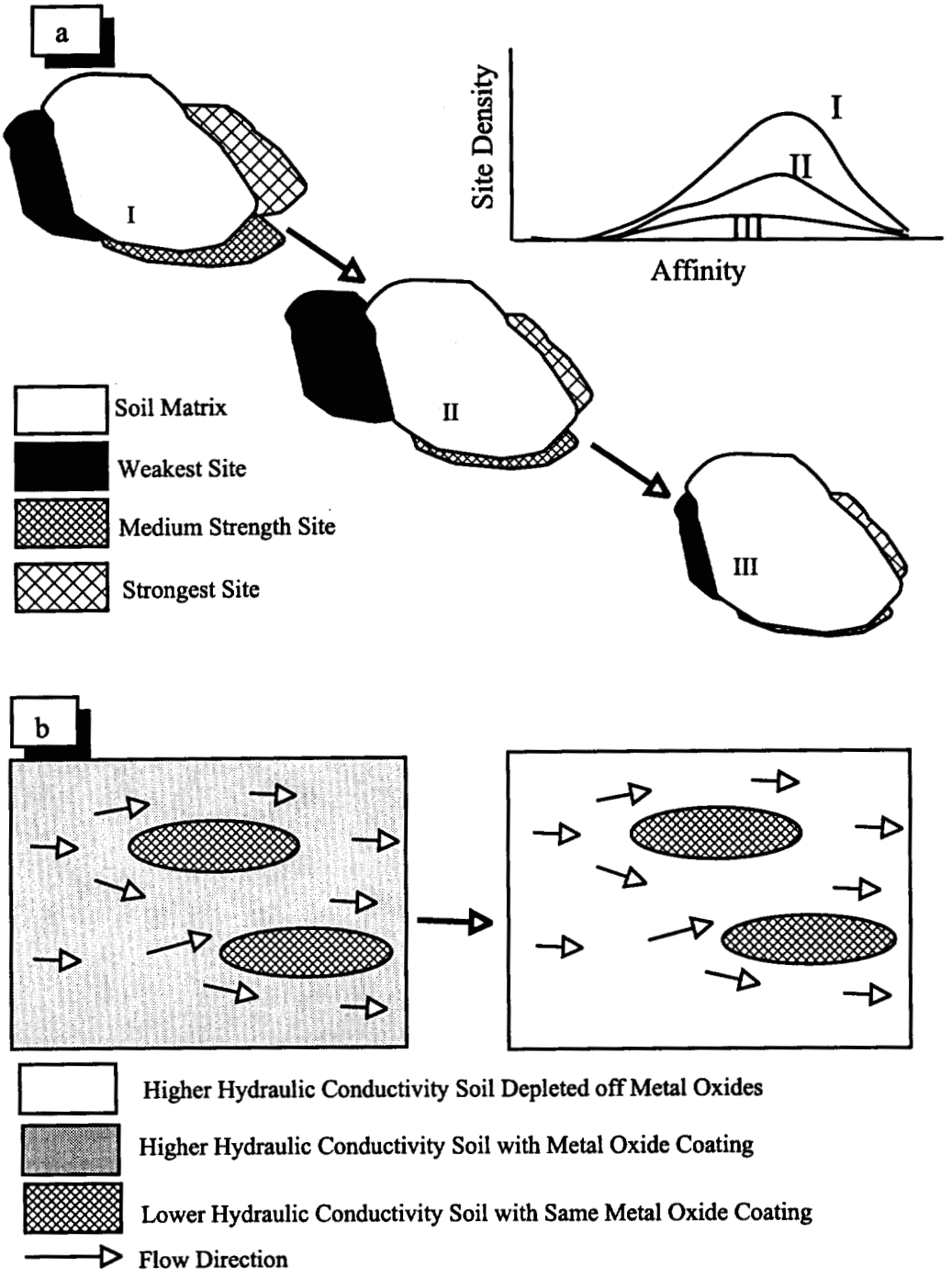

Figure 7.1. Geochemical Evolution of a) microscale adsorption heterogeneity, and b) macroscale adsorption heterogeneity.

Although ligands naturally present in soil change the soil adsorption properties, the change is accelerated in soils contaminated with high concentration of ligands. The role of such evolution is important for understanding the 1) long term mobility of solute in soils, 2) effect of flushing ligands though soils to clean up metal contamination, 3) effect of generating protons during electrokinetic remediation, and 4) whether dissolution of adsorption sites during laboratory experiments will change the sorbent property being studied.

The goal of this research was to quantify the changes in adsorption heterogeneity due to weathering induced loss of adsorption sites. We used samples of two sands naturally coated with varying amounts of Fe and Al oxides. Oxalate was used to promote the dissolution of surficial metal oxides because oxalate is found in both contaminated and natural environments. The change in the surface was studied with scanning electron microscopy (SEM). Changes in adsorption properties were probed with isotherms and pH edges for oxalate, Cu, and Cu in the presence of oxalate (denoted here as Cu*-Ox).

We found that adsorption parameters were only minimally affected by weathering until nearly all of the surficial oxides were removed. The changes in adsorption was modeled by a reduced N_s, a loss of stronger adsorption sites, and a decrease in the average binding strength.

7.3 The Strategy for Modeling Changes in Adsorption Properties

We modeled the edges for oxalate, Cu, and Cu*-Ox with the Diffuse Layer Model (DLM) and the Continuous Distribution Model (CDM) (*23*). We modeled the isotherms only with the CDM.

7.3.1 The DLM Approach

The Diffuse Layer Model, the Constant Capacitance Model, and the Triple Layer Model accurately reproduce the adsorption edges for low to moderate surface coverage (Chapters 3 and 4). We modeled the adsorption edges for oxalate, Cu, and Cu*-Ox with the homogeneous-site DLM because it is simple and has the fewest adjustable parameters. We were unable to reproduce the isotherms with DLM because of the apparent heterogeneity in adsorption energies.

MC and MU have small specific surface areas (3 m^2/g and 2 m^2/g, respectively). We assumed that dissolution of surficial Fe and Al will not substantially change the surface area of coated sands because the samples will not have any significant micropores. It was demonstrated in Chapters 3 and 4 that fitting with surface complexation models is insensitive to the choice of surface protonation constants (pK_a). It is also difficult to quantify unambiguously small difference in pK_a for the weathered samples of MC and MU because of experimental error and modeling limitations. We assumed the values of pK_a to be the same for the weathered and unweathered samples of MC and MU.

We fit the adsorption data with FITEQL 3.1 and analyzed the DLM results by, 1) comparing the goodness of fit (V_Y) for the optimized effective surface complexation constant (K^{eff}) while fixing N_s for all samples in a weathering sequence, and 2) optimizing both the K^{eff} and the N_s (for the best V_Y) and then examining changes in these parameters. Although significant deviation of V_Y from unity for different data sets suggest worsening of the fit, strict comparison of V_Y values is not possible because of the difference in the inherent noise in the data. A change in N_s can be related to the change in the amount of Fe and Al on the surface but cannot by itself be related to loss of sites of particular strengths. However, K^{eff} is a measure of the average strength of binding of an adsorbate. We will obtain a larger value of K^{eff} when the adsorbate binds to the stronger sites and a smaller value when it binds to weaker sites. The K^{eff} values for homologous samples (same sample but different surficial Fe and Al) will increase if stronger sites are generated or weaker sites are lost. The K^{eff} values decrease if stronger sites are lost and the adsorbate binds to the weaker sites.

We modeled the edges with the species used in Chapters 3 and 4 (listed in Table 7.1). The DLM was calibrated to the pK_a of goethite. We analyzed the oxalate edges only for pH $\geq$ 6 so that we could neglect the competition between dissolved metal and the surface for the oxalate in solution.

7.3.2 The CDM Approach

The CDM approach (*23*) estimates a continuous distribution of adsorption energies. These distributions are approximations and do not represent the "real" variation of energies. Although this simplistic approach may not accurately estimate the range of site strengths of

Table 7.1. Equilibrium expressions for the surface complexation reactions used to reproduce the adsorption of Cu, oxalate, and Cu in the presence of oxalate in the Diffuse Layer Model (DLM). The same surface species were shown to reproduce the adsorption in Chapters 3 and 4.

Oxalate
$[\equiv XC_2O_4^-] = [\equiv XOH^o]\{C_2O_4^{2-}\}\{H^+\}\exp(F\psi_o/RT)K_{XOx2}$
$[\equiv XOC_2O_4^{3-}] = [\equiv XOH^o]\{C_2O_4^{2-}\}\{H^+\}^{-1}\exp(3F\psi_o/RT)K_{XOx3}$
Copper
$[\equiv XOCu^+] = [\equiv XOH^o]\{Cu^{2+}\}\{H^+\}^{-1}\exp(-F\psi_o/RT)K_{XOCu}$

individual sorbents, it can be effectively used for describing the changes in the range of adsorption energies for weathered and unweathered samples.

Kinniburgh et al. (*23*) derive expressions for composite isotherms for the General Freundlich, Langmuir-Freundlich, Discrete-Site Langmuir, and Tóth approaches. They conclude that the Tóth equation (Eq. 7.1) is the best and we have used it to analyze the adsorption data:

$$S^* = \frac{SAN_s^T 10^{\kappa}}{a(1 + 10^{\beta\kappa})^{1/\beta}} \qquad (7.1)$$

where, S^* is the amount adsorbed per unit sorbent and $\kappa = {}^cp_m + \tilde{n}pH + \log c$. The exchange stoichiometry is $\tilde{n}$, c is the equilibrium concentration in solution, N_s^T is the site density calculated with the Tóth isotherm equation, S is the solids concentration (g/L), A is the specific surface area (m^2/g), a is the Avogadro number, β is the heterogeneity index ($0 < \beta < 1$), and ${}^cp_m$ is the optimized value of the relative affinity. The adjustable parameters are ${}^cp_m$, $\tilde{n}$, N_s^T, and β. Based on assumptions of site affinity distribution function, Kinniburgh et al. (*23*) derive an expression for the dimensionless distribution of site strength ($V({}^cp)$):

$$V({}^cp) = \frac{\ln 10}{\pi}(1 + 2.10^{\beta\tau}\cos \pi\beta + 10^{2\beta\tau})^{-1/2\beta}\sin\left(\frac{1}{\beta}\tan^{-1}\left(\frac{\sin \pi\beta}{10^{-\beta\tau} + \cos \pi\beta}\right)\right) \qquad (7.2)$$

where, ${}^cp$ is the relative affinity, and $\tau = {}^cp - {}^cp_m$. This distribution is skewed to the right and gives a low affinity tail. Our strategy was to fit Eq. 7.1 to the edges and isotherms to obtain

values for $^{c}p_m$, $\bar{n}$, N_s^T, and β. These values were then substituted in Eq. 7.2 to obtain a range of adsorption site strengths. The ordinate of the distribution was plotted in terms of MV(^{c}p) (where, M = N_s^TSA/a) to convert the distribution from a dimensionless scale to an absolute scale (concentration of sites per unit sorbent). MV(^{c}p) = number of sites with ^{c}p between ^{c}p and $^{c}p + d^{c}p$ per unit adsorbent. The abscissa was the normalized relative affinity - τ.

For constant β, N_s^T, and $\bar{n}$, changing the value of $^{c}p_m$ changes only the position of the distribution on the affinity axis and not its shape. When all other parameters are held constant, a decrease in N_s^T lowers the maximum height of the distribution without shifting its position. A decrease in β reduces the maximum peak value, broadens the distribution, and shifts the peak to the lower affinity region. A change in the distribution due to diminished N_s^T suggests a greater loss of medium strength sites and smaller loss of low or high strength sites. A peak shifted to the lower affinity region has more sites of smaller strength. A change in $\bar{n}$ does not directly influence the shape of the distribution because its value is not used for calculating (V^{c}p) with Eq. 7.2. However, different values of $\bar{n}$ effect the optimized values of $^{c}p_m$, β, and N_s^T. This then indirectly influences the calculated range of site strengths. Loss of adsorption sites will decrease the value of N_s^T. A change in the range of adsorption energies will be reflected by a change in the optimal value of β.

For the adsorption edges, Eq. 7.1 was fitted with the nonlinear Levenburg-Marquardt algorithm using SigmaPlot (Jandel Scientific). When $^{c}p_m$, β, N_s^T, and $\bar{n}$ were all used as fitting parameters the solution was sensitive to the initial guess. We were unable to minimize the standard error to obtain the best fit because of a very shallow minimum. For the unweathered samples we fixed $\bar{n}$ to a generally accepted value and N_s^T to the total adsorbate concentration, and used $^{c}p_m$ and β as adjustable parameters. The value of $^{c}p_m$, obtained for the unweathered sample, and $\bar{n}$ were fixed for subsequent nonlinear fits of the weathered samples. It is possible to use this approach to estimate changes in both adsorption capacity and intensity from anion edges because the fraction adsorbed decreases for larger sorbate/sorbent ratio (*24*). Cation edges shift towards higher pH for large sorbate/sorbent ratios but span the same fraction adsorbed range (0% to 100%). Hence, for cations it is not possible to differentiate between change in adsorption capacity and adsorption intensity.

For the adsorption isotherms, the nonlinear fitting for Eq. 7.1 was done with Levenburg-Marquardt algorithm using TableCurve (Jandel Scientific). The fitting was sensitive to the initial guess when ${}^{c}p_m$, β, N_s^T, and $\bar{n}$ were used as adjustable parameters. We modeled the isotherm for the unweathered sample by using ${}^{c}p_m$, β, N_s^T, and $\bar{n}$ as adjustable parameters. For the weathered samples, we fixed the value of ${}^{c}p_m$ (to the value obtained for the unweathered sample) and used β, M, and $\bar{n}$ as adjustable parameters.

7.4 Experimental Methods

We conducted experiments on samples of two sands naturally coated with varying amounts of Fe and Al oxides, Milford Coated (MC) and Milford Uncoated (MU) which were obtained from the Pacific Northwest Laboratory, Richland, WA. They were collected from adjacent subsurface strata in Delaware. Details of sample preparation and experimental conditions are presented in Chapter 2.

To eliminate the abrasion of particles in stirred reactors we dissolved the surficial metal oxides in a mini-column manifold (Fig. 6.1). Details of experimental methodology for dissolution is presented in Chapter 6. We removed the mini-columns at various stages of dissolution. We removed the cores, washed the weathered samples with DI water, and NaOH solution (pH ~ 10.5) to desorb the adsorbed oxalate. Washing desorbed > 90% of the adsorbed oxalate after 48 hours. Washing also removed coatings from the weathered sample and the total mass of fines generated during washing was the same when the weathered samples were washed with DI water or with solution containing 0.01, 0.05, and 0.1 M NaCl. We removed more coating from MC and MU with Ox_T = 100 μM than the operationally defined "oxalate extractable" portion of the coating (listed in Table 7.2). Washing with DI water and NaOH solution liberated oxide-rich fines from the coated samples because of physical abrasion. We filtered and removed the fines from the weathered samples and lost some of the metal oxide coating. The samples in a weathering sequence are labelled as MC or MU followed by the sequence number (e.g., MC0, MC1, etc. listed in Table 7.2). We air

Table 7.2. The surficial Fe and Al determined by extraction of sub-samples of weathered and unweathered samples of MC and MU with 6 N HCl and ammonium oxalate/oxalic acid (NH_4-Ox).

Soil	6 N HCl				NH_4-Ox	
Sample	Fe (mg/g)	% of Total	Al(mg/g)	% of Total	Fe (mg/g)	Al (mg/g)
MC0	0.75	100%	1.3	100%	0.2	0.11
MC1	0.45	60%	0.9	69%		
MC2	0.21	28%	0.42	32%		
MC3	0.05	7%	0.23	18%		
MU0	0.12	100%	0.5	100%	0.06	0.07
MU1	0.06	50%	0.4	80%		
MU2	0.04	33%	0.2	40%		
MU3	0.01	8.3%	0.11	22%		

dried the samples and used them for subsequent adsorption experiments. The "total" surficial Fe and Al of the homologous samples of MC and MU were measured by extracting subsamples with 6 N HCl (Table 7.2). The "amorphous" portion of the surficial Fe and Al was measured for the unweathered samples by extracting subsamples with ammonium oxalate/oxalic acid solution (Table 7.2). Details of extraction procedure is presented in Chapter 2.

We obtained the adsorption edges for oxalate concentration (Ox_T) of 10 μM and 50 μM, Cu concentration (Cu_T) of 15 μM, and Cu_T = 27 μM in the presence of Ox_T = 1 mM. We also obtained adsorption isotherms at pH 7 for oxalate and Cu in the presence of Ox_T = 1 mM. The solution was buffered at pH 7 with 0.01 M MOPS, a non-interfering biological buffer. Oxalate partitioning was measured with radiolabeled ^{14}C oxalate (NEN Research Products, 98.1 % purity). An aliquot of filtrate (750 μL) was added to 3 mL scintillation liquid (Ecolite, ICN Pharmaceuticals, Inc.) and the ^{14}C activity in solution was measured in a scintillation counter. Cu in solution was analyzed with atomic absorption

spectrophotometry (AAS), using either flame or graphite furnace atomization. The adsorbed amount was calculated as the difference between the total concentration and the concentration in solution.

We used scanning electron microscopy (SEM; Zeiss DSM-960) and semi-quantitative Energy Dispersive X-ray (EDX) to document visually changes in the surface and to analyze the changes in the surface elemental composition for unweathered and weathered samples. We placed air dried samples of MC and MU on stainless steel stubs and coated them with Au-Pd to prevent charging of the surface during imaging.

7.5 Results

7.5.1 Surface Microscopy

The surfaces of MC and MU grains in Figures 7.2a and 7.3a were relatively smooth prior to weathering with oxalate solution. The semi-quantitative EDX analysis of the unweathered sample, illustrated in Figure 7.2c and 7.3c, revealed both Fe and Al in the unweathered sample of MC and Al in the unweathered sample of MU. This correlates well with the data obtained with chemical extraction (Table 7.2). For the weathered samples, we analyzed MC3 (contained 7% of the 6N HCl extractable Fe and 18% of the 6 N HCl extractable Al, Table 7.2) and MU3 (contained 8.3% of the 6N HCl extractable Fe and 22% of the 6 N HCl extractable Al, Table 7.2) with SEM because they represent the end points of weathering in our experiments. After dissolution the surface of MC3 (shown in Fig. 7.2b) became rougher and surface elemental composition changed (see Fig. 7.2d). Unlike MC, the surface of MU (in Figure 7.3b) did not change. Although MC3 and MU3 lost the same proportion of 6 N HCl extractable coating, semi-quantitative EDX analysis of the weathered samples revealed Al for MC3 (Fig. 7.2d) but not for MU3 (Fig.7.3d). We were unable to detect surficial Fe in MC3 and MU3.

7.5.2 Probing Change in Adsorption Properties with Adsorption Isotherms and Edges

7.5.2.1 Oxalate Isotherm: For unweathered MC (MC0), the isotherm (at pH 7) illustrated in Figure 7.4a was saturating Freundlich with slope < 1 and transitioned gradually towards

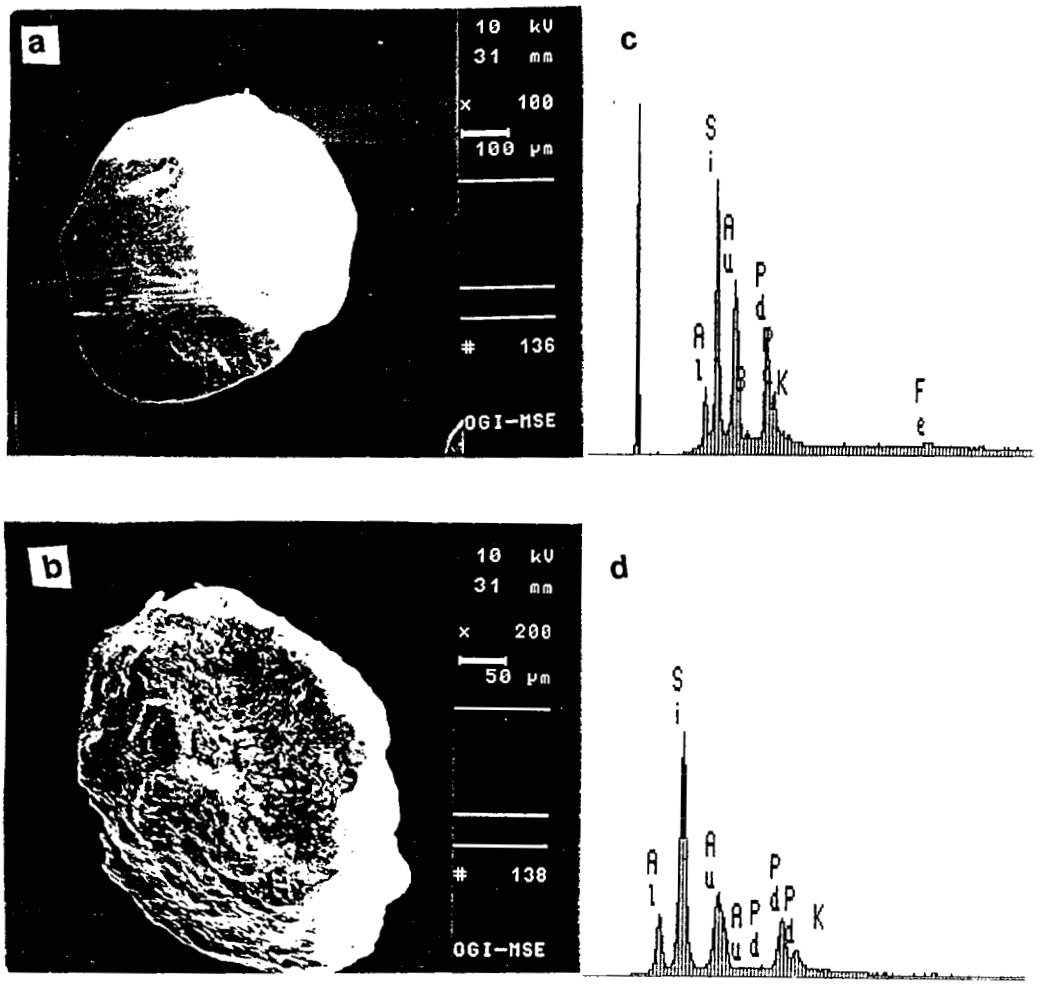

Figure 7.2 Scanning Electron Micrographs of a)unweathered Milford Coated (MC0) and b) weathered Milford Coated (MC3). The energy dispersive X-ray are shown in a) MC0 and b) MC3.

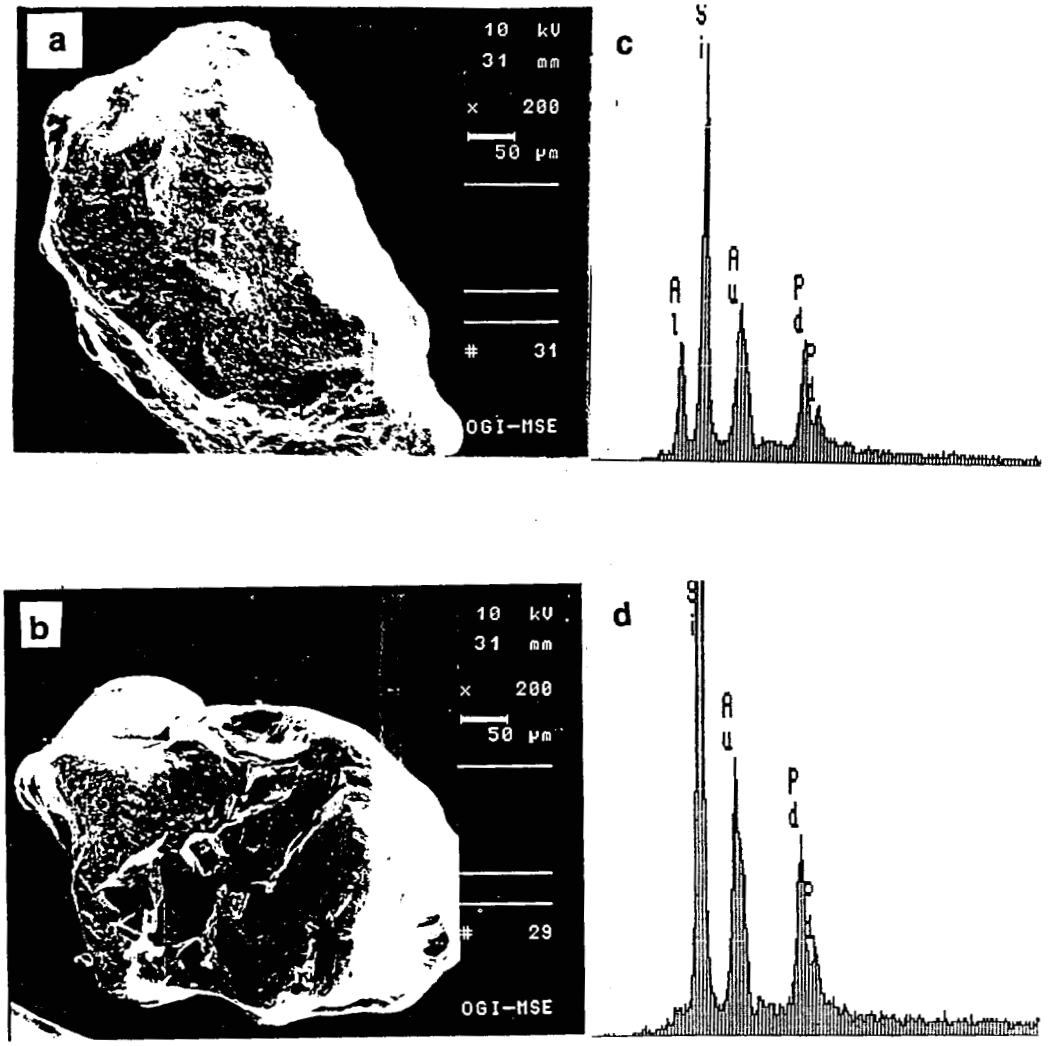

Figure 7.3 Scanning Electron Micrographs of a)unweathered Milford Uncoated (MU0) and b) weathered Milford Uncoated (MU3). The energy dispersive X-ray are shown in a) MU0 and b) MU3.

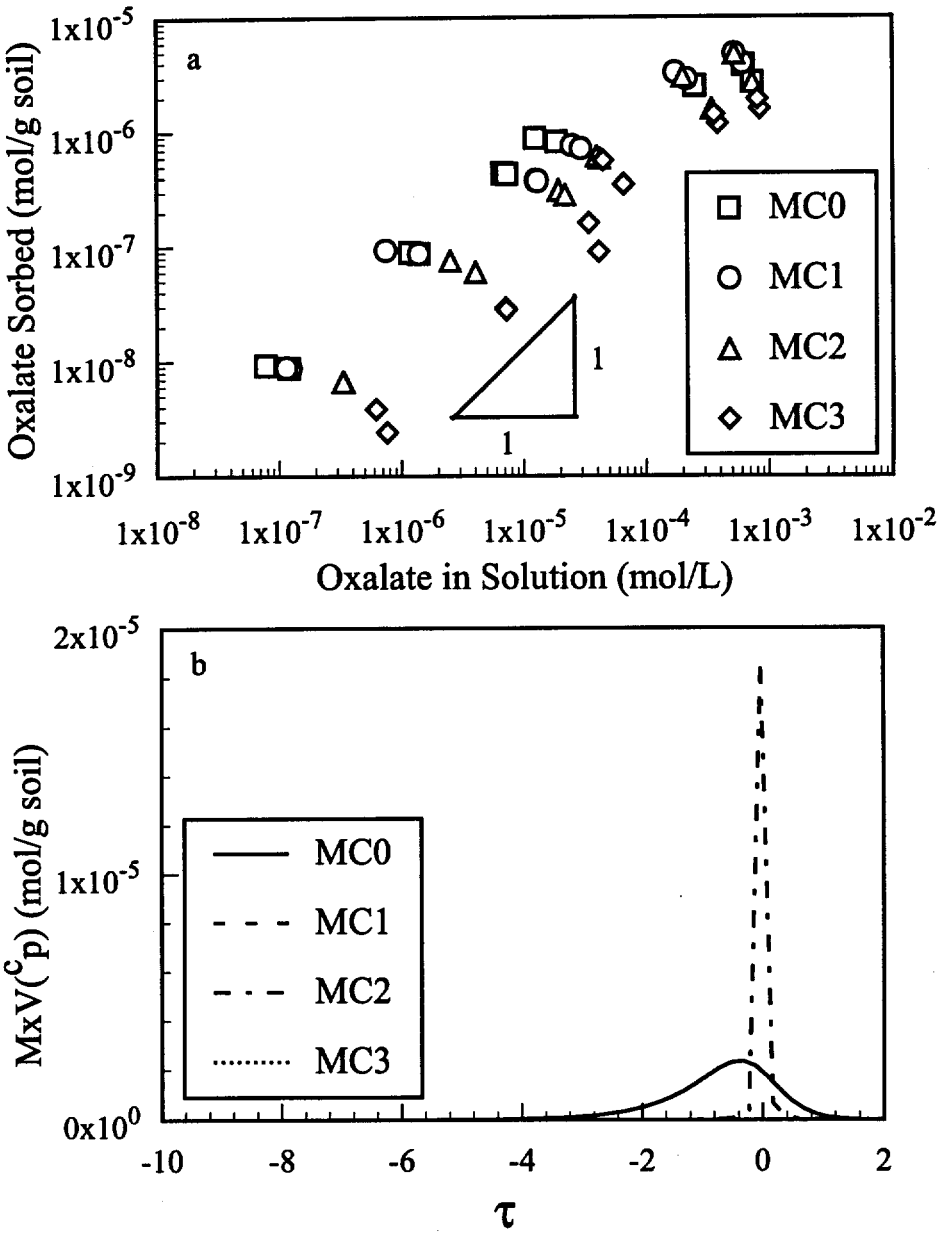

Figure 7.4. Data for a) oxalate isotherm, and b) the range of site strengths calculated with the continuous distribution model at pH 7 for samples of MC. The weathering sequence is indicated by sample name followed by a number. The surficial metal oxide for the samples is listed in Table 7.2. Lines for MC0 and MC1 are overlapping and MC3 is indistinquishable from the horizontal axis.

Table 7.3. Results of Continuous Distribution Model (CDM) fits for adsorption of oxalate, Cu, and Cu in the presence of oxalate (denoted here as Cu*-Ox) onto weathered and unweathered samples of MC.

Sample	Ox_T = 10 μM		Ox_T = 50 μM		Ox Isotherm		Cu_T = 15 μM		Cu*-Ox		Cu*-Ox Isotherm	
^cp_m	15.7		15.7		15.5		-4.7		-7.9		-10.6	
$\bar{n}$	-1.0		-1.0		-1.5		2.0		2.0		2.0	
Sample	N_s^T	β	N_s^T	β	N_s^T	β	N_s^T	β	N_s^T	β	N_s^T	β
MC0	0.02	0.32	0.10	0.24	0.88	0.54	0.03	1.00	0.05	0.41	0.21	1.00
MC1	0.02	0.34	0.08	0.25	0.88	0.54	0.03	0.97	0.05	0.36	0.19	1.00
MC2	0.01	1.00	0.05	0.43	0.88	0.99	0.03	0.64	0.05	0.31	0.14	1.00
MC3	0.01	1.00	0.04	1.00	0.48	1.00	0.03	0.42	0.05	0.23	0.03	1.00

an adsorption maximum. When ~ 40% of the 6 N HCl extractable oxide coating (MC1; listed in Table 7.2) was removed the isotherm showed visible change. Removal of ~ 70% of the coating resulted in a slight decrease in adsorption maximum, an increase in the slope to unity, and a sharper transition to the adsorption maximum. Removal of more coating further decreased the adsorption of oxalate in MC3. For the CDM analysis, the value of N_s^T (listed in Table 7.3) decreased only for MC3 (an apparent loss of adsorption sites) when nearly all of the extractable coating was removed. The β values were the same for MC0 and MC1 but increased to 0.99 (a decrease in heterogeneity) for MC2. MC0 and MC1 revealed the same distribution of site strengths in Figure 7.4b. When compared to the other samples MC3 did not reveal any distribution of site strengths.

Unlike MC, the slope of the oxalate isotherm for unweathered MU (at pH 7) in Figure 7.5 was ≈ 1. The heterogeneity was revealed by a gradual transition to the adsorption maximum. The oxalate isotherms onto weathered samples of MU remained unchanged until nearly all the surficial coating was removed. At that point, MU3 had a diminished adsorption and there was a sharper transition from the linear region to the adsorption maximum. The Tóth equation (Eq. 7.1) was unable to reproduce accurately the gradual transition of the isotherm from the linear region to the adsorption maximum. The CDM analysis (results presented in Table 7.4) detected a decrease in the value of N_s^T while the value of β was always unity.

7.5.2.2 Cu*-Ox Isotherm: The isotherm for adsorption of Cu with Ox_T = 1 mM onto MC0 (illustrated in Fig. 7.6) had a slope ≈ 1 and transitioned gradually to maximum adsorption. The isotherm changed for MC2 when nearly 70% of the oxide coating was removed. For MC3, there was no change in slope but the adsorption maximum decreased. The larger scatter in the data for the weathered sample was because of measurement errors associated with measuring small concentration of adsorbed Cu. The values of β obtained from the CDM analysis (listed in Table 7.3) was equal to 1 for all samples but the value of N_s^T decreased with loss of surficial coating. We were unable to obtain Cu*-Ox isotherm onto MU because Ox_T = 1 mM effectively competed with Cu and saturated the surface sites.

7.5.2.3 Oxalate pH Edges: The edges for Ox_T = 10 μM onto samples of MC (shown in Fig.

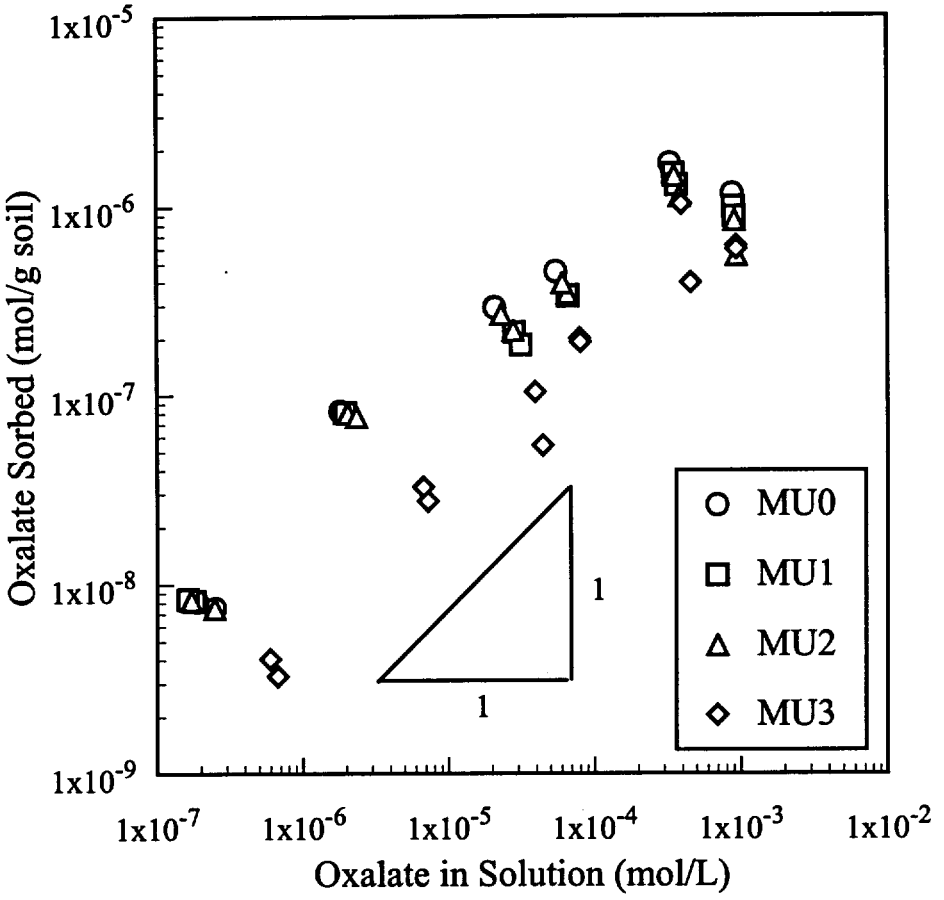

Figure 7.5. Data for oxalate isotherm at pH 7 for samples of MU. The samples in the weathering sequence are referenced by samples name followed by a number. The surficial metal oxide for the samples are listed in Table 7.2.

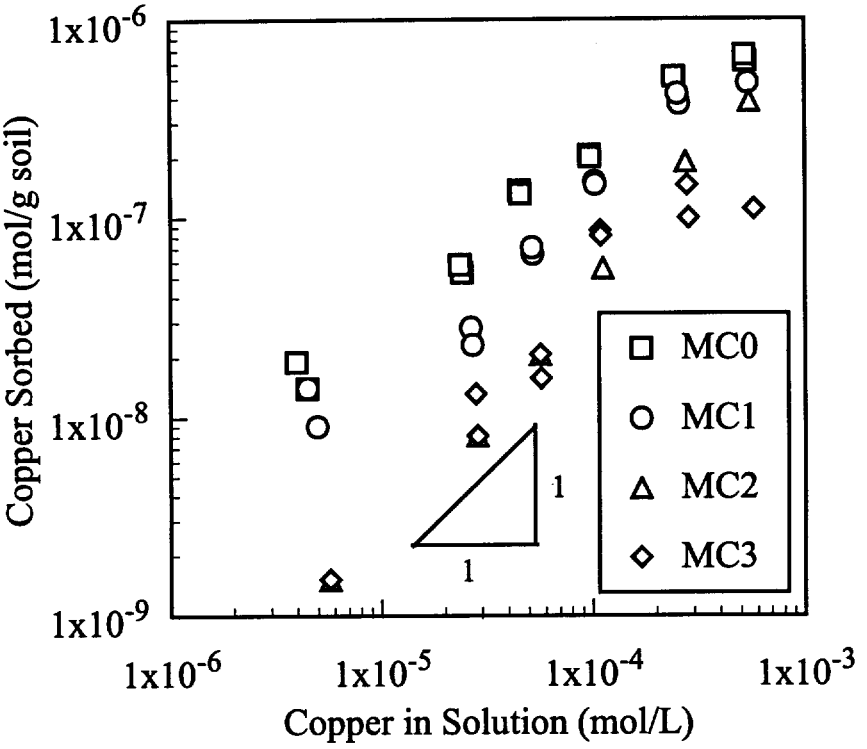

Figure 7.6. Data for adsorption isotherm of Cu with 1 mM oxalate at pH 7 for samples of MC.

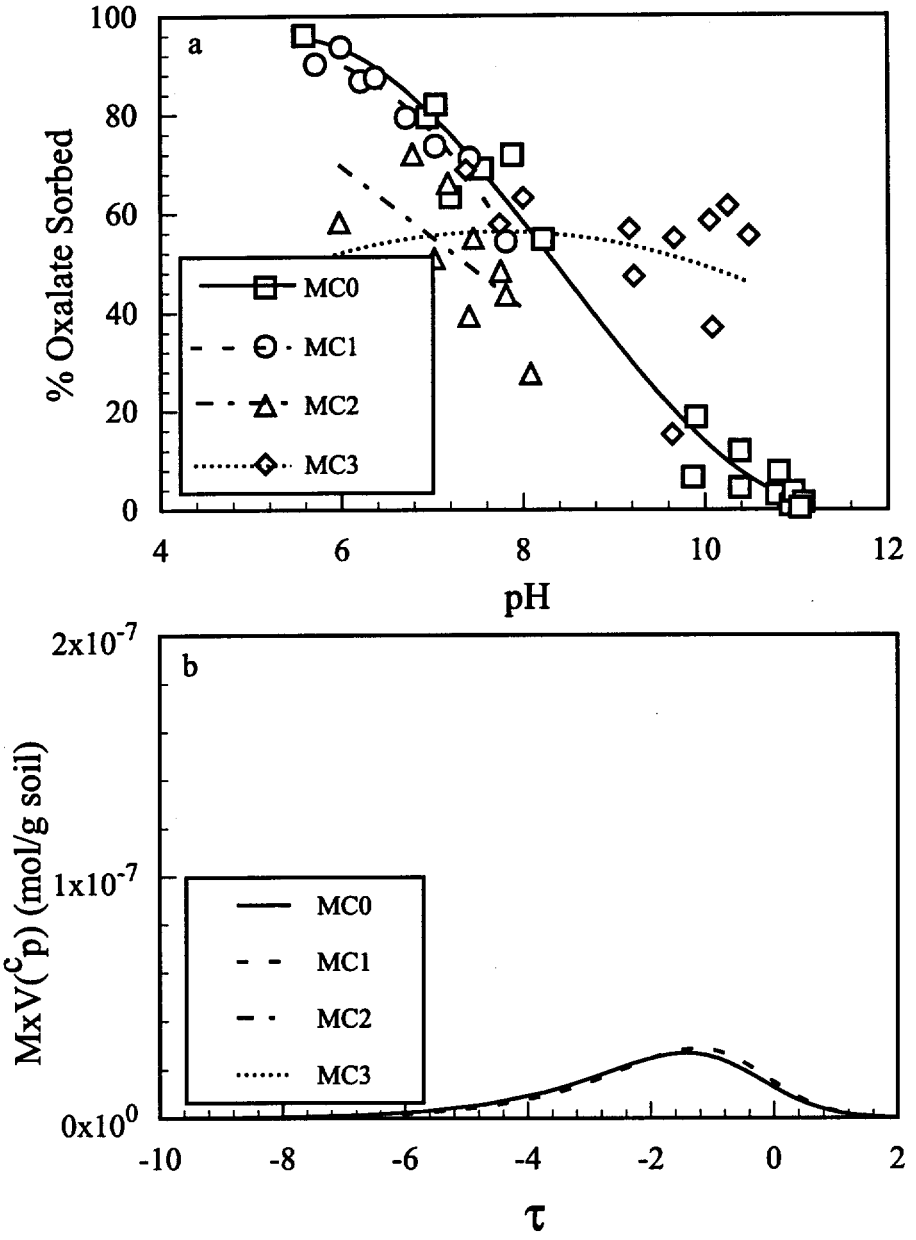

Figure 7.7. Data for a) pH edge, and b) range of site strengths calculated with the continuous distribution model for Ox_T = 10 μM onto samples of MC. The lines in Fig. 7.7a are the CDM fits for the data. The corresponding lines in Fig. 7.7b are the calculated range of site strengths. The site strength distribtion for MC2 and MC3 are indistinquishable from the horizontal axis.

Table 7.4. Results of CDM fits for adsorption of oxalate, Cu, and Cu*-Ox onto weathered and unweathered samples of MU.

Sample	Ox_T = 10 μM		Ox Isotherm		Cu_T = 15 μM		Cu*-Ox Edge	
^cp_m	15.7		10.2		-4.7		-9.9	
$\bar{n}$	-1.0		-0.9		2.0		2.0	
Sample	N_s^T	β	N_s^T	β	N_s^T	β	N_s^T	β
MU0	0.03	0.31	0.42	1.00	0.04	0.58	0.081	0.48
MU1	0.03	0.30	0.41	1.00	0.04	0.50	0.081	0.47
MU2	0.03	0.28	0.36	1.00	0.04	0.37	0.081	0.47
MU3	0.02	0.19	0.24	1.00	0.03	0.29	0.081	0.37

7.7a) changed for MC2 when nearly 70% of the 6 N HCl extractable Fe and Al were removed. Interestingly, the adsorption was constant for MC3 over pH 6 - 10. A value of N_s = 0.4 sites/nm^2 reproduced oxalate adsorption onto samples of MC with the DLM. The results of FITEQL optimization is listed in Table 7.5. FITEQL did not converge on optimal DLM parameters for MC3 because it was unable to account for constant adsorption for pH 6 - 10. The value of log K_{XOx2} decreased for samples with smaller oxide coating whereas log K_{XOx3} had no discernible trend. The decrease in log K^{eff} suggests a loss of stronger adsorption sites. For MC2 and MC3, reducing the N_s (as listed in Table 7.5) better reproduced the edge. The value of N_s^T, calculated with the CDM, decreased and the value of β increased to 1. The results are listed in Table 7.3. The range of adsorption energies (shown in Fig. 7.7b) was nearly the same for MC0 and MC1 but was nonexistent for MC2 and MC3.

The adsorption of Ox_T = 50 μM slightly decreased for MC1 when 6 N HCl extractable Fe was decreased by nearly 40% (to ~ 0.45 mg/g) and Al was decreased by 30% (to ~ 0.9 mg/g) (see Fig. 7.8a). The adsorption decreased further for MC2 and MC3 when more oxide coating was removed. With DLM we fit the adsorption edge using N_s = 0.4 sites/nm^2. The fit for samples with smaller coating became progressively worse. As detailed in Table 7.5, V_Y increased when the same N_s was employed to model edges onto samples with smaller coating. The value of log K_{XOx2} was smaller for samples with less coating suggesting loss of stronger adsorption sites. The edges for samples with smaller coating were better modeled with smaller N_s. This suggested that there was a loss of sites with loss of surficial Fe and Al. A similar loss of binding sites with loss of oxides was detected by CDM for Ox_T = 50 μM (see Fig. 7.8b) and the optimum N_s^T for the weathered samples decreased (Table 7.3). The CDM revealed an increase in β suggesting a narrower range of site strengths. The difference between MC0 and MC1 may be primarily due to sparse data for MC1. For MC2, the increase in the range of adsorption energies was probably due to grain-scale heterogeneity induced by uneven removal of the coating during dissolution.

The adsorption of Ox_T = 10 μM onto MU (shown in Fig. 7.9a) decreased with a loss of > 90 % of the 6 N HCl extractable Fe and > 60 % of the 6 N HCl extractable Al. The DLM reproduced the adsorption edges for the weathered and unweathered samples of MU

Table 7.5. Optimal DLM parameters fitted to edges for Ox_T = 10 μM and 50 μM onto weathered and unweathered MC and MU. Left hand columns present best fit parameters assuming that N_s is fixed for samples of MC at 0.4 sites/nm^2 and for samples of MU at 0.3 sites/nm^2. Right hand columns present best-fit parameters when N_s is allowed to vary.

Sample	Constant N_s (sites/nm^2)				Best V_Y			
	N_s	V_Y	log K_{XOx2}	log K_{XOx3}	N_s	V_Y	log K_{XOx2}	log K_{XOx3}
	Oxalate = 10 μM							
MC0	0.40	0.59	11.45±0.25	-5.06±0.15	0.40	0.59	11.45±0.25	-5.06±0.15
MC1	0.40	0.10	10.68±0.35	-4.75±0.24	0.40	0.10	10.68±0.35	-4.75±0.24
MC2	0.40	1.60	9.53±0.41	-4.90±0.09	0.20	0.96	11.36±0.17	-4.24±0.14
MC3	0.40	N.C.[¶]			0.012	1.70	15.48±0.52	-3.20±0.32
	Oxalate = 50 μM							
MC0	0.40	3.21	11.04±0.04	-4.26±0.04	0.40	3.21	11.04±0.04	-4.26±0.04
MC1	0.40	6.34	10.55±0.09	-4.34±0.04	0.20	2.16	12.19±0.05	-4.57±0.05
MC2	0.40	5.23	10.06±0.06	-4.25±0.08	0.40	5.23	10.06±0.06	-4.25±0.08
MC3	0.40	12.23	10.09±0.08	-4.09±0.03	0.12	5.34	12.93±0.07	-4.28±0.04
	Oxalate = 10 μM							
MU0	0.3	1.11	12.41±0.08	-5.20±0.20	0.3	1.11	12.41±0.08	-5.20±0.20

Table 7.5 (Continued). Optimal DLM parameters fitted to edges for Ox_T = 10 μM and 50 μM onto weathered and unweathered MC and MU. Left hand columns present best fit parameters assuming that N_s is fixed for samples of MC at 0.4 sites/nm^2 and for samples of MU at 0.3 sites/nm^2. Right hand columns present best-fit parameters when N_s is allowed to vary.

Sample	Constant N_s (sites/nm^2)				Best V_Y			
	N_s	V_Y	log K_{XOx2}	log K_{XOx3}	N_s	V_Y	log K_{XOx2}	log K_{XOx3}
MU1	0.3	1.18	11.78±0.17	-4.59±0.10	0.3	1.18	11.78±0.17	-4.59±0.10
MU2	0.3	1.08	11.49±0.13	-4.81±0.12	0.3	1.08	11.49±0.13	-4.81±0.12
MU3	0.3	0.29	9.87±0.07	-5.45±0.25	0.0075	0.97	15.1±0.45	-5.50±0.76

[1]N.C. = No Convergence

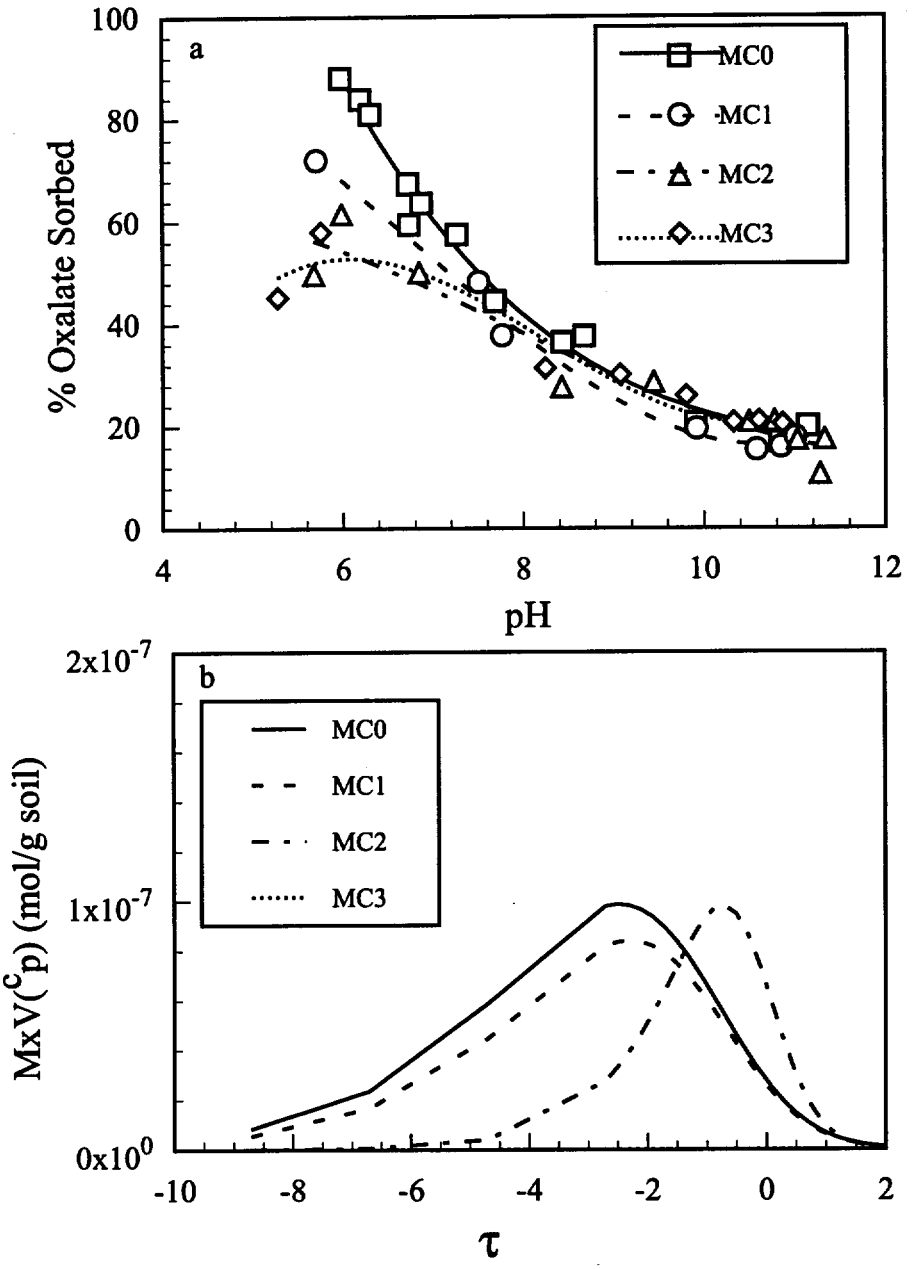

Figure 7.8. Data for a) pH edge, and b) range of site strengths calculated with the continuous distribution model for Ox_T = 50 μM for samples of MC. The lines in Fig. 7.8a are the CDM fits for the data. The corresponding lines in Fig. 7.8b are the calculated range of site strengths. The line for MC3 in Fig. 7.8b is indistinquishable from the horizontal axis.

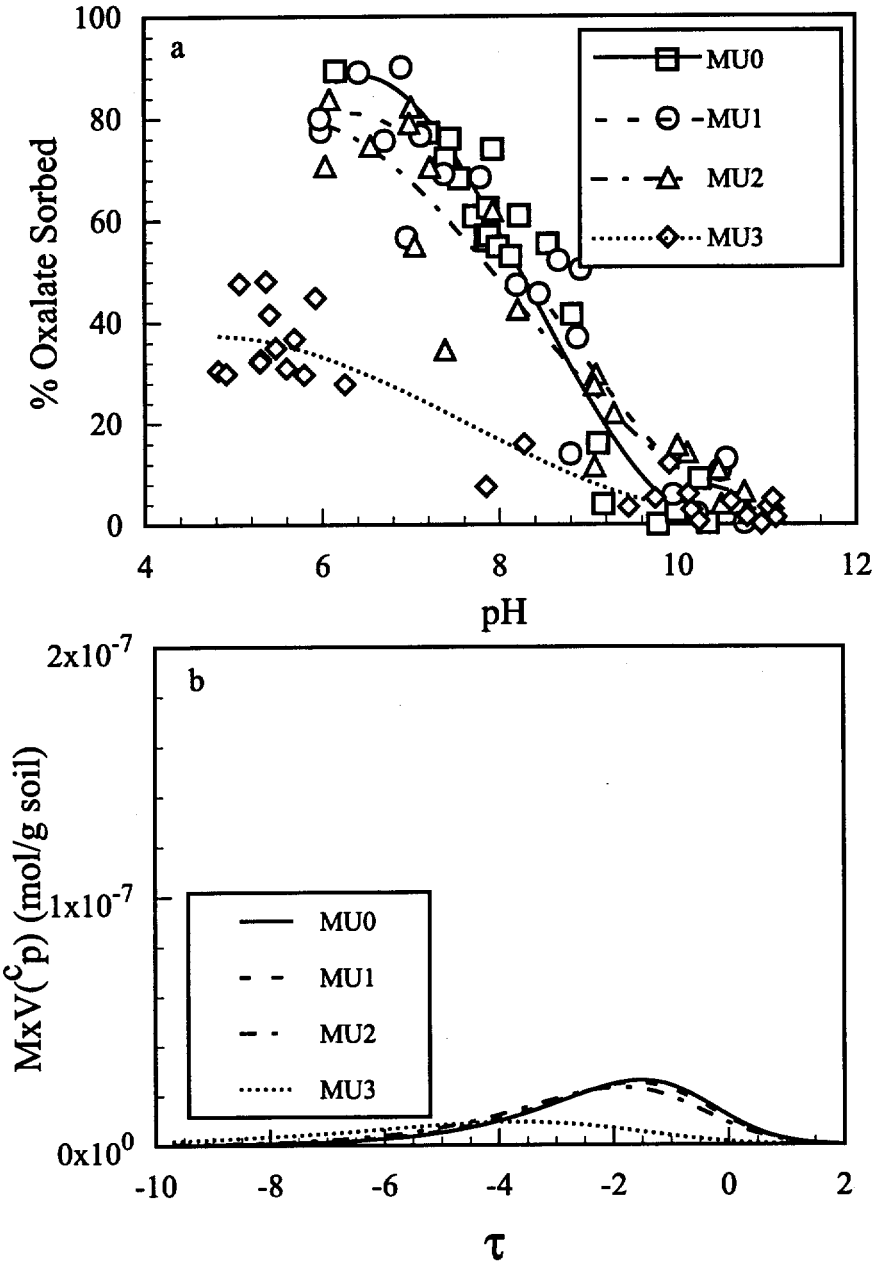

Figure 7.9. Data for a) pH edge, and b) range of site strengths calculated with the continuous distribution model for Ox_T = 10 μM onto samples of MU. The lines in Fig. 7.9a are the CDM fits for the data. The corresponding lines in Fig. 7.9b are the calculated range of strengths.

with N_s = 0.3 sites/nm^2 (modeling results in Table 7.5). The value of log K_{XOx2} decreased while that of log K_{XOx3} showed no discernible trend. Although the edges for MU0, MU1, and MU2 were best modeled with the same N_s, the edge for MU3 was modeled accurately with a smaller N_s. The values of N_s^T and β (listed in Table 7.4) also remained nearly the same until most of the surficial Fe and Al were removed. The site strength distribution revealed by CDM changed for MU3, when nearly all of the coating was removed (Fig. 7.9b).

7.5.2.4 Cu pH Edges: The edges for Cu_T = 15 μM (shown in Fig. 7.10a) changed only for MC3 when ~ 90% of the 6 N HCl extractable coating was removed. The shift in the edge was due to saturation of adsorption sites at larger sorbate/sorbent ratio. The edges for adsorption of Cu were suitably modeled with DLM using N_s = 0.4 sites/nm^2 (Table 7.6). Cu adsorption modeling is insensitive to N_s (as shown in Chapter 3) and we did not obtain better fits with smaller N_s. The fit was poor for MC3 and we were unable to improve the fit by changing N_s. The value of log K_{XOCu} (listed in Table 7.4) decreased with loss of coating. Unlike oxalate, the value of β (listed in Table 7.3) increased for samples with less coating and the range of site strengths (shown in Fig. 7.10b) was greater for MC2 and MC3 than for MC0 and MC1.

As with MC, edges for Cu_T = 15 μM onto the samples of MU (shown in Fig. 7.11a) changed only for MU3. A N_s fixed at 0.3 sites/nm^2 reproduced the edges and the value of log K_{XOCu} (listed in Table 7.6) was smaller for samples with less coating. The slight shift in the edge for samples with less coating was reproduced in the site strength distribution with a broad curve, reduction in the maximum height, and loss of stronger adsorption sites (illustrated in Fig. 7.11b).

7.5.2.5 Cu*-Ox Edge: The edge for adsorption of Cu onto samples of MC in the presence of oxalate (illustrated in Fig. 7.12a) changed and shifted towards the higher pH only for MC3 when 90% of the 6 N HCl extractable Fe and Al was removed. A fixed N_s gave progressively poorer fits for samples of MC containing smaller surficial Fe and Al and log K_{XOCuOx} values (listed in Table 7.6) for the samples with lesser coating decreased. We invoked smaller N_s to obtain better fit for the edges for samples with smaller coating. The CDM analysis of Cu*-Ox edge onto MC0 revealed a narrow range of site strengths in Figure 7.12b. The decrease in

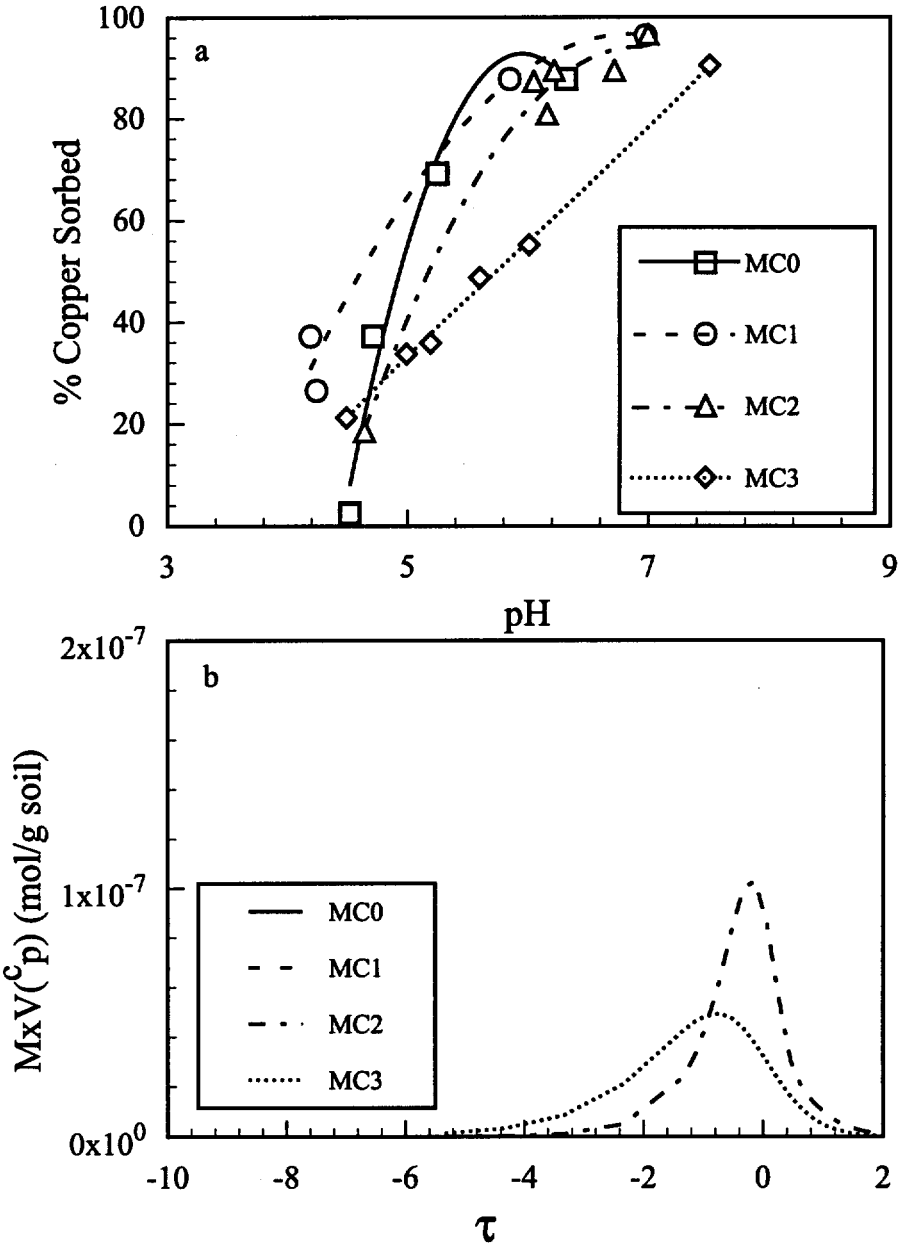

Figure 7.10. Data for a) pH edge, and b) range of site strengths calculated with the continuous distribution model for Cu_T = 15 μM onto samples of MC. The lines in Fig. 7.10a are the CDM fits for the data. The corresponding lines in Fig. 7.10b are the calculated range of site strengths. The lines for MC0 and MC1 in Fig. 7.10b are indistinquishable from the horizontal axis.

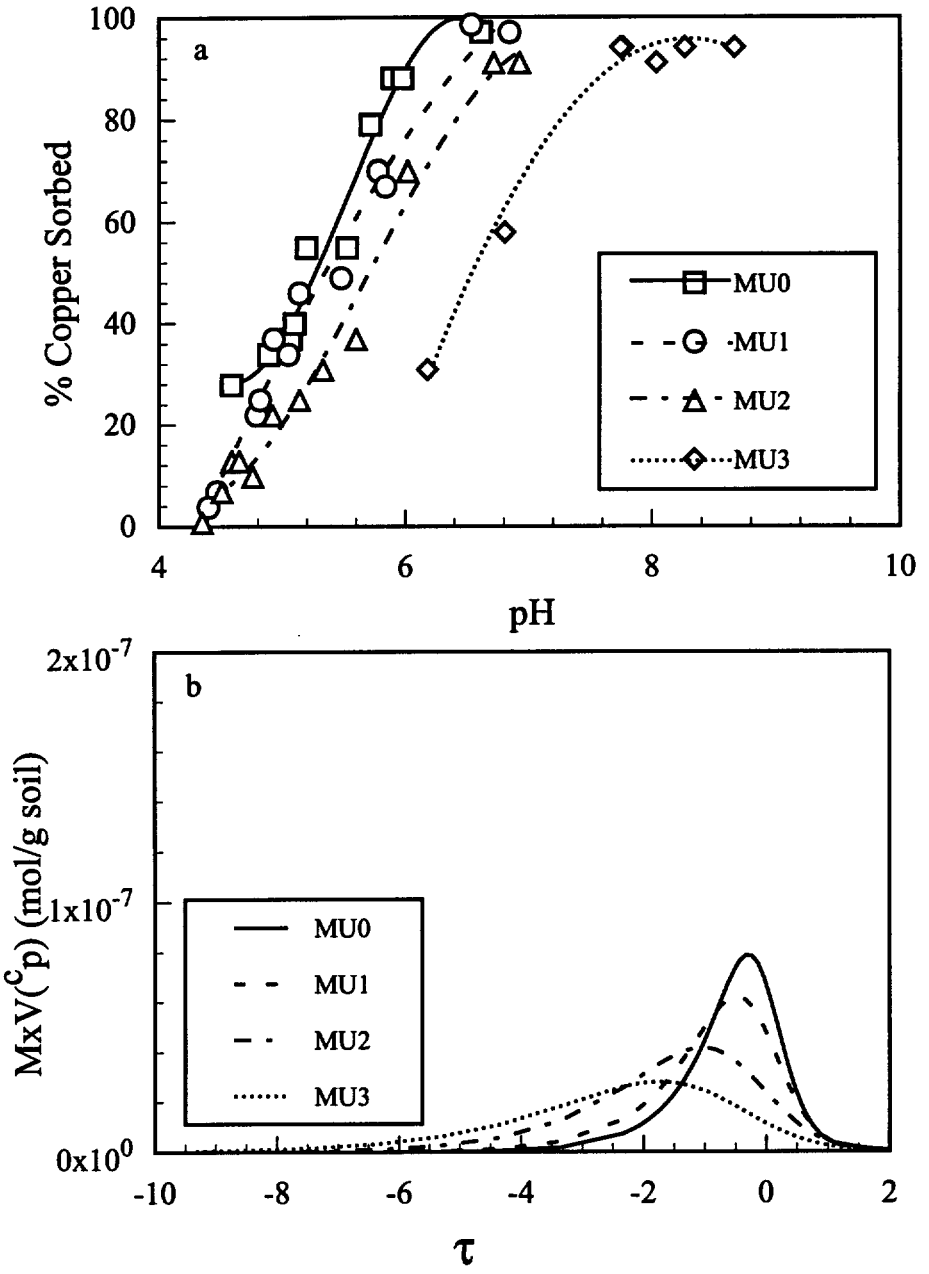

Figure 7.11. Data for a) pH edge, and b) range of site strengths calculated with the continuous distribution model for Cu_T = 15 μM onto samples of MU. The lines in Fig. 7.11a are the CDM fits for the data. The corresponding lines if Fig. 7.11b are the calculated range of site strengths.

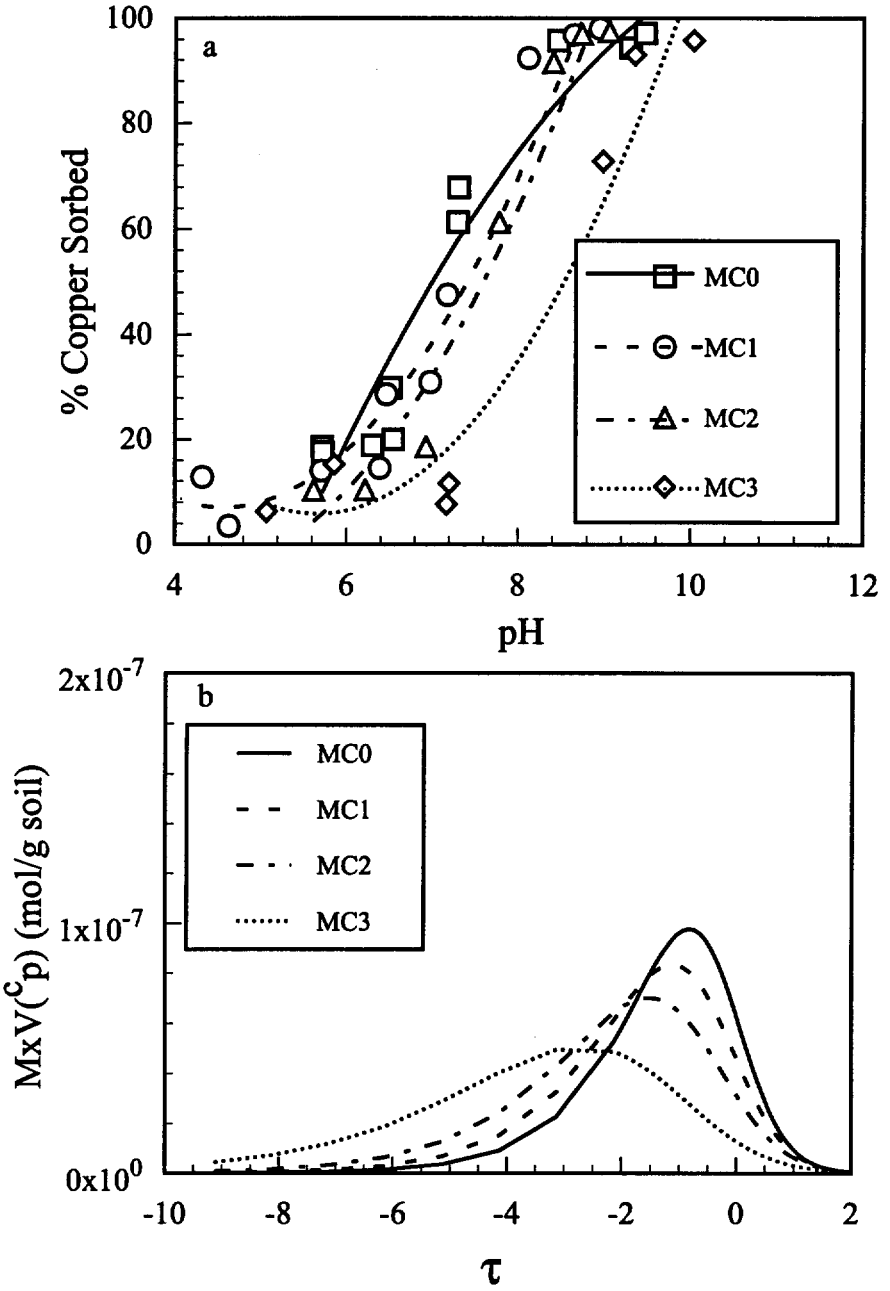

Figure 7.12. Data for a) pH edge, and b) range of site strengths calculated with the continuous distribution model for Cu_T = 27 μM with Ox_T = 1 mM for samples of MC. The lines in Fig. 7.12a are CDM fits for the data. The corresponding lines in Fig. 7.12b are the calculated range of site strengths.

Table 7.6. Optimal DLM parameters fitted to pH edges for Cu_T = 15 μM and for Cu_T = 27 μM in the presence of Ox_T = 1 mM onto weathered and unweathered samples of MC and MU. Changing N_s did not change the fit for Cu adsorption hence results are equivalent to fits with the best V_Y.

Soil	Constant N_s (sites/nm^2)			Best V_Y		
	N_s	V_Y	log K_{XOCu}	N_s	V_Y	log K_{XOCu}
	Cu_T = 15 μM					
MC0	0.4	2.19	1.89±0.13			
MC1	0.4	1.68	3.00±0.11			
MC2	0.4	1.66	1.82±0.21			
MC3	0.4	22.55	3.05±0.17			
	Cu_T = 15 μM					
MU0	0.3	1.93	1.74±0.08			
MU1	0.3	1.92	1.71±0.08			
MU2	0.3	1.67	0.96±0.11			
MU3	0.3	0.68	-0.81±0.16			
	Cu_T = 27 μM with Ox_T = 100 μM					
MC0	0.40	7.51	1.94±0.05	0.40	7.51	1.94±0.05
MC1	0.40	11.53	1.53±0.05	0.40	11.53	1.53±0.05
MC2	0.40	4.82	0.91±0.06	0.10	4.20	1.47±0.09
MC3	0.40	4.82	0.91±0.05	0.08	4.02	1.60±0.08
	Cu_T = 27 μM with Ox_T = 100 μM					
MU0	0.30	3.57	1.15±0.04	0.30	3.57	1.15±0.04
MU1	0.30	3.42	0.79±0.04	0.30	3.42	0.79±0.04
MU2	0.30	1.52	0.66±0.04	0.30	1.52	0.66±0.04
MU3	0.30	40.7	0.83±0.07	0.30	40.7	0.83±0.07

surficial Fe and Al resulted in a slightly broader distribution of site strengths (Fig. 7.12b) caused by a smaller value of β (listed in Table 7.3).

As with oxalate and Cu, Cu*-Ox edge for MU3 (in Figure 7.13a) shifted slightly towards higher pH. The adsorption edges of Cu*-Ox on MU0, MU1, and MU2 were modeled with N_s = 0.30 sites/nm^2 (Table 7.6). The value of log K_{XOCu} (listed in Table 7.6) decreased for samples with less coating. We were unable to accurately reproduce the edge for MU3 even by reducing the N_s. Cu*-Ox revealed a narrow distribution of adsorption energies (shown in Fig. 7.13b) for MU0. The values of β (listed in Table 7.4) decreased for MU3 and this was accompanied by broadening of the distribution of site strengths.

7.6 Discussion

For MC, oxalate adsorption edges and isotherms changed only after nearly 70% of the 6 N HCl extractable surficial coating was removed whereas the Cu edges in the absence and presence of oxalate changed when nearly 90% of the 6 N HCl extractable coating was removed. For MU the adsorption of Cu, oxalate, and Cu*-Ox decreased when ~ 90% of the coating was removed. Although optimal N_s and N_s^T did not change significantly for weathered samples until nearly all of the coating was removed, the range of site strength distributions and the K^{eff} values were much more sensitive to loss of coating.

Loss of surficial Fe and Al increases the adsorbate/adsorbent ratio and shifts the edge in predictable ways (*24*). For larger adsorbate/adsorbent ratios, the fraction of oxalate adsorbed decreased at the lower pH and the Cu edges (in the absence and presence of oxalate) shifted towards the higher pH. The absence of an appreciable shift in the edge, even after loss of surficial coating, indicates a proportional relationship between the adsorption density and the adsorbate concentration. The edge shifts only when the adsorption is nonproportional, either because of multiple site types or saturation of available sites (*24*). We obtained a wide range of adsorbate/adsorbent ratios for which the adsorption density was proportional to the adsorbate concentration. Only when > 70% of the coating was removed did this proportionality change.

Adsorption edges for samples of MC and MU change because of a decrease in

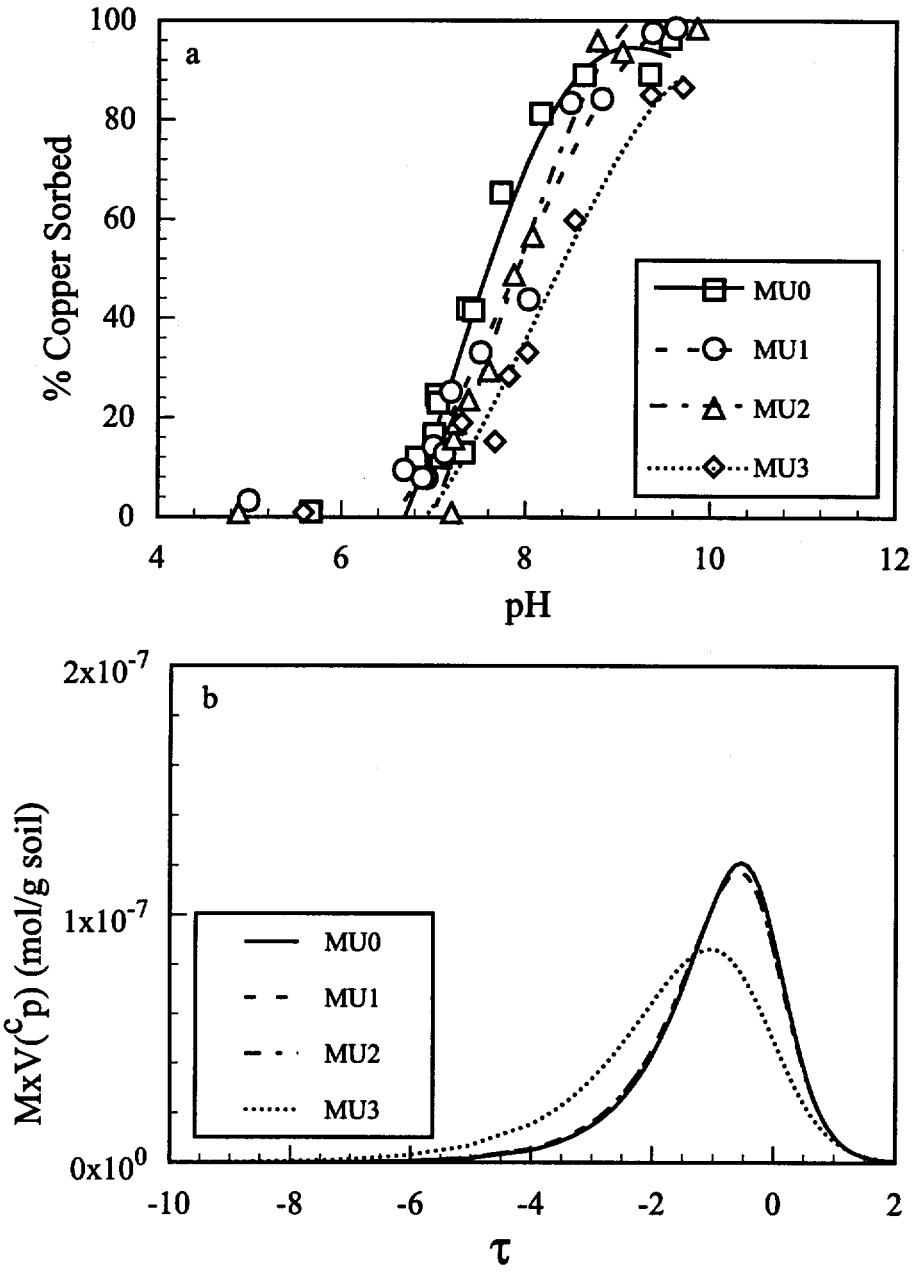

Figure 7.13. Data for a) pH edge, and b) range of site strengths calculated with the continuous distribution model for Cu_T = 27 μM with Ox_T = 1 mM for samples of MU. The lines in Fig. 7.13a are the CDM fits for the data. The corresponding lines in Fig. 7.13b are the calculated range of site strengths. The distribution of site strengths for MU0 and MU1 are overlapping.

adsorption capacity and intensity but the edges, by themselves, do not provide insight into the contribution of one over the other. The is reflected in the DLM results where we can either estimate change in log K^{eff} (keeping N_s constant) or change in N_s (best V_Y results).

For MC, oxalate adsorption was slightly more sensitive to changes in surface properties than Cu. For MU, oxalate and Cu were equally insensitive to changes in adsorption properties. This may be due to formation of pits (shown Fig. 7.2b) and a possible uncovering of fixed charged sites on clays in MC during weathering. For Cu adsorption, loss of variable charge sites may be compensated by the freshly uncovered fixed charged sites. Oxalate on the other hand does not bind to fixed negatively charged sites and hence is more sensitive to changes in oxide coating.

Interestingly, the optimal N_s obtained with the DLM was insensitive to loss of coating. For all adsorbates nearly the same N_s modeled the adsorption of the weathered and unweathered samples (see Tables 7.5 and Table 7.6). Only when nearly all of the 6 N HCl extractable coating was removed did we need to use a smaller N_s. The K^{eff} values on the other hand decreased progressively for weathered samples (see log K_{XOx2} and log K_{XOCu} and Tables 7.5 and 7.6) suggesting loss of stronger adsorption sites.

The N_s^T values obtained for edges and isotherms also did not change significantly for the weathered samples (see Table 7.3 and 7.4). The β values, on the other hand, changed considerably, once again indicating a change in the range of adsorption energies. An increase in β values (for MC: Ox_T = 10 μM, 50 μM, and oxalate isotherm) revealed a narrow range of adsorption energies for the coated samples. A decrease in β values (for Cu, Cu*-Ox for MC and MU, and oxalate for MU) revealed a loss of stronger adsorption sites and a general broadening of the distribution. A narrow range of adsorption energies indicates a loss of both stronger and weaker sites, hence a decrease in the range of site strengths (i.e., a diminished capacity and heterogeneity). A general broadening of the distribution of site strengths indicates a loss of sites but an expansion of the range of site strengths, i.e., a diminished capacity and an increase in site heterogeneity. There is a loss of stronger adsorption sites but more weaker sites apparent are exposed for adsorption.

The adsorption of oxalate and Cu in the presence and absence of oxalate did not

change appreciably until a substantial portion of the surficial metal oxide was removed from the subsoil particles. The relative insensitivity of N_s and N_s^T and the greater sensitivity of K^{eff} and β to loss of coating is probably because adsorption may be taking place on one or two atomic layers on the surface. Loss of oxide coating exposes fresh coating for adsorption and the adsorption capacity does not change. The freshly exposed coating may have a different site heterogeneity than the original coating. In this particular case the freshly exposed oxide layers are less heterogeneous than the original coating.

The site density that can model the adsorption is insensitive to the loss of oxide coating. However, the optimal K^{eff} values decrease by more than an order or magnitude for the weathered samples. This suggests that the mobility of solutes through a weathering subsoil medium may be substantially enhanced over extended period of time. Such change in solute mobility will be accelerated in ligand contaminated sites or metal contaminated subsoils being remediated by flushing strong ligand through them.

7.7 References

(1) Adams, J.B.; Palmer, F.; and Stanley, J.T. *Geomicrobiol. J.*, **1992**, 10:99-114.

(2) Neilands, J.B. "Iron and its Role on Microbial Physiology," in. J.B. Neilands (ed.) *Microbial Iron Metabolism: A Comprehensive Treatise*, **1974**, pp. 4-19, Academic Press, New York.

(3) Basu, A. *Geology*, **1981**, 9:132-133.

(4) Knoll, M.A. and James, W.C. *Geology*, **1987**, 15:1099-1102.

(5) Grandstaff, D.E. "The Dissolution Rate of Forsterite Olivine from Hawaiian Beach Sand," in *Rates of Chemical Weathering of Rocks and Minerals*, Colman, S.E. and Dethier, D.P. (ed.), **1986**, pp. 41-59, Academic Press, Inc.

(6) Welch, S.A. and Ullman, W.J. *Geochim. Cosmochim. Acta*, **1993**, 57:2725-2736.

(7) Birkeland, P.W. *Soils and Geomorphology*, **1984**, Oxford University Press, New York.

(8) Ugolini, F.C. "Processes and Rates of Weathering in Cold and Polar Desert Environments," in *Rates of Chemical Weathering of Rocks and Minerals*, Colman, S.M. and Dethier, D. (eds.), **1986**, 1993-235, Academic Press, Orlando, FL.

(9) Suter, D.; Banwart, S.; and Stumm, W. *Langmuir*, **1991**, 7:809-813.

(10) Stumm, W.; Furrer, G.; and Kunz, B. *Croat. Chemica Acta*, **1983**, 56(4)593-611.

(11) Benett, P.C. *Geochim. Cosmochim Acta*, **1991**, 55:1781-1798.

(12) Lovely, D.R. *Geomicrobiol. J.*, **1987**, 5:375-399.

(13) Lovely, D.R. and Phillips, E.J.P. *Appl. Environ. Microbial.*, **1988**, 54:1472-1480.

(14) Wieland, E.; Wehrli, B.; and Stumm, W. *Geochim. Cosmochim. Acta*, **1988**, 52:1969-1981.

(15) Zinder, B.; Furrer, G.; and Stumm, W. *Geochim. Cosmochim Acta*, **1986**, 50:1861-1869.

(16) Wieland, E. and Stumm, W. *Geochim. Cosmochim. Acta*, **1992**, 56:3339-3355.

(17) Furrer, G. and Stumm, W. *Geochim. Cosmochim Acta*, **1986**, 50:1847-1860.

(18) Stumm, W.; Furrer, G.; Wieland, E.; and Zinder, B.; "The Effects of Complex-Forming Ligands on the Dissolution of Oxides and Aluminosilicates," in *The Chemistry of Weathering*, J.L. Drever (ed.), **1985**, 55-74, Reidel Publishing Co.

(19) Hering, J. and Stumm W. 1990, "Oxidative and Reductive Dissolution of Minerals," in *Mineral-Water Interface Geochemistry*, Hochella, M.F. and White, A.F. (ed.), Reviews in Mineralogy, **1990**, 23:427-465.

(20) Waite, T.D. and Morel, F.M.M. *J. Colloid Interface Sci.*, **1984a**, 102(1):121-137.

(21) Waite, T.D. and Morel, F.M.M. *Environ. Sci. Technol.*, **1984b**, 18(11):860-868.

(22) Lundström, U.S. *J. Soil Sci.*, **1993**, 44:121-133.

(23) Kinniburgh, D.G.; Barker, J.A.; and Whitfield, M. *J. Colloid Interface Sci.*, **1983**, 95(2):370- 384.

(24) Dzombak, D.A. and Morel, F.M.M. *Surface Complexation Modeling: Hydrous Ferric Oxide*. John Wiley & Sons. **1990**.

CHAPTER 8

SUMMARY, IMPLICATIONS, AND FUTURE DIRECTIONS

8.1 Summary

8.1.1 Adsorption Modeling

Sands coated with varying amounts of metal oxide were heterogeneous at the microscale and contained a wide range of adsorption energies. The extent of this apparent heterogeneity depended on the nature and concentration of the adsorbate. A weakly binding anion (oxalate) revealed a greater site heterogeneity than the strongly binding metal (Cu). A metal-ligand (Cu-Oxalate) complex revealed intermediate heterogeneity that depended on the concentration of the ligand.

Such site heterogeneity of oxide coated sand was often modeled accurately with homogeneous-site formulations of various elaborations of the surface complexation model (SCM). Only for the highest sorbate concentration (100 μM oxalate) the fit with the homogeneous-site model was statistically poorer. The Diffuse Layer and Constant Capacitance models required a physically unrealistic species $\equiv XOC_2O_4^{3-}$ to reproduce the broad edge (wide inflection) of oxalate. The Triple Layer Model (TLM) did not require such an unrealistic species when oxalate was assumed to form an outer-sphere complex. The TLM may model the electrostatic interactions more realistically at the higher pH and near the pristine point of zero charge. The fit with various SCMs was insensitive to the protonation constants and the electric double layer structure but was somewhat sensitive to the choice of site density. Interestingly, individual edges gave slightly different values of the effective surface complexation constant (K^{eff}). The difference in the K^{eff} values was due to concentration dependent site heterogeneity. Thus, it was not always possible to use K^{eff} for one sorbate concentration to reproduce adsorption of another concentration of the same

sorbate.

Using a small number of sites, we modeled adsorption of all concentration of single adsorbate Cu and Cu in the presence of oxalate but were unable to model all of the oxalate edges with the discrete pK_a spectrum (DPS) approach. It was also not always possible to conveniently select a set of surface sites to consistently model various adsorbates and adsorbate concentrations.

8.1.2 Dissolution of Coating and its Effect on Metal Contaminant Subsoil Remediation

Dissolution of surficial metal from artificially and naturally coated samples was transport limited. The dissolution of surficial Fe-oxide from both samples was strongly dependent on the pore velocity when the influent oxalate solution was not buffered. In the presence of buffered oxalate, the pore velocity affected the dissolution from only the naturally coated sample. Calculation of conditional stability constants suggests that the presence of dissolved Fe will reduce the efficiency of metal contaminant removal by complexing with the ligand. In some cases, the rapidly dissolving Al may also reduce the efficiency of metal contaminant removal.

8.1.3 Change of Adsorption due to Dissolution of Coating

For weathered Milford Coated sands, the adsorption of oxalate changed measurably when nearly 70% of the 6 N HCl extractable surficial Fe and Al were removed. The edges for Cu in the presence and absence of oxalate changed when nearly all the surficial Fe and Al were lost. For weathered Milford Uncoated samples, adsorption of oxalate, Cu, and Cu in the presence of oxalate changed when nearly all of the oxide coating was removed. The change in the adsorption characteristics was represented by a diminished site density, a decline in the average binding strength, and a loss of sites with stronger adsorption energies.

8.2 Importance of the Results

Adsorption onto metal oxide coated sands, which are more complex than pure-phase metal oxides but are simpler than many of the soils, can be modeled for a moderately wide range of concentration with SCMs. The fits are not always good for higher sorbate concentration. The insensitivity of SCM fits to N_s and pK_a make it a convenient method for

modeling adsorption onto natural materials because it is difficult to obtain accurate estimates of these parameters for natural material. This insensitivity makes SCMs an ineffective tool for accurately diagnosing the molecular scale adsorption processes. The K^{eff} values obtained from modeling different adsorbate concentrations are slightly different. Hence, it is not always possible to reproduce adsorption of one concentration with K^{eff} values obtained from another concentration. Since it may not be possible to obtain data for all conditions encountered in the subsoil formations, it is desirable to extrapolate K^{eff} values obtained from a small data set to conditions encountered in the field. Extrapolation may result in uncertain estimates of solute mobility and one should be careful in selecting constants. The uncertainty will be smaller for single sorbate adsorption and greater for multiple adsorbates.

The DPS approach does have distinct advantages for modeling adsorption of a wide range of concentration of metal, in single adsorbate or multiple adsorbate, onto somewhat heterogeneous adsorbents. Its advantages in modeling anion adsorption may be limited. One may need to invoke larger number of sites, i.e., more adjustable parameters, to model adsorption over a wide range of concentration. Hence, the DPS model provides greater flexibility in modeling adsorption onto heterogeneous adsorbents but also increases the arbitrariness in choosing parameters.

Ligands in natural and contaminated soils may dissolve surficial oxide but the loss of such adsorption sites may not influence the adsorption of ions until a substantial amount of the coating is removed. Although the site density that can model the adsorption of oxalate and Cu in the presence and absence of oxalate does not change until nearly all of the oxide coating is removed, the optimal K^{eff} values decrease by more than an order or magnitude for the weathered samples. The mobility of solutes through a weathering subsoil medium may be substantially enhanced over extended period of time. Such change in solute mobility will be accelerated in ligand contaminated sites or metal contaminated subsoils being remediated by flushing ligand through them.

Since the dissolution of metal oxide from soil may be transport limited, remediation of metal contaminated subsoils may not be accelerated by increasing the rate at which ligands are flushed through the subsurface formations. Large concentration of dissolved metal may

complex with the ligand and may reduce the amount of metal contaminant removed from the subsurface. The inability to control pH during remediation of soil may also increase the uncertainty related to objectively evaluating the progress of the remediation of a site.

8.3 Future Directions

Interestingly, the K^{eff} values depended on the total adsorbate concentration. More work should be done to verify this for other mineralogically complex soils and attempts should be made to correlate the surficial coating and the adsorbate concentrations with the optimized K^{eff}. Empirical regression function may help effective extrapolation of K^{eff} values.

Although $\equiv XOC_2O_4^{3-}$ is an unrealistic species, it is required for reproducing the broad edge of oxalate. Attempts should be made to identify the species that may be occurring at pH > 7, identify other strategies for modeling the broad edge without including the unrealistic species, or rethink the validity of the assumed electric double layer structure in some conditions.

The DPS model has to be improved before it is widely used for modeling adsorption on naturally complex subsoil particles. The model should be able to identify the sites that do not contribute to adsorption and Westall (*1*) is working on changing FITEQL to solve this problem.

More research is needed to identify the role of various side reactions in affecting the remediation of metal contaminated subsoils. Such side reaction may greatly increase the time required to remediate the site. It may not always be possible to control the pH because buffers may often be used as substrate by microbes. Lack of buffering will increase the pH during dissolution and may increase the adsorption of metals. Conversely, excess buffer will add to the cost of remediation. Ex-situ treatment of the dissolved metal-ligand complex before disposal will also increase the cost of remediation.

We estimated changes in effective surface complexation constant with loss of oxide coating. Such a change in constants will influence the solute mobility and research on other soil samples will validate the universality of this phenomena.

8.4 References

(1) Westall, J.C. Personal Communication, **1996**, Oregon State University, Corvallis, Oregon.

APPENDIX A

DATA FOR ADSORPTION ONTO ARTIFICIALLY COATED SAMPLE

Table A.1. Data for oxalate adsorption isotherm onto AC at pH 7

Ox_T (M)	Oxalate in Solution (M)	Oxalate Sorbed (mol/g)
$1.00x10^{-03}$	$7.34x10^{-04}$	$2.66x10^{-06}$
$1.00x10^{-03}$	$8.07x10^{-04}$	$1.93x10^{-06}$
$5.00x10^{-04}$	$3.13x10^{-04}$	$1.87x10^{-06}$
$5.00x10^{-04}$	$3.00x10^{-04}$	$2.00x10^{-06}$
$1.00x10^{-04}$	$2.80x10^{-05}$	$7.20x10^{-07}$
$1.00x10^{-04}$	$3.66x10^{-05}$	$6.34x10^{-07}$
$5.00x10^{-05}$	$1.21x10^{-05}$	$3.79x10^{-07}$
$5.00x10^{-05}$	$1.14x10^{-05}$	$3.86x10^{-07}$
$1.00x10^{-05}$	$1.18x10^{-06}$	$8.82x10^{-08}$
$1.00x10^{-05}$	$4.50x10^{-07}$	$9.55x10^{-08}$
$1.00x10^{-06}$	$2.67x10^{-08}$	$9.73x10^{-09}$
$1.00x10^{-06}$	$3.86x10^{-08}$	$9.61x10^{-09}$

Table A.2. Data for adsorption of Ox_T = 100 μM onto AC

pH	Oxalate in Solution (M)	Oxalate Sorbed (mol/g)
3.14	$2.61x10^{-06}$	$9.74x10^{-07}$
3.35	$1.55x10^{-06}$	$9.84x10^{-07}$
3.69	$5.28x10^{-07}$	$9.95x10^{-07}$
3.93	$3.42x10^{-07}$	$9.97x10^{-07}$
4.12	$5.45x10^{-07}$	$9.95x10^{-07}$
4.64	$6.22x10^{-07}$	$9.94x10^{-07}$
5.20	$1.03x10^{-06}$	$9.90x10^{-07}$
5.64	$1.04x10^{-06}$	$9.90x10^{-07}$
6.33	$3.94x10^{-06}$	$9.61x10^{-07}$
6.35	$7.55x10^{-06}$	$9.25x10^{-07}$
6.69	$4.06x10^{-06}$	$9.59x10^{-07}$
6.70	$6.49x10^{-06}$	$9.35x10^{-07}$
7.03	$2.43x10^{-05}$	$7.57x10^{-07}$
7.16	$1.88x10^{-05}$	$8.12x10^{-07}$
7.18	$2.48x10^{-05}$	$7.52x10^{-07}$
7.27	$4.90x10^{-05}$	$5.10x10^{-07}$
7.36	$3.30x10^{-05}$	$6.70x10^{-07}$
7.58	$5.33x10^{-05}$	$4.67x10^{-07}$
8.27	$4.34x10^{-05}$	$5.66x10^{-07}$
8.62	$5.19x10^{-05}$	$4.81x10^{-07}$
9.12	$6.62x10^{-05}$	$3.38x10^{-07}$
9.20	$5.91x10^{-05}$	$4.09x10^{-07}$
9.26	$6.16x10^{-05}$	$3.84x10^{-07}$
10.10	$8.61x10^{-05}$	$1.39x10^{-07}$
10.41	$9.42x10^{-05}$	$5.76x10^{-08}$

Table A.3. Data for adsorption of Ox_T = 50 μM onto AC

pH	Oxalate in Solution (M)	Oxalate Sorbed (mol/g)
2.77	$6.54x10^{-06}$	$4.35x10^{-07}$
3.60	$5.24x10^{-07}$	$4.95x10^{-07}$
3.67	$9.16x10^{-07}$	$4.91x10^{-07}$
4.07	$3.44x10^{-07}$	$4.97x10^{-07}$
4.36	$3.06x10^{-07}$	$4.97x10^{-07}$
4.53	$5.55x10^{-07}$	$4.94x10^{-07}$
4.91	$6.46x10^{-07}$	$4.94x10^{-07}$
5.07	$4.40x10^{-07}$	$4.96x10^{-07}$
5.43	$1.17x10^{-06}$	$4.88x10^{-07}$
5.57	$5.89x10^{-07}$	$4.94x10^{-07}$
5.77	$1.01x10^{-06}$	$4.90x10^{-07}$
5.83	$5.93x10^{-07}$	$4.94x10^{-07}$
6.02	$1.25x10^{-06}$	$4.88x10^{-07}$
6.33	$3.60x10^{-06}$	$4.64x10^{-07}$
6.25	$1.84x10^{-06}$	$4.82x10^{-07}$
6.46	$1.94x10^{-06}$	$4.81x10^{-07}$
6.82	$2.69x10^{-06}$	$4.73x10^{-07}$
6.87	$4.93x10^{-06}$	$4.51x10^{-07}$
6.94	$7.46x10^{-06}$	$4.25x10^{-07}$
7.15	$6.84x10^{-06}$	$4.32x10^{-07}$
7.41	$9.84x10^{-06}$	$4.02x10^{-07}$
7.74	$1.76x10^{-05}$	$3.24x10^{-07}$
8.43	$2.16x10^{-05}$	$2.84x10^{-07}$
9.64	$2.71x10^{-05}$	$2.29x10^{-07}$
9.76	$2.46x10^{-05}$	$2.54x10^{-07}$
9.92	$3.06x10^{-05}$	$1.94x10^{-07}$

Table A.3 (Continued). Data for adsorption of Ox_T = 50 μM onto AC

pH	Oxalate in Solution (M)	Oxalate Sorbed (mol/g)
10.25	2.81×10^{-05}	2.19×10^{-07}
10.72	4.23×10^{-05}	7.70×10^{-08}
10.81	4.05×10^{-05}	9.47×10^{-08}
11.04	3.91×10^{-05}	1.09×10^{-07}

Table A.4. Data for adsorption of Ox_T = 10 μM onto AC

pH	Oxalate in Solution (M)	Oxalate Sorbed (mol/g)
4.91	1.39×10^{-07}	9.86×10^{-08}
5.22	1.88×10^{-11}	1.00×10^{-07}
5.77	1.41×10^{-07}	9.86×10^{-08}
6.06	4.26×10^{-08}	9.96×10^{-08}
6.13	1.05×10^{-07}	9.89×10^{-08}
6.60	1.22×10^{-07}	9.88×10^{-08}
6.71	8.07×10^{-07}	9.92×10^{-08}
6.92	1.76×10^{-07}	9.82×10^{-08}
7.21	1.84×10^{-07}	9.82×10^{-08}
7.31	1.17×10^{-07}	9.88×10^{-08}
7.35	1.09×10^{-06}	8.91×10^{-08}
7.83	1.17×10^{-06}	8.83×10^{-08}
8.23	3.98×10^{-06}	6.02×10^{-08}
8.51	5.03×10^{-06}	4.97×10^{-08}
9.41	7.50×10^{-06}	2.50×10^{-08}
9.94	9.41×10^{-06}	5.87×10^{-08}
10.09	8.34×10^{-06}	1.66×10^{-08}

Table A.5. Data for adsorption of Cu_T = 5.7 μM onto AC

pH	Copper in Solution (M)	Copper Sorbed (mol/g)
2.82	$1.32x10^{-05}$	$2.39x10^{-08}$
3.04	$1.20x10^{-05}$	$1.21x10^{-08}$
3.05	$1.24x10^{-05}$	$2.79x10^{-08}$
3.38	$1.36x10^{-05}$	$2.79x10^{-08}$
4.29	$5.54x10^{-07}$	$4.37x10^{-08}$
4.41	$4.89x10^{-06}$	$5.15x10^{-08}$
5.12	$1.04x10^{-05}$	$9.89x10^{-08}$
5.17	$9.63x10^{-06}$	$1.02x10^{-07}$
5.42	$4.60x10^{-06}$	$1.02x10^{-07}$
5.64	$4.60x10^{-06}$	$1.28x10^{-07}$
6.01	$1.20x10^{-05}$	$1.42x10^{-07}$
6.12	$1.97x10^{-06}$	$1.41x10^{-07}$
6.17	$6.57x10^{-07}$	$1.45x10^{-07}$

Table A.6. Data for adsorption of Cu_T = 15 μM onto AC

pH	Copper in Solution (M)	Copper Sorbed (mol/g)
4.27	$4.06x10^{-06}$	$1.63x10^{-08}$
4.30	$4.06x10^{-06}$	$1.63x10^{-08}$
4.41	$3.55ex10^{-06}$	$2.14x10^{-08}$
4.44	$3.03x10^{-06}$	$2.66x10^{-08}$
4.34	$3.55x10^{-06}$	$2.14x10^{-08}$
4.70	$2.52x10^{-06}$	$3.17x10^{-08}$
5.19	$9.78x10^{-07}$	$4.71x10^{-08}$
5.29	$2.07x10^{-07}$	$5.48x10^{-08}$
5.20	$4.64x10^{-07}$	$5.23x10^{-08}$
5.67	$2.07x10^{-07}$	$5.48x10^{-08}$
5.72	$1.04x10^{-07}$	$5.59x10^{-08}$

Table A.7. Data for adsorption of Cu_T = 27 μM with Ox_T = 1 mM onto AC

pH	Copper in Solution (M)	Copper Sorbed (mol/g)
4.91	$2.44x10^{-05}$	$2.27x10^{-08}$
5.67	$2.37x10^{-05}$	$2.90x10^{-08}$
5.94	$2.34x10^{-05}$	$3.22x10^{-08}$
6.03	$2.28x10^{-05}$	$3.86x10^{-08}$
6.28	$2.25x10^{-05}$	$4.18x10^{-08}$
6.72	$1.90x10^{-05}$	$7.67x10^{-08}$
7.19	$1.01x10^{-05}$	$1.66x10^{-07}$
7.37	$1.36x10^{-05}$	$1.30x10^{-07}$
7.66	$9.40x10^{-06}$	$1.72x10^{-07}$
7.69	$4.71x10^{-06}$	$2.19x10^{-07}$
7.89	$1.89x10^{-06}$	$2.47x10^{-07}$
7.98	$5.20x10^{-07}$	$2.61x10^{-07}$

Table A.8. Data for adsorption of Cu_T = 121 μM with Ox_T = 1 mM onto AC

pH	Copper in Solution (M)	Copper Sorbed (mol/g)
7.27	$8.54x10^{-05}$	$3.52x10^{-07}$
7.58	$4.72x10^{-05}$	$7.34x10^{-07}$
7.66	$4.22x10^{-05}$	$7.85x10^{-07}$
7.92	$2.35x10^{-05}$	$9.72x10^{-07}$
8.16	$1.84x10^{-05}$	$1.02x10^{-06}$
8.21	$1.05x10^{-05}$	$1.10x10^{-06}$
8.53	$1.26x10^{-05}$	$1.08x10^{-06}$
8.62	$2.56x10^{-06}$	$1.18x10^{-06}$
8.98	$1.83x10^{-06}$	$1.19x10^{-06}$
9.30	$1.11x10^{-06}$	$1.20x10^{-06}$

Table A.9. Data for adsorption of Cu_T = 38 μM with Ox_T = 100 μM onto AC

pH	Copper in Solution (M)	Copper Sorbed (mol/g)
3.39	$3.67x10^{-05}$	$1.60x10^{-08}$
3.47	$3.82x10^{-05}$	$4.28x10^{-10}$
3.53	$3.74x10^{-05}$	$8.34x10^{-09}$
3.63	$3.58x10^{-05}$	$2.42x10^{-09}$
3.67	$3.74x10^{-05}$	$8.34x10^{-09}$
3.69	$3.82x10^{-05}$	$4.28x10^{-10}$
3.70	$3.74x10^{-05}$	$8.34x10^{-09}$
3.75	$3.62x10^{-05}$	$2.02x10^{-08}$
3.81	$3.62x10^{-05}$	$2.02x10^{-08}$
3.86	$3.47x10^{-05}$	$3.60x10^{-08}$
3.99	$3.62x10^{-05}$	$2.02x10^{-08}$
4.16	$3.62x10^{-05}$	$2.02x10^{-08}$
4.19	$3.44x10^{-05}$	$3.86x10^{-08}$
4.32	$3.62x10^{-05}$	$2.02x10^{-08}$
4.37	$3.18x10^{-05}$	$6.50x10^{-08}$
4.54	$3.03x10^{-05}$	$8.01x10^{-08}$
4.59	$3.14x10^{-05}$	$6.88x10^{-08}$
4.69	$2.76x10^{-05}$	$1.07x10^{-07}$
4.87	$2.76x10^{-05}$	$1.07x10^{-07}$
4.87	$2.72x10^{-05}$	$1.10x10^{-07}$
4.89	$2.46x10^{-05}$	$1.37x10^{-07}$
5.18	$2.50x10^{-05}$	$1.33x10^{-07}$
5.31	$2.26x10^{-05}$	$1.57x10^{-07}$
5.52	$1.82x10^{-05}$	$2.01x10^{-07}$
5.75	$1.18x10^{-05}$	$2.65x10^{-07}$
5.98	$1.99x10^{-05}$	$1.84x10^{-07}$
6.72	$9.91x10^{-06}$	$2.84x10^{-07}$

Table A.9 (Continued). Data for adsorption of Cu_T = 38 μM with Ox_T = 100 μM onto AC

pH	Copper in Solution (M)	Copper Sorbed (mol/g)
6.87	$2.67x10^{-06}$	$3.56x10^{-07}$
7.15	$7.19x10^{-06}$	$3.11x10^{-07}$
7.58	$2.67x10^{-06}$	$3.56x10^{-07}$
7.72	$4.13x10^{-07}$	$3.78x10^{-07}$

Table A.10. Data for adsorption of Cu_T = 8.3 μM with Ox_T = 100 μM onto AC

pH	Copper in Solution (M)	Copper Sorbed (mol/g)
3.45	$7.39x10^{-06}$	$8.69x10^{-09}$
3.62	$7.39x10^{-06}$	$8.69x10^{-09}$
3.65	$7.76x10^{-06}$	$4.95x10^{-09}$
3.75	$7.76x10^{-06}$	$4.95x10^{-09}$
3.85	$6.64x10^{-06}$	$1.62x10^{-08}$
3.87	$7.39x10^{-06}$	$8.69x10^{-09}$
3.92	$6.64x10^{-06}$	$1.62x10^{-08}$
3.97	$6.64x10^{-06}$	$1.62x10^{-08}$
4.02	$6.64x10^{-06}$	$1.62x10^{-08}$
4.19	$5.90x10^{-06}$	$2.36x10^{-08}$
4.23	$6.27x10^{-06}$	$1.99x10^{-08}$
4.37	$6.27x10^{-06}$	$1.99x10^{-08}$
4.56	$5.19x10^{-06}$	$3.07x10^{-08}$
4.69	$5.19x10^{-06}$	$3.07x10^{-08}$
4.89	$4.52x10^{-06}$	$3.74x10^{-08}$
4.99	$3.17x10^{-06}$	$5.09x10^{-08}$
5.16	$3.50x10^{-06}$	$4.76x10^{-08}$
5.17	$2.49x10^{-06}$	$5.77x10^{-08}$
5.57	$2.15x10^{-06}$	$6.11x10^{-08}$
5.60	$2.03x10^{-06}$	$6.23x10^{-08}$
6.01	$1.14x10^{-06}$	$7.12x10^{-08}$
5.97	$1.47x10^{-06}$	$6.78x10^{-08}$
6.53	$7.98x10^{-07}$	$7.46x10^{-08}$
6.48	$7.98x10^{-07}$	$7.46x10^{-08}$
6.61	$1.64x10^{-07}$	$8.09x10^{-08}$

Table A.11. Data for adsorption of Ox_T = 100 μM with Cu_T = 38 μM onto AC

pH	Oxalate in Solution (M)	Oxalate Sorbed (mol/g)
3.51	$2.09x10^{-06}$	$9.79x10^{-07}$
4.06	$5.21x10^{-06}$	$9.48x10^{-07}$
4.60	$4.04x10^{-06}$	$9.60x10^{-07}$
4.65	$4.62x10^{-06}$	$9.54x10^{-07}$
5.04	$1.05x10^{-05}$	$8.95x10^{-07}$
5.64	$8.28x10^{-06}$	$9.17x10^{-07}$
5.68	$8.20x10^{-06}$	$9.18x10^{-07}$
5.94	$1.97x10^{-05}$	$8.03x10^{-07}$
6.04	$9.81x10^{-06}$	$9.02x10^{-07}$
6.04	$1.42x10^{-05}$	$8.58x10^{-07}$
6.27	$1.24x10^{-05}$	$8.76x10^{-07}$
6.37	$1.10x10^{-05}$	$8.90x10^{-07}$
6.43	$1.08x10^{-05}$	$8.92x10^{-07}$
6.47	$1.63x10^{-05}$	$8.37x10^{-07}$
6.49	$1.47x10^{-05}$	$8.53x10^{-07}$
7.15	$3.46x10^{-05}$	$6.54x10^{-07}$
7.31	$4.67x10^{-05}$	$5.33x10^{-07}$
7.47	$2.12x10^{-05}$	$7.88x10^{-07}$
7.48	$4.41x10^{-05}$	$5.59x10^{-07}$
7.88	$6.97x10^{-05}$	$3.03x10^{-07}$
7.85	$6.36x10^{-05}$	$3.64x10^{-07}$
7.95	$6.94x10^{-05}$	$3.06x10^{-07}$
8.43	$7.97x10^{-05}$	$2.03x10^{-07}$
8.67	$7.23x10^{-05}$	$2.77x10^{-07}$

Table A.12. Data for adsorption of Ox_T = 100 μM with Cu_T = 8.3 μM onto AC

pH	Oxalate in Solution (M)	Oxalate Sorbed (mol/g)
3.52	$4.71x10^{-06}$	$9.53x10^{-07}$
4.24	$1.09x10^{-06}$	$9.89x10^{-07}$
4.89	$1.38x10^{-06}$	$9.86x10^{-07}$
4.91	$1.75x10^{-06}$	$9.82x10^{-07}$
5.34	$4.24x10^{-06}$	$9.58x10^{-07}$
5.90	$5.89x10^{-06}$	$9.41x10^{-07}$
6.22	$7.78x10^{-06}$	$9.22x10^{-07}$
6.30	$9.56x10^{-06}$	$9.04x10^{-07}$
6.45	$1.01x10^{-05}$	$8.99x10^{-07}$
6.45	$5.31x10^{-06}$	$9.47x10^{-07}$
6.90	$2.12x10^{-05}$	$7.88x10^{-07}$
7.16	$2.78x10^{-05}$	$7.22x10^{-07}$
7.62	$4.89x10^{-05}$	$5.11x10^{-07}$
7.65	$6.23x10^{-05}$	$3.77x10^{-07}$
7.66	$5.92x10^{-05}$	$4.08x10^{-07}$
7.69	$6.24x10^{-05}$	$3.76x10^{-07}$
7.88	$5.66x10^{-05}$	$4.34x10^{-07}$
8.07	$6.98x10^{-05}$	$3.02x10^{-07}$
8.21	$7.87x10^{-05}$	$2.13x10^{-07}$
8.45	$8.53x10^{-05}$	$1.47x10^{-07}$
8.45	$7.97x10^{-05}$	$2.03x10^{-07}$
9.35	$9.50x10^{-05}$	$5.02x10^{-08}$
9.36	$9.41x10^{-05}$	$5.94x10^{-07}$
9.71	$8.65x10^{-05}$	$1.35x10^{-07}$

APPENDIX B

DATA FOR ADSORPTION ONTO UNWEATHERED MILFORD COATED SAMPLE

Table B.1. Data for oxalate adsorption isotherm onto MC at pH 7

Ox_T (M)	Oxalate in Solution (M)	Oxalate Sorbed (mol/g)
$1.00x10^{-03}$	$6.21x10^{-04}$	$7.81x10^{-06}$
$1.00x10^{-03}$	$7.32x10^{-04}$	$2.67x10^{-06}$
$5.00x10^{-04}$	$2.51x10^{-04}$	$2.48x10^{-06}$
$5.00x10^{-04}$	$2.48x10^{-04}$	$2.51x10^{-06}$
$1.00x10^{-04}$	$1.85x10^{-05}$	$8.14x10^{-07}$
$1.00x10^{-04}$	$1.24x10^{-05}$	$8.75x10^{-07}$
$5.00x10^{-05}$	$6.70x10^{-06}$	$4.32x10^{-07}$
$5.00x10^{-05}$	$7.29x10^{-06}$	$4.27x10^{-07}$
$1.00x10^{-05}$	$1.38x10^{-06}$	$8.61x10^{-08}$
$1.00x10^{-05}$	$1.17x10^{-06}$	$8.82x10^{-08}$
$1.00x10^{-06}$	$1.19x10^{-07}$	$8.81x10^{-09}$
$1.00x10^{-06}$	$7.72x10^{-07}$	$9.23x10^{-09}$

Table B.2. Data for adsorption edge onto MC; Ox_T = 100 μM

pH	Oxalate in Solution (M)	Oxalate Sorbed (mol/g)
4.54	$4.18x10^{-05}$	$5.82x10^{-07}$
4.81	$4.42x10^{-05}$	$5.58x10^{-07}$
4.89	$4.66x10^{-05}$	$5.34x10^{-07}$
4.92	$3.35x10^{-05}$	$6.65x10^{-07}$
5.33	$3.47x10^{-05}$	$6.53x10^{-07}$
5.63	$2.18x10^{-05}$	$7.82x10^{-07}$
5.94	$2.67x10^{-05}$	$7.34x10^{-07}$
5.95	$2.57x10^{-05}$	$7.43x10^{-07}$
6.09	$3.85x10^{-05}$	$6.15x10^{-07}$
6.12	$3.93x10^{-05}$	$6.07x10^{-07}$
6.42	$3.50x10^{-05}$	$6.50x10^{-07}$
6.65	$3.55x10^{-05}$	$6.45x10^{-07}$
6.99	$4.22x10^{-05}$	$5.78x10^{-07}$
7.50	$5.47x10^{-05}$	$4.53x10^{-07}$
7.62	$5.62x10^{-05}$	$4.38x10^{-07}$
8.35	$6.96x10^{-05}$	$3.04x10^{-07}$
9.21	$8.06x10^{-05}$	$1.94x10^{-07}$
9.88	$8.73x10^{-05}$	$1.27x10^{-07}$
10.05	$8.87x10^{-05}$	$1.13x10^{-07}$
10.08	$8.86x10^{-05}$	$1.14x10^{-07}$
10.73	$9.59x10^{-05}$	$4.09x10^{-08}$

Table B.3. Data for adsorption edge onto MC; Ox_T = 50 μM

pH	Oxalate in Solution (M)	Oxalate Sorbed (mol/g)
4.31	$1.20x10^{-05}$	$3.80x10^{-07}$
4.32	$1.43x10^{-05}$	$3.57x10^{-07}$
4.68	$1.42x10^{-05}$	$3.58x10^{-07}$
4.73	$1.35x10^{-05}$	$3.65x10^{-07}$
4.78	$8.49x10^{-05}$	$4.15x10^{-07}$
5.07	$6.21x10^{-06}$	$4.38x10^{-07}$
5.33	$6.71x10^{-06}$	$4.33x10^{-07}$
5.41	$5.41x10^{-06}$	$4.46x10^{-07}$
5.47	$4.01x10^{-06}$	$4.60x10^{-07}$
5.75	$3.90x10^{-06}$	$4.61x10^{-07}$
5.98	$5.95x10^{-06}$	$4.41x10^{-07}$
6.20	$8.03x10^{-06}$	$4.20x10^{-07}$
6.31	$9.52x10^{-06}$	$4.05x10^{-07}$
6.73	$1.63x10^{-05}$	$3.37x10^{-07}$
6.74	$2.02x10^{-05}$	$2.98x10^{-07}$
6.88	$1.82x10^{-05}$	$3.18x10^{-07}$
7.27	$2.12x10^{-05}$	$2.88x10^{-07}$
7.69	$2.78x10^{-05}$	$2.22x10^{-07}$
8.44	$3.18x10^{-05}$	$1.82x10^{-07}$
8.68	$3.12x10^{-05}$	$1.88x10^{-07}$
9.91	$3.97x10^{-05}$	$1.03x10^{-07}$
10.84	$4.16x10^{-05}$	$8.43x10^{-08}$
11.15	$4.00x10^{-05}$	$1.00x10^{-07}$

Table B.4. Data for adsorption edge onto MC; Ox_T = 10 μM

pH	Oxalate in Solution (M)	Oxalate Sorbed (mol/g)
4.43	$1.98x10^{-06}$	$8.02x10^{-08}$
4.47	$1.82x10^{-06}$	$8.18x10^{-08}$
4.94	$9.01x10^{-07}$	$9.10x10^{-08}$
4.98	$8.12x10^{-07}$	$9.19x10^{-08}$
5.17	$5.02x10^{-07}$	$9.50x10^{-08}$
5.28	$5.36x10^{-07}$	$9.46x10^{-08}$
5.58	$4.02x10^{-07}$	$9.60x10^{-08}$
5.59	$3.90x10^{-07}$	$9.61x10^{-08}$
6.95	$2.06x10^{-07}$	$7.94x10^{-08}$
7.04	$1.80x10^{-07}$	$8.20x10^{-08}$
7.20	$3.67x10^{-06}$	$6.33x10^{-08}$
7.88	$2.82x10^{-06}$	$7.18x10^{-08}$
7.55	$3.10x10^{-06}$	$6.90x10^{-08}$
8.22	$4.53x10^{-06}$	$5.47x10^{-08}$
9.87	$9.34x10^{-06}$	$6.58x10^{-09}$
9.90	$8.13x10^{-06}$	$1.87x10^{-08}$
10.79	$9.69x10^{-06}$	$3.09x10^{-09}$
10.38	$9.56x10^{-06}$	$4.40x10^{-09}$
10.38	$8.81x10^{-06}$	$1.19x10^{-08}$
10.81	$9.22x10^{-06}$	$7.78x10^{-09}$
10.94	$9.92x10^{-06}$	$8.10x10^{-10}$
10.97	$9.64x10^{-06}$	$3.64x10^{-09}$
11.08	$9.85x10^{-06}$	$1.46x10^{-09}$
11.04	$9.96x10^{-06}$	$3.78x10^{-10}$

Table B.5. Data for adsorption edge onto MC; Cu_T = 15 μM

pH	Oxalate in Solution (M)	Oxalate Sorbed (mol/g)
4.52	$1.44x10^{-05}$	$3.82x10^{-09}$
4.71	$9.21x10^{-06}$	$5.57x10^{-08}$
5.25	$4.42x10^{-06}$	$1.04x10^{-07}$
6.32	$1.63x10^{-06}$	$1.32x10^{-07}$

Table B.6. Data for adsorption edge onto MC; Cu_T = 5.7 μM

pH	Oxalate in Solution (M)	Oxalate Sorbed (mol/g)
3.79	$5.60x10^{-06}$	$8.52x10^{-10}$
3.93	$5.60x10^{-06}$	$8.52x10^{-10}$
4.03	$5.60x10^{-06}$	$8.52x10^{-10}$
4.10	$5.35x10^{-06}$	$3.42x10^{-09}$
4.12	$5.09x10^{-06}$	$5.99x10^{-09}$
4.27	$4.58x10^{-06}$	$1.11x10^{-08}$
4.39	$4.06x10^{-06}$	$1.63x10^{-08}$
4.50	$3.81x10^{-06}$	$1.88x10^{-08}$
4.49	$3.96x10^{-06}$	$1.73x10^{-08}$
4.54	$3.81x10^{-06}$	$1.88x10^{-08}$
4.54	$3.96x10^{-06}$	$1.73x10^{-08}$
4.63	$4.42x10^{-06}$	$1.27x10^{-08}$
4.68	$3.55x10^{-06}$	$2.14x10^{-08}$
4.69	$3.96x10^{-06}$	$1.73x10^{-08}$
4.71	$3.03x10^{-06}$	$2.66x10^{-08}$
4.76	$3.96x10^{-06}$	$1.73x10^{-08}$
4.84	$3.50x10^{-06}$	$2.19x10^{-08}$
4.86	$3.03x10^{-06}$	$2.66x10^{-08}$
4.98	$2.11x10^{-06}$	$3.58x10^{-08}$
5.08	$1.65x10^{-06}$	$4.04x10^{-08}$
5.22	$1.18x10^{-06}$	$4.51x10^{-08}$
5.31	$6.18x10^{-07}$	$5.07x10^{-08}$
5.35	$4.29x10^{-07}$	$5.26x10^{-08}$
5.99	$9.52x10^{-08}$	$5.59x10^{-08}$

Table B.7. Data for adsorption edge onto MC; Cu_T = 27 μM with Ox_T = 1 mM

pH	Oxalate in Solution (M)	Oxalate Sorbed (mol/g)
3.17	$2.15x10^{-05}$	$5.10x10^{-08}$
3.58	$2.12x10^{-05}$	$5.43x10^{-08}$
3.61	$2.09x10^{-05}$	$5.76x10^{-08}$
3.73	$2.35x10^{-05}$	$3.12x10^{-08}$
4.00	$2.15x10^{-05}$	$5.10x10^{-08}$
4.35	$2.22x10^{-05}$	$4.44x10^{-08}$
4.79	$2.25x10^{-05}$	$4.11x10^{-08}$
5.08	$2.12x10^{-05}$	$5.43x10^{-08}$
5.72	$2.16x10^{-05}$	$5.03x10^{-08}$
5.73	$2.19x10^{-05}$	$4.77x10^{-08}$
6.31	$2.15x10^{-05}$	$5.10x10^{-08}$
6.52	$1.86x10^{-05}$	$8.08x10^{-08}$
6.55	$2.12x10^{-05}$	$5.40x10^{-08}$
7.30	$1.01x10^{-05}$	$1.66x10^{-07}$
7.31	$8.30x10^{-06}$	$1.83x10^{-07}$
8.47	$7.90x10^{-07}$	$2.58x10^{-07}$
9.31	$1.16x10^{-06}$	$2.55x10^{-07}$
9.48	$4.18x10^{-07}$	$2.62x10^{-07}$

Table B.8. Data for adsorption edge onto MC; Cu_T = 121 μM with Ox_T = 1 mM

pH	Oxalate in Solution (M)	Oxalate Sorbed (mol/g)
6.46	$1.19x10^{-04}$	$2.13x10^{-08}$
6.68	$1.15x10^{-04}$	$5.73x10^{-08}$
6.69	$1.14x10^{-04}$	$6.45x10^{-08}$
6.69	$1.12x10^{-04}$	$8.61x10^{-08}$
6.93	$1.08x10^{-04}$	$1.22x10^{-07}$
7.06	$9.90x10^{-05}$	$2.17x10^{-07}$
7.10	$1.01x10^{-04}$	$2.01x10^{-07}$
7.14	$7.90x10^{-05}$	$4.17x10^{-07}$
7.22	$9.26x10^{-05}$	$2.81x10^{-07}$
7.31	$8.46x10^{-05}$	$3.60x10^{-07}$
7.32	$8.38x10^{-05}$	$3.69x10^{-07}$
7.54	$6.66x10^{-05}$	$5.40x10^{-07}$
7.55	$5.97x10^{-05}$	$6.09x10^{-07}$
7.66	$5.29x10^{-05}$	$6.77x10^{-07}$
7.67	$5.57x10^{-05}$	$6.49x10^{-07}$
7.90	$2.92x10^{-05}$	$9.15x10^{-07}$
8.18	$1.65x10^{-05}$	$1.04x10^{-06}$
8.37	$1.81x10^{-05}$	$1.03x10^{-06}$
8.59	$6.12x10^{-06}$	$1.15x10^{-06}$
8.73	$4.52x10^{-06}$	$1.16x10^{-06}$
8.98	$2.12x10^{-06}$	$1.19x10^{-06}$
9.49	$5.19x10^{-07}$	$1.20x10^{-06}$

Table B.9. Data for adsorption edge onto MC; Cu_T = 38 μM with Ox_T = 100 μM

pH	Oxalate in Solution (M)	Oxalate Sorbed (mol/g)
3.47	$3.74x10^{-05}$	$8.41x10^{-09}$
3.93	$3.59x10^{-05}$	$2.35x10^{-08}$
4.05	$3.40x10^{-05}$	$4.24x10^{-08}$
4.15	$3.36x10^{-05}$	$4.61x10^{-08}$
4.20	$3.55x10^{-05}$	$2.73x10^{-08}$
4.30	$3.36x10^{-05}$	$4.61x10^{-08}$
4.33	$3.63x10^{-05}$	$1.97x10^{-08}$
4.39	$3.14x10^{-05}$	$6.88x10^{-08}$
4.48	$3.21x10^{-05}$	$6.12x10^{-08}$
4.55	$3.03x10^{-05}$	$8.01x10^{-08}$
4.61	$3.25x10^{-05}$	$5.75x10^{-08}$
4.64	$3.43x10^{-05}$	$3.94x10^{-08}$
4.72	$3.29x10^{-05}$	$5.37x10^{-08}$
4.85	$3.34x10^{-05}$	$4.85x10^{-08}$
5.05	$3.52x10^{-05}$	$3.04x10^{-08}$
5.30	$3.07x10^{-05}$	$7.56x10^{-08}$
5.47	$2.89x10^{-05}$	$9.37x10^{-08}$
5.88	$2.80x10^{-05}$	$1.03x10^{-07}$
6.22	$2.17x10^{-05}$	$1.66x10^{-07}$
6.74	$1.08x10^{-05}$	$2.75x10^{-07}$
6.85	$9.91x10^{-06}$	$2.84x10^{-07}$
7.08	$9.91x10^{-06}$	$2.84x10^{-07}$
7.39	$6.29x10^{-06}$	$3.20x10^{-07}$
7.66	$2.67x10^{-06}$	$3.56x10^{-07}$

Table B.10. Data for adsorption edge onto MC; Cu_T = 8.3 μM with Ox_T = 100 μM

pH	Oxalate in Solution (M)	Oxalate Sorbed (mol/g)
3.42	$7.76x10^{-06}$	$4.95x10^{-09}$
3.52	$7.76x10^{-06}$	$4.95x10^{-09}$
3.60	$7.76x10^{-06}$	$4.95x10^{-09}$
3.65	$7.02x10^{-06}$	$1.24x10^{-08}$
3.70	$7.76x10^{-06}$	$4.95x10^{-09}$
3.74	$7.76x10^{-06}$	$4.95x10^{-09}$
3.79	$7.39x10^{-06}$	$8.68x10^{-09}$
3.85	$7.76x10^{-06}$	$4.95x10^{-09}$
3.97	$7.02x10^{-06}$	$1.24x10^{-08}$
4.05	$7.76x10^{-06}$	$4.95x10^{-09}$
4.13	$7.76x10^{-06}$	$4.95x10^{-09}$
4.35	$7.02x10^{-06}$	$1.24x10^{-08}$
4.59	$5.42x10^{-06}$	$2.84x10^{-08}$
4.85	$5.42x10^{-06}$	$2.84x10^{-08}$
5.19	$5.08x10^{-06}$	$3.18x10^{-08}$
5.19	$4.74x10^{-06}$	$3.51x10^{-08}$
5.48	$4.07x10^{-06}$	$4.19x10^{-08}$
5.92	$3.73x10^{-06}$	$4.53x10^{-08}$
6.05	$3.39x10^{-06}$	$4.87x10^{-08}$
6.69	$1.69x10^{-06}$	$6.57x10^{-08}$
6.78	$1.01x10^{-06}$	$7.25x10^{-08}$
6.80	$1.01x10^{-06}$	$7.25x10^{-08}$
7.27	$1.64x10^{-07}$	$8.09x10^{-08}$
7.75	$6.24x10^{-08}$	$8.20x10^{-08}$

Table B.10. Data for adsorption edge onto MC; Ox_T = 100 μM with Cu_T = 8.3 μM

pH	Oxalate in Solution (M)	Oxalate Sorbed (mol/g)
3.47	$5.95x10^{-05}$	$4.05x10^{-07}$
4.09	$6.16x10^{-05}$	$3.84x10^{-07}$
4.48	$5.51x10^{-05}$	$4.49x10^{-07}$
4.59	$4.76x10^{-05}$	$5.24x10^{-07}$
4.93	$4.71x10^{-05}$	$5.29x10^{-07}$
5.23	$4.12x10^{-05}$	$5.88x10^{-07}$
5.47	$4.33x10^{-05}$	$5.67x10^{-07}$
5.66	$3.90x10^{-05}$	$6.10x10^{-07}$
5.79	$3.43x10^{-05}$	$6.57x10^{-07}$
6.02	$3.55x10^{-05}$	$6.45x10^{-07}$
6.71	$5.09x10^{-05}$	$4.91x10^{-07}$
6.80	$4.42x10^{-05}$	$5.58x10^{-07}$
6.99	$5.23x10^{-05}$	$4.77x10^{-07}$
7.26	$5.15x10^{-05}$	$4.85x10^{-07}$
7.47	$5.50x10^{-05}$	$4.50x10^{-07}$
7.48	$5.81x10^{-05}$	$4.19x10^{-07}$
7.48	$5.14x10^{-05}$	$4.86x10^{-07}$
7.72	$5.86x10^{-05}$	$4.14x10^{-07}$
8.20	$6.38x10^{-05}$	$3.62x10^{-07}$
8.62	$8.21x10^{-05}$	$1.79x10^{-07}$
9.05	$9.38x10^{-05}$	$6.24x10^{-08}$

APPENDIX C

DATA FOR ADSORPTION ONTO WEATHERED MILFORD COATED SAMPLES

MC1

Table C.1. Data for oxalate adsorption isotherm at pH 7.

Ox_T [M]	Oxalate in Solution (M)	Oxalate Sorbed (mol/g)
$1.00x10^{-03}$	$6.08x10^{-04}$	$3.92x10^{-06}$
$1.00x10^{-03}$	$5.23x10^{-04}$	$4.77x10^{-06}$
$5.00x10^{-04}$	$2.14x10^{-04}$	$2.86x10^{-06}$
$5.00x10^{-04}$	$1.72x10^{-04}$	$3.28x10^{-06}$
$1.00x10^{-04}$	$2.49x10^{-05}$	$7.51x10^{-07}$
$1.00x10^{-04}$	$2.94x10^{-05}$	$7.06x10^{-07}$
$5.00x10^{-05}$	$1.26x10^{-05}$	$3.74x10^{-07}$
$5.00x10^{-05}$	$1.29x10^{-05}$	$3.71x10^{-07}$
$1.00x10^{-05}$	$7.43x10^{-07}$	$9.26x10^{-08}$
$1.00x10^{-05}$	$1.39x10^{-06}$	$8.61x10^{-08}$
$1.00x10^{-06}$	$1.24x10^{-07}$	$8.76x10^{-09}$
$1.00x10^{-06}$	$1.14x10^{-07}$	$8.86x10^{-09}$

Table C.2. Data for adsorption edge at Ox_T = 50 μM onto MC1.

pH	Oxalate in Solution (M)	Oxalate Sorbed (mol/g)
4.79	$2.19x10^{-05}$	$2.81x10^{-07}$
5.14	$1.99x10^{-05}$	$3.01x10^{-07}$
5.35	$1.59x10^{-05}$	$3.41x10^{-07}$
5.71	$1.40x10^{-05}$	$3.60x10^{-07}$
7.51	$2.59x10^{-05}$	$2.41x10^{-07}$
7.77	$3.11x10^{-05}$	$1.89x10^{-07}$
9.92	$4.02x10^{-05}$	$9.76x10^{-08}$
10.58	$4.23x10^{-05}$	$7.69x10^{-08}$
10.85	$4.20x10^{-05}$	$7.96x10^{-08}$
11.01	$4.11x10^{-05}$	$8.93x10^{-08}$
11.25	$3.86x10^{-05}$	$1.14x10^{-07}$

Table C.3. Data for adsorption edge at Ox_T = 10 μM onto MC1.

pH	Oxalate in Solution (M)	Oxalate Sorbed (mol/g)
4.71	$2.00x10^{-06}$	$8.00x10^{-08}$
4.89	$1.79x10^{-06}$	$8.21x10^{-08}$
5.18	$1.18x10^{-06}$	$8.82x10^{-08}$
5.34	$8.53x10^{-07}$	$9.15x10^{-08}$
5.71	$9.85x10^{-07}$	$9.02x10^{-08}$
5.99	$6.35x10^{-07}$	$9.37x10^{-08}$
6.21	$1.33x10^{-06}$	$8.67x10^{-08}$
6.37	$1.26x10^{-06}$	$8.74x10^{-08}$
6.71	$2.06x10^{-06}$	$7.94x10^{-08}$
$7.^{-03}$	$2.64x10^{-06}$	$7.36x10^{-08}$
7.41	$2.89x10^{-06}$	$7.11x10^{-08}$
7.81	$4.57x10^{-06}$	$5.43x10^{-08}$

Table C.4. Data for copper adsorption isotherm at pH 7 with Ox_T = 1 mM.

Cu_T (M)	Copper in Solution (M)	Copper Sorbed (mol/g)
$5.87x10^{-04}$	$5.39x10^{-04}$	$4.75x10^{-07}$
$5.87x10^{-04}$	$5.39x10^{-04}$	$4.75x10^{-07}$
$2.93x10^{-04}$	$2.56x10^{-04}$	$3.73x10^{-07}$
$2.93x10^{-04}$	$2.51x10^{-04}$	$4.19x10^{-07}$
$1.17x10^{-04}$	$1.02x10^{-04}$	$1.51x10^{-07}$
$1.17x10^{-04}$	$1.03x10^{-04}$	$1.46x10^{-07}$
$5.87x10^{-05}$	$5.21x10^{-05}$	$6.58x10^{-08}$
$5.87x10^{-05}$	$5.16x10^{-05}$	$7.08x10^{-08}$
$2.93x10^{-05}$	$2.65x10^{-05}$	$2.81x10^{-08}$
$2.93x10^{-05}$	$2.70x10^{-05}$	$2.31x10^{-08}$
$5.87x10^{-06}$	$4.96x10^{-06}$	$9.04x10^{-09}$
$5.87x10^{-06}$	$4.46x10^{-06}$	$1.40x10^{-08}$

Table C.5. Data for adsorption edge at Cu_T = 15 μM onto MC1.

pH	Copper in Solution (M)	Copper Sorbed (mol/g)
4.19	$9.21x10^{-06}$	$5.57x10^{-08}$
4.24	$1.08x10^{-05}$	$3.97x10^{-08}$
5.85	$1.63x10^{-06}$	$1.32x10^{-07}$
6.98	$3.34x10^{-07}$	$1.44x10^{-07}$

Table C.6. Data for adsorption edge at Cu_T = 27 μM with Ox_T = 1 mM onto MC1.

pH	Copper in Solution (M)	Copper Sorbed (mol/g)
3.17	$2.38x10^{-05}$	$2.79x10^{-08}$
3.28	$2.15x10^{-05}$	$5.10x10^{-08}$
3.55	$2.38x10^{-05}$	$2.79x10^{-08}$
3.71	$2.12x10^{-05}$	$5.43x10^{-08}$
3.88	$2.25x10^{-05}$	$4.11x10^{-08}$
4.31	$2.35x10^{-05}$	$3.12x10^{-08}$
4.32	$2.32x10^{-05}$	$3.45x10^{-08}$
4.63	$2.57x10^{-05}$	$9.42x10^{-09}$
4.75	$2.19x10^{-05}$	$4.77x10^{-08}$
5.09	$2.19x10^{-05}$	$4.77x10^{-08}$
5.71	$2.29x10^{-05}$	$3.78x10^{-08}$
6.39	$2.27x10^{-05}$	$3.91x10^{-08}$
6.47	$1.89x10^{-05}$	$7.75x10^{-08}$
6.98	$1.83x10^{-05}$	$8.37x10^{-08}$
7.18	$1.38x10^{-05}$	$1.28x10^{-07}$
8.12	$1.69x10^{-06}$	$2.49x10^{-07}$

MC2

Table C.7. Data for oxalate adsorption isotherm at pH 7 onto MC2.

Ox_T (M)	Oxalate in Solution (M)	Oxalate Sorbed (mol/g)
$1.00x10^{-03}$	$7.32x10^{-04}$	$2.68x10^{-06}$
$1.00x10^{-03}$	$5.24x10^{-04}$	$4.76x10^{-06}$
$5.00x10^{-04}$	$1.99x10^{-04}$	$3.01x10^{-06}$
$5.00x10^{-04}$	$3.43x10^{-04}$	$1.57x10^{-06}$
$1.00x10^{-04}$	$4.20x10^{-05}$	$5.80x10^{-07}$
$1.00x10^{-04}$	$3.95x10^{-05}$	$6.05x10^{-07}$
$5.00x10^{-05}$	$1.92x10^{-05}$	$3.08x10^{-07}$
$5.00x10^{-05}$	$2.17x10^{-05}$	$2.83x10^{-07}$
$1.00x10^{-05}$	$4.03x10^{-06}$	$5.97x10^{-08}$
$1.00x10^{-05}$	$2.50x10^{-06}$	$7.50x10^{-08}$
$1.00x10^{-06}$	$3.38x10^{-07}$	$6.62x10^{-09}$
$1.00x10^{-06}$	$3.31x10^{-07}$	$6.69x10^{-09}$

Table C.8. Data for adsorption edge at Ox_T = 50 μM onto MC2.

pH	Oxalate in Solution (M)	Oxalate Sorbed (mol/g)
5.17	$2.91x10^{-05}$	$2.09x10^{-07}$
5.68	$2.51x10^{-05}$	$2.49x10^{-07}$
5.99	$1.92x10^{-05}$	$3.08x10^{-07}$
6.85	$2.49x10^{-05}$	$2.51x10^{-07}$
8.43	$3.61x10^{-05}$	$1.39x10^{-07}$
9.45	$3.57x10^{-05}$	$1.43x10^{-07}$
10.50	$3.95x10^{-05}$	$1.05x10^{-07}$
10.78	$3.94x10^{-05}$	$1.06x10^{-07}$
11.01	$4.13x10^{-05}$	$8.68x10^{-08}$
11.12	$3.83x10^{-05}$	$1.17x10^{-07}$
11.28	$4.47x10^{-05}$	$5.35x10^{-08}$
11.33	$4.12x10^{-05}$	$8.76x10^{-08}$

Table C.9. Data for adsorption edge at Ox_T = 10 μM onto MC2.

pH	Oxalate in Solution (M)	Oxalate Sorbed (mol/g)
5.19	$4.05x10^{-06}$	$5.95x10^{-08}$
5.97	$4.17x10^{-06}$	$5.83x10^{-08}$
6.78	$2.80x10^{-06}$	$7.20x10^{-08}$
7.02	$4.91x10^{-06}$	$5.09x10^{-08}$
7.17	$3.39x10^{-06}$	$6.61x10^{-08}$
7.40	$6.07x10^{-06}$	$3.93x10^{-08}$
7.45	$4.51x10^{-06}$	$5.49x10^{-08}$
7.75	$5.17x10^{-06}$	$4.83x10^{-08}$
7.81	$5.64x10^{-06}$	$4.36x10^{-08}$
7.99	$4.43x10^{-06}$	$5.57x10^{-08}$
8.08	$7.24x10^{-06}$	$2.76x10^{-08}$
10.03	$5.15x10^{-06}$	$4.85x10^{-08}$

Table C.10. Data for copper adsorption isotherm at pH 7 with Ox_T = 1 mM.

Cu_T (M)	Copper in Solution (M)	Copper Sorbed (mol/g)
$5.87x10^{-04}$	$5.48x10^{-04}$	$3.84x10^{-07}$
$2.93x10^{-04}$	$2.74x10^{-04}$	$1.91x10^{-07}$
$1.17x10^{-04}$	$1.12x10^{-04}$	$5.59x10^{-08}$
$5.87x10^{-05}$	$5.66x10^{-05}$	$2.07x10^{-08}$
$2.93x10^{-05}$	$2.85x10^{-05}$	$8.09x10^{-09}$
$5.87x10^{-06}$	$5.71x10^{-06}$	$1.52x10^{-09}$

Table C.11. Data for adsorption edge at Cu_T = 15 μM onto MC2.

pH	Copper in Solution (M)	Copper Sorbed (mol/g)
4.64	$1.20x10^{-05}$	$2.78x10^{-08}$
6.05	$1.69x10^{-06}$	$1.31x10^{-07}$
6.16	$2.65x10^{-06}$	$1.21x10^{-07}$
6.22	$1.37x10^{-06}$	$1.34x10^{-07}$
6.72	$1.37x10^{-06}$	$1.34x10^{-07}$
7.00	$2.98x10^{-07}$	$1.45x10^{-07}$

Table C.12. Data for adsorption edge at Cu_T = 27 μM with Ox_T = 1 mM onto MC2.

pH	Copper in Solution (M)	Copper Sorbed (mol/g)
3.40	$2.42x10^{-05}$	$2.46x10^{-08}$
3.66	$2.25x10^{-05}$	$4.11x10^{-08}$
3.79	$2.25x10^{-05}$	$4.11x10^{-08}$
4.29	$2.32x10^{-05}$	$3.45x10^{-08}$
5.62	$2.38x10^{-05}$	$2.79x10^{-08}$
6.22	$2.38x10^{-05}$	$2.80x10^{-08}$
6.93	$2.16x10^{-05}$	$5.03x10^{-08}$
7.78	$1.01x10^{-05}$	$1.66x10^{-07}$
8.41	$1.90x10^{-06}$	$2.47x10^{-07}$

MC3

Table C.13. Data for oxalate adsorption isotherm at pH 7 onto MC3.

Ox_T (M)	Oxalate in Solution (M)	Oxalate Sorbed (mol/g)
$1.00x10^{-03}$	$8.43x10^{-04}$	$1.57x10^{-06}$
$1.00x10^{-03}$	$8.09x10^{-04}$	$1.91x10^{-06}$
$5.00x10^{-04}$	$3.83x10^{-04}$	$1.17x10^{-06}$
$5.00x10^{-04}$	$3.60x10^{-04}$	$1.40x10^{-06}$
$1.00x10^{-04}$	$4.46x10^{-05}$	$5.54x10^{-07}$
$1.00x10^{-04}$	$6.56x10^{-05}$	$3.44x10^{-07}$
$5.00x10^{-05}$	$4.11x10^{-05}$	$8.90x10^{-08}$
$5.00x10^{-05}$	$3.40x10^{-05}$	$1.60x10^{-07}$
$1.00x10^{-05}$	$7.11x10^{-06}$	$2.89x10^{-08}$
$1.00x10^{-05}$	$7.21x10^{-06}$	$2.79x10^{-08}$
$1.00x10^{-06}$	$7.60x10^{-07}$	$2.40x10^{-09}$
$1.00x10^{-06}$	$6.18x10^{-07}$	$3.82x10^{-09}$

Table C.14. Data for adsorption edge at Ox_T = 50 μM onto MC3.

pH	Oxalate in Solution (M)	Oxalate Sorbed (mol/g)
5.28	$2.74x10^{-05}$	$2.26x10^{-07}$
5.76	$2.10x10^{-05}$	$2.90x10^{-07}$
8.25	$3.43x10^{-05}$	$1.57x10^{-07}$
9.08	$3.50x10^{-05}$	$1.50x10^{-07}$
9.81	$3.70x10^{-05}$	$1.30x10^{-07}$
10.33	$3.96x10^{-05}$	$1.04x10^{-07}$
10.61	$3.95x10^{-05}$	$1.05x10^{-07}$
10.87	$3.98x10^{-05}$	$1.02x10^{-07}$
11.08	$3.72x10^{-05}$	$1.28x10^{-07}$
11.14	$3.54x10^{-05}$	$1.46x10^{-07}$
11.22	$3.81x10^{-05}$	$1.19x10^{-07}$

Table C.15. Data for adsorption edge at Ox_T = 10 μM onto MC3.

pH	Oxalate in Solution (M)	Oxalate Sorbed (mol/g)
5.91	$5.56x10^{-06}$	$4.44x10^{-08}$
7.37	$3.12x10^{-06}$	$6.88x10^{-08}$
7.74	$4.23x10^{-06}$	$5.77x10^{-08}$
8.00	$3.69x10^{-06}$	$6.31x10^{-08}$
9.17	$4.33x10^{-06}$	$5.67x10^{-08}$
9.22	$5.28x10^{-06}$	$4.72x10^{-08}$
9.64	$8.48x10^{-06}$	$1.52x10^{-08}$
9.66	$4.52x10^{-06}$	$5.48x10^{-08}$
10.05	$4.16x10^{-06}$	$5.84x10^{-08}$
10.08	$6.31x10^{-06}$	$3.69x10^{-08}$
10.25	$3.86x10^{-06}$	$6.14x10^{-08}$
10.48	$4.47x10^{-06}$	$5.53x10^{-08}$

Table C.16. Data for copper adsorption isotherm at pH 7 with Ox_T = 1 mM.

Cu_T (M)	Copper in Solution (M)	Copper Sorbed (mol/g)
$5.87x10^{-04}$	$5.76x10^{-04}$	$1.10x10^{-07}$
$5.87x10^{-04}$	$5.76x10^{-04}$	$1.10x10^{-07}$
$2.93x10^{-04}$	$2.83x10^{-04}$	$9.92x10^{-08}$
$2.93x10^{-04}$	$2.79x10^{-04}$	$1.45x10^{-07}$
$1.17x10^{-04}$	$1.09x10^{-04}$	$8.60x10^{-08}$
$1.17x10^{-04}$	$1.09x10^{-04}$	$8.10x10^{-08}$
$5.87x10^{-05}$	$5.66x10^{-05}$	$2.07x10^{-08}$
$5.87x10^{-05}$	$5.71x10^{-05}$	$1.57x10^{-08}$
$2.93x10^{-05}$	$2.80x10^{-05}$	$1.31x10^{-08}$
$2.93x10^{-05}$	$2.85x10^{-05}$	$8.09x10^{-09}$
$5.87x10^{-06}$	$5.71x10^{-06}$	$1.52x10^{-09}$
$5.87x10^{-06}$	$5.71x10^{-06}$	$1.52x10^{-09}$

Table C.17. Data for adsorption edge at Cu_T = 15 μM onto MC3.

pH	Copper in Solution (M)	Copper Sorbed (mol/g)
4.49	$1.16x10^{-05}$	$3.18x10^{-08}$
4.99	$9.73x10^{-06}$	$5.05x10^{-08}$
5.19	$9.41x10^{-06}$	$5.37x10^{-08}$
5.60	$7.48x10^{-06}$	$7.30x10^{-08}$
6.01	$6.51x10^{-06}$	$8.27x10^{-08}$
7.51	$1.23x10^{-06}$	$1.36x10^{-07}$

Table C.18. Data for adsorption edge at Cu_T = 27 μM with Ox_T = 1 mM onto MC3.

pH	Copper in Solution (M)	Copper Sorbed (mol/g)
3.02	$2.48x10^{-05}$	$1.80x10^{-08}$
3.22	$2.48x10^{-05}$	$1.80x10^{-08}$
3.40	$2.32x10^{-05}$	$3.45x10^{-08}$
3.52	$2.38x10^{-05}$	$2.79x10^{-08}$
3.63	$2.35x10^{-05}$	$3.12x10^{-08}$
3.99	$2.35x10^{-05}$	$3.12x10^{-08}$
4.12	$2.29x10^{-05}$	$3.78x10^{-08}$
4.36	$2.42x10^{-05}$	$2.46x10^{-08}$
5.07	$2.49x10^{-05}$	$1.68x10^{-08}$
5.86	$2.25x10^{-05}$	$4.11x10^{-08}$
7.17	$2.46x10^{-05}$	$2.06x10^{-08}$
7.20	$2.35x10^{-05}$	$3.12x10^{-08}$
8.99	$6.98x10^{-06}$	$1.97x10^{-07}$
9.36	$1.53x10^{-06}$	$2.51x10^{-07}$
10.04	$7.90x10^{-07}$	$2.58x10^{-07}$

APPENDIX D

DATA FOR ADSORPTION ONTO UNWEATHERED MILFORD UNCOATED SAMPLE

Table D.1. Data for oxalate adsorption isotherm onto MU at pH 7

Ox_T (M)	Oxalate in Solution (M)	Oxalate Sorbed (mol/g)
$1.00x10^{-03}$	$9.11x10^{-04}$	$8.90x10^{-07}$
$1.00x10^{-03}$	$8.85x10^{-04}$	$1.15x10^{-06}$
$5.00x10^{-04}$	$3.49x10^{-04}$	$1.51x10^{-06}$
$5.00x10^{-04}$	$3.33x10^{-04}$	$1.67x10^{-06}$
$1.00x10^{-04}$	$5.52x10^{-05}$	$4.48x10^{-07}$
$1.00x10^{-04}$	$5.49x10^{-05}$	$4.52x10^{-07}$
$5.00x10^{-05}$	$2.08x10^{-05}$	$2.92x10^{-07}$
$5.00x10^{-05}$	$2.10x10^{-05}$	$2.90x10^{-07}$
$1.00x10^{-05}$	$1.81x10^{-06}$	$8.19x10^{-08}$
$1.00x10^{-05}$	$1.96x10^{-06}$	$8.04x10^{-08}$
$1.00x10^{-06}$	$2.49x10^{-07}$	$7.51x10^{-09}$
$1.00x10^{-06}$	$1.88x10^{-07}$	$8.12x10^{-09}$

Table D.2. Data for adsorption edge onto MU for Ox_T = 100 μM

pH	Oxalate in Solution (M)	Oxalate Sorbed (mol/g)
4.49	$5.56x10^{-05}$	$4.44x10^{-07}$
4.71	$6.69x10^{-05}$	$3.31x10^{-07}$
5.02	$6.61x10^{-05}$	$3.39x10^{-07}$
5.23	$5.70x10^{-05}$	$4.30x10^{-07}$
5.51	$4.12x10^{-05}$	$5.88x10^{-07}$
5.91	$3.96x10^{-05}$	$6.04x10^{-07}$
5.95	$4.46x10^{-05}$	$5.54x10^{-07}$
5.96	$4.82x10^{-05}$	$5.18x10^{-07}$
6.13	$4.88x10^{-05}$	$5.12x10^{-07}$
6.41	$4.93x10^{-05}$	$5.07x10^{-07}$
6.43	$5.16x10^{-05}$	$4.84x10^{-07}$
6.53	$3.69x10^{-05}$	$6.31x10^{-07}$
6.73	$5.89x10^{-05}$	$4.11x10^{-07}$
7.11	$6.18x10^{-05}$	$3.82x10^{-07}$
7.45	$6.95x10^{-05}$	$3.05x10^{-07}$
7.53	$6.64x10^{-05}$	$3.36x10^{-07}$
8.27	$7.02x10^{-05}$	$2.98x10^{-07}$
8.42	$8.78x10^{-05}$	$1.22x10^{-07}$
8.91	$8.48x10^{-05}$	$1.52x10^{-07}$
9.03	$9.35x10^{-05}$	$6.47x10^{-08}$
9.55	$9.83x10^{-05}$	$1.71x10^{-08}$
9.70	$9.75x10^{-05}$	$2.53x10^{-08}$
9.94	$9.2x10^{-05}$	$7.44x10^{-08}$
10.04	$8.60x10^{-05}$	$1.40x10^{-07}$
10.19	$9.78x10^{-05}$	$2.21x10^{-08}$
10.37	$9.75x10^{-05}$	$2.45x10^{-08}$

Table D.3. Data for adsorption edge onto MU for Ox_T = 50 μM

pH	Oxalate in Solution (M)	Oxalate Sorbed (mol/g)
3.77	$2.58x10^{-05}$	$2.42x10^{-07}$
4.08	$2.56x10^{-05}$	$2.44x10^{-07}$
4.51	$2.39x10^{-05}$	$2.61x10^{-07}$
4.89	$2.24x10^{-05}$	$2.76x10^{-07}$
5.11	$2.44x10^{-05}$	$2.56x10^{-07}$
5.25	$2.15x10^{-05}$	$2.85x10^{-07}$
5.47	$1.81x10^{-05}$	$3.19x10^{-07}$
5.48	$2.05x10^{-05}$	$2.95x10^{-07}$
5.73	$2.17x10^{-05}$	$2.83x10^{-07}$
5.93	$1.71x10^{-05}$	$3.29x10^{-07}$
6.15	$1.77x10^{-05}$	$3.23x10^{-07}$
6.59	$1.93x10^{-05}$	$3.07x10^{-07}$
6.72	$1.83x10^{-05}$	$3.17x10^{-07}$
6.99	$1.70x10^{-05}$	$3.30x10^{-07}$
7.02	$2.46x10^{-05}$	$2.54x10^{-07}$
7.05	$2.61x10^{-05}$	$2.39x10^{-07}$
7.20	$3.08x10^{-05}$	$1.92x10^{-07}$
8.09	$3.43x10^{-05}$	$1.57x10^{-07}$
8.15	$3.54x10^{-05}$	$1.46x10^{-07}$
8.17	$3.83x10^{-05}$	$1.17x10^{-07}$
8.57	$3.26x10^{-05}$	$1.74x10^{-07}$
8.84	$3.94x10^{-05}$	$1.06x10^{-07}$
9.30	$3.48x10^{-05}$	$1.52x10^{-07}$
9.52	$3.88x10^{-05}$	$1.12x10^{-07}$
9.60	$4.45x10^{-05}$	$5.50x10^{-08}$
10.38	$4.69x10^{-05}$	$3.11x10^{-08}$
10.62	$4.86x10^{-05}$	$1.35x10^{-08}$

Table D.4. Data for adsorption edge onto MU for Ox_T = 10 μM

pH	Oxalate in Solution (M)	Oxalate Sorbed (mol/g)
4.14	$5.88x10^{-06}$	$4.12x10^{-08}$
4.32	$4.55x10^{-06}$	$5.45x10^{-08}$
4.61	$3.59x10^{-06}$	$6.41x10^{-08}$
4.75	$3.94x10^{-06}$	$6.06x10^{-08}$
4.83	$3.58x10^{-06}$	$6.42x10^{-08}$
5.09	$3.13x10^{-06}$	$6.87x10^{-08}$
5.14	$3.03x10^{-06}$	$6.97x10^{-08}$
5.42	$1.98x10^{-06}$	$8.02x10^{-08}$
5.71	$1.70x10^{-06}$	$8.30x10^{-08}$
6.16	$1.06x10^{-06}$	$8.94x10^{-08}$
7.21	$2.29x10^{-06}$	$7.71x10^{-08}$
7.40	$2.79x10^{-06}$	$7.21x10^{-08}$
7.45	$2.40x10^{-06}$	$7.60x10^{-08}$
7.55	$3.18x10^{-06}$	$6.82x10^{-08}$
7.72	$3.92x10^{-06}$	$6.08x10^{-08}$
7.85	$4.29x10^{-06}$	$5.71x10^{-08}$
7.86	$4.39x10^{-06}$	$5.61x10^{-08}$
7.88	$3.76x10^{-06}$	$6.24x10^{-08}$
7.89	$4.30x10^{-06}$	$5.70x10^{-08}$
7.93	$2.61x10^{-06}$	$7.39x10^{-08}$
7.99	$4.51x10^{-06}$	$5.49x10^{-08}$
8.13	$4.70x10^{-06}$	$5.30x10^{-08}$
8.23	$3.91x10^{-06}$	$6.09x10^{-08}$
8.55	$4.46x10^{-06}$	$5.54x10^{-08}$
8.82	$5.85x10^{-06}$	$4.15x10^{-08}$
9.11	$8.40x10^{-06}$	$1.60x10^{-08}$
9.17	$9.60x10^{-06}$	$4.04x10^{-09}$

Table D.4 (Continued). Data for adsorption edge onto MU for Ox_T = 10 μM

pH	Oxalate in Solution (M)	Oxalate Sorbed (mol/g)
9.78	$9.99x10^{-06}$	$6.96x10^{-11}$
9.99	$9.74x10^{-06}$	$2.59x10^{-09}$
10.25	$9.10x10^{-06}$	$9.04x10^{-09}$
10.34	$9.97x10^{-06}$	$3.19x10^{-10}$

Table D.5. Data for adsorption edge onto MU for Cu_T = 15 μM

pH	Copper in Solution (M)	Copper Sorbed (mol/g)
4.59	$9.52x10^{-06}$	$3.62x10^{-08}$
4.89	$8.74x10^{-06}$	$4.40x10^{-08}$
5.07	$8.35x10^{-06}$	$4.79x10^{-08}$
5.10	$7.95x10^{-06}$	$5.19x10^{-08}$
5.20	$6.00x10^{-06}$	$7.14x10^{-08}$
5.53	$6.00x10^{-06}$	$7.14x10^{-08}$
5.72	$2.87x10^{-06}$	$1.03x10^{-07}$
5.90	$1.70x10^{-06}$	$1.14x10^{-07}$
5.98	$1.70x10^{-06}$	$1.14x10^{-07}$
6.62	$5.24x10^{-07}$	$1.26x10^{-07}$

Table D.6. Data for adsorption edge onto MU for Cu_T = 5.7 μM

pH	Copper in Solution (M)	Copper Sorbed (mol/g)
4.54	$5.52x10^{-06}$	$1.65x10^{-09}$
4.66	$4.83x10^{-06}$	$8.59x10^{-09}$
4.69	$5.29x10^{-06}$	$3.96x10^{-09}$
4.83	$4.83x10^{-06}$	$8.59x10^{-09}$
4.90	$4.37x10^{-06}$	$1.32x10^{-08}$
4.96	$3.91x10^{-06}$	$1.78x10^{-08}$
5.19	$2.98x10^{-06}$	$2.71x10^{-08}$
5.52	$2.52x10^{-06}$	$3.17x10^{-08}$
5.83	$4.28x10^{-07}$	$5.26x10^{-08}$
6.12	$2.20x10^{-07}$	$5.47x10^{-08}$
6.55	$6.71x10^{-08}$	$5.62x10^{-08}$
6.60	$5.81x10^{-08}$	$5.63x10^{-08}$

Table D.7. Data for adsorption edge onto MU for Cu_T = 27 μM with Ox_T = 1 mM

pH	Copper in Solution (M)	Copper Sorbed (mol/g)
5.67	$2.63x10^{-05}$	$2.88x10^{-09}$
6.82	$2.34x10^{-05}$	$3.23x10^{-08}$
7.01	$2.21x10^{-05}$	$4.51x10^{-08}$
7.03	$2.00x10^{-05}$	$6.63x10^{-08}$
7.05	$2.04x10^{-05}$	$6.21x10^{-08}$
7.08	$2.34x10^{-05}$	$3.23x10^{-08}$
7.33	$2.31x10^{-05}$	$3.50x10^{-08}$
7.37	$1.53x10^{-05}$	$1.13x10^{-07}$
7.43	$1.54x10^{-05}$	$1.12x10^{-07}$
7.73	$8.98x10^{-06}$	$1.77x10^{-07}$
8.16	$4.70x10^{-06}$	$2.19x10^{-07}$
8.63	$2.57x10^{-06}$	$2.41x10^{-07}$
9.56	$6.16x10^{-07}$	$2.60x10^{-07}$
9.34	$2.55x10^{-06}$	$2.41x10^{-07}$

Table D.8. Data for adsorption edge onto MU for Cu_T = 121 μM with Ox_T = 1 mM

pH	Copper in Solution (M)	Copper Sorbed (mol/g)
6.67	$1.18x10^{-04}$	$2.92x10^{-08}$
6.81	$1.13x10^{-04}$	$7.96x10^{-08}$
6.95	$1.14x10^{-04}$	$6.52x10^{-08}$
7.09	$1.12x10^{-04}$	$8.68x10^{-08}$
7.48	$8.89x10^{-05}$	$3.17x10^{-07}$
7.42	$1.11x10^{-04}$	$9.40x10^{-08}$
7.77	$6.66x10^{-05}$	$5.41x10^{-07}$
8.06	$5.43x10^{-05}$	$6.63x10^{-07}$
8.45	$1.91x10^{-05}$	$1.02x10^{-06}$
8.28	$3.20x10^{-05}$	$8.86x10^{-07}$
9.04	$7.53x10^{-06}$	$1.13x10^{-06}$
9.36	$1.77x10^{-06}$	$1.19x10^{-06}$

Table D.9. Data for adsorption edge onto MU for Cu_T = 38 μM with Ox_T = 100 μM

pH	Copper in Solution (M)	Copper Sorbed (mol/g)
4.61	$3.79x10^{-05}$	$3.50x10^{-09}$
4.90	$3.79x10^{-05}$	$3.50x10^{-09}$
5.18	$3.70x10^{-05}$	$1.25x10^{-08}$
5.49	$3.52x10^{-05}$	$3.06x10^{-08}$
5.84	$3.43x10^{-05}$	$3.96x10^{-08}$
6.46	$2.44x10^{-05}$	$1.39x10^{-07}$
6.73	$1.71x10^{-05}$	$2.11x10^{-07}$
7.14	$9.00x10^{-06}$	$2.93x10^{-07}$
7.45	$6.29x10^{-06}$	$3.20x10^{-07}$
7.71	$1.77x10^{-06}$	$3.65x10^{-07}$
8.49	$8.65x10^{-07}$	$3.74x10^{-07}$
8.82	$8.65x10^{-07}$	$3.74x10^{-07}$

Table D.10. Data for adsorption edge onto MU for Cu_T = 8.3 μM with Ox_T = 100 μM

pH	Copper in Solution (M)	Copper Sorbed (mol/g)
4.79	$7.45x10^{-06}$	$8.05x10^{-09}$
5.07	$7.45x10^{-06}$	$8.05x10^{-09}$
5.52	$7.11x10^{-06}$	$1.14x10^{-08}$
5.59	$6.10x10^{-06}$	$2.16x10^{-08}$
6.45	$4.74x10^{-06}$	$3.52x10^{-08}$
6.60	$3.72x10^{-06}$	$4.53x10^{-08}$
6.97	$3.39x10^{-06}$	$4.87x10^{-08}$
7.37	$6.73x10^{-07}$	$7.59x10^{-08}$
7.87	$1.64x10^{-07}$	$8.09x10^{-08}$

Table D.11. Data for adsorption edge onto MU for Ox_T = 100 μM with Cu_T = 38 μM.

pH	Oxalate in Solution (M)	Oxalate Sorbed (mol/g)
3.41	$7.59x10^{-05}$	$2.41x10^{-07}$
3.90	$7.80x10^{-05}$	$2.20x10^{-07}$
4.19	$7.69x10^{-05}$	$2.31x10^{-07}$
4.38	$7.53x10^{-05}$	$2.47x10^{-07}$
4.95	$6.48x10^{-05}$	$3.52x10^{-07}$
5.02	$7.34x10^{-05}$	$2.66x10^{-07}$
5.21	$6.21x10^{-05}$	$3.79x10^{-07}$
5.28	$6.85x10^{-05}$	$3.15x10^{-07}$
5.72	$6.66x10^{-05}$	$3.34x10^{-07}$
5.73	$4.90x10^{-05}$	$5.10x10^{-07}$
6.09	$5.87x10^{-05}$	$4.13x10^{-07}$
6.48	$6.26x10^{-05}$	$3.74x10^{-07}$
6.55	$6.41x10^{-05}$	$3.59x10^{-07}$
6.77	$7.54x10^{-05}$	$2.46x10^{-07}$
6.77	$6.29x10^{-05}$	$3.71x10^{-07}$
6.98	$5.87x10^{-05}$	$4.13x10^{-07}$
7.29	$6.98x10^{-05}$	$3.02x10^{-07}$
7.63	$7.29x10^{-05}$	$2.72x10^{-07}$
7.78	$7.05x10^{-05}$	$2.95x10^{-07}$
7.79	$7.13x10^{-05}$	$2.87x10^{-07}$
8.02	$7.22x10^{-05}$	$2.78x10^{-07}$
8.60	$8.35x10^{-05}$	$1.65x10^{-07}$
8.83	$8.77x10^{-05}$	$1.23x10^{-07}$
9.41	$8.92x10^{-05}$	$1.08x10^{-07}$

Table D.12. Data for adsorption edge onto MU for Ox_T = 100 μM with Cu_T = 8.3 μM.

pH	Oxalate in Solution (M)	Oxalate Sorbed (mol/g)
3.40	$7.46x10^{-05}$	$2.54x10^{-07}$
4.12	$6.20x10^{-05}$	$3.80x10^{-07}$
4.29	$7.07x10^{-05}$	$2.93x10^{-07}$
4.61	$6.80x10^{-05}$	$3.20x10^{-07}$
5.12	$6.48x10^{-05}$	$3.52x10^{-07}$
5.17	$6.13x10^{-05}$	$3.87x10^{-07}$
5.58	$6.03x10^{-05}$	$3.97x10^{-07}$
5.79	$5.19x10^{-05}$	$4.81x10^{-07}$
6.07	$5.87x10^{-05}$	$4.13x10^{-07}$
6.37	$5.25x10^{-05}$	$4.75x10^{-07}$
6.59	$5.49x10^{-05}$	$4.51x10^{-07}$
7.04	$7.21x10^{-05}$	$2.79x10^{-07}$
7.20	$7.66x10^{-05}$	$2.34x10^{-07}$
7.31	$7.44x10^{-05}$	$2.56x10^{-07}$
7.36	$7.02x10^{-05}$	$2.98x10^{-07}$
7.47	$7.54x10^{-05}$	$2.46x10^{-07}$
8.33	$8.91x10^{-05}$	$1.09x10^{-07}$
8.45	$8.97x10^{-05}$	$1.03x10^{-07}$
8.53	$9.39x10^{-05}$	$6.12x10^{-08}$
9.18	$9.43x10^{-05}$	$5.70x10^{-08}$
9.40	$9.45x10^{-05}$	$5.50x10^{-08}$
9.67	$9.24x10^{-05}$	$7.59x10^{-08}$
10.30	$9.97x10^{-05}$	$2.72x10^{-09}$

APPENDIX E

DATA FOR ADSORPTION ONTO WEATHERED MILFORD UNCOATED SAMPLE

MU1

Table E.1. Data for adsorption isotherm onto MU1 at pH 7

Ox_T (M)	Oxalate in Solution (M)	Oxalate Sorbed (mol/g)
$1.00x10^{-03}$	$9.01x10^{-04}$	$9.89x10^{-07}$
$1.00x10^{-03}$	$9.13x10^{-04}$	$8.74x10^{-07}$
$5.00x10^{-04}$	$3.53x10^{-04}$	$1.47x10^{-06}$
$5.00x10^{-04}$	$3.72x10^{-04}$	$1.28x10^{-06}$
$1.00x10^{-04}$	$6.66x10^{-05}$	$3.34x10^{-07}$
$1.00x10^{-04}$	$6.63x10^{-05}$	$3.37x10^{-07}$
$5.00x10^{-05}$	$2.85x10^{-05}$	$2.15x10^{-07}$
$5.00x10^{-05}$	$3.16x10^{-05}$	$1.84x10^{-07}$
$1.00x10^{-05}$	$1.94x10^{-06}$	$8.06x10^{-08}$
$1.00x10^{-05}$	$1.98x10^{-06}$	$8.02x10^{-08}$
$1.00x10^{-06}$	$1.80x10^{-07}$	$8.20x10^{-09}$
$1.00x10^{-06}$	$1.62x10^{-07}$	$8.38x10^{-09}$

Table E.2. Data for oxalate adsorption edge onto MU1 Ox_T = 10 μM

pH	Oxalate in Solution (M)	Oxalate Sorbed (mol/g)
3.91	$3.99x10^{-06}$	$6.01x10^{-08}$
3.96	$2.95x10^{-06}$	$7.05x10^{-08}$
4.13	$3.63x10^{-06}$	$6.38x10^{-08}$
4.18	$4.45x10^{-06}$	$5.55x10^{-08}$
4.32	$2.96x10^{-06}$	$7.04x10^{-08}$
4.46	$3.30x10^{-06}$	$6.70x10^{-08}$
4.64	$3.05x10^{-06}$	$6.95x10^{-08}$
4.72	$4.09x10^{-06}$	$5.91x10^{-08}$
4.80	$2.77x10^{-06}$	$7.23x10^{-08}$
5.23	$2.76x10^{-06}$	$7.24x10^{-08}$
5.55	$1.85x10^{-06}$	$8.15x10^{-08}$
5.98	$2.01x10^{-06}$	$8.00x10^{-08}$
5.99	$2.25x10^{-06}$	$7.75x10^{-08}$
6.42	$1.09x10^{-06}$	$8.91x10^{-08}$
6.71	$2.44x10^{-06}$	$7.56x10^{-08}$
6.90	$9.95x10^{-07}$	$9.01x10^{-08}$
6.96	$4.33x10^{-06}$	$5.67x10^{-08}$
7.12	$2.34x10^{-06}$	$7.66x10^{-08}$
7.38	$3.10x10^{-06}$	$6.91x10^{-08}$
7.79	$3.16x10^{-06}$	$6.84x10^{-08}$
8.20	$5.27x10^{-06}$	$4.73x10^{-08}$
8.45	$5.44x10^{-06}$	$4.56x10^{-08}$
8.67	$4.79x10^{-06}$	$5.21x10^{-08}$
8.80	$8.61x10^{-06}$	$1.39x10^{-08}$
8.88	$6.31x10^{-06}$	$3.69x10^{-08}$

Table E.2 (Continued). Data for oxalate adsorption edge onto MU1 Ox_T = 10 μM

pH	Oxalate in Solution (M)	Oxalate Sorbed (mol/g)
8.92	$4.96x10^{-06}$	$5.04x10^{-08}$
9.95	$9.41x10^{-06}$	$5.86x10^{-09}$
10.22	$9.79x10^{-06}$	$2.14x10^{-09}$
10.48	$8.93x10^{-06}$	$1.07x10^{-08}$
10.55	$8.71x10^{-06}$	$1.29x10^{-08}$
10.64	$9.60x10^{-06}$	$3.99x10^{-09}$
10.75	$9.96x10^{-06}$	$3.56x10^{-10}$

Table E.3. Data for Cu adsorption edge onto MU1; Cu_T = 15 μM

pH	Copper in Solution (M)	Copper Sorbed (mol/g)
4.40	$1.26x10^{-05}$	$4.93x10^{-09}$
4.47	$1.23x10^{-05}$	$8.84x10^{-09}$
4.79	$1.03x10^{-05}$	$2.84x10^{-08}$
4.82	$9.91x10^{-06}$	$3.23x10^{-08}$
4.93	$8.35x10^{-06}$	$4.79x10^{-08}$
5.05	$8.74x10^{-06}$	$4.40x10^{-08}$
5.14	$7.17x10^{-06}$	$5.97x10^{-08}$
5.48	$6.78x10^{-06}$	$6.36x10^{-08}$
5.78	$4.04x10^{-06}$	$9.10x10^{-08}$
5.84	$4.43x10^{-06}$	$8.70x10^{-08}$
6.54	$3.28x10^{-07}$	$1.28x10^{-07}$
6.85	$5.24x10^{-07}$	$1.26x10^{-07}$

Table E.4. Data for adsorption edge onto MU1 for Cu_T = 27 μM with Ox_T = 1 mM.

pH	Copper in Solution (M)	Copper Sorbed (mol/g)
4.99	$2.63x10^{-05}$	$8.90x10^{-09}$
6.68	$2.47x10^{-05}$	$2.56x10^{-08}$
6.88	$2.51x10^{-05}$	$2.13x10^{-08}$
6.93	$2.51x10^{-05}$	$2.13x10^{-08}$
7.00	$2.34x10^{-05}$	$3.83x10^{-08}$
7.12	$2.38x10^{-05}$	$3.46x10^{-08}$
7.19	$2.04x10^{-05}$	$6.80x10^{-08}$
7.51	$1.83x10^{-05}$	$8.93x10^{-08}$
8.03	$1.54x10^{-05}$	$1.18x10^{-07}$
8.48	$4.70x10^{-06}$	$2.25x10^{-07}$
8.82	$4.47x10^{-06}$	$2.27x10^{-07}$
9.37	$8.72x10^{-07}$	$2.63x10^{-07}$
9.62	$6.15x10^{-07}$	$2.66x10^{-07}$
10.06	$6.15x10^{-07}$	$2.66x10^{-07}$

MU2

Table E.5. Data for adsorption isotherm onto MU2 at pH 7

Ox_T (M)	Oxalate in Solution (M)	Oxalate Sorbed (mol/g)
$1.00x10^{-03}$	$9.16x10^{-04}$	$8.38x10^{-07}$
$1.00x10^{-03}$	$9.45x10^{-04}$	$5.47x10^{-07}$
$5.00x10^{-04}$	$3.56x10^{-04}$	$1.44x10^{-06}$
$5.00x10^{-04}$	$3.88x10^{-04}$	$1.12x10^{-06}$
$1.00x10^{-04}$	$6.56x10^{-05}$	$3.44x10^{-07}$
$1.00x10^{-04}$	$6.08x10^{-05}$	$3.92x10^{-07}$
$5.00x10^{-05}$	$2.80x10^{-05}$	$2.20x10^{-07}$
$5.00x10^{-05}$	$2.31x10^{-05}$	$2.69x10^{-07}$
$1.00x10^{-05}$	$2.04x10^{-06}$	$7.96x10^{-08}$
$1.00x10^{-05}$	$2.35x10^{-06}$	$7.65x10^{-08}$
$1.00x10^{-06}$	$2.47x10^{-07}$	$7.53x10^{-09}$
$1.00x10^{-06}$	$1.71x10^{-07}$	$8.29x10^{-09}$

Table E.6. Data for adsorption edge onto MU2 for Ox_T = 10 μM.

pH	Oxalate in Solution (M)	Oxalate Sorbed (mol/g)
3.89	$3.18x10^{-06}$	$6.82x10^{-08}$
3.90	$4.73x10^{-06}$	$5.27x10^{-08}$
4.00	$3.12x10^{-06}$	$6.88x10^{-08}$
4.00	$3.68x10^{-06}$	$6.32x10^{-08}$
4.27	$4.61x10^{-06}$	$5.39x10^{-08}$
4.28	$3.83x10^{-06}$	$6.17x10^{-08}$
4.66	$2.81x10^{-06}$	$7.19x10^{-08}$
4.98	$4.00x10^{-06}$	$6.00x10^{-08}$
5.06	$2.58x10^{-06}$	$7.42x10^{-08}$
5.10	$2.55x10^{-06}$	$7.45x10^{-08}$
5.29	$1.16x10^{-06}$	$8.84x10^{-08}$
5.34	$2.14x10^{-06}$	$7.86x10^{-08}$
6.04	$2.92x10^{-06}$	$7.08x10^{-08}$
6.09	$1.62x10^{-06}$	$8.38x10^{-08}$
6.55	$2.53x10^{-06}$	$7.47x10^{-08}$
6.99	$2.09x10^{-06}$	$7.91x10^{-08}$
7.01	$1.77x10^{-06}$	$8.23x10^{-08}$
7.05	$4.49x10^{-06}$	$5.51x10^{-08}$
7.22	$2.95x10^{-06}$	$7.05x10^{-08}$
7.39	$6.54x10^{-06}$	$3.46x10^{-08}$
7.93	$3.82x10^{-06}$	$6.19x10^{-08}$
8.21	$5.74x10^{-06}$	$4.26x10^{-08}$
9.07	$7.25x10^{-06}$	$2.75x10^{-08}$
9.07	$8.84x10^{-06}$	$1.16x10^{-08}$
9.09	$7.03x10^{-06}$	$2.97x10^{-08}$

Table E.6 (Continued). Data for adsorption edge onto MU2 for Ox_T = 10 μM.

pH	Oxalate in Solution (M)	Oxalate Sorbed (mol/g)
9.29	$7.80x10^{-06}$	$2.20x10^{-08}$
10.00	$8.44x10^{-06}$	$1.56x10^{-08}$
10.11	$8.58x10^{-06}$	$1.42x10^{-08}$
10.46	$8.91x10^{-06}$	$1.09x10^{-08}$
10.49	$9.59x10^{-06}$	$4.07x10^{-09}$
10.75	$9.35x10^{-06}$	$6.50x10^{-09}$
10.80	$9.78x10^{-06}$	$2.17x10^{-09}$

Table E.7. Data for adsorption edge onto MU2 for Cu_T = 15 μM.

pH	Copper in Solution (M)	Copper Sorbed (mol/g)
4.35	$1.30x10^{-05}$	$1.02x10^{-09}$
4.51	$1.23x10^{-05}$	$8.84x10^{-09}$
4.59	$1.15x10^{-05}$	$1.67x10^{-08}$
4.65	$1.15x10^{-05}$	$1.67x10^{-08}$
4.76	$1.19x10^{-05}$	$1.27x10^{-08}$
4.92	$1.03x10^{-05}$	$2.84x10^{-08}$
5.14	$9.91x10^{-06}$	$3.23x10^{-08}$
5.33	$9.13x10^{-06}$	$4.01x10^{-08}$
5.60	$8.35x10^{-06}$	$4.79x10^{-08}$
6.02	$4.04x10^{-06}$	$9.10x10^{-08}$
6.72	$1.31x10^{-06}$	$1.18x10^{-07}$
6.93	$1.31x10^{-06}$	$1.18x10^{-07}$

Table E.8. Data for adsorption edge onto MU2 for Cu_T = 27 μM. and Ox_T = 1 mM..

pH	Copper in Solution (M)	Copper Sorbed (mol/g)
4.88	$2.70x10^{-05}$	$2.47x10^{-09}$
7.22	$2.30x10^{-05}$	$4.26x10^{-08}$
7.20	$2.70x10^{-05}$	$2.47x10^{-09}$
7.24	$2.21x10^{-05}$	$5.10x10^{-08}$
7.38	$2.08x10^{-05}$	$6.38x10^{-08}$
7.60	$1.93x10^{-05}$	$7.96x10^{-08}$
7.87	$1.40x10^{-05}$	$1.32x10^{-07}$
8.07	$1.19x10^{-05}$	$1.53x10^{-07}$
8.77	$1.30x10^{-06}$	$2.59x10^{-07}$
9.04	$1.90x10^{-06}$	$2.53x10^{-07}$
9.85	$6.15x10^{-07}$	$2.66x10^{-07}$
10.01	$6.15x10^{-07}$	$2.66x10^{-07}$

MU3

Table E.9. Data for adsorption isotherm onto MU3 at pH 7

Ox_T (M)	Oxalate in Solution (M)	Oxalate Sorbed (mol/g)
$1.00x10^{-03}$	$9.38x10^{-04}$	$6.16x10^{-07}$
$1.00x10^{-03}$	$9.41x10^{-04}$	$5.89x10^{-07}$
$5.00x10^{-04}$	$3.98x10^{-04}$	$1.02x10^{-06}$
$5.00x10^{-04}$	$4.61x10^{-04}$	$3.92x10^{-07}$
$1.00x10^{-04}$	$8.01x10^{-05}$	$1.99x10^{-07}$
$1.00x10^{-04}$	$8.10x10^{-05}$	$1.90x10^{-07}$
$5.00x10^{-05}$	$4.46x10^{-05}$	$5.39x10^{-08}$
$5.00x10^{-05}$	$3.97x10^{-05}$	$1.03x10^{-07}$
$1.00x10^{-05}$	$6.75x10^{-06}$	$3.25x10^{-08}$
$1.00x10^{-05}$	$7.26x10^{-06}$	$2.74x10^{-08}$
$1.00x10^{-06}$	$5.95x10^{-07}$	$4.05x10^{-09}$
$1.00x10^{-06}$	$6.71x10^{-07}$	$3.29x10^{-09}$

Table E.10. Data for adsorption edge onto MU3 for Ox_T = 10 μM.

pH	Oxalate in Solution (M)	Oxalate Sorbed (mol/g)
4.83	$6.95x10^{-06}$	$3.05x10^{-08}$
4.90	$7.34x10^{-06}$	$2.66x10^{-08}$
4.92	$7.02x10^{-06}$	$2.99x10^{-08}$
5.07	$5.24x10^{-06}$	$4.76x10^{-08}$
5.30	$6.78x10^{-06}$	$3.22x10^{-08}$
5.31	$6.73x10^{-06}$	$3.27x10^{-08}$
5.37	$5.19x10^{-06}$	$4.81x10^{-08}$
5.41	$5.85x10^{-06}$	$4.15x10^{-08}$
5.48	$6.51x10^{-06}$	$3.49x10^{-08}$
5.60	$6.91x10^{-06}$	$3.09x10^{-08}$
5.69	$6.33x10^{-06}$	$3.67x10^{-08}$
5.80	$7.04x10^{-06}$	$2.96x10^{-08}$
5.93	$5.52x10^{-06}$	$4.48x10^{-08}$
6.26	$7.22x10^{-06}$	$2.78x10^{-08}$
7.85	$9.25x10^{-06}$	$7.50x10^{-09}$
8.28	$8.41x10^{-06}$	$1.59x10^{-08}$
9.45	$9.66x10^{-06}$	$3.43x10^{-09}$
9.75	$9.48x10^{-06}$	$5.21x10^{-09}$
9.91	$8.80x10^{-06}$	$1.20x10^{-08}$
10.12	$9.40x10^{-06}$	$6.02x10^{-09}$
10.16	$9.71x10^{-06}$	$2.85x10^{-09}$
10.24	$9.94x10^{-06}$	$6.22x10^{-10}$
10.60	$9.55x10^{-06}$	$4.53x10^{-09}$
10.78	$9.85x10^{-06}$	$1.51x10^{-09}$
10.94	$9.99x10^{-06}$	$9.92x10^{-11}$

Table E.10 (Continued). Data for adsorption edge onto MU3 for Ox_T = 10 μM.

pH	Oxalate in Solution (M)	Oxalate Sorbed (mol/g)
11.02	$9.65x10^{-06}$	$3.46x10^{-09}$
11.07	$9.49x10^{-06}$	$5.07x10^{-09}$
11.07	$9.70x10^{-06}$	$2.95x10^{-09}$
11.10	$9.86x10^{-06}$	$1.36x10^{-09}$

Table E.11. Data for adsorption edge onto MU3 for Cu_T = 15 μM.

pH	Copper in Solution (M)	Copper Sorbed (mol/g)
6.18	$9.13x10^{-06}$	$4.01x10^{-08}$
6.81	$5.61x10^{-06}$	$7.53x10^{-08}$
7.75	$9.15x10^{-07}$	$1.22x10^{-07}$
7.75	$9.15x10^{-07}$	$1.22x10^{-07}$
7.77	$9.15x10^{-07}$	$1.22x10^{-07}$
8.04	$1.31x10^{-06}$	$1.18x10^{-07}$
8.27	$9.15x10^{-07}$	$1.22x10^{-07}$
8.67	$9.15x10^{-07}$	$1.22x10^{-07}$
9.31	$2.09x10^{-06}$	$1.11x10^{-07}$
9.72	$3.65x10^{-06}$	$9.49x10^{-08}$
9.85	$4.04x10^{-06}$	$9.10x10^{-08}$
10.02	$4.43x10^{-06}$	$8.70x10^{-08}$

Table E.12. Data for adsorption edge onto MU3 for Cu_T = 27 μM. and Ox_T = 1 mM.

pH	Copper in Solution (M)	Copper Sorbed (mol/g)
5.59	$2.70x10^{-05}$	$2.47x10^{-09}$
7.31	$2.21x10^{-05}$	$5.10x10^{-08}$
7.67	$2.31x10^{-05}$	$4.10x10^{-08}$
7.82	$1.96x10^{-05}$	$7.65x10^{-08}$
8.02	$1.83x10^{-05}$	$8.93x10^{-08}$
8.53	$1.11x10^{-05}$	$1.62x10^{-07}$
9.35	$4.27x10^{-06}$	$2.29x10^{-07}$
9.70	$3:85x10^{-06}$	$2.34x10^{-07}$
10.07	$3.66x10^{-08}$	$2.72x10^{-07}$
10.45	$3.66x10^{-08}$	$2.72x10^{-07}$
10.59	$3.66x10^{-08}$	$2.72x10^{-07}$
10.78	$3.66x10^{-08}$	$2.72x10^{-07}$

APPENDIX F

DATA FOR LIGAND-PROMOTED DISSOLUTION OF METAL-OXIDE COATINGS IN MINI-COLUMNS

Table F.1. Data for dissolution of Fe from AC with buffered Ox_T = 1 mM at pH 4

Pore Velocity (pv/hr)	Dissolved Fe (mM)	Dissolution Rate (μmol/hr/gm)
$5.73x10^{-01}$	$3.32x10^{-01}$	$1.95x10^{-01}$
$6.29x10^{-01}$	$4.30x10^{-01}$	$2.77x10^{-01}$
$6.36x10^{-01}$	$4.21x10^{-01}$	$2.74x10^{-01}$
$7.30x10^{-01}$	$4.17x10^{-01}$	$3.12x10^{-01}$
$1.89x10^{-01}$	$4.17x10^{-01}$	$8.08x10^{-02}$
$3.42x10^{-02}$	$4.34x10^{-01}$	$1.52x10^{-02}$
$9.01x10^{-01}$	$4.10x10^{-01}$	$3.79x10^{-01}$
$6.97x10^{-01}$	$4.39x10^{-01}$	$3.14x10^{-01}$
$3.73x10^{-01}$	$4.39x10^{-01}$	$1.68x10^{-01}$
$4.00x10^{-01}$	$3.80x10^{-01}$	$1.56x10^{-01}$
$3.88x10^{-01}$	$3.80x10^{-01}$	$1.51x10^{-01}$
$3.74x10^{-01}$	$3.80x10^{-01}$	$1.46x10^{-01}$
$3.63x10^{-01}$	$3.75x10^{-01}$	$1.39x10^{-01}$
$4.50x10^{-01}$	$3.73x10^{-01}$	$1.72x10^{-01}$

Table F.2. Data for dissolution of Fe from AC with unbuffered Ox_T = 1 mM; $pH_{initial}$ = 4

Pore Velocity (pv/hr)	pH_{final} - $pH_{initial}$	Dissolved Fe (mM)	Rate (μmol/hr/gm)
$3.72x10^{-01}$	3.50	$2.29x10^{-04}$	$5.46x10^{-05}$
$3.35x10^{-01}$	2.65	$4.79x10^{-02}$	$1.03x10^{-02}$
$2.85x10^{-01}$	1.88	$1.99x10^{-01}$	$3.63x10^{-02}$
$2.52x10^{-01}$	1.93	$1.96x10^{-01}$	$3.17x10^{-02}$
$1.77x10^{-01}$	2.09	$2.08x10^{-01}$	$2.36x10^{-02}$
$1.55x10^{-01}$	1.95	$2.10x10^{-01}$	$2.08x10^{-02}$
$1.31x10^{-01}$	1.95	$1.77x10^{-01}$	$1.48x10^{-02}$
$1.13x10^{-01}$	2.02	$1.75x10^{-01}$	$1.26x10^{-02}$
$1.00x10^{-01}$	2.15	$1.55x10^{-01}$	$9.97x10^{-03}$
$9.85x10^{-02}$	2.23	$1.52x10^{-01}$	$9.60x10^{-03}$
$8.76x10^{-02}$	2.19	$1.37x10^{-01}$	$7.69x10^{-03}$
$6.99x10^{-02}$	1.78	$1.38x10^{-01}$	$6.19x10^{-03}$
$6.30x10^{-02}$	2.14	$1.07x10^{-01}$	$4.32x10^{-03}$
$5.03x10^{-02}$	2.15	$9.76x10^{-02}$	$3.15x10^{-03}$
$4.43x10^{-02}$	2.43	$7.56x10^{-02}$	$2.15x10^{-03}$
$3.92x10^{-02}$	2.36	$5.67x10^{-02}$	$1.43x10^{-03}$
$3.37x10^{-02}$	2.43	$1.87x10^{-02}$	$4.03x10^{-04}$
$2.65x10^{-02}$	2.35	$3.00x10^{-02}$	$5.08x10^{-04}$
$2.44x10^{-02}$	2.65	$2.28x10^{-02}$	$3.56x10^{-04}$

Table F.3. Data for dissolution of Fe from MC with buffered Ox_T = 1 mM at pH 4

Pore Velocity (pv/hr)	Dissolved Fe (mM)	Dissolution Rate (μM/hr/gm)
$4.72x10^{-01}$	$4.23x10^{-02}$	$1.78x10^{-02}$
$4.54x10^{-01}$	$4.34x10^{-02}$	$1.76x10^{-02}$
$4.40x10^{-01}$	$4.11x10^{-02}$	$1.61x10^{-02}$
$5.06x10^{-01}$	$3.77x10^{-02}$	$1.63x10^{-02}$
$4.82x10^{-01}$	$3.59x10^{-02}$	$1.48x10^{-02}$
$5.00x10^{-01}$	$3.65x10^{-02}$	$1.56x10^{-02}$
$4.05x10^{-01}$	$3.55x10^{-02}$	$1.23x10^{-02}$
$3.85x10^{-01}$	$3.63x10^{-02}$	$1.19x10^{-02}$
$2.54x10^{-01}$	$5.40x10^{-02}$	$1.17x10^{-02}$
$2.26x10^{-01}$	$4.56x10^{-02}$	$8.80x10^{-03}$
$1.85x10^{-01}$	$5.00x10^{-02}$	$7.91x10^{-03}$
$1.67x10^{-01}$	$4.53x10^{-02}$	$6.47x10^{-03}$
$1.54x10^{-01}$	$5.00x10^{-02}$	$6.59x10^{-03}$
$1.34x10^{-01}$	$5.00x10^{-02}$	$5.72x10^{-03}$
$1.22x10^{-01}$	$4.95x10^{-02}$	$5.17x10^{-03}$
$1.42x10^{-01}$	$4.79x10^{-02}$	$5.83x10^{-03}$
$9.68x10^{-02}$	$5.39x10^{-02}$	$4.46x10^{-03}$
$2.95x10^{-02}$	$7.54x10^{-02}$	$1.90x10^{-03}$
$1.52x10^{-01}$	$3.84x10^{-02}$	$4.98x10^{-03}$

Table F.4. Data for dissolution of Fe from MC with unbuffered Ox_T = 1 mM; $pH_{initial}$ = 4

Pore Velocity (pv/hr)	pH_{final} - $pH_{initial}$	Dissolved Fe (mM)	Rate (μmol/hr/gm)
$3.63x10^{-01}$	1.40	$7.11x10^{-03}$	$1.33x10^{-03}$
$3.29x10^{-01}$	2.31	$5.30x10^{-02}$	$8.97x10^{-03}$
$2.96x10^{-01}$	2.21	$8.77x10^{-02}$	$1.33x10^{-03}$
$2.21x10^{-01}$	2.00	$9.67x10^{-02}$	$1.10x10^{-02}$
$1.82x10^{-01}$	1.88	$9.94x10^{-02}$	$9.30x10^{-03}$
$1.47x10^{-01}$	1.81	$1.04x10^{-01}$	$7.82x10^{-03}$
$1.64x10^{-01}$	1.55	$1.09x10^{-01}$	$9.19x10^{-03}$
$1.62x10^{-01}$	1.19	$8.73x10^{-02}$	$7.27x10^{-03}$
$1.39x10^{-01}$	1.41	$8.55x10^{-02}$	$6.11x10^{-03}$
$1.26x10^{-01}$	1.62	$8.79x10^{-02}$	$5.69x10^{-03}$
$1.15x10^{-01}$	1.79	$7.58x10^{-02}$	$4.50x10^{-03}$
$1.08x10^{-01}$	1.94	$7.79x10^{-02}$	$4.33x10^{-03}$
$9.81x10^{-02}$	1.95	$7.73x10^{-02}$	$3.90x10^{-03}$
$9.12x10^{-02}$	2.04	$6.61x10^{-02}$	$3.10x10^{-03}$
$7.92x10^{-02}$	1.97	$6.68x10^{-02}$	$2.72x10^{-03}$
$6.56x10^{-02}$	2.40	$6.24x10^{-02}$	$2.11x10^{-03}$
$5.37x10^{-02}$	2.43	$5.66x10^{-02}$	$1.56x10^{-03}$
$4.96x10^{-02}$	2.38	$4.87x10^{-02}$	$1.24x10^{-03}$
$3.87x10^{-02}$	2.46	$3.34x10^{-02}$	$6.64x10^{-04}$
$3.43x10^{-02}$	2.74	$1.49x10^{-02}$	$2.62x10^{-04}$
$2.78x10^{-01}$	0.88	$2.34x10^{-02}$	$3.35x10^{-03}$
$9.12x10^{-02}$	2.02	$3.40x10^{-02}$	$1.60x10^{-03}$

VITA

The author was born in Patna, India and spend his formative years in Calcutta, India. After graduating from South Point High School in 1982, he studied geology for a year at Jadavpur University, Calcutta. He joined the Department of Mining Engineering at the Indian School of Mines, Dhanbad in 1983. In 1987, he graduated after completing his thesis entitled "Cost Analysis of Underground Mines". Vowing never to go back to school he joined Coal India Ltd. and worked for a year in the underground and open pit coal mines as a Mining Engineer responsible for production and safety. During this period he published two articles in mining engineering journals (*1, 2*). He then took up a job with IDL Chemicals Ltd., Hyderabad as Assistant Manager - Technical Services.

August 1989 saw him move to the United States for a M.S. in Mining Engineering at the Southern Illinois University at Carbondale. He focussed on the environmental problems related to mining and in 1991 completed his thesis entitled "Large Diameter Column Study of the Alkaline Recharge Pool Approach for Acid Seep Abatement". He learned a great deal about the geochemistry and remediation of acid mine drainage and the endeavor resulted in a journal publication (*3*). In the desire to get formally trained in environmental science and engineering he decided to pursue a Ph.D. He joined the research group of Dr. William Fish in the Department of Environmental Science and Engineering at the Oregon Graduate Institute of Science & Technology. He started working on research related to a municipal landfill but then moved on to work on the effect of site heterogeneity on adsorption of ions. His research also included investigating the role of ligands in remediating metal contaminated subsoils. He has published one article (*4*) and is looking forward to publishing more articles from his thesis. After a prolonged long distance relationship with Preeti, he married her in June 1993. They had a son, Ankit, in June 1994.

He is now moving on to the "real world" in search for a satisfying and fruitful career. He hopes to find more time for his wife and son.

PUBLICATIONS

(1) Kumar, A. and Dash, S.K. *Mine Safety Journal*, **1987**.

(2) Kumar, A. and Dash, S.K. *Minetech*, **1988**, Vol. 9, No. 5, Nov-Dec.

(3) Kumar, A.; Paul, B.C. and Chugh, Y.P. *Journal of the Environment in the Mineral and Energy Industry*, **1993**, 155-162.

(4) Kumar, A. and Fish, W. *Colloids and Surfaces A: Physicochemical and Engineering Aspects*, In Press.